REAL-TIME NON-CONTACT MEASUREMENT AND ANALYSIS FOR THE CONTROL OF DISTORTION DURING WELDING

by
Gökhan Göktuğ

B.Sc. in Civil Engineering, İstanbul Technical University
İstanbul, 1986

S.M. in Civil Engineering, Massachusetts Institute of Technology
Cambridge, 1990

S.M. in Naval Architecture an Marine Engineering, Massachusetts Institute of Technology
Cambridge, 1994

Ocean Engineer, Massachusetts Institute of Technology
Cambridge, 1994

SUBMITTED TO THE DEPARTMENT OF OCEAN ENGINEERING IN PARTIAL FULFILLMENT OF THE REQUIREMENTS FOR THE DEGREE

OF

DOCTOR OF PHILOSOPHY IN ADVANCED MANUFACTURING

at the
MASSACHUSETTS INSTITUTE OF TECHNOLOGY
June 1994

Signature of Author_____
Department of Ocean Engineering
June, 1994

Certified by_____
Koichi Masubuchi
Thesis Supervisor

Accepted by_____
Douglas A. Carmichael
Chairman, Committee for Graduate Studies

REAL-TIME NON-CONTACT MEASUREMENT AND ANALYSIS FOR THE CONTROL OF DISTORTION DURING WELDING

by

Gökhan Göktuğ

Submitted to the Department of Ocean Engineering in June, 1994 in partial fulfillment of the requirements for the degree of Doctor of Philosophy in Advanced Manufacturing.

Abstract

The problem of controlling distortion due to welding has been acknowledged by designers and manufacturers as a matter of extreme importance. The two causes of welding distortion are the relative movement of joining parts until the weld freezes and the distortion caused by thermal plastic strains formed during welding. These strains have been studied and formulated to some extent by many scientists. Nevertheless, it is the relative motion that has the paramount effect on final distortion. Since its measurement and analysis are very complicated, few researchers have attempted to formalize this problem involving rigid body motion which occurs in a short time and in small magnitudes. In addition, the intense light source interferes with optical measurement and high temperatures prevent access to the vicinity of weld area.

The purpose of this study is to determine the behavior of the metal movement of pieces being joined and effect of movement on the residual values of distortion that remain permanently in the structure. At first, a real-time non-contact measurement technique was developed to measure metal movement during and after welding. This measurement technique, which consists of high accuracy, 8 μm, non-contact laser displacement sensors, was used to measure the out-of-plane metal movement due to elastic-plastic strains and rigid-body motion. With this technique, the behavior of out-of-plane distortion in washer pipe fixture of fiber optic connectors used in electronic industry was determined. A practical solution was suggested to the manufacturer of the fiber optic connectors to reduce distortion by up to 70%.

To study transient metal movements during joining three sets of experiments were performed. In the first set, a stainless steel plate was examined at three different configurations of solid plate, plate with a slit and two separate plates. The second set of experiments involved the bead-on-plate and butt welded restrained beam models. In the last set, the transient out-of-plane distortion of butt welded steel plates was investigated. A fundamental difference in the mechanism of metal movement and resulting distortion between restrained joint and unrestrained free joint was determined after the completion of the experiments.

Experimental results of bead-on-plane welded solid stainless steel plates were supported by a numerical approach used to analyze the physical quantities involved in the welding process. A finite element model for welding process was developed and utilized in ADINA and ADINA-T to analyze the transient temperature field, transient strains, distortion and plastic strains. The numerical predictions showed good agreement with the experimental results.

Thesis Supervisor: Koichi Masubuchi
Title: Kawaski Professor of Engineering

Acknowledgment

I would like to express my warmest gratitude to my advisor Prof. Koichi Masubuchi, for his invaluable guidance and financial and emotional support when I needed it the most.

My sincere appreciation goes to my committee members, Professors Tomasz Wierzbicki and Alan Brown. Both of them gave me priceless advice in my thesis and their contribution in this study is deeply acknowledged.

Special thanks to Mr. Koga for his involvement and help throughout this thesis. I am also grateful to him for his friendship and help in my work. Without him, I would have to work twice as much to finish. I would like to express my appreciation to Mr. N. Eckhouse for providing the data-acquisition software.

Thanks to Mr. Hijikata, Mr. Ichikawa, Mr. Kaito, Mr. Meada, Mr. Mukai, Mr. Nakamura, Mr. Shimizu, Mr. Tanizawa and Mr. Umekuni, for their friendship and the fun we shared.

Deep thanks to Ms. Ipek Ilter for proof-reading the text, helping me with some of the drawings and text. Her input in script is invaluable. My warm appreciation also goes to Ms. C. Brooke, Ms. T. Garalis, Ms. M. Grenhamm, Ms. Judy Sheitanian, Ms. S. Trohon and Ms. B. Tuths for making life easy for me in the department.

Finally, I would like to thank my friends here at MIT, İpek, İbo, Hasan, Yüksel, Serhat, Erol, Gürkan, Rıfat and Çınar, for sticking with me in good and bad times. I also thank my friends, Charis, Diane, Gebran, Hayat, John, Soren, Noah, and all others that I could not mention here for all the good times we had together.

Table of Contents

List of Figures

List of Tables

Chapter 1

1. Introduction

Residual stresses and distortion are major problems associated with the welding fabrication of large, complex structures including ships, railroad tracks, and offshore structures. Moreover, with the advance of computer technology, welding has become one of the most common joining processes for manufacturing the components of electronic devices. This has necessitated a total solution to the problem related to distortion.

The main problem associated with welding is that when a weldment is locally heated by the heat source used, complex thermal stresses occur during the welding, and residual stresses and distortion remain after the work is completed. These stresses and distortions have various consequences, most of which are detrimental to the integrity of welded structures. Similarly, they reduce the efficiency of the manufactured electronic components. Therefore, distortion becomes a very important factor and correcting unacceptable distortion is very expensive and in some cases impossible. In the last decade engineers in all fields of the industry were faced with several problems arising from residual stresses and distortion, such as mismatches and residual stresses with values almost as high as that of the yielding stress of the material that remains in the structure etc. There are several reasons that cause such problems:

- We are using increasingly thinner sections which tend to distort more,
- In order to produce more compact parts, we reduce the dimensions of the parts as much as possible. However, the heat input cannot be reduced as much as the dimensions of the parts. Hence, these small products are subjected to relatively more heat inputs than large ones,

- We are using an increasing number of aluminum alloys and other non-ferrous alloys which tend to cause more distortion problems,

- In order to provide required accuracy, some structures such as microchips and mechanical parts of electronic devices must be fabricated with increasingly less tolerance for distortion.

We believe that the best way of dealing with these problems is to develop technologies for controlling and reducing residual stresses and distortion during fabrication. The best method to accomplish this is to utilize real-time controls during welding, even as non-elastic strains causing these stresses and strains are being formed, along with transient metal movement. The difficulty here is that necessary control must be maintained during welding while the weldment undergoes complex changes of thermal stresses. In order to have correct and consistent controls, one must have the following capabilities:

- Sensing capability. One must have a proper device or devices that are able to detect whether what should be happening is actually taking place.

- Prediction capability. One must have a proper prediction capability, either by analysis, prior experiments, and/or experience on:

  (a) how the studied weldment deforms

  (b) how to perform proper controls to change the distortion being considered.

- Control capability. If one finds out what is actually happening is different from what is supposed to happen, it is important to have the capability to make necessary changes, in real-time if necessary.

1.1 Literature Review and Background Discussion

The behavior of metal movement during welding is a very complex subject to measure and predict. This difficulty is well understood and acknowledged by scientists and engineers working in the welding field. The first researchers started to study the subject in the late 1930's. However, to the best of our knowledge, most of the studies executed and published until now discussed the final values of stresses and distortion after cooling.

Spraragen and co-workers [119, 120, 121], published several review reports which included a series of comprehensive research on residual stresses and distortion. Some time later, researchers in the United Kingdom, Japan and U.S.S.R., also became interested in the subject of residual stresses and distortion. Several books were written on welding distortion and residual stresses. A most comprehensive book on welding titled 'Analysis of Welded Structures' was written by Prof. K. Masubuchi [62] in 1980. This book covers all the previous studies and the information gathered in the USA, Japan, and the European countries.

The early studies of residual stresses and distortion were limited to empirical approaches mostly associated with simple weldments. Besides those, there were some analytical studies on residual stresses and shrinkage. Naka [88] started the pioneering work in Japan on the analytical study of weld shrinkage around 1940's. His work included both experiments and analytical examination. He reduced the mathematical complication of the nature of welding into a one dimensional problem and neglected the effects of shrinkage in the welding direction and the behavior of shrinkage in butt welds.

The metal movement during welding was first investigated by Matsui [83]. He studied the shrinkage process during first pass welding. In this study, Matsui introduced the behavior of metal movement in the axial direction of butt welded beams. He concluded that about 80% to 90% of weld shrinkage occurred at base metal and the rest of it, approximately 15%, came from the shrinkage of the weld metal. However, his work was limited to the motions in the plane and to a very basic analytical analysis due to lack of technology.

These early studies were mostly experimental or very simple cases, such as one dimensional problems, axisymmetric stress and temperature field in spot welding applications and instant heating on the edges of strip geometries where the temperature and stress are only functions of lateral distance from the weld line. Even these simple cases, required many hours of computational time by the computer technology of that day.

In the 1960's, with the advancement of computer technology, extensive applications of welding models were developed. In the early 60's, Tall [124, 125], introduced a weld model for bead-on-plate welding along the center of a rectangular strip. While the temperature field was considered in two dimensions, stress calculations were made in one dimension by considering the longitudinal stress component as a function of the lateral distance from the weld line and other components of stress tensor as identically equal to zero.

Based on Tall's method, in the late 60's, Masubuchi [82], and other scientists from research institutes developed computer software written in FORTRAN for thermal stresses during welding [82]. Later, these programs were improved by researchers at M.I.T. under the supervision of Prof. Masubuchi and they were applied to various kinds of geometrical shapes and materials. The predicted results were verified with experimental data and good correlations were generally reported [11].

All of these analytical studies suffered from the nonlinearity of metal properties at elevated temperatures. The resulting predictions were poor due to the fact that the properties of the material at higher temperatures were ignored. This shortcoming of the analytical approach led researchers to use numerical methods to handle the highly nonlinear nature of welding problems. In this area, the finite element method became very popular in the early 70's. Hibbit and Marchal [42] developed a thermo-mechanical numerical model of welding process by using this method. The model included material nonlinearities and complex boundary conditions, such as the deposition of molten beads and radiation heat losses. Following this, there were many other finite element programs developed with rather limited capabilities to calculate the stresses and strains. With the development of commercial multi-purpose finite element programs in the early 80's, the researchers and engineers utilized these programs to develop specific models [85,96,136]. Today, there are more than several hundred finite element programs available commercially all over the world. However, only a few of them are capable of handling complicated models that include material nonlinearities at elevated temperatures.

The limitation of mathematical modeling is that one has to know the physical behavior of the system being analyzed. In welding, restraining and metal movement are the most important factors on the final values of distortion and residual stresses. However, most studies in this field which generally cover the subject of residual stress and final distortion, do not pay the required attention to the formation of the metal movement while welding is being performed. An accurate model can only be developed if the actual history of the behavior of the system is understood.

A numerical model does not provide an accurate result unless it simulates the physical behavior of the system under investigation. It means that physical behavior needs to measured which is not very easy in welding applications. To have a factual measurement, one has to determine

first what and where to measure. It is stressed by Masubuchi [62, 70] that the plastic strains developed around the weld metal are the cause of the final residual distortion. However, this area is exposed to the very high values of temperature resulting from the welding arc. The accuracy and the speed of data readings required in the measurements is very important. The quantities which need to be determined in welding processes are the temperature distribution, stresses and strains, and distortion. Temperature is measured with thermocouples and there are almost no problems until thermocouples are exposed directly to the welding arc. If one wants to understand the behavior of distortion, there is no need to measure residual stresses because they do not give us any information about how the system is forced to behave. On the other hand, residual stresses are mostly measured by relaxation technique which has to be performed after everything else is completed. The only quantity not measured is distortion, i.e. metal movement and strains. Researchers have used strain gauges to measure the transient strains. If the geometry of the tested specimen is very simple, such as a beam, then it is easy to calculate the distortion and transient displacement from strain gauge readings. However, if the geometry is complicated such as in plates, shells, etc. it is almost impossible to compute the distortion from strains. Moreover, strain gauges require a relatively large specimen and they have to be mounted quite a distance away from the weld line. An almost untouched quantity which is the last and most important is distortion or metal movement. Distortion is measured by dial gauges. Although they have very low accuracy and it is difficult to collect data through them, mechanical dial gauges have been used very extensively in the measurement of weld distortion. However, this is a very inefficient method of measurement. It has low accuracy and has to be placed on a certain large area which will not be affected by the heat. Moreover, the readings are performed by the naked eye and logged on paper. Therefore, this part of the study in welding applications was left alone and people did not pay special attention to improve the techniques to elicit an accurate measurement of metal movement especially during welding.

1.2 Methodology

Many studies have been executed and published on the subject of distortion and shrinkage behavior of welded joints. There are a few papers which describe the metal movement process during welding and cooling. However, most of them discussed the final distortions after the welded joint was cooled down. Studying the metal movement of the welded structures from the point of view of residual distortions, restraining stresses of the welded joint and weld cracking is very important, as those may be serious problems in actual welding procedure.

It should be noted that there is a difference in the metal movement of the welded joint between the first and later passes. In the first pass, plates that were at first separate are joined. On the other hand, in the second and later passes, plates are no longer separate but were already joined together by the first welding pass. Distortion, that is metal movement, due to welding consists of two parts. The first part is the relative movement of joining parts until the weld freezes. Although it was known that this is the most dominant factor in the size of final distortion, a few scientists have attempted to formalize this problem involving rigid body motion. This is a fact that makes the analysis of distortion extremely complicated based on the present data. The second part, which was studied and formulated to some extent by scientists, is distortion caused by the incompatible strains formed after the weld is frozen. These incompatible strains give rise to self-equilibrating stresses that remain in the welded structure after it is cooled down to ambient temperature, thus producing the so-called residual stresses and plastic deformations in turn.

Matsui [] performed an experimental and analytical study on shrinkage process during first pass welding. This is one of the limited studies that investigates the contraction and expansion processes. However, it should be noted that Matsui studied axial metal movement in transverse direction of butt welded joints. Therefore, his work is limited to in-plane metal

movement of joining pieces. As a result of his study, he concluded that most of the metal movement comes from the expansion of the base metal and the rest belongs to the contraction of weld metal which only accounts for 10 to 15 % of the whole shrinkage. Moreover, he reported that contraction is mainly affected by two factors, the plate thickness and gauge length[1]. However, due to the difficulty of measurement and analysis, he did not consider the rigid-body motion of unrestrained free parts welded.

In this study, the rigid-body motion and metal movement of bead-on-plate and butt welds were studied. First, a real time non-contact measurement technique was developed to determine the behavior of out-of-plane metal movement and then this technique was successfully applied to the following welding applications:

- washer pipe fixture of fiber optic connectors used in electronic industry,
- a free plate model used extensively in experiments with three different joining configurations, a solid plate, plate with a slit reaching half way its thickness, and two separate pieces.
- a restrained beam model with and without a slit at two different thicknesses, 1" and 2" respectively.
- a restrained H-joint plate machined and butt welded.

Finally, a 2-D FEM model was developed for bead-on-plate condition of solid plates. A commercial FEM software, ADINA-T and ADINA[2], was used to incorporate the welding model.

---

[1]The gauge length is defined as the length between the supports or restraining.

[2]Automatic Dynamic Incremental Nonlinear Analysis

1.3 Characteristics of the Problem

In terms of the characteristics of the problem, this thesis can be considered as consisting of two parts. The first part was performed under contract and it consisted of controlling the out-of-plane distortion in washer pipe connectors. This part of the project was concerned with the control of vertical displacement of pipe-washer connectors used in the fiber optic packages developed by AT&T, Bell Laboratories Solid State, Technology Center, Breiningsville. The connectors were very small, 0.18" for the diameter of the washer and 0.1" for the diameter of the pipe. The required control of distortion was in the order of microns. This was a rather unusual geometry for researchers working in shipbuilding, and a challenging and different work.

Performing the experiment by using conventional measurement techniques used in welding experiments for many years was not possible. A state-of-the-art measurement technique was needed to be able to take measurements on very small specimens and to detect and measure very small movements of the parts . Additionally, laser pulse welding method which is performed in 8 msec. was used in the actual manufacturing. 8 msec. welding time is an extremely short duration to take an accurate measurement. Also, as mentioned earlier, metal movement during welding is another very important factor that needs to be determined. To develop a very accurate, real-time, fast and non-contact technique, a study was initiated under the supervision of Prof. Masubuchi in the Welding Systems Laboratory at M.I.T.

In order to develop a suitable measurement technique, this study started with a very broad literature survey in the rather unfamiliar field of electronic industry. State-of-art laser displacement sensors, with 8 μm accuracy, manufactured by KEYENCE/Japan and meeting all the qualifications desired, were found after two months of search. To understand the physical behavior of the washer-pipe connectors and to find the causes of the distortion which caused

loss of efficiency in the actual function of fiber optic packages, a year and a half long series of experiments were performed with specimens ten times enlarged. During this period, many meetings were held between the researchers at M.I.T. and AT&T Bell Laboratories. The behavior of the metal movement during and after welding was well determined to the order of millimeters. Based on the results of the experiments, the causes of distortion and methods of control were reported to AT&T in six progress reports. However, although the individual behavior of the movements of the parts was determined, the interaction between the washer and the pipe could not be entirely established until the weld froze. The very complicated nature of welding and the geometry did not allow us to perform a mathematical verification of experimental results.

In the second part, with this newly developed tool, a basic study was started to fill in the gaps left out by past studies due to lack of technology. First, a series of experiments were performed to study the transient movement of stainless steel plates due to heating by a stationary gas tungsten arc. Three different types of specimens were prepared; namely, a solid plate, a plate with a slit, and two separate plates. The tendency of the metal movement in the two separate plates was entirely different than the others. However, a different tendency was interestingly observed in all three specimens which was that of restraining before and after welding.

Second, after seeing the effect of restraining, effort was made to clarify this phenomenon in detail. Therefore, a specimen was machined to simulate the perfect cantilever boundary condition in the manufacturing of railroad tracks. This part of the project was supported by the Japanese National Railway Company, JR. The effect of restraining on the vertical displacement of railroad tracks was determined in real-time.

Third, and the last experiment of this thesis, was sponsored by the US Navy. The transient out-of-plane distortions of H-shaped restrained butt joints were measured. Experiments were performed on two types of specimens, bead-on-plate (no slit) and butt weld (with a slit.) The whole scenario of metal movement during and after welding is successfully determined.

The results of the bead-on-plate conditions of the solid plate experiment were supported by the finite element model developed by using ADINA, Automatic Dynamic Incremental Nonlinear Analysis.

This measurement technique, its utilization for the various applications of welding processes and the presentation of the different behaviors between unrestrained free joints and restrained bead-on-plates and butt welded joints, constitutes the uniqueness and the contribution of the five years of research and effort made towards this doctoral dissertation. It is believed that this method will provide a clearer picture of metal movement during joining which is the most complicated and important phenomena of the welding process. Moreover, it is hoped that the present study will fill a large gap left out in past studies.

1.4 Objective of the Thesis

The main objective of this thesis is to conduct a study on the out-of-plane distortion during welding by developing a non-contact real-time measurement method which is able to follow the actual behavior of metal movement during and after welding. In other words, this thesis is mainly concerned with the sensing capability during welding. A secondary objective is to extend the possible theoretical analysis into the numerical prediction of heat flow and thereby generating an examination of deformation phenomena. The third and last objective is to control distortion based on the results obtained by the experimental data and numerical prediction.

In summary, the objective of this research can be outlined as follows:

1- Performing a study on the out-of-plane distortion during welding in order to determine the rigid-body motion and transient distortion caused by incompatible strains. Therefore, a technique needs to be developed to measure the transient distortion. This technique should satisfy the following requirements:

- The technique should require minimum preparation and instrumentation.
- Since a measurement in the vicinity of weld is desired, the specimen should not be touched during measurement because of the very high temperatures in that area after welding.
- Measurement during and after welding must be made in real-time .
- The technique should be applicable to various types of weldments including very large and very small structures.
- For micro devices used in electronic industry, the technique has to be very accurate in order to be able to make precise measurements of movements up to the order of 100 microns.

2- Modeling the welding heat transfer and perform stress analysis using the finite element method. Compare the results with the experiment.

3- Controlling distortion based on the results obtained experimentally and numerically.

1.5 Organization and Outline of the Thesis

In Chapter 2, a general background in the field of distortion and residual stresses is summarized. The most common distortion patterns, transfer shrinkage and angular distortion, are emphasized and a literature survey with related subjects is presented.

In Chapter 3, laser displacement sensors which measure transient deformations and their applications to various geometries are introduced. Performed experiments and data obtained in the experiments are presented. Suggestions to reduce the distortion, which are also supported by experiments, are outlined.

In Chapter 4, the heat flow analysis of the welding process is considered. The available analytical solutions are presented with their limitations on usage. A two dimensional finite element model is introduced for welding problems considering the material nonlinearities at high temperatures. The results obtained with the nonlinear finite element program ADINA-T are presented.

In Chapter 5, the finite element model of welding process is introduced to predict transient deformation, residual stresses, thermal stresses and plastic strains. ADINA results of computed quantities are presented.

In Chapter 6, the comparison of experimental results with numerically predicted ones are given. The experimentally obtained temperature history and transient distortion are compared with ADINA and ADINA-T predictions.

In Chapter 7, the conclusion and recommendations for future studies are given.

Chapter 2

2. Fundamental Characteristics of Residual Stresses and Distortion in Welded Structures

2.1. Basic Discussion

Residual stresses and distortion in welded structures are similar to each other as follows:

(a) Both residual stresses and distortion are produced by non-elastic strains produced during welding in the regions near the weld

(b) Residual stresses and distortion are interrelated. When a joint is more highly restrained, residual stresses tend to increase, while distortion tends to decrease.

Residual stresses cannot be easily measured, and it is difficult to control their magnitude. In many cases, tensile residual stresses that exist in regions near the weld are as high as the yield stress of the material. On the other hand, distortion is measurable, and it is possible, in many cases, to control distortion within a tolerable limit by using proper techniques.

The basic problems in analyzing and controlling distortion are:

(1) A variety of distortion types. Various types of distortion occur, as shown in Figure 1 [62]. Even a simple butt weld, for example, can cause transverse shrinkage, longitudinal shrinkage, angular distortion, bending distortion, and buckling distortion (when large thin plates are welded), as will be discussed later. Distortion of a complex welded structure is extremely complicated.

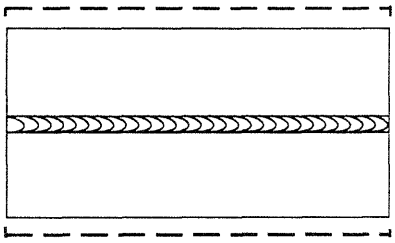

a) Transverse Shrinkage

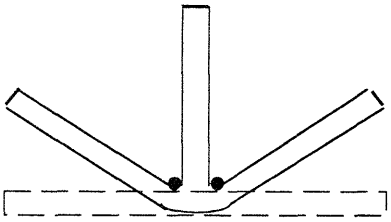

b) Angular Change

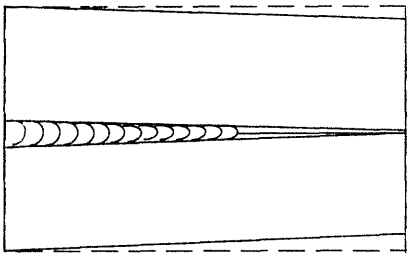

c) Rotational Distortion

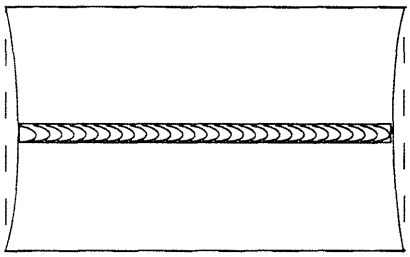

d) Longitudinal Shrinkage

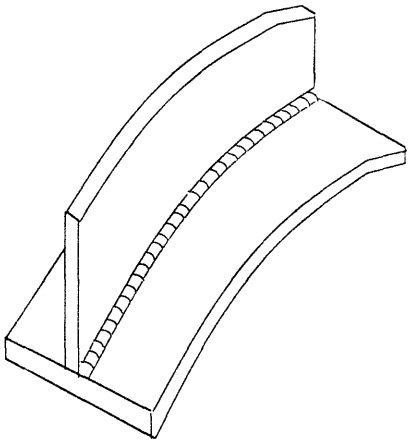

e) Longitudinal Bending Distortion

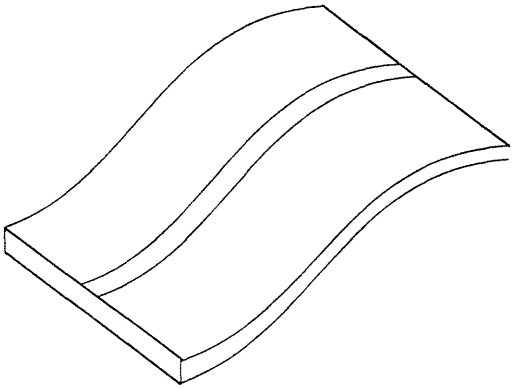

f) Buckling Distortion

Figure 2.1 Various types of distortion[62]

(2) Effects of welding parameters. The amount of distortion is affected by many welding parameters including joint design, welding processes, and welding conditions including welding current, arc voltage, and arc travel speed.

(3) Effects of fabrication procedures. The amount of distortion is also affected by various fabrication procedures including joint restraint, welding sequence, etc.

A major problem which makes the analysis and control of distortion produced by arc welding very complex, is that two separate parts are joined to become one by heating with a moving heat source. The parts being joined make complex movements while joining takes place. Whether or not the parts are restrained has a significant effect on the transient metal movement and final distortion. After the weld metal solidifies, the joint moves as a single body as the temperature decreases. Therefore, in the analysis and control of distortion, it is extremely important to understand the mechanisms of transient metal movement and the final distortion. In the case of multipass welding of a butt joint, for example, metal movement during the first pass and the movement during subsequent passes can be very different.

2.2 Examples of Thermal Stresses and Metal Movement During Welding

Discussed here are some basic characteristics of transient metal movement and distortion of some simple welds, as follows:

(1) Transient heat flow and thermal stresses during bead-on-plate welding

(2) Transient metal movement and distortion during bead-on-edge welding of a rectangular plate

(3) Control of joint mismatch (rotational distortion) during butt welding

(4) Bending deformation of a flat plate by line heating with a laser beam

(5) Transient vertical (or lateral) movements during butt welding of steel plates

(6) Transient out-of-plane movements during butt welding of steel plates.

2.2.1 Transient Heat Flow and Thermal Stresses During Bead-on-Plate Welding

Figure 2.2 schematically shows the changes in temperature and thermal stresses during bead-on-plate welding. A weld bead is being laid along the x-axis of a large flat plate. The welding arc, which is presently located at the origin, O, is moving at a speed, v (see Figure 2.1-a).

Figure 2.2-b shows temperature distributions along several cross sections [62, 68]. Along Section A-A, which is ahead of the welding arc, the temperature changes due to welding, ΔT, are almost zero, as shown in Figure 2.1-b-1. Along Section B-B, which crosses the origin, temperature distribution is very steep, as shown in Figure 2.2-b-2. Along Section C-C, which is some distance behind the arc, the distribution of temperature change is as shown in Figure 2.2-b-3. Along Section D-D, which is very far behind the arc, the temperature change due to welding diminishes again, as shown in Figure 2.2-b-4.

Figure 2.2-c shows distributions of thermal stresses in the x-direction, σ_x, along these sections. Stresses in the y-direction, σ_y, and shearing stress, τ_{xy}, also exist in a two-dimensional stress field. A simplified analysis which only considers σ_x has been developed. This analysis is called the "one-dimensional analysis" in this report. Along Section A-A, thermal stresses caused by the welding arc are almost zero. The stress distribution along Section B-B, is shown in Figure 2.2-c-2. Because the molten metal does not support a load, stresses underneath the welding arc are close to zero. Stresses in regions near the arc are compressive, because thermal expansions in these areas are restrained by the surrounding regions that are heated to lower temperatures. Since the temperatures of these regions are quite high and the yield stresses of the material are low, stresses in these regions are as high as the yield stresses of the material at corresponding temperatures. Stresses in regions away from the weld are tensile to balance the compressive stresses in areas near the weld.

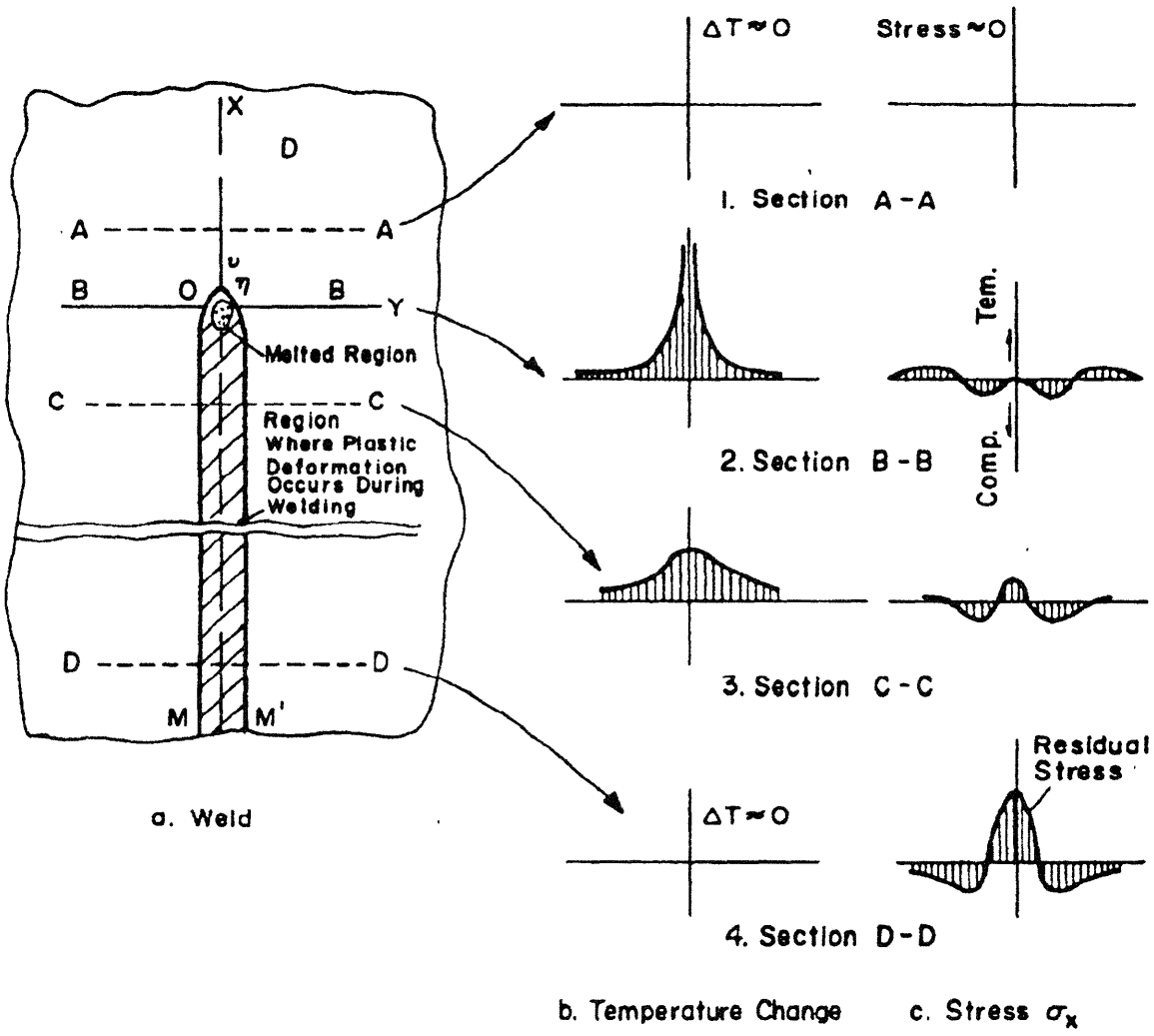

Figure 2.2 Schematic representation of changes of temperatures and thermal stresses during bead-on-plate welding[62]

Stresses are distributed along Section C-C as shown in Figure 2-c-3. Since the weld metal and base metal regions near the weld have cooled, they try to shrink causing tensile stresses in regions near the weld. Figure 2.2-c-4 shows the stress distribution along Section D-D. High tensile stresses are produced in regions near the weld, while compressive stresses are produced in regions away from the weld. The distribution of residual stresses that remain after welding is shown in Figure 2.2-c-4.

The cross-hatched area, MM', in Figure 2.2-a shows the region where plastic deformation has occurred due to welding. The small, egg-shaped region near the origin indicates the region where the metal is in the molten stage. The region outside the cross-hatched area has remained elastic during the entire welding thermal cycle.

2.2.2 Transient Metal Movement During Bead-on-Edge Welding of a Rectangular Plate

Figure 2.3 shows schematically how a rectangular plate deforms when arc welding is performed along the upper longitudinal edge [68,70]. Since temperatures are higher in regions near the upper edge, these regions expand more than those near the lower edge causing upward movement of the center of the plate, δ, as shown by Curve OA in Figure 3. When welding is completed and the metal starts to cool, the plate deforms in the opposite direction. If the material were completely elastic in the entire region of the plate, during the entire period of the heating and cooling cycle, the plate would deform as shown by Curve AB'C' returning to its original shape with no residual distortion. However, this does not happen in the welding of a real material, be it steel, aluminum, or titanium. In the case of welding a real material, plastic deformations occur in regions near the upper edge while temperatures are high and yield stresses of the material are low. As a result of the compressive plastic strains (shrinkage) that are produced in regions near the upper edge, the plate continues to deform after passing its

original shape (or the horizontal line) resulting in the negative final distortion, δ_f, when the plate cools to its initial temperature (see Curve OABC).

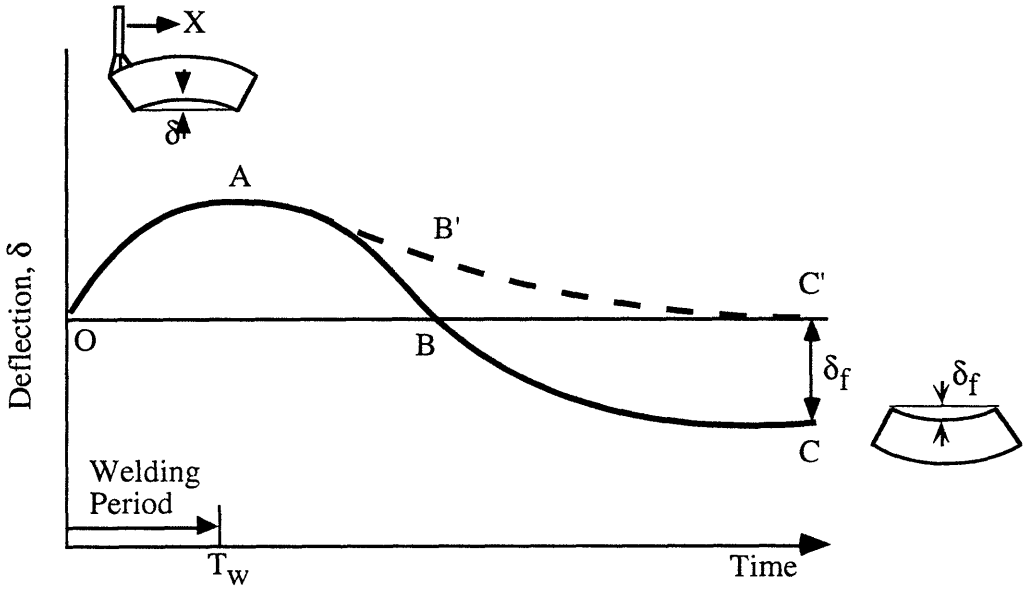

Figure 2.3 Transient deformation of rectangular plate during and after welding along the upper edge of a rectangular plate[3]

It is believed that the most effective way for reducing distortion is to control the formation of plastic strains produced in regions near the weld. The difficulty here is that the necessary control must be made during welding. If the control performed is correct, the final distortion will be reduced. If the control is incorrect, on the other hand, the final distortion will be increased. In order to perform correct controls consistently, one must have the following capabilities:

(1) Sensing capability. One must have a proper device or devices to sense whether what should happen is actually happening.

(2) Control capability. If one finds that what is actually happening is different from what is supposed happen, it is important that one has the capability of making necessary changes, in real time.

2.2.3 Control of Joint Mismatch (Rotational Distortion) Produced During Butt Welding

Figure 2.4 (a) shows metal movements when two free plates are butt welded, schematically. Since each of the two plates being welded deforms as shown by Curve OABC in Figure 2.2, the unwelded portion of the joint opens resulting in a joint mismatch [70]. Masubuchi called this type of distortion "rotational distortion" [62]. A common method of coping with rotational distortion is to hold the joint with tack welds. This can be done relatively easily in manual welding of small parts. In the case of automatic welding, however, dealing with the rotational distortion becomes an important problem. When welding is performed by a robot, for example, tack welds must be made by a human welder requiring additional manpower and cost. On many occasions, tack welds are made by inexperienced persons resulting in less than perfect welds. Also, tack welds, even though they are perfectly made, act as major hazards during the subsequent root pass welding. In fact, it is difficult to completely melt tack welds during the root pass welding thereby causing lack of penetration and other types of defects [52]. In submerged arc welding of thick plates, forces acting on tack welds are so huge that tack welds often break during welding. In fact, Japanese shipbuilders experienced longitudinal cracking of the finishing end when they first introduced one-side submerged arc welding of large ship plates [35].

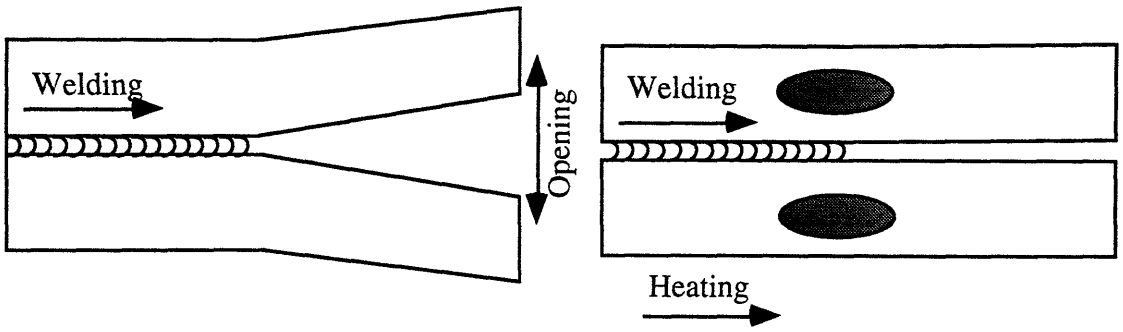

Figure 2.4 Formation mechanism of joint mismatch and a method of reducing it by side heating during welding[70]

Chang, Park, and Miyachi of M.I.T. performed experimental and analytical studies for reducing forces acting on tack welds during butt welding [20,100,85]. The basic idea used by Chang was to reduce the joint mismatch or the rotational distortion by side heating, as schematically shown in Figure 2.4 (b). By performing side heating during welding, it may be possible to produce additional thermal stresses that can counteract those produced by welding. It is important, however, that the additional heating does not produce additional residual stresses. Figure 2.5 (a) shows the experimental setup used by Chang [20]. Instead of using tack welds for holding plates to be joined, two semi-circular rings were attached to both ends of the joint. The rings were equipped with strain gauges in order to measure changes of deformation at these ends. Although the rings were welded to the plates in the experiments, these rings can be designed in such a way that they can be clamped to plates to be welded in actual fabrication. Efforts were made to reduce the opening of the finishing end by altering the thermal pattern in the weldment during welding. Two oxygen torches were mounted on a frame with welding head so that the side heating system could be moved along with the welding arc. The position of the heating system relative to the welding head could be adjusted in three directions, x, y, and z (see Figure 2.5 (a)), in order to control the side heating procedure.

Figure 2.5 (b) shows typical results obtained on low-carbon steel weldments, 36 inches long, 24 inches wide, and 0.5 inch thick. The left figure shows results obtained on a weld made with no side heating, while the right figure shows results obtained on a weld made with side heating. It can be seen in the figure that very soon after the start of welding, the starting end began to shrink. Note that when closing of a joint occurs, strains measured on gauges attached on the outer surface of the ring would be tensile. On the specimen without side heating, the finishing end first opened a considerable amount and it began to shrink after welding was completed. Welding was completed in 165 seconds, but it took approximately 1800 seconds (30 minutes) before forces acting on the rings were fully developed. The major difference between the movement of the starting end and that of the finishing end was produced during welding. The maximum load in the ring attached at the finishing end was 1125 lb. The results show that very large forces exist in the joint during welding.

The side heating caused little effect on forces acting on the ring attached to the starting end. On the other hand, forces acting on the ring attached to the finishing end were greatly affected by the side heating. The maximum load in the ring attached at the finishing end was reduced to only 105 lb. Results show that the deformation at the starting end was barely affected by the side heating. This indicates that the measurement at the starting end can be used as a control. In other words, the joint mismatch can be minimized as long as the strain measurements on the finishing end are similar to those obtained on the starting end.

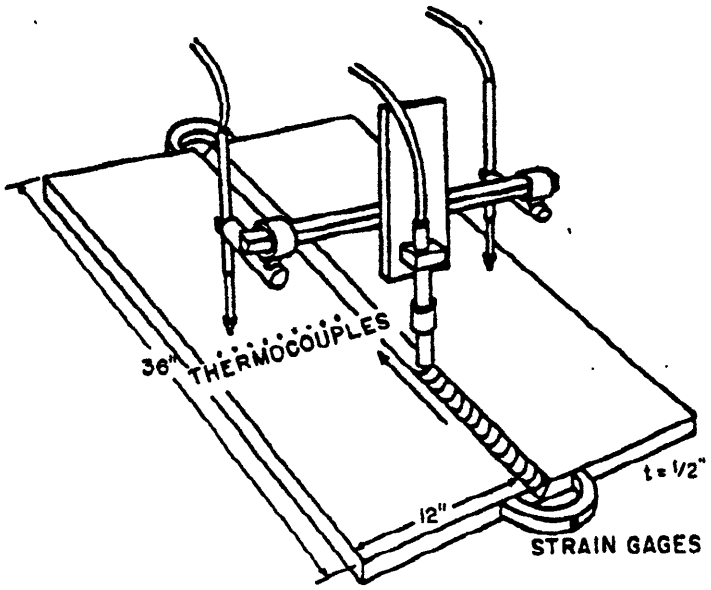

(a) Heating System

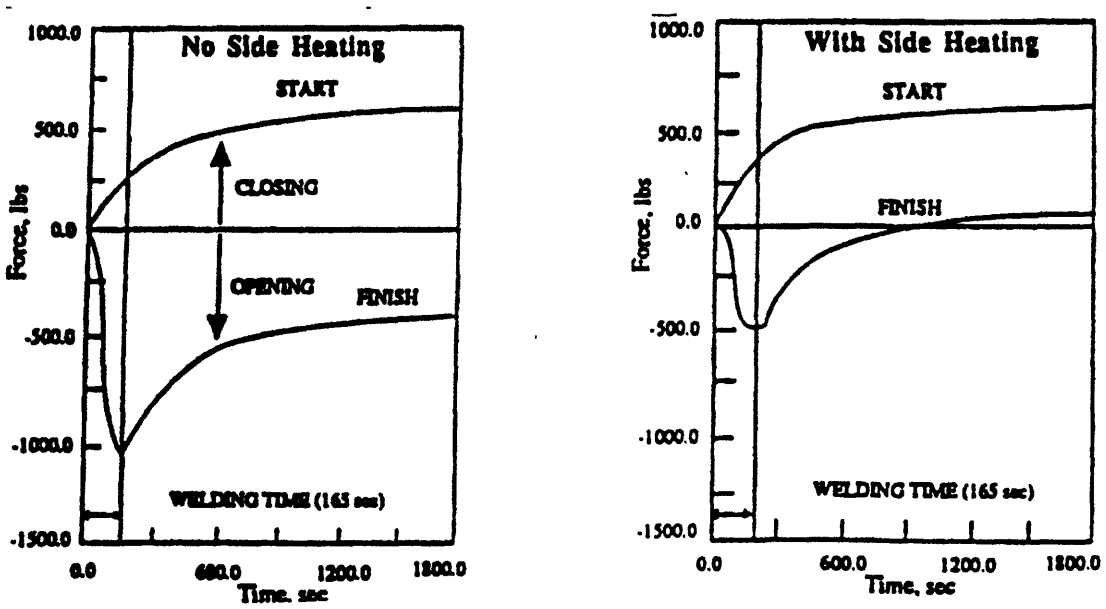

(b) Experimental Results

Figure 2.5 Reduction of forces acting on rings attached to starting and finishing ends of a butt weld[70]

An analytical study was made to determine optimum conditions for side heating using a one-dimensional program that analyzes longitudinal stress only. It has been found that the most desirable side heating is to heat wide regions away from the weld to moderate temperatures (around 200°F) to accomplish the following:

(a) Side heating should provide thermal stresses large enough to counteract those produced by welding

(b) Side heating should not produce additional residual stresses.

Aluminum Welds. A limited study on aluminum welds was performed by Park [100]. First, experiments were performed to study the effects of side heating on forces acting on rings attached to both ends of aluminum butt joints 36 x 24 x 0.5 in. in size. Results were disappointing. For example, the maximum force observed on a ring attached to the finishing end increased from 300 lb. on a weld without side heating to 700 lb. on a weld with side heating. This is probably due to the combined effects of the following:

(1) Compared to steel, aluminum has a larger (approximately 5 times) heat conductivity. In order to produce, by side heating, thermal stresses large enough to counteract those produced by welding, we must have uneven temperatures caused by both welding and side heating. In an aluminum weld heat spreads so rapidly that the temperature rise produced by welding and produced by side heating cannot be well separated.

(2) Compared to steel, aluminum has a larger (approximately 3.5 times) coefficient of linear thermal expansion. Therefore, the best method of reducing the distortion in an aluminum weld is to minimize the temperature rise, not to increase the temperature rise by side heating.

It was decided to study the effects of forced cooling on the joint mismatch during welding of an aluminum butt joint. Cooling was done by placing crushed dry ice particles on surface regions near the weld. Then the maximum force observed on a ring attached to the finishing end decreased from 300 lb. without forced cooling to a mere 30 lb. with cooling. The results show that the key for reducing the joint mismatch in an aluminum weld is to keep the temperature rise due to welding as small as possible.

2.2.4 Out-of-Plane Distortion of a Plate Due to Line Heating

Techniques involving heating with an acetylene torch have been used for straightening distorted plates as well as forming plates into various shapes [62]. Japanese shipyards extensively use line heating for bending steel plates. A research project was performed at M.I.T. for the U. S. Navy through Todd Pacific Shipyards Corporation to investigate whether steel plates can be formed by line heating with a high-power laser beam (5-10 kilowatts in power) instead of an oxyacetylene torch [72,76,78,113]. In most experiments, steel plates 18 inches wide and 24 inches long were heated with a laser power source moving along the center line of a plate, as shown in Figure 2.6 (a). In order to avoid excessively concentrated heating of the plate, the laser beam was defocused. The plate thickness studied ranged from 1/4 to 1 inch. Materials used were low-carbon steel and three types of high-strength steels including: HY-80 steel, K-TEN80CF steel manufactured by Kobe Steel, and ASTM A710 steel. K-TEN80CF has a minimum ultimate tensile strength of 80 kg/mm^2 (114 ksi). Compared with HY-80 steel, K-TEN80CF and A710 steels have lower carbon equivalent values and improved weldability. Experiments included measurements of (a) changes of temperatures, (b) transient thermal strains, and (c) out-of-plane deformation (angular change).

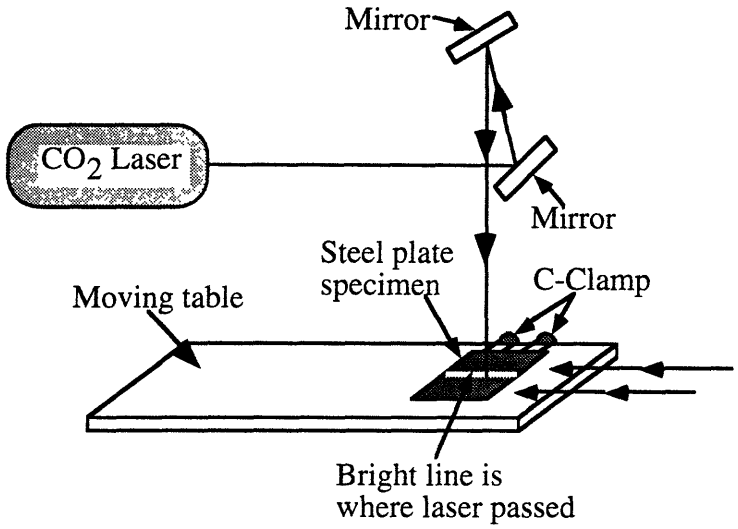

a-) Experimental setup

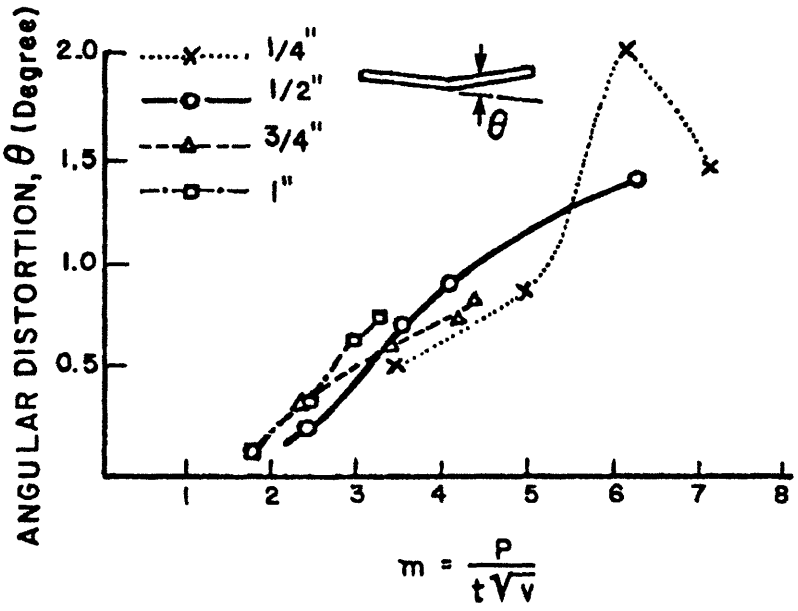

b-) Effects of experimental parameters on angular distortion in low carbon steel plates

Figure 2.6 Bending of steel plates by line heating with high-power laser[72,76,78,113]

Effects of Heat Input and Plate Thickness. Figure 2.6 (b) shows effects of various experimental parameters on values of angular change in low-carbon steel plates 1/4, 1/2, 3/4, and 1 inch thick. Used in the abscissa is a parameter, m, which is expressed as follows:

$$m = \frac{p}{t\sqrt{v}} \tag{1}$$

where,

P = power of the laser beam, KW (kilowatt)

t = plate thickness, in

v = travel speed of the laser heat source, ipm (inches per minute).

By using this parameter, data for different thicknesses are arranged within a range. The amount of angular change increased as the parameter "m" increased; however, when the value of m exceeded a certain value (around 6), the amount of angular change started to decrease.

Similar tendencies have been reported by Watanabe and Satoh who studied angular distortions produced in fillet welds, as shown in Figure 2.7 [62,137]. In fact, the parameter, "m," was developed by prior knowledge on the results shown in Figure 2.7.

Effects of Specimen Length. A limited study was conducted on the effects of specimen length on angular change due to laser line heating. A 24 inch long specimen was cut into three pieces, one inch, 10 inches, and 12 inches long. These three pieces were assembled having the one-inch long piece in the middle, and laser line heating was performed along the center line of the assembled pieces. This set-up was used in order to assure that the heat flow patterns in these pieces would be as similar to each other as possible. Figure 8 shows transient metal movements of the three plates 3/8 inch thick heated with a laser power (P = 6 KW) moving at a speed of 9 inches per minute. Heating of the entire assembly of 23 inches long was completed in 153 seconds. Significant movements of the pieces occurred while the pieces were being

heated, and it took much longer (around 500 to over 1000 seconds) before the distortion finally settled. The final distortion of the one-inch long piece was far less than those of 10- and 12-inch long pieces. Similar results were obtained with specimens of different thicknesses (1/2 and 5/8 inch) heated under different conditions. These results may be explained as follows:

(1) One-Inch Long Piece. When the top surface of the piece was heated, regions near the top surface expanded more than the bottom regions thus causing negative distortion. But the plastic strains produced in regions near the top region were not so large, since the entire piece deformed easily. When the piece cooled, distortions in the opposite direction occurred, but the final distortion was rather small.

(2) 10- and 12-inch Long Pieces. When the top surface was heated by a moving heat source, top regions directly below this heat source which were heated to high temperatures tried to expand. But the expansion was restrained by materials located ahead and behind the moving heat source where temperatures were lower than those directly below the heat source. Therefore, the amount of plastic compressive strains produced in the regions below the moving heat source were more than those produced in the 1-inch long piece, resulting in larger final distortions.

These results demonstrate that the dimensions of the specimen sometimes cause significant effects on distortion. One way to avoid possible confusion is to obtain experimental data on transient metal movement during heating treatment. It is easy to understand a certain phenomenon once we understand its mechanisms of formation. Without developing a good understanding of the mechanisms of the formation of this phenomenon, we are often confused by the results.

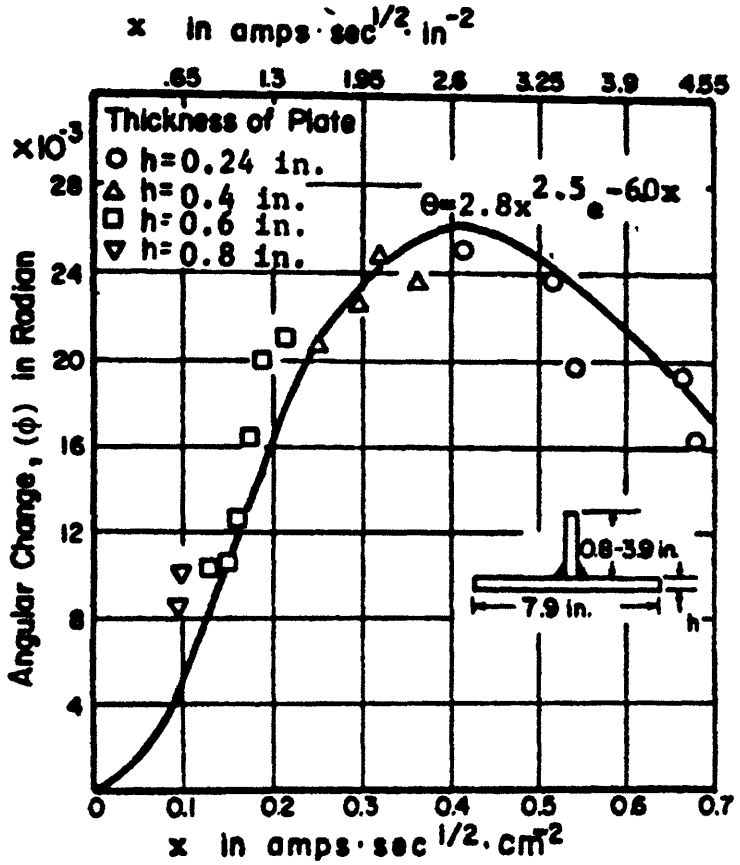

Where $x = 10^{-3} \frac{I}{h\sqrt{vh}}$

I = Current, amp

h = Thickness

v = Welding speed

e = Base of the common logarithm.

Figure 2.7 Effects of welding parameters on angular changes of free fillet welds[62,137]

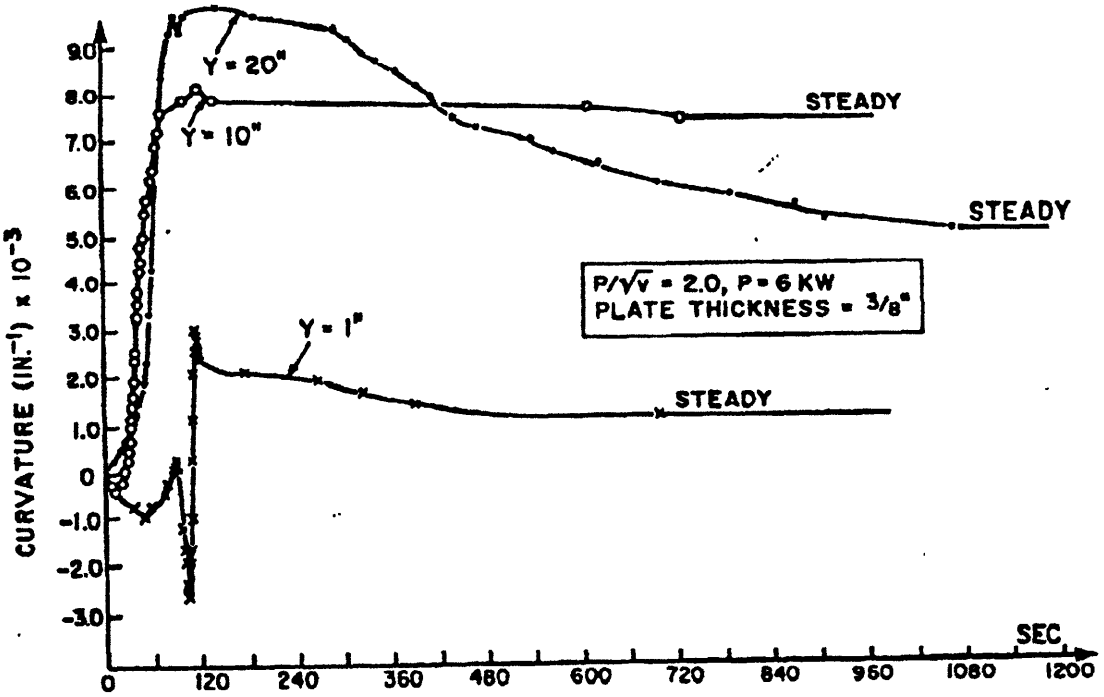

Figure 2.8 Effects of specimen length on transient angular distortions of steel plates being line heated by the laser beam[78]

Chapter 3

3. Experiment

3.1 Introduction

As mentioned earlier, metal movement during welding is a very complex and complicated subject to be measured and predicted. Past studies in this field which generally cover the subject of residual stress and final distortion, did not consider the importance of the formation of the metal movement while welding is performed. This experimental work covers a wide range of geometries used in the joining process to understand the behavior of metal movement during welding time and at the cooling stage. The necessity to do this comes from the fact that the final values of distortion and residual stresses produced are due to the complicated path of metal movement during the melting and solidification of welded metal.

After the objective of the study, this chapter outlines the steps of experimental investigation. A short explanation of the instruments used in the experiment are given in the corresponding subsections. The experimental procedure is explained in detail in order to provide more familiarity with the work. Selection of the welding procedure is explained separately. Materials used in the experiment are presented with their physical and mechanical properties since their variation with temperature has an essential importance on the accuracy of the predicted results. Finally, the results of the experiments are shown with graphic illustrations.

3.2 The Objective of Experimental Investigation

The objective of this experimental investigation is to obtain a series of real-time data which

accurately display the formation of the distortion during and after welding in various geometries commonly used in the fabrication of ships, railroad tracks, ocean structures, etc. and the manufacture of micro-devices such as fiber optic connectors in computer industry. The specific goal of the entire investigation is to understand what happens and how the structure deforms during welding and how to control the distortion before it develops. However, to measure the residual stress and transient micro strains, the geometries of the specimens under investigation are small enough not to allow one to use commonly utilized measurement devices for welding problems, such as strain and dial gauges. Therefore, in this study, for the first time in welding applications, non-contact, high accuracy, 8 μm, frequency laser displacement sensors are used to observe transient metal movement. However, laser displacements sensors are able to perform the same functions for larger structures as well.

Moreover, since some of the work performed was performed under contract to outside firms and industry, special attention was paid to solve the problems as directed and methods acceptable to these firms were proposed to fulfill the contract requirements.

3.3 Real-Time Non-Contact Measurement of Distortion

3.3.1 Necessity of Real-Time Non-Contact Measurement in Welding

The methods used to measure distortion in welded structures are limited due to the nature of the welding procedure. Dial gauges are widely used to measure distortion in welding. However, the location of the dial gauges is controlled by the welding process and specimen sizes. In the previous studies[7, 96, 136], researchers have measured the distortion at relatively far distances from the welding line. As is known in welding distortion, the final value of the distortion stresses is very closely related to the size of the plastic zone where they happen to exist in the vicinity of the weld line. Moreover, the reading of data from the dial gauge is a

time-delayed procedure. A high frequency measurement technique is required in order to follow the formation of deformation accurately. In other words, to picture the whole scenario, the measurement technique must be faster than the response of the structure. On the other hand, since welding produces a high heat input into the structure especially around the weld, the measurement device should not be affected by the heat. However, this is almost impossible for a mechanical device to perform. Therefore, a high frequency real-time non-contact measurement of distortion in the close neighborhood of the weld line is a must.

3.4 Materials Used in Experiment and Their Properties

In this section, characteristics of materials used in the experiment are summarized. The temperature-dependent physical and mechanical properties are tabulated. Moreover, the chemical composition range, along with the physical and mechanical properties and annealed material at room temperature are shown separately.

3.4.1 304 Stainless Steel

304 Stainless steel is a low-carbon (max. 0.08% C), unstabilized austenitic stainless steel specially developed for better corrosion resistance and for restriction of carbide precipitation during welding.

The chemical composition of 304 stainless steel is shown in Table 3.1[7]

The mechanical properties of the 304 stainless steel are summarized in Table 3.2. The properties at elevated temperatures are given for mechanical properties in Table 3.3 .

Element	Percentage
C	0.080 max.
Mn	2.00 max.
Si	1.00 max.
Ni	8.00-10.50(or 11.)
Cr	18.00-20.0
Mo	0.50 max.
S	0.039 max.
P	0.045 max.

Table 3.1 Compositional range of 304 Stainless Steel[7]

Yield strength, σ_y	254.4 MPa
Ultimate tensile strength, (UTS)	578.6 MPa
Elongation, % in 50.4 mm	50 %
Hardness	Bhn 149
Reduction in area	60 %
Density	8000 kg/m^3

Table 3.2 Mechanical properties of 304 stainless steel at room temperature [7]

The temperature dependent mechanical properties of 304 stainless steels are summarized in Table 3.3. The data was collected from several books and theses works performed at M.I.T. The names of the books and the thesis are given in the reference section of this work.

Temperature, °C	Young's Modulus, E N/cm^2x10^6	Poisson's Ratio, ν	Yield Stress, σ_y, N/cm^2x10^3	Strain Hardening Modulus, N/cm^2x10^6	Thermal Expansion Coefficient, $\mu cm/cm°C$
0	21.00	0.288	25440.0	0.5250	17.02
20	21.00	0.288	25440.0	0.5250	17.02
38	20.00	0.297	24410.0	0.5000	17.06
93	19.24	0.302	21100.0	0.4810	17.22
149	18.82	0.307	19100.0	0.4705	17.37
204	18.41	0.310	17580.0	0.4603	17.53
260	17.93	0.313	16550.0	0.4483	17.69
316	17.65	0.315	15510.0	0.4413	17.85
371	17.03	0.317	15030.0	0.4258	18.01
427	16.62	0.319	14270.0	0.4155	18.17
538	15.51	0.322	13240.0	0.3878	18.48
593	15.03	0.323	12480.0	0.3758	18.64
649	14.55	0.325	11930.0	0.3638	18.80
704	14.07	0.327	11170.0	0.3518	18.96
760	13.38	0.327	9920.0	0.3345	19.12
816	12.48	0.329	7860.0	0.3120	19.28
871	10.00	0.330	5100.0	0.2500	20.00
1000	5.33	0.330	100.0	0.1333	20.00
1093	2.66	0.330	10.0	0.0665	20.00
1200	1.33	0.330	10.0	0.0333	20.00

Table 3.3 Temperature-dependent mechanical properties of 304 stainless steel[7]

3.5 Experimental Set-Up

3.5.1 Experimental Instruments

Experimental instruments consist of four main parts:

- Welding process and power supply
- Laser displacement sensors
- Thermocouples
- Data acquisition system

3.5.1.1 Welding Process and Power Supply

Gas Tungsten Arc Welding (G.T.A.W.) process was utilized for the whole experiment because it is one of the cleanest welding processes. Moreover, laser displacement sensors were placed a very close distance from the weld line and they are very sensitive to the sparks and fumes produced by the welding torch. A stationary arc without filler metal was used. Two MILLER welding machines were used to produce a dual welding torch and they were operated at the same time by a custom made power switch mechanism.

3.5.1.1.1 Welding Conditions Used in the Experiment

Spot G.T.A.W. process was applied without a filler metal supply, to simulate a YAG laser irradiation. A couple of welding arcs were turned on simultaneously, and were maintained for five through six seconds to create molten pools of sufficient size. Welding parameters were investigated previously, and set up as shown in Table 3.4. In the case of cylindrical geometry, after the first welding pass, the test bench was rotated 90 degrees and the second welding pass was applied to the specimen in the same way as described above.

Polarity	Direct Current Straight Polarity (Electrode Minus)
Welding Current	150 A
Arc Voltage	13 V
Shielding Gas	Argon
Welding Time	5 ~ 6 sec (Manual Control)

Table 3.4 Gas-Tungsten-Arc-Welding Condition

For the plane specimens, only a single welding torch shown in Figure 3.1 is used under the same conditions summarized in Table 3.4 above.

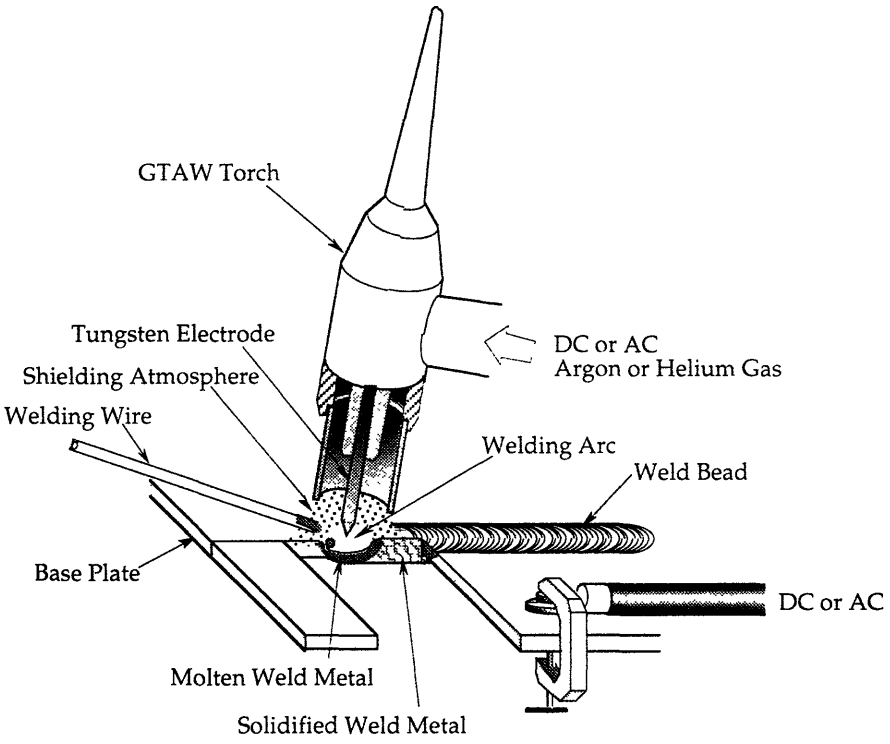

Figure 3.1 Gas tungsten arc welding operation and torch assembly

3.5.1.2 Non-contact Laser Displacement Sensors

A non-contact laser displacement sensor was used to measure the vertical displacement pattern of the specimen. In addition, the out-of-plane motion of the welded specimen was also measured to understand its deformation behavior. The main features of the laser displacement sensor used in this experiment are shown in Table 4.

Maker		KEYENCE Corporation
Model	Sensor Head	LB - 081
	Controller	LB - 1101
Light Source		Semi-conductor Laser Wave Length : 780 nm
Reference Distance		80 mm
Measuring Range		± 15 mm
Linearity		0.25% of F.S.
Resolution		8 μm
Response Frequency		36 Hz

Table 3.5 Main features of the laser displacement sensor

The KEYENCE laser displacement sensor, model LB-081, is a high accuracy measurement device which operates under FUZZY logic control circuit to stabilize the moving targets. Moreover, it can be easily set to a reference point by AUTO ZERO function.

During the experiments, the fumes and the light produced by welding caused noise interference with the laser sensors. In order to avoid this problem, several modifications were made on the experimental setup. However, the following suggestions in general prevent this interference

- Isolating the power cable and connecting the sensor cable from the power line to the welding torch.
- Case grounding the sensor head. If noise occurs at the mounting position of the sensor head, install insulating material between the mounting position and the sensor head.
- Covering the sensor with a metal casing to prevent radiation noise interference. Make sure noise does not enter the metal case.
- Shielding the cables with metal or using independent metal conduits to prevent radiation noise and inductive noise interference.
- Earth-grounding the frame grounding terminal.
- Using only compatible pairs, as each head is designed for a specific controller in order to get more accurate results.

3.5.1.3 Thermocouples

In this investigation, standard OMEGA Engineering type OST probe termination thermocouples with standard 12" length, and 1/8" diameter probe were used. A K type thermocouple was chosen because of its wide range of temperature measurement capability, simplicity, and sturdiness. The data was plotted against time by using a self calibrated chart recorder provided by the same company, OMEGA Engineering.

3.5.1.4 Data-Acquisition System

The laser displacement sensors are interfaced with a 486 PC compatible microcomputer via an analog to digital converter. The heart of the system is a 16 channel, 12 bit A/D board manufactured by Metrabyte Corporation. It is controlled by custom software written in C and developed for this project at the M.I.T. Welding Systems Laboratory. The position of the laser sensors is sampled at a frequency of 10 Hz/channel, and logged to a data file on the PC. Resolution of the system is approximately 8 μm. Up to six channels were used to collect the data from laser sensors. However, in order to eliminate the interference between the sensors, one of the channels was grounded and a single channel was connected to the sensor. Once the data is acquired, it is analyzed and plotted with EasyPlot, a scientific data visualization package manufactured by Spiral Systems.

3.5.2 Specimens

3.5.2.1 Cylindrical Geometry

At first austenitic stainless steel (304 SUS) was used as a material for the test washer and the test tube, because it has a high thermal expansion rate (large welding deformation is expected), good weldability and a convenient supply. Second, the original material kovar was used.

Figure 3.2 (a), (b), and (c) show the dimensions of the stainless steel washer and tube specimens respectively. Outer diameters of the specimens -2.10 inch for the washer and 1.00 inch for the tube- are both ten times as large as the original ones. As for the washer, thought to play the most important role to the displacement behavior of the tube, two types of the configurations were prepared; flat-type washers of various thicknesses (0.20, 0.40, 0.80 and

1.20 inch) and a step-type washer (a washer with a small projection). The gap between the washer and the tube was controlled within 0.005ths of an inch in diameter.

All the kovar specimens shown in Figure 3.3 with their dimensions were machined and supplied to M.I.T. by AT&T. The dimensions of the kovar specimens were slightly different than the 304 stainless steel, due to the limitation of the size of the original material and cost. The length of the test tube was shortened from 4 to 3 inches. The outer diameter of the test washer was also reduced from 2 inches to 1.85 inches.

To investigate the influence of the gap between the tube and the washer, two kinds of combinations were prepared: a tightly fitted combination in which the gap was controlled within 0.005ths of an inch, and a loosely fitted combination where the gap was controlled from 0.008 to 0.01sts of an inch.

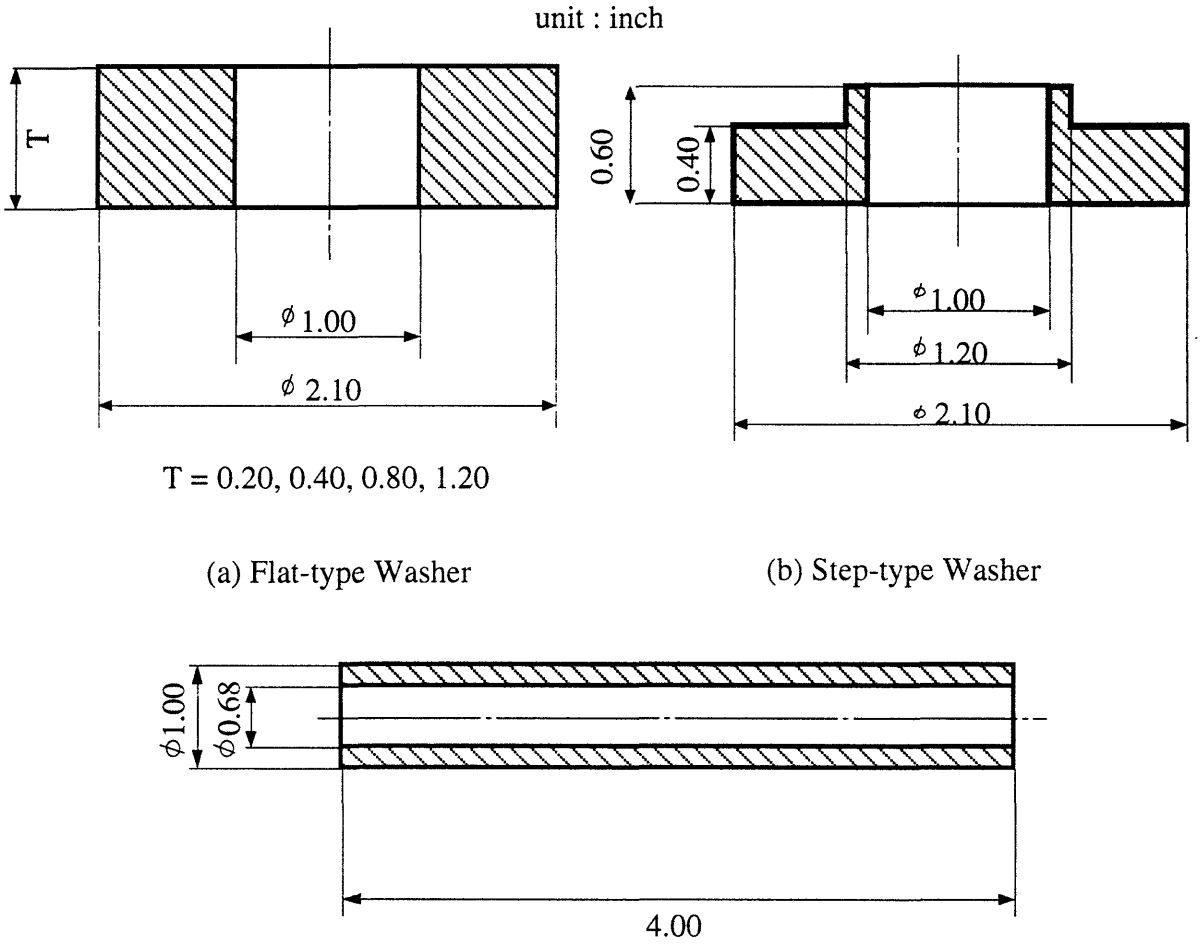

Figure 3.2 Dimensions of stainless steel test specimens

unit : inch

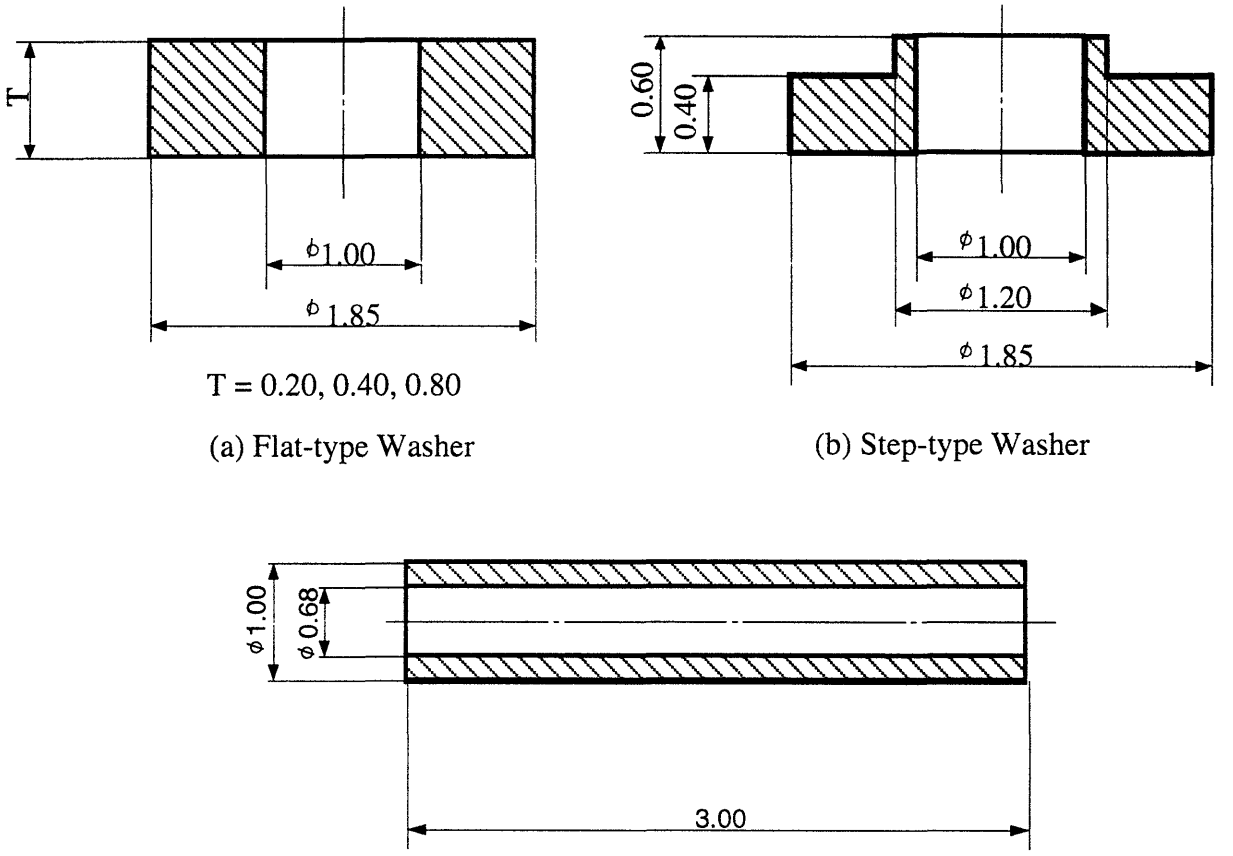

T = 0.20, 0.40, 0.80

(a) Flat-type Washer

(b) Step-type Washer

(c) Tube specimen

Figure 3.3 Dimensions of kovar specimens

In order to study the effect of the clearance between the washer and the tube more effectively, a solid piece to go between these two was machined. The solid washer tube configuration is shown in Figure 3.4. 304 Stainless steel is used as the material and the same experimental procedure is applied to the system.

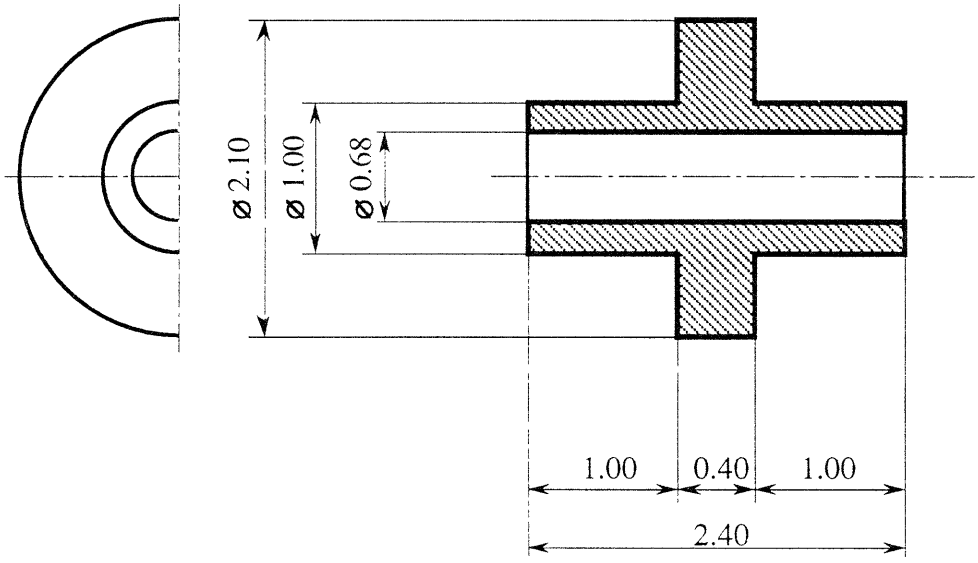

Figure 3.4 Dimensions of a solid washer-pipe configuration

3.5.2.2 Plane Geometry

The different specimen sizes were investigated in plane geometry. The first one is a stainless steel plate model shown in Figure 3.5 with its dimensions. This specimen style, was designed for three different configurations as follows:

- A solid 2x5x0.25 plate,
- Another plate with the same dimensions but with a 5/8 inch slit , Figure 3.6,
- Two solid plates put together to simulate two separate pieces.

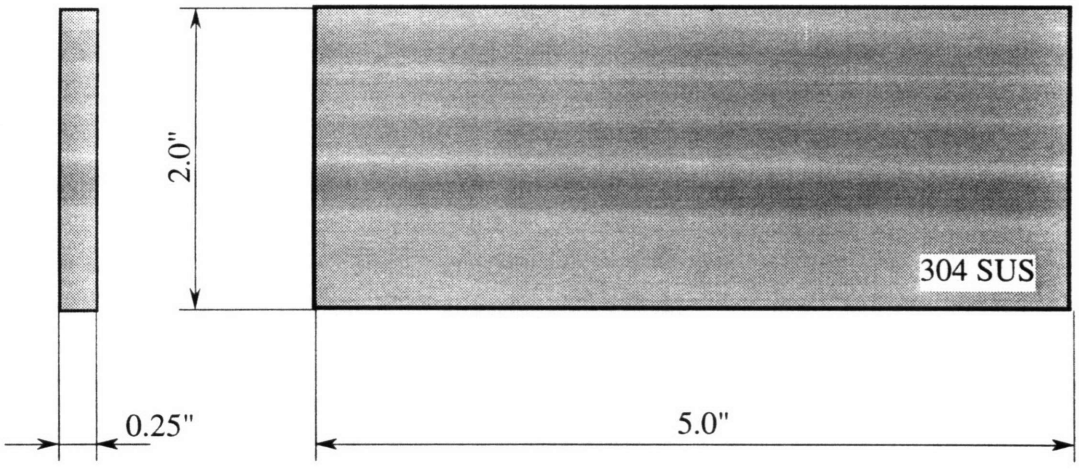

Figure 3.5 Dimensions of plane specimens without slit

In this part of the experiment, our aim was to study the basics of welding distortion and to support the results of the experiments with mathematical analysis. The considered geometry is the most common geometry in welding applications. By assuming uniform heating in depth direction which is direction x pointing out of the plane, the problem can be handled as a two dimensional distortion field, that is defined in the z and y plane.

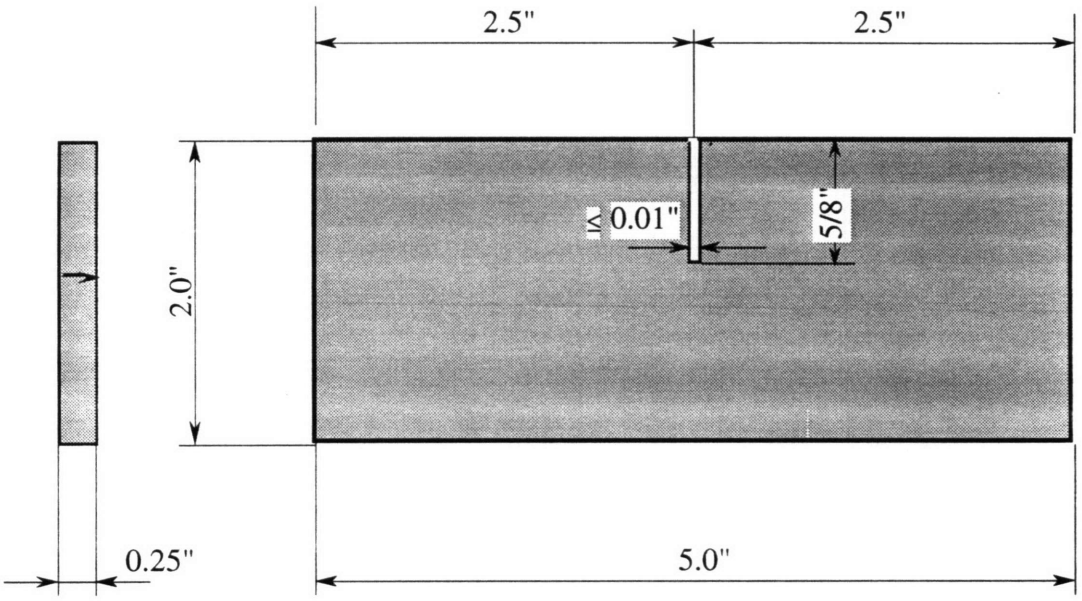

Figure 3.6 Dimensions of plane specimens with slit

Second, a larger size is considered in order to study the effect of restraining and size. Figure 3.7 shows the specimens with slit used in the experiment. Two thickness sizes of the beam model were considered with two configurations. One a solid beam with no cut and the other a cut beam with a 1/16" clearance in between.

Third, a plate specimen was prepared in dimensions, 12x7x0.25 in. Low-carbon steels were utilized as material. Longitudinal and transverse slits were made to prepare an H-shaped restrained joint. The geometry of the specimen is shown in Figure 3.12.

Efforts were made to keep the parameters, such as welding conditions, welding method, the location of welding torch, etc. constant. Only, geometrical constraints were allowed to vary in the whole experimental part of this investigation.

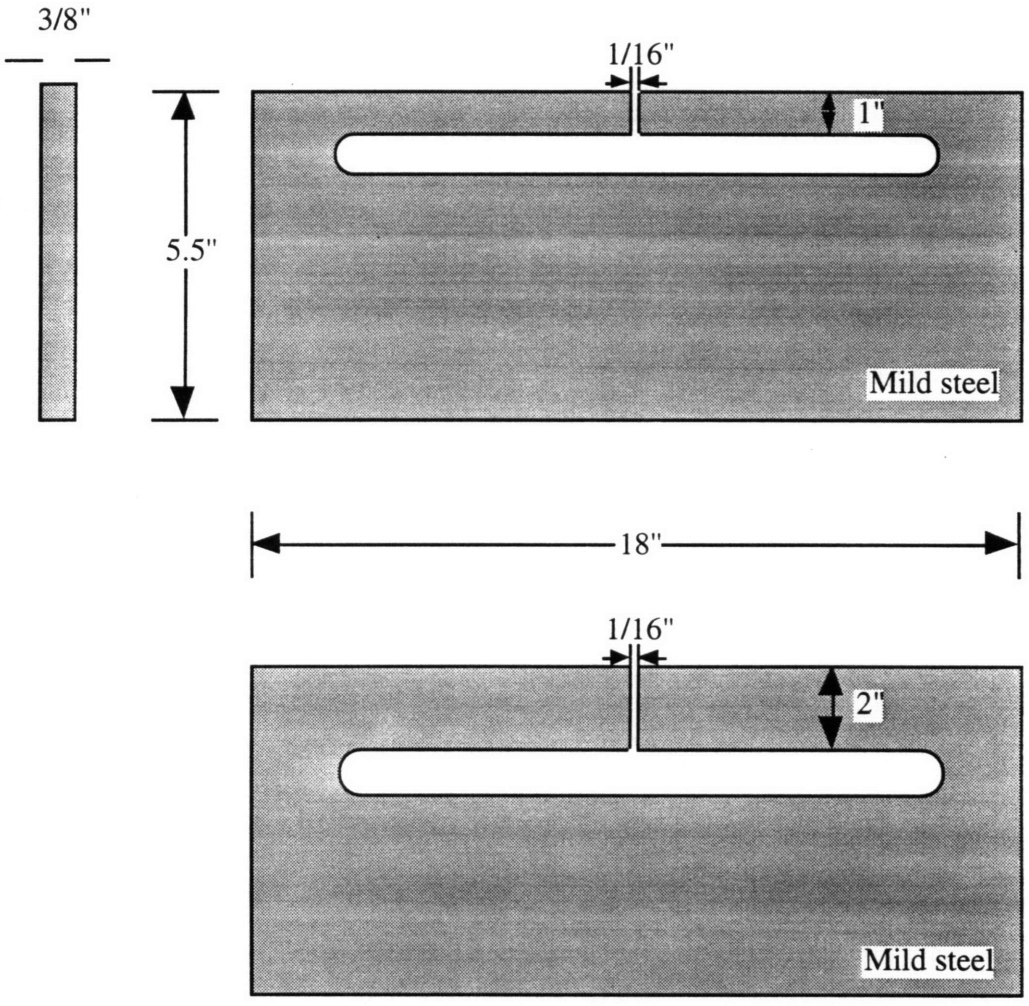

Figure 3.7 Dimensions of beam model with slit

3.5.3 Experiment Configuration

3.5.3.1 Configuration of Cylindrical Geometry

Figure 3.8 shows a general arrangement of the experimental setup. A test washer and a test tube were set on a test bench made of carbon steel. The tube was attached to the test bench with the screw in the fixture, and the washer fixed by a couple of tack welds using G.T.A.W. Dual G.T.A.W. torches, connected to independent welding power sources, were mounted over the washer symmetrically as shown in the figure.

Two laser sensors were placed under the bench where the interference of the light of the welding torch utilizing a laser beam could be minimized. All the specimens were cleaned very carefully to remove all the grease and the dust from the surface in order to avoid fumes formed as a result of burning. Laser sensors were connected to controllers which convert readings from the laser beams into volts.

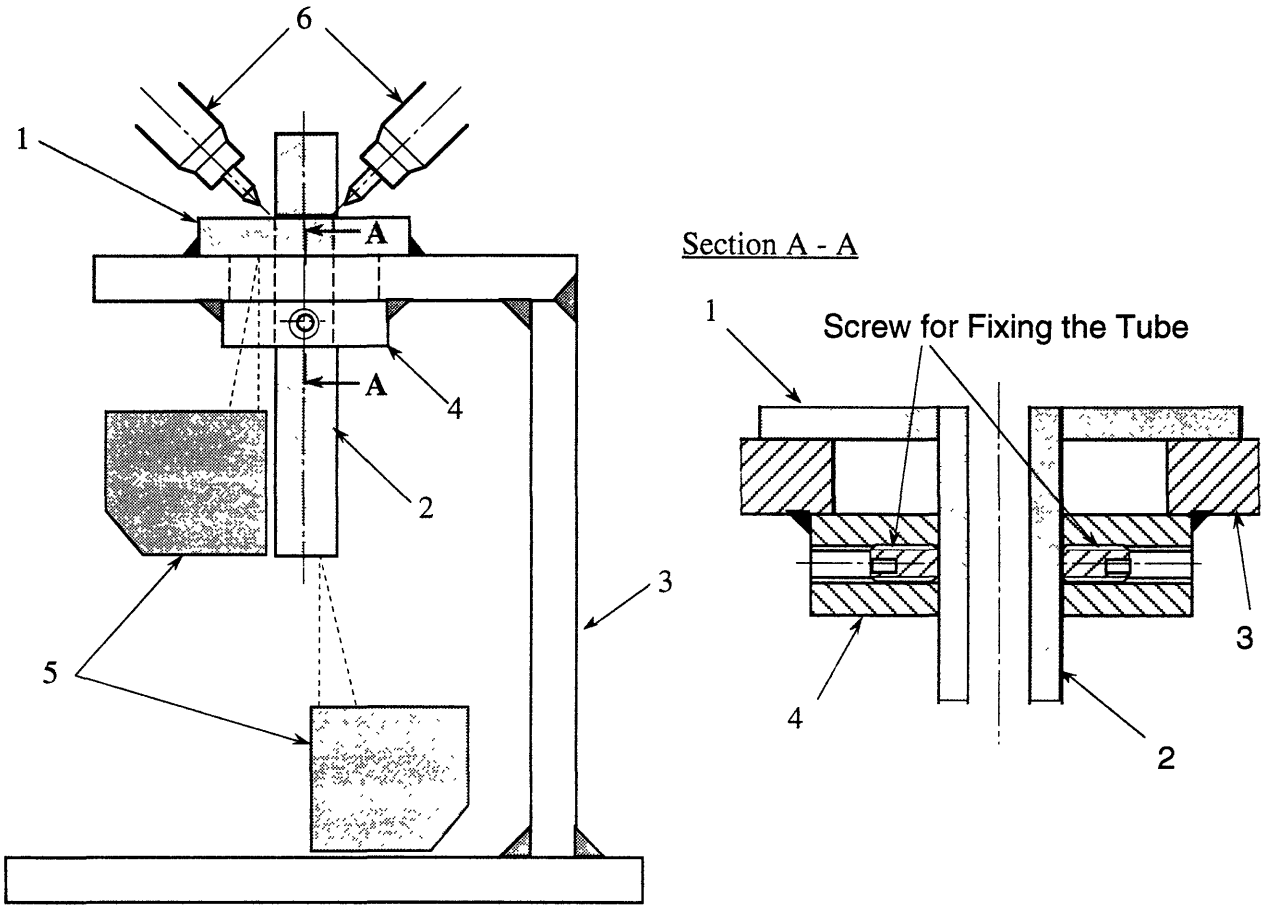

1. Test Washer : 304 Stainless Steel
2. Test Tube : 304 Stainless Steel
3. Test Bench : Carbon Steel
4. Tube Fixture : Carbon Steel + Screw
5. Laser Displacement Sensor : KEYENCE Model LB-081
6. Gas Tungsten Arc Welding Torches

Figure 3.8 Experimental setup for cylindrical specimens and location of displacement measurements

3.5.3.2 Configuration of Plane Geometry

3.5.3.2.1 Temperature Measurement with Thermocouple

Four thermocouples were placed on the plane stainless steel specimens as shown in Figure 3.9. Transient temperature history of four points, 0.6", 0.8", 1.2", and 1.6" were recorded through a chart. It was not possible to approach the weld line any closer than 0.6 " due to the direct heat effect of the welding arc on the thermocouple. However, it was necessary that the locations the thermocouples were mounted on be chemically clean and free of all greases, oil, scale or oxidation. In order to obtain the best results, the following steps are recommended:

- Remove all foreign matter (oil, paint, oxide, scale, etc.) from the surface with disc sander, grinder, or mill file, leaving the surface smooth,
- Indicate the locations by using a blade,
- Clean the surface with gauze saturated with Methyl Ethyl Ketons,
- Apply a metal conditioner to the surface with a cotton swab and remove with one stroke of clean tissue,
- Clean fingers with Neutralizer and cotton applicator,
- After applying the Neutralizer to the surface with cotton, remove it with one stroke of clean tissue.

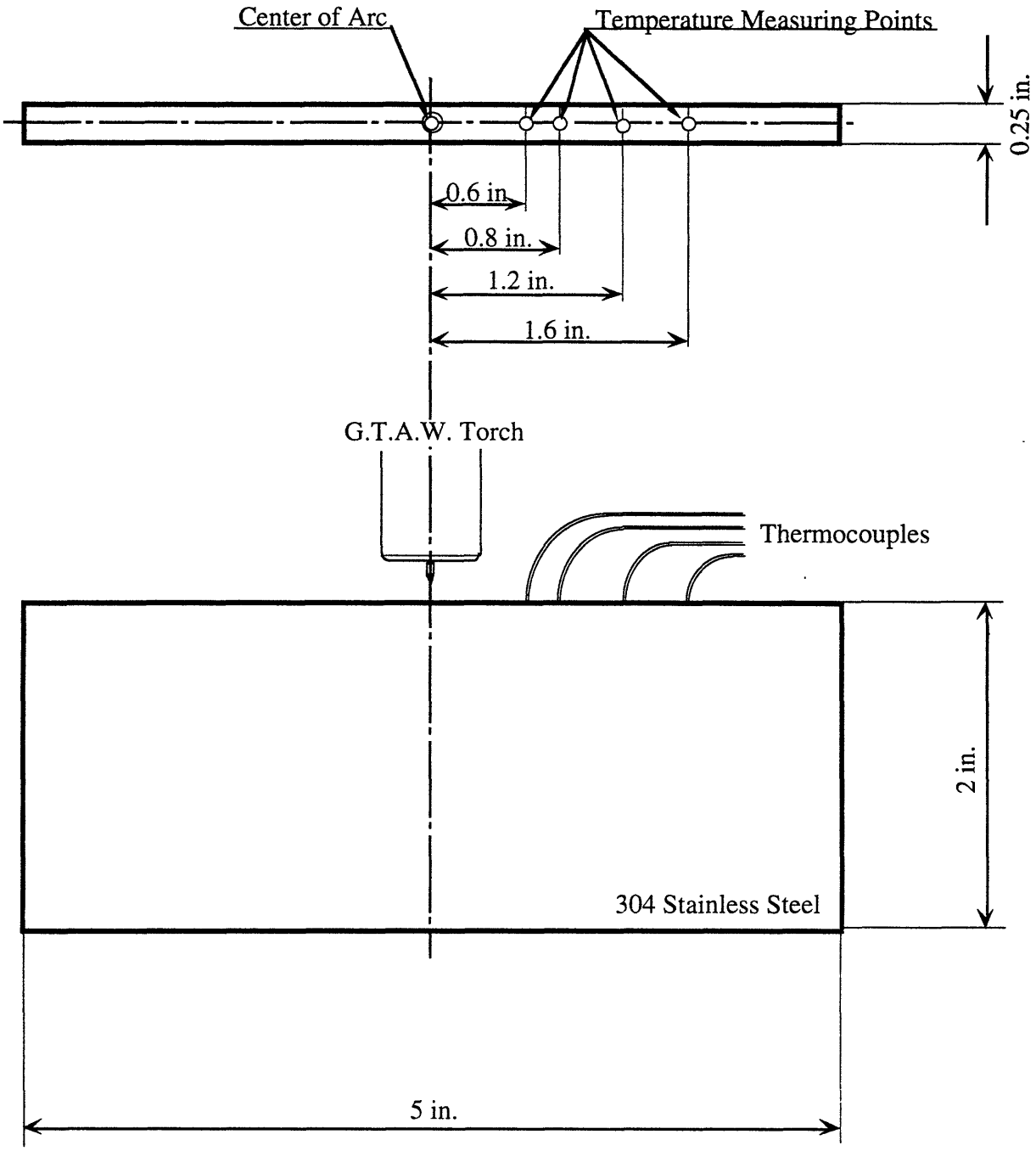

Figure 3.9 Experimental setup for plane specimens and location of thermocouples

3.5.3.2.2 Displacement Measurements with Laser Sensors

The transient displacement of plate due to welding was measured at four locations during and after welding. Four laser sensors were placed on the top and bottom surfaces of the plate as shown in Figure 3.10. Controllers were connected to the 16 channel, 12 bit A/D board installed on a 486 PC compatible microcomputer through a converter box. However, only four out of 16 channels were utilized for this specific experiment. The data was stored in a file as volts by a custom written C code.

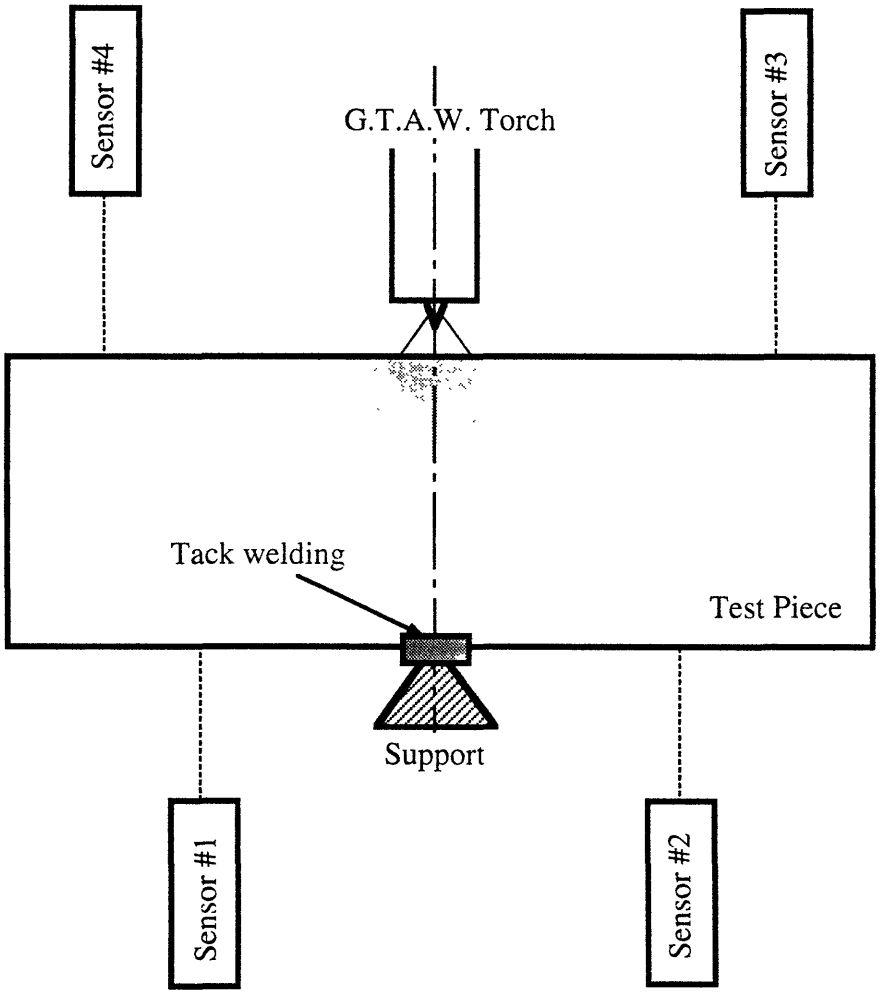

Figure 3.10 Experimental setup for plane specimens and locations of laser displacement sensors

The transient vertical displacement of the beam model is measured in the same way with five different laser sensors. One of the sensors was used to check the symmetry of the system. The contact surface between the welding arc and laser beams was covered with a black metal piece because it is well known that the brightness of the arc in G.T.A.W. is the one of the strongest among welding arcs. Therefore, in the experiment, special attention was paid the keep the welding arc as isolated as possible from the laser beams.

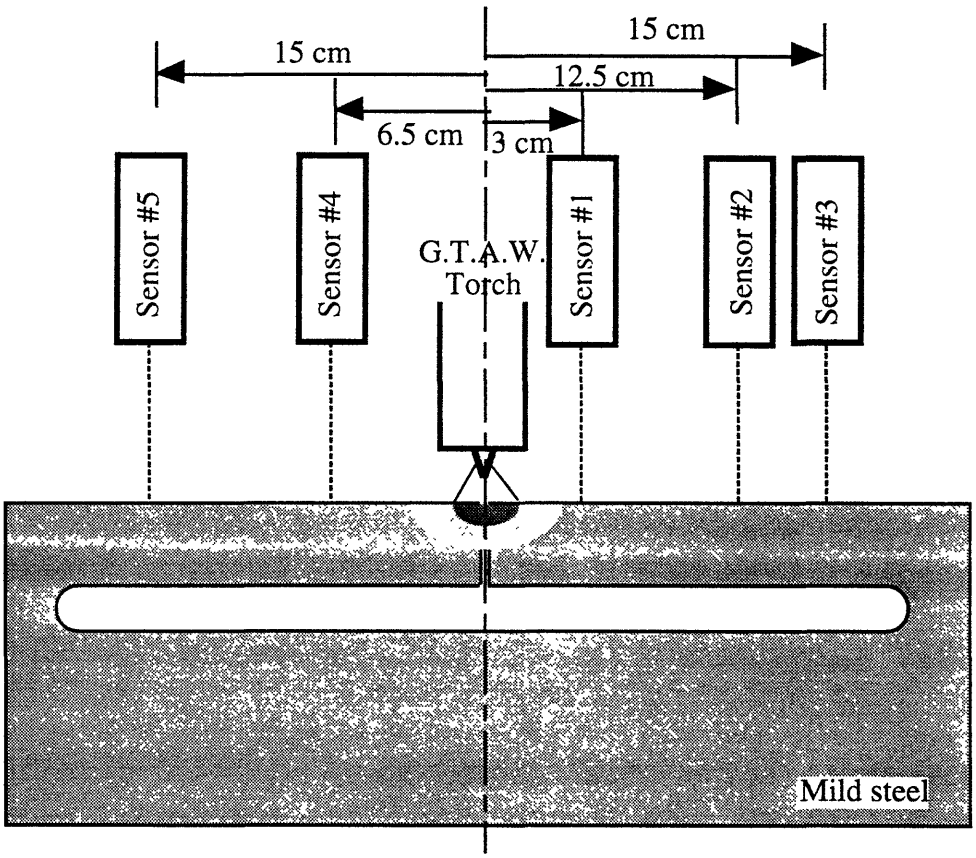

Figure 3.11 Experimental setup for the beam model and locations of laser displacement sensors

Since the specimen size was large enough there was no need to use tack welds to fix the plate to the bench. Hence, the beam model was assumed to exist in a continuum and there were two cantilever beams siding each other from 1/16" distance. However, the specimen without a slit is a two-sided cantilever beam and bead-on-plate welding condition is applied to the middle of its upper surface.

Figure 3.12 shows the experimental setup for the measurement of transient out-of-plane movement during the butt welding of steel plates. Four laser sensors were used to detect the transient distortion.

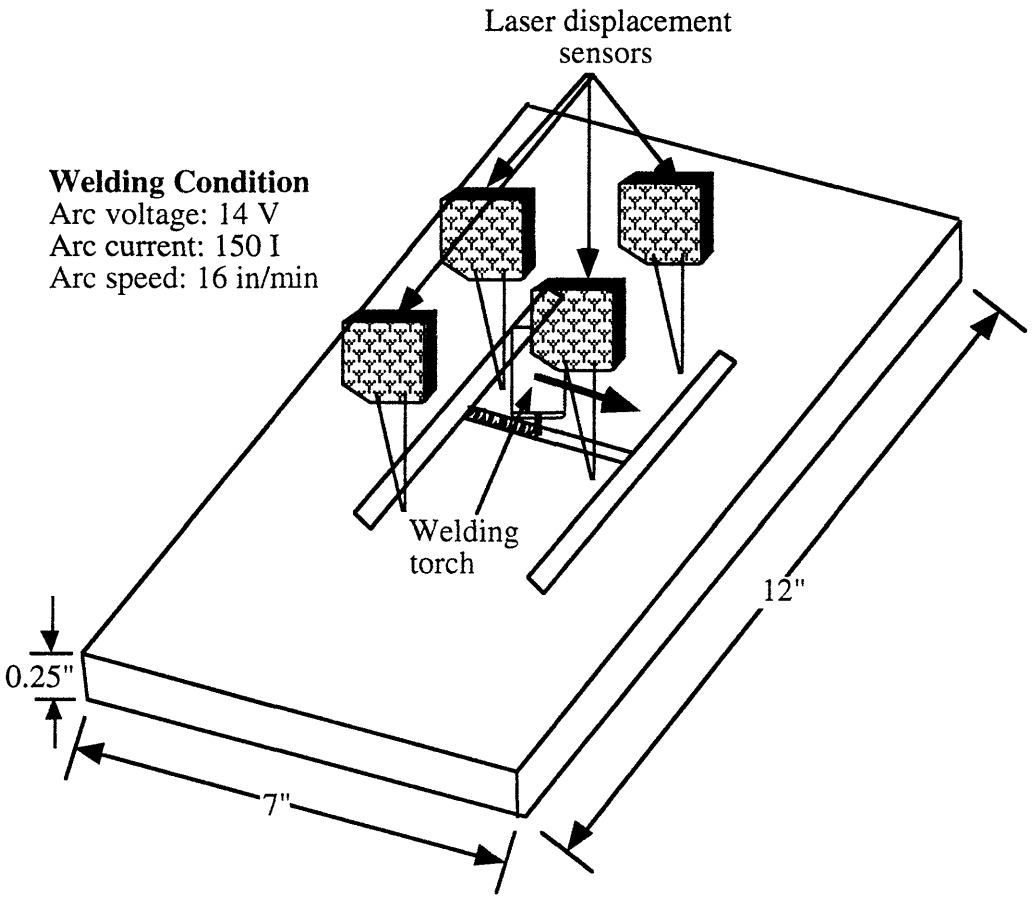

Figure 3.12 Experimental setup for measurement of transient movements during butt welding of steel plates

3.6 Experimental Results

3.6.1 Results of Fiber-Optic Fixture Model (Cylindrical Geometry)

The individual displacement measurements of each component of the system are presented in the following subsections. After the explanation of the tendency of the system to deform, experimental results are shown.

3.6.1.1 Deformation of the Tube

The structure of the system consists of two main parts. In this part of the research, the tube deformation or displacement was controlled and reduced. The second part is concerned with the washer which is responsible for the displacement of the tube. The individual and combined interaction of these two parts to each other are outlined in the following paragraphs.

3.6.1.1.1 Displacement Tendency of the Tube

In the experiment, as mentioned before, the tube was combined with washers of various shapes. All through our welding trials, however, the tube showed an unchanged tendency in its displacement behavior. A typical transient vertical displacement history of the tube observed in the experiment is illustrated in Figure 3.13.

In the first welding pass, as drawn with a solid line in the figure, the tube moves upward while the welding arc is turned on. Immediately after the arc is turned off the tube starts to move downward. The speed of its downward movement decreases with time, and finally the amount of the displacement approaches a certain value, *Df*. The tube also showed a similar displacement behavior in the second welding pass. However, *Df* of the second welding pass

(dashed line in the figure) was much smaller than that of the first pass. Moreover, in the second pass, the washer and the tube moved together and there was no relative motion between the washer and tube.

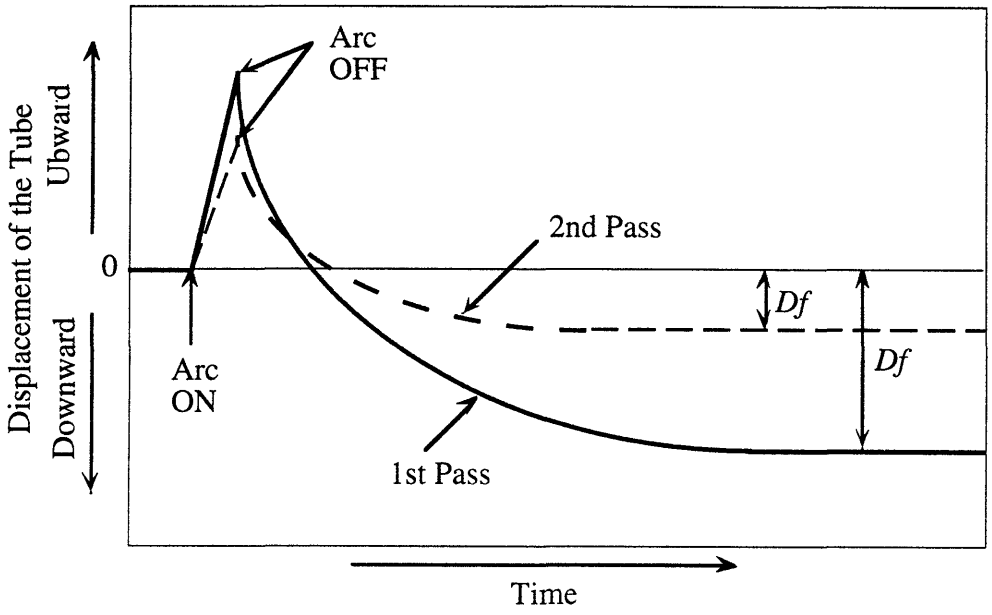

Figure 3.13 Schematic drawing of the tube displacement during the welding process

In the actual laser welding process, this part of the experiment was conducted under contract to AT&T Bell Laboratories. According to their specifications, *Df* had to be minimized in order to perform the required increase in the efficiency of data transmission from the fiber optic to the micro-chip in the laser package. In the following section, therefore, the decrease in *Df* in the first welding pass was diligently observed, by varying several conditions including the configuration of the washer and fixing the strength of the tube to the test bench by using a couple of embedded screws in the welded plate.

3.6.1.2 Experiments on Stainless Steel

3.6.1.2.1 Effect of the Thickness of the Washer on Df

Four different thickness sizes of flat-type washers were used in the experiment. The history of the tube displacement during the welding process in each thickness of the washer is shown in Figures 3.14, 3.15, 3.16, and 3.17. Regardless of the thickness of the washer, the displacement of the tube shows the same tendency as mentioned before.

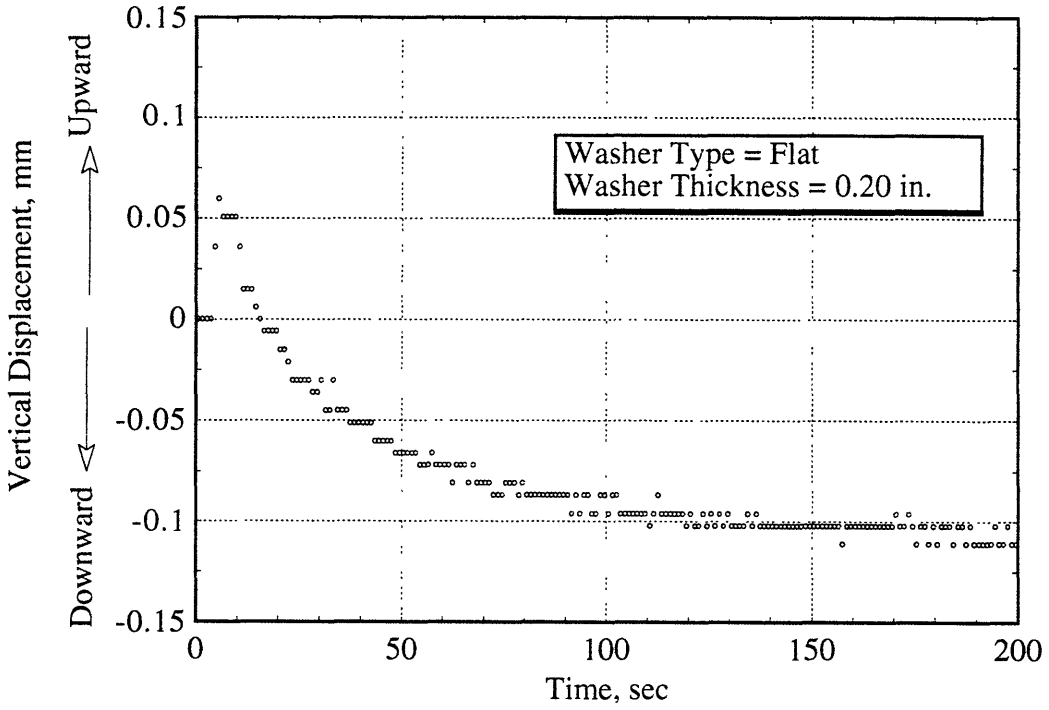

Figure 3.14 Displacement history of the tube with a washer thickness of 0.20"

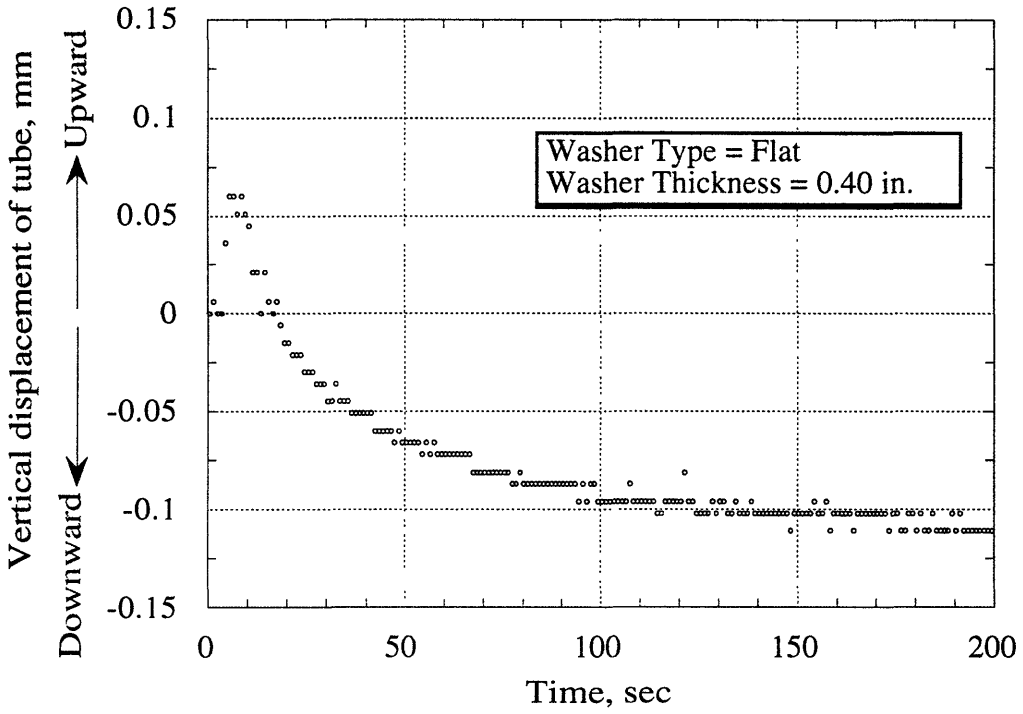

Figure 3.15 Displacement history of the tube with a washer thickness of 0.40 "

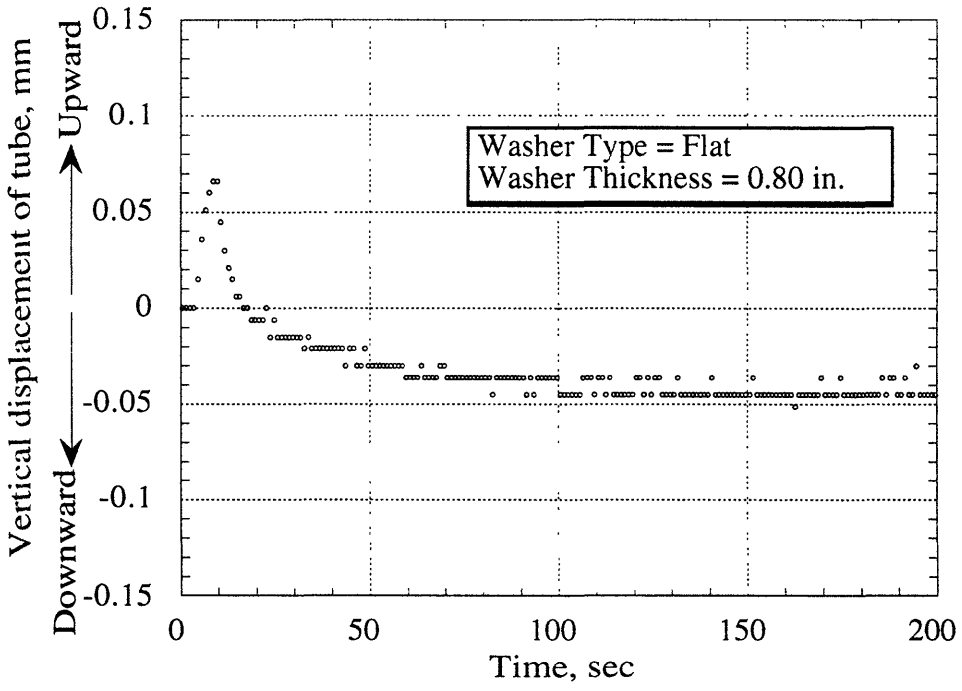

Figure 3.16 Displacement history of the tube with a washer thickness of 0.80 "

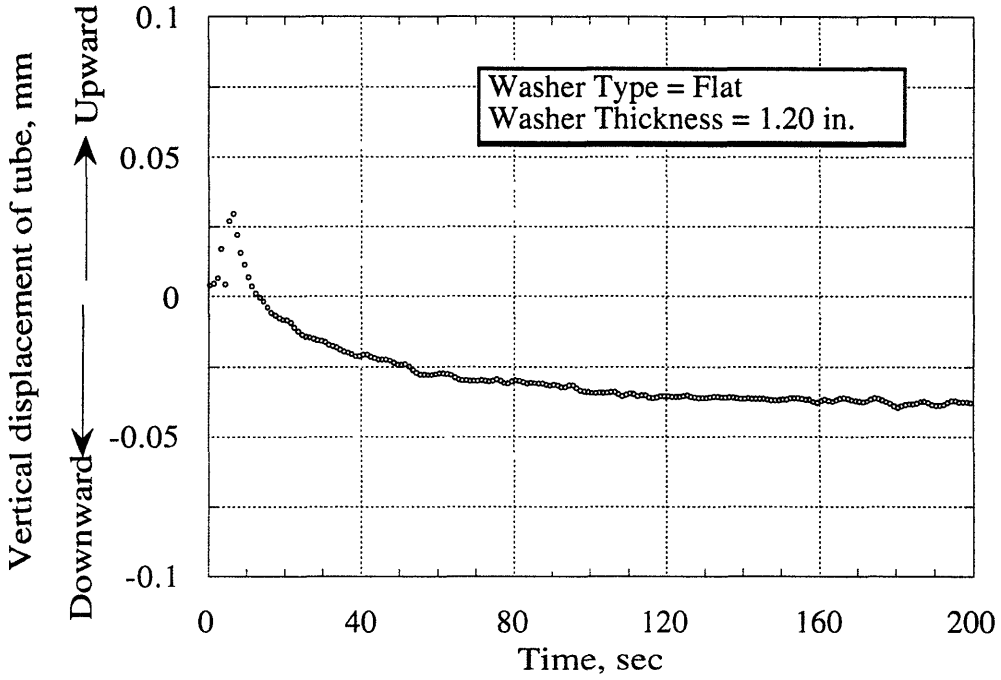

Figure 3.17 Displacement history of the tube with a washer thickness of 1.20"

On the other hand, *Df* decreases noticeably as the thickness of the washer increases. Figure 3.18 shows the relation between *Df* and the thickness of the washer. From the figure, the *Df* for the 1.20" thick washer is approximately one fourth of *Df* for the 0.20" thick washer. It can be said, therefore, that the increased rigidity of the washer makes the displacement of the tube smaller. However, the decrease rate of *Df* becomes smaller as the thickness of the washer increases. *Df* approaches to approximately 40 μm, where the thickness of the washer is over an inch.

3.6.1.2.2 Effect of the Projection on the Movement of Washer

In this part of the experiment, the step-type test washer as shown in Figure 3.2 (b) was used. A small projection on the washer was expected to decrease the thermal deformation of the

washer, because the projection absorbs the heat and melts before it deforms. Therefore a part of the heat transferred from the arc is being dumped to the environment and used for melting the piece of metal. Moreover, the rest of the washer is subjected to a smaller amount of heat.

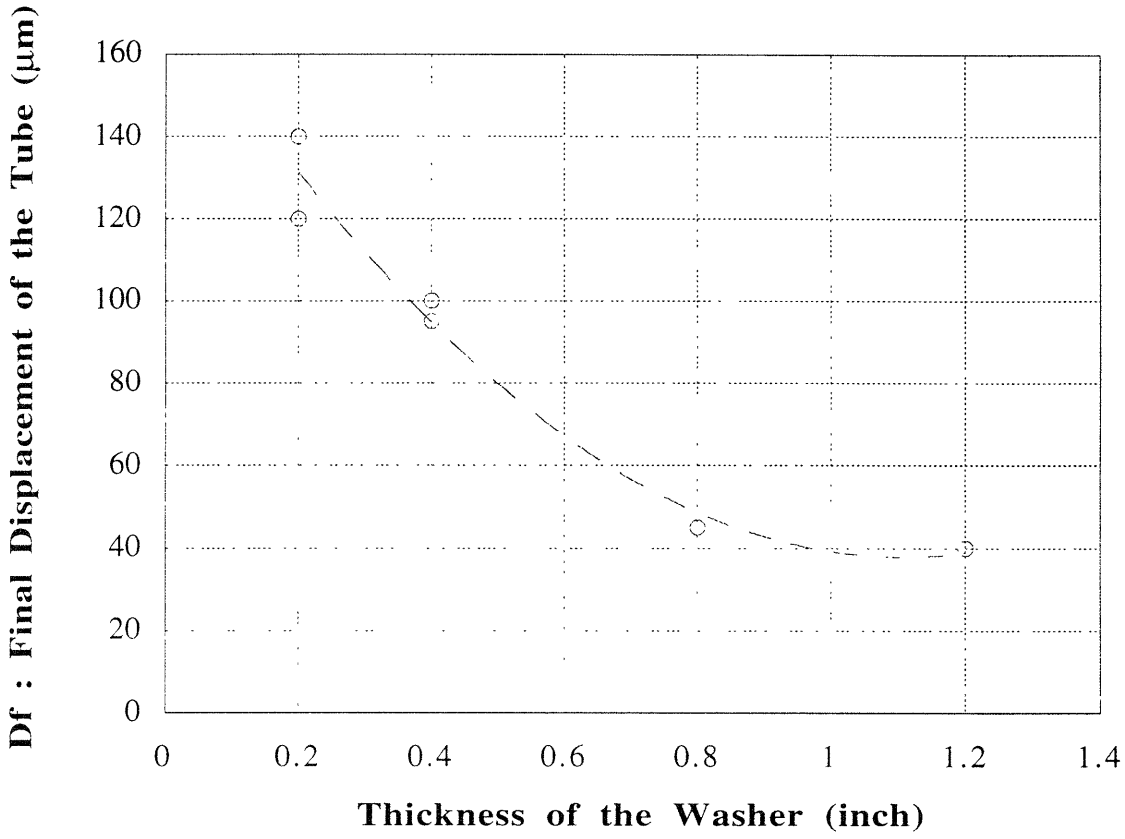

Figure 3.18 Relation between Df and the thickness of the washer

Figure 3.19 shows a history of the tube displacement for the step-type washer. The result of the flat type washer of the same thickness is also indicated with a dashed line. Both curves show the same manner of sequential displacement. However, it should be noted that in the case of the step-type washer, *Df* is approximately half as much as the flat-type washer.

Consequently, the small projection on the washer was found to be effective in reducing the displacement of the tube.

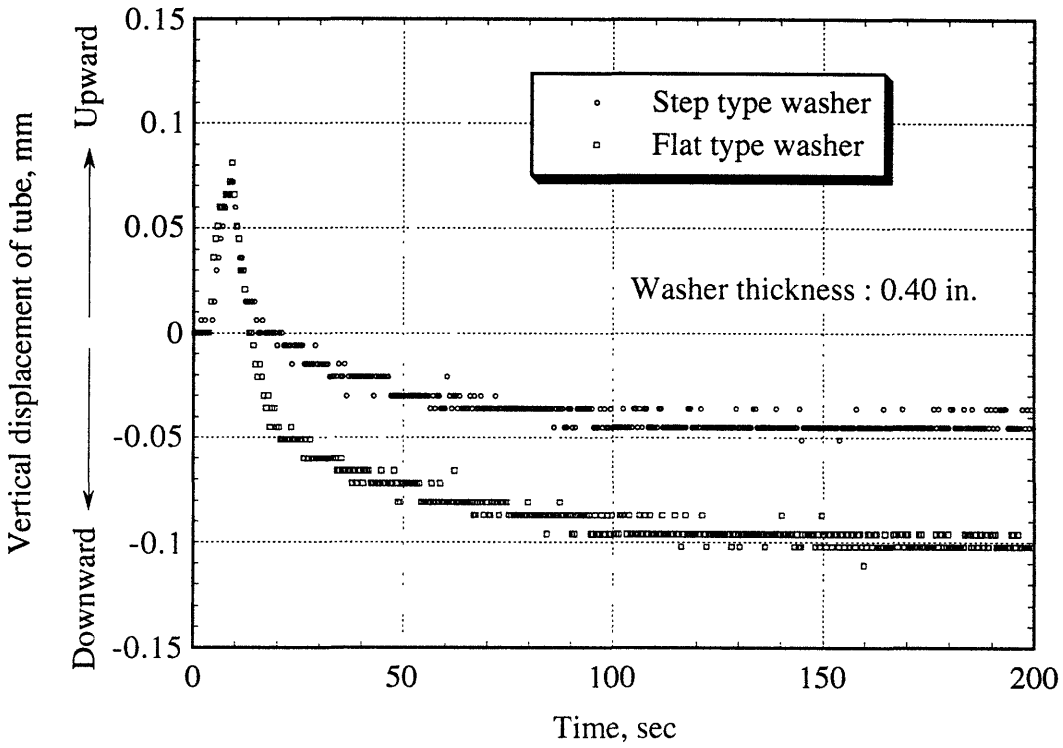

Figure 3.19 Displacement of the tube with two different types of washer

3.6.1.2.3 Effect of the Fixing Strength on the Movement of Tube

As mentioned in 3.5, the tube was attached with a couple of screws to the test bench prior to the welding trial. In order to understand the effect of the fixture of the tube on its vertical motion, the tightening strength of the screws into two levels was varied as follows,

- Tight *Fix*: Tightening the screw strongly with a hexagonal wrench
  (All the experiments mentioned above were done in the same way)
- Loose *Fix*: Loosening the screw until it is just enough to hold the tube

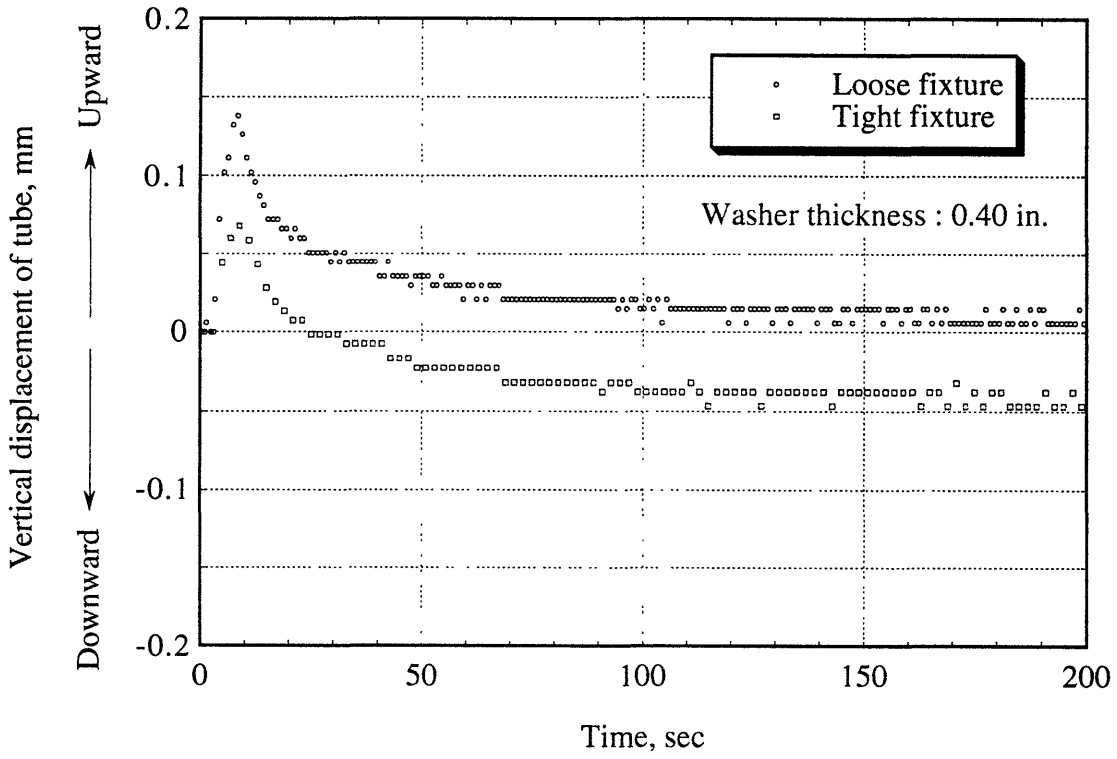

Figure 3.20 Displacement history of tube with different restraints

Figure 3.20 shows the comparison of the tube displacement behaviors between the *Tight Fix* case and the *Loose Fix* case. During welding, the difference of the upward displacement between these two cases is remarkable. This can be seen easily in Figure 3.20. In the case of *Loose Fix*, the tube is raised much higher than the *Tight Fix* case. Moreover, during the cooling stage the tube returns almost to its initial location. Hence, it was concluded that the displacement of the tube could be reduced sharply by making the tube free from the fixture in the vertical motion.

3.6.1.2.4 Deformation of the Washer

The displacement of the bottom surface of the washer was measured with the laser displacement sensor. An example of the measured displacement history is shown in Figure 3.21. As shown in the figure, the bottom surface of the washer moves upward while the welding arc is turned on, and comes down after the arc is turned off. Then it gradually returns to its initial position. Speaking qualitatively, the motion of the bottom surface of the washer is similar to the motion of the tube, but the amount of the upward displacement of the washer while the arc is turned on, is much smaller than that of the tube.

To determine the actual deformation behavior of the washer that directly influences the tube displacement, the top surface of the washer should be measured, because the tube is welded to the upper part of the washer. It was, however, difficult to measure the displacement of the top surface of the washer, due to an existence of the welding arc that disturbed the laser sensor by its strong light. Therefore, all the measurements were performed on the bottom surfaces of tube and the washer.

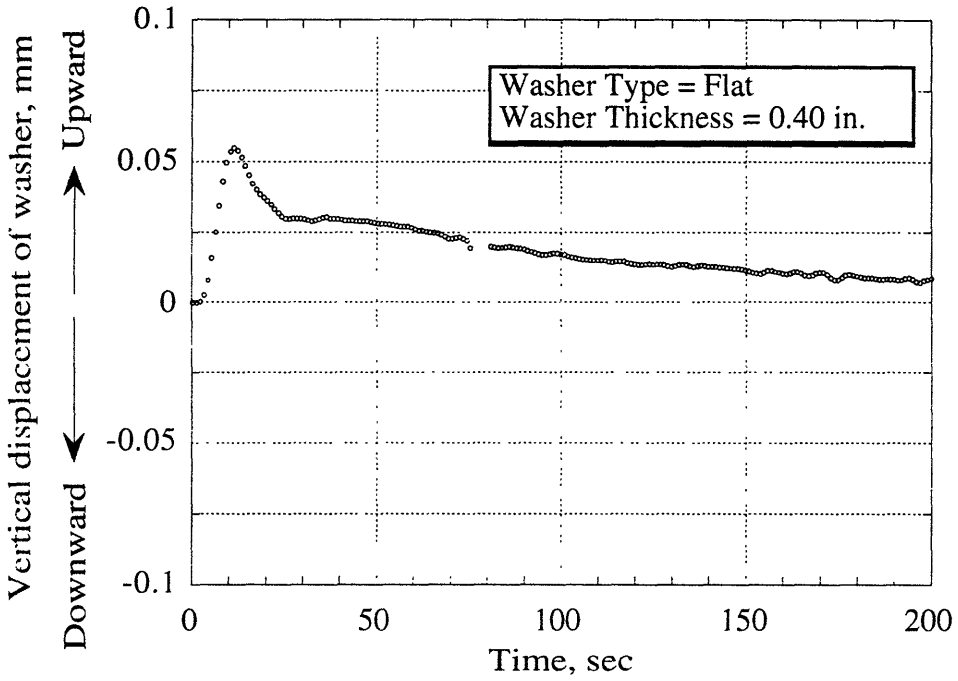

Figure 3.21 Displacement history of the washer

3.6.1.2.5 Effect of the Clearance between the Tube and Washer on Displacement of Tube

This section describes the results of experiments to clarify the influence of the gap the tube and the washer. In the experiments, loosely fitted test washers and tubes were used, and results were compared with the data of the tightly fitted test pieces. Center holes of washers were carefully machined so that the gap between the tube and the washer was controlled from 0.008" to 0.010" (In previous experiments, the gap was controlled within 0.005".)

Figure 3.22 shows the vertical displacement histories of the tube with flat-type test washers during welding. In the figure, three curves, each of which shows the data with the test washer of 0.20, 0.40 and 0.80 inch thicknesses respectively, are drawn.

All curves show the same tendency. While the welding arc was turned on, unlike the previous experiment (washers and tubes fit each other tightly), the tube did not move up as much as before. Immediately after the arc was turned off, the tube started to move down and finally the displacement of the tube approached a certain amount. The amount of the final displacement of the tube, *Df*, changed with the thickness of the test washer. *Df* decreased by using a thicker washer. Here, it should be noted that the *Df* with the loosely fitted tube and washer combination is much larger than the Df with the tightly fitted combinations (obtained in the previous experiment; see Figure 3.24.)

Test results with a step-type washer are shown in Figure 3.26. The displacement history of the tube showed the same tendency, as with flat-type washers. However, *Df* with a step-type washer was much less than *Df* with flat-type washer of the same thickness (0.40 inch).

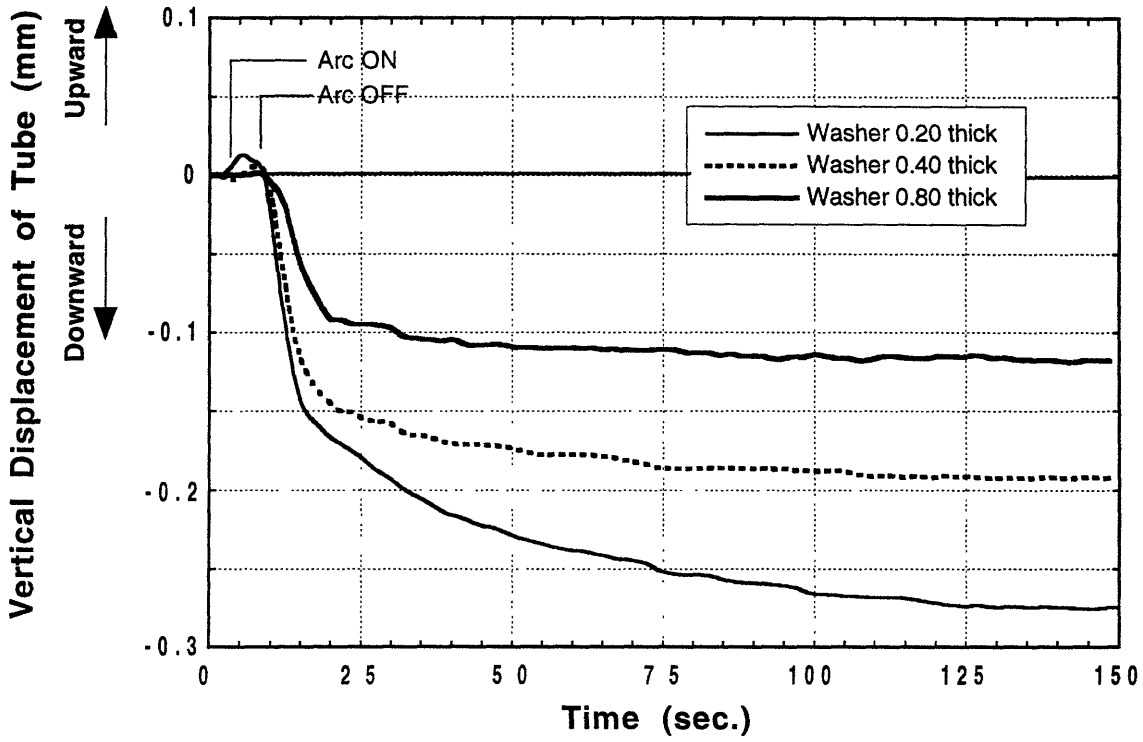

Figure 3.22 Displacement history of the tube for larger clearance

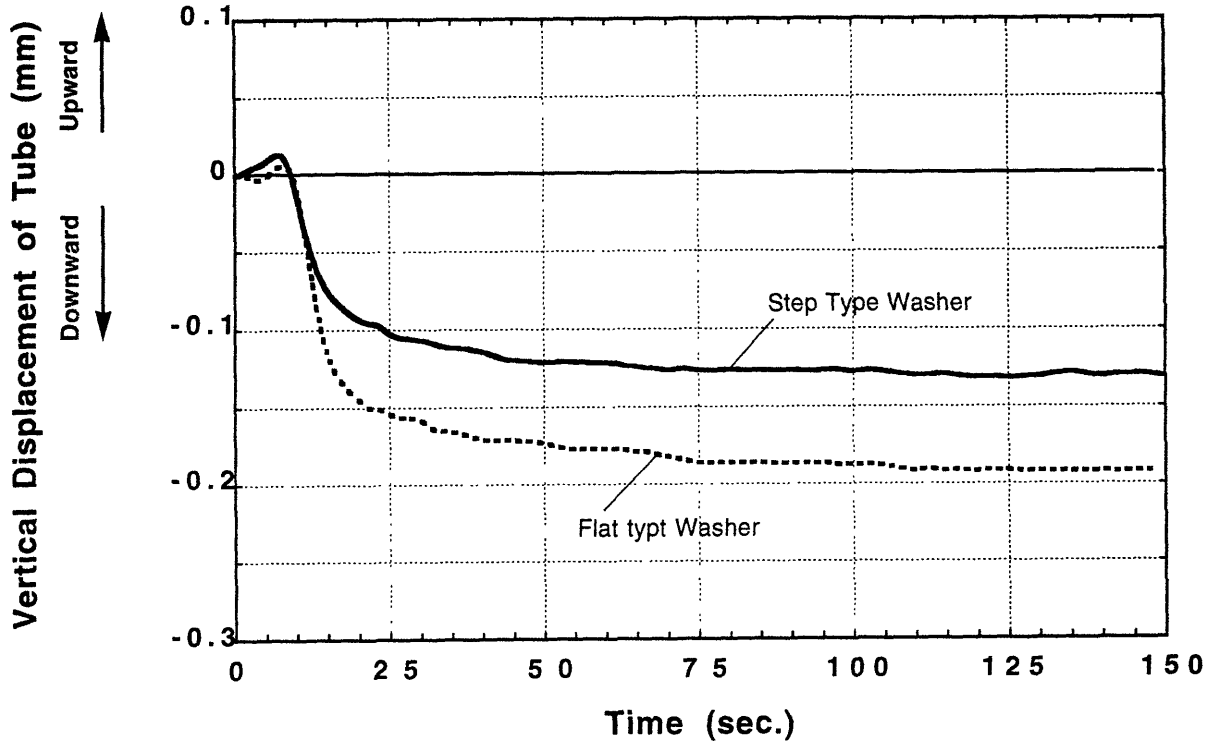

Figure 3.23 Displacement history of the tube for different shapes at a larger clearance

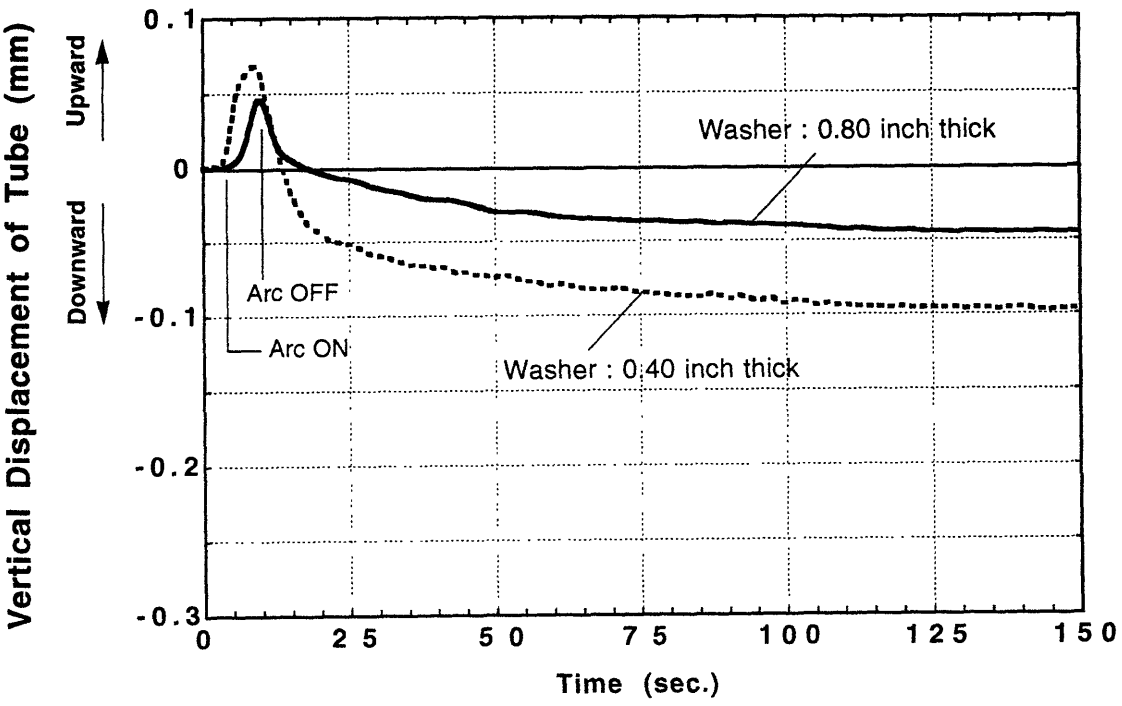

Figure 3.24 Displacement history of the tube for tight clearance

3.6.1.3 Kovar Experiments

3.6.1.3.1 Displacement of the Tube with Loosely Fitted Washer

Figure 3.25 shows the vertical displacement histories of test tubes loosely fitted with flat type test washers during welding. In the figure, three curves, showing the data with test washers of 0.20, 0.40 and 0.80 inches thickness, are shown respectively. Figure 3.26 shows results obtained from experiments performed previously under the same condition using the 304 stainless steel.

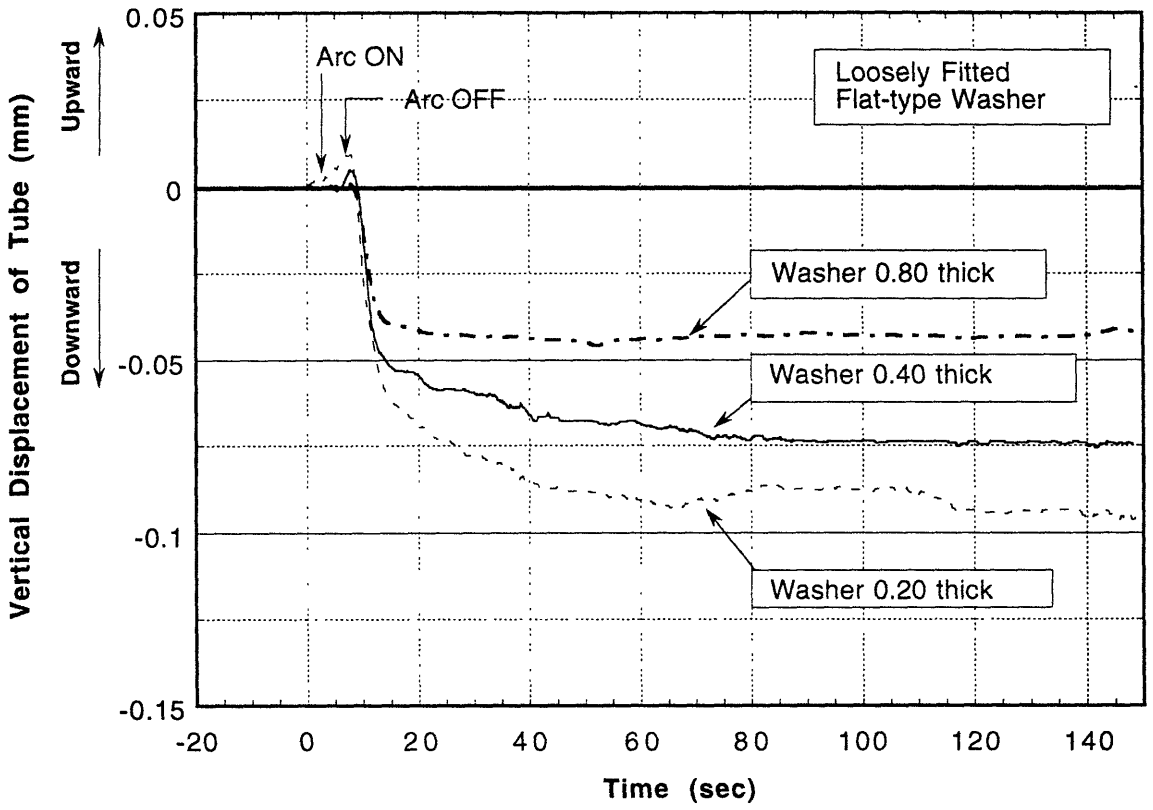

Figure 3.25 Displacement history of the tube at various washer thicknesses of kovar

When comparing Figure 3.25 and Figure 3.26, first it is obvious that the amount of the displacement of the kovar specimen is much smaller than that of the stainless steel. Second, as the most important result, the displacement history of test tubes of kovar showed exactly the same tendency as stainless steel. While the welding arc was turned on, the tube was pushed up a little, and after the arc was switched off, it went down rapidly below its initial level. Finally, the amount of the displacement of the tube approached a certain value. This permanent displacement of the tube decreased as the thickness of the test washer increased.

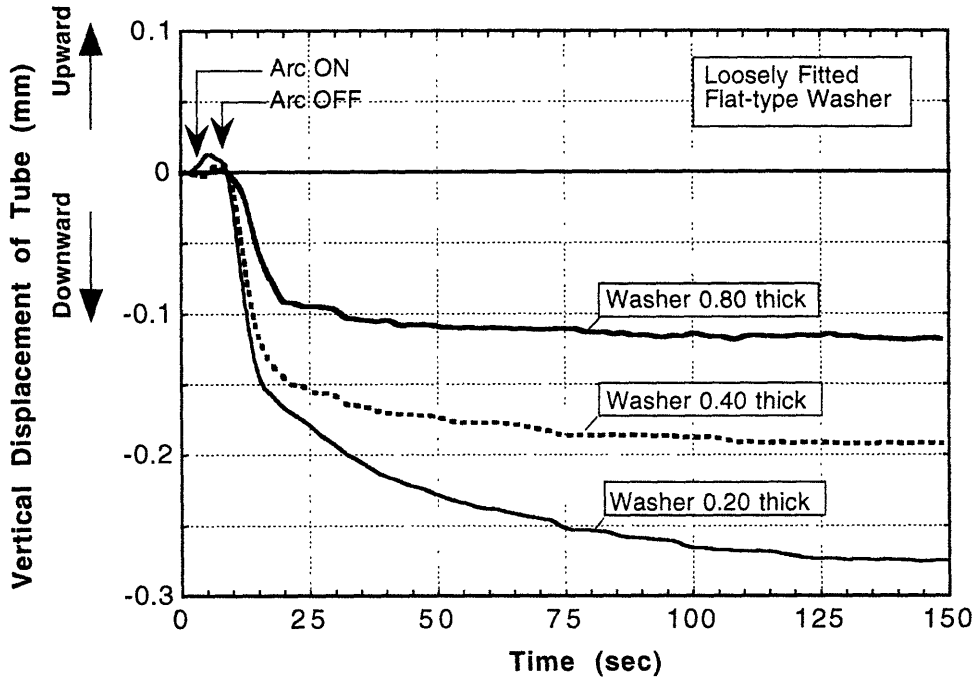

Figure 3.26 Displacement history of the tube at various washer thicknesses of stainless steel

3.6.1.3.2 Displacement of the Tube with Tightly Fitted Washer

Fig. 3.27 shows the vertical displacement history of test tubes tightly fitted with test washers. In the figure, two curves are shown, each of which illustrates the data for test washers of 0.20 and 0.40 inch thickness respectively.

Unlike results obtained from a loosely fitted combination of tubes and washers, tubes followed the upward movement of the washer while the arc was turned on in this experiment. The final displacements of tubes, therefore, were much smaller than those shown in the loosely fitted combinations of tubes and washers. The use of the thicker washer (0.40 inch thick) resulted in a smaller vertical displacement of the tube.

Figure 3.28 shows the difference between the tightly and loosely fitted washer tube configuration. It is very clear that the tube could not follow the upward motion of the washer but it had to move together with the washer after the weld froze. This caused a large residual distortion although the washer only came back to its initial state.

3.6.1.3.3 Effect of the Projection on the Washer on the Displacement of Tube

Figure 3.29 shows the vertical displacement history of the tube with a step-type washer of 0.40 inch thickness. A curve which shows the result obtained with a flat-type washer of the same thickness is also shown in the figure for comparison. As shown in the figure, the final displacement of the tube with the step-type washer was much smaller than that of the one with the flat-type washer of the same thickness.

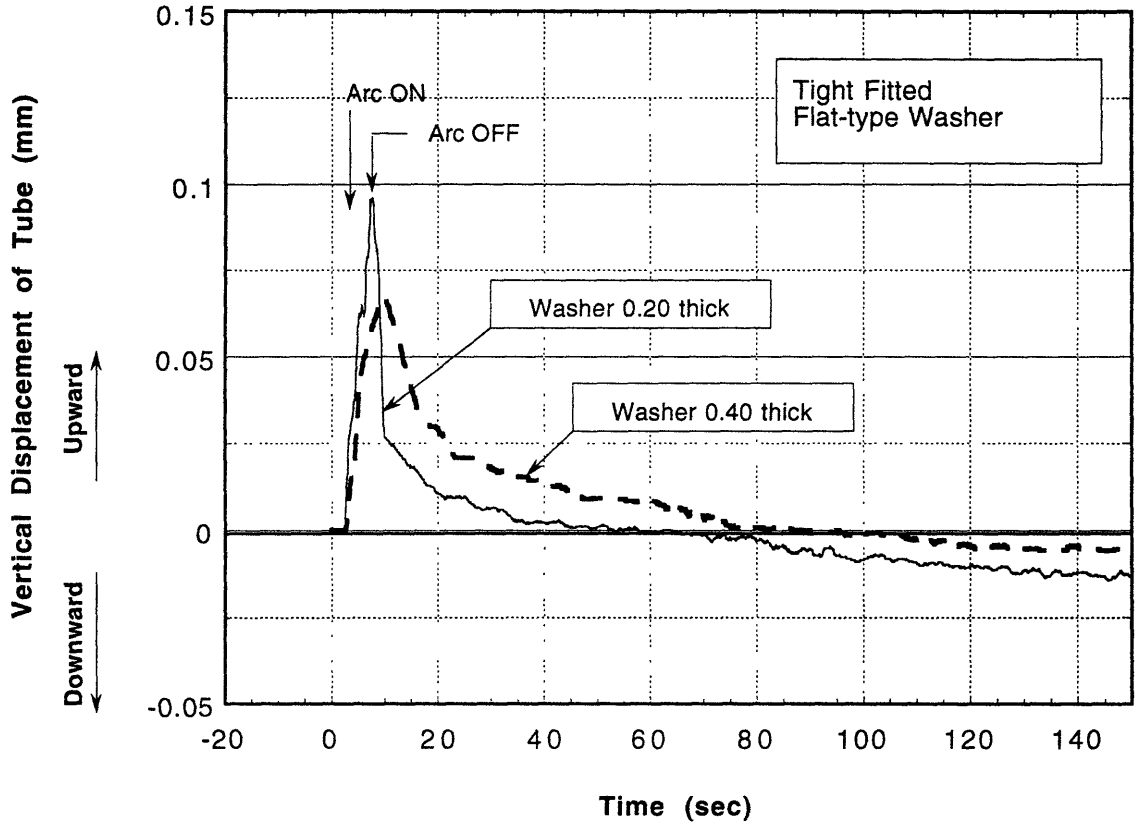

Figure 3.27 History of the displacement of the tube at a tightly fitted configuration

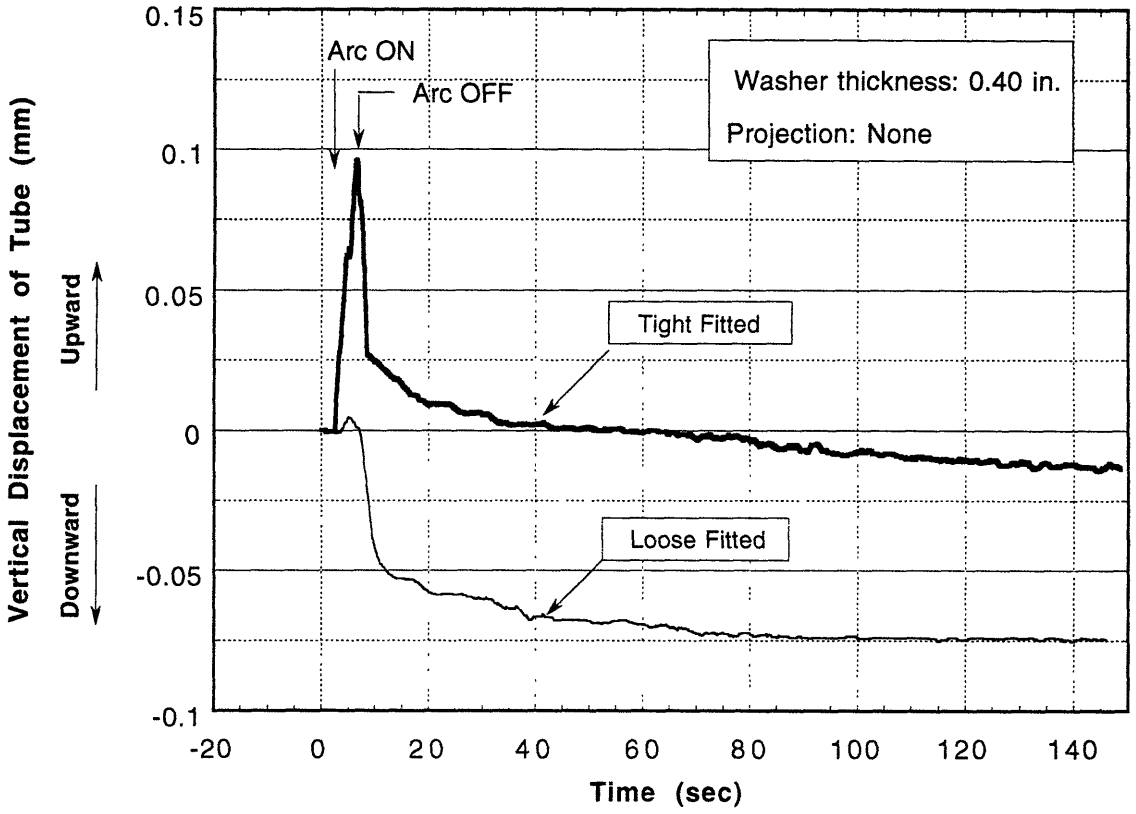

Figure 3.28 History of the displacement of the tube at a tightly and loosely fitted configuration

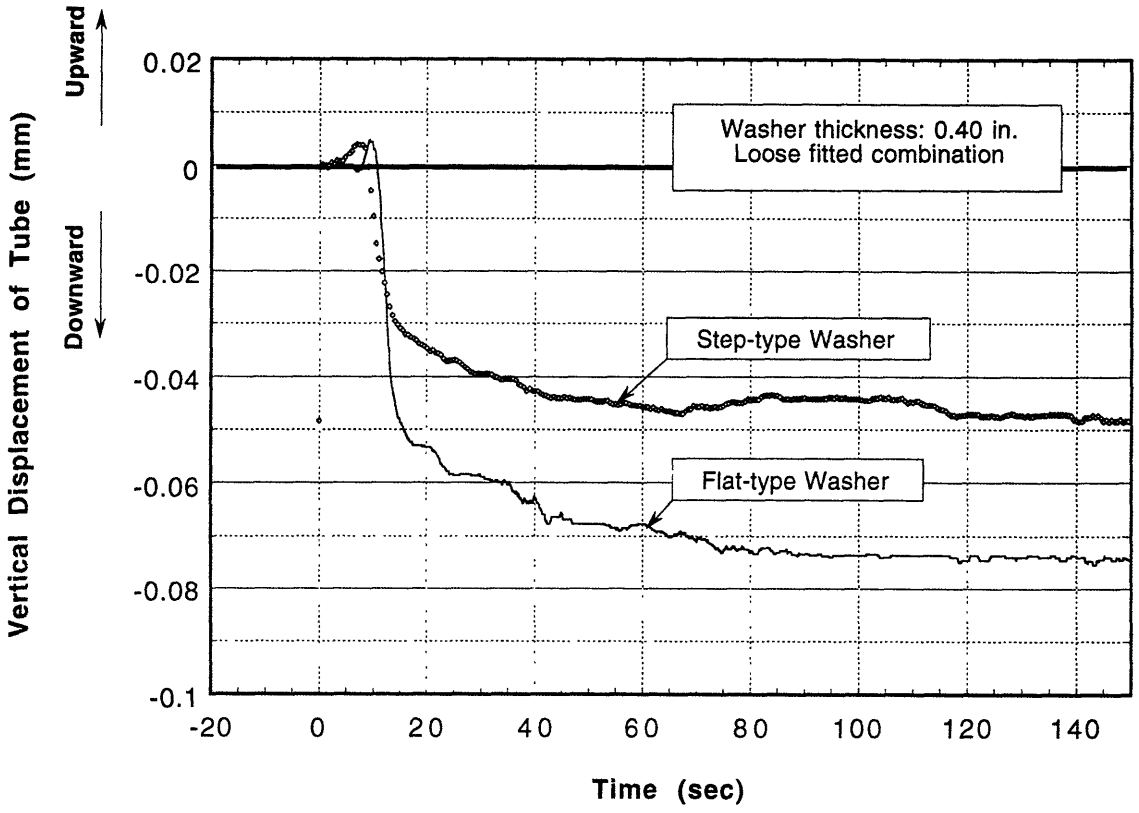

Figure 3.29 Displacement history of the tubes with different shapes

3.6.2 Results of Plane Plate

3.6.2.1 Plate Model

During welding time, 5 sec., the upper surface of the plate is heated more than the lower edge of the plate. Therefore, the heated area tends to expand. As a result of this, since the plate is fixed in the middle of the lower edge, the plate starts to bend and the points away from the weld line move downward as shown in Figures 3.30 and 3.31. However, in the regions near the weld, when the metal tries to expand it is restrained by the surrounding metals at lower temperatures.

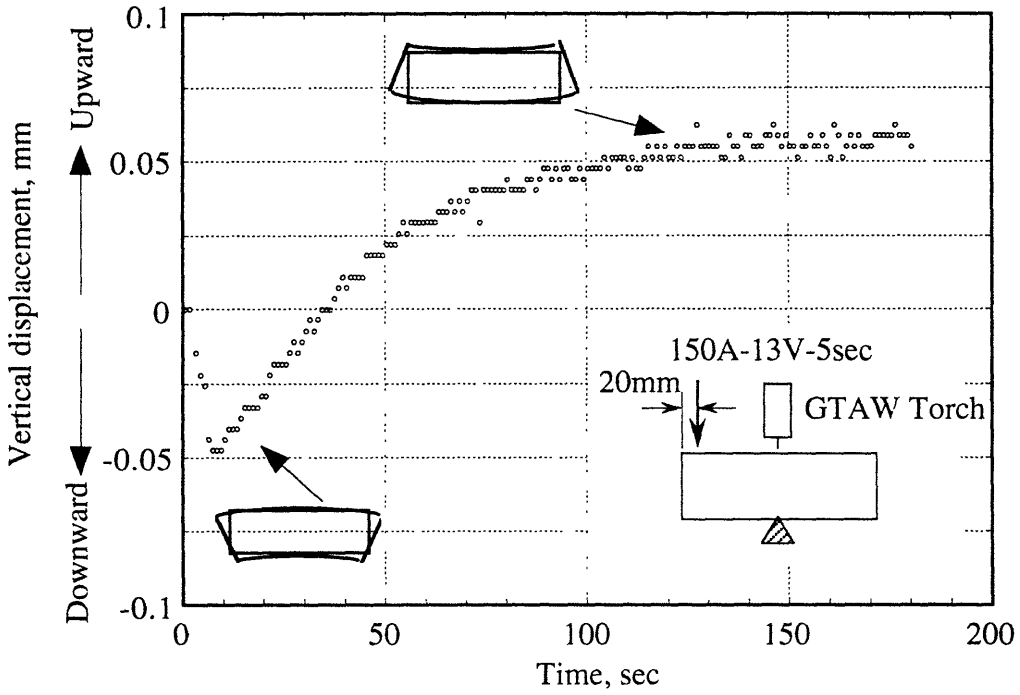

Figure 3.30 Transient deformation of plate during and after welding measured at the upper surface

Consequently, under this restraint and lower yield stress due to temperature, the region near the weld yields plastically. Moreover, compressive stresses and compressive plastic strains develop in this region. After welding is finished, the cooling stage starts. At this stage, the plate starts to bend in the opposite direction, that is, upward. This point corresponds with the minimum in Figures 3.30 and 3.31. If the system was totally elastic, the plate would stop when it reached the initial position. However, this does not take place due to the existence of compressive plastic strains, as can be clearly seen by the figures. Plates continue to bend in the opposite direction and finally approach a certain residual value. This value is the final distortion of the plate due to welding.

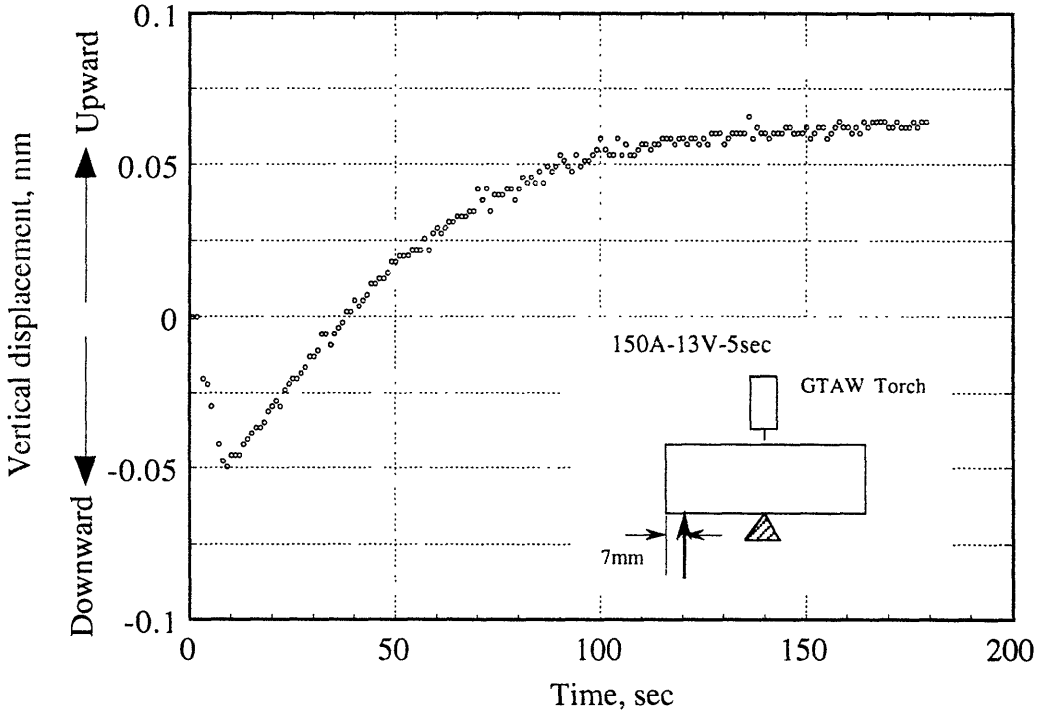

Figure 3.31 Transient deformation of the plate during and after welding as measured at the lower surface

In the case of joining two plates, the event that takes place is entirely different. First, let's consider the plate with a slit up to its middle thickness. The same welding condition is applied to this plate as it was to the non-slit specimen. As it is seen in Figures 3.32 and 3.33, the downward deformation and final distortion of the plate in the opposite direction is smaller than the values obtained from the non-slit specimen. The slit, here, enables the upper surface to expand into the direction of the center of the plate. This reduces the downward movement of the plate during the welding period. However, after welding is completed, with the start of the cooling stage, the direction of the motion is reversed, and the plate starts to bend in the opposite direction. The frozen weld, which is at a higher temperature than the rest of the plate, starts to shrink due to its lowered yielding strength during cooling. The system again reaches final distortion after it cools down. However, this value is smaller than the value of the specimen without the slit.

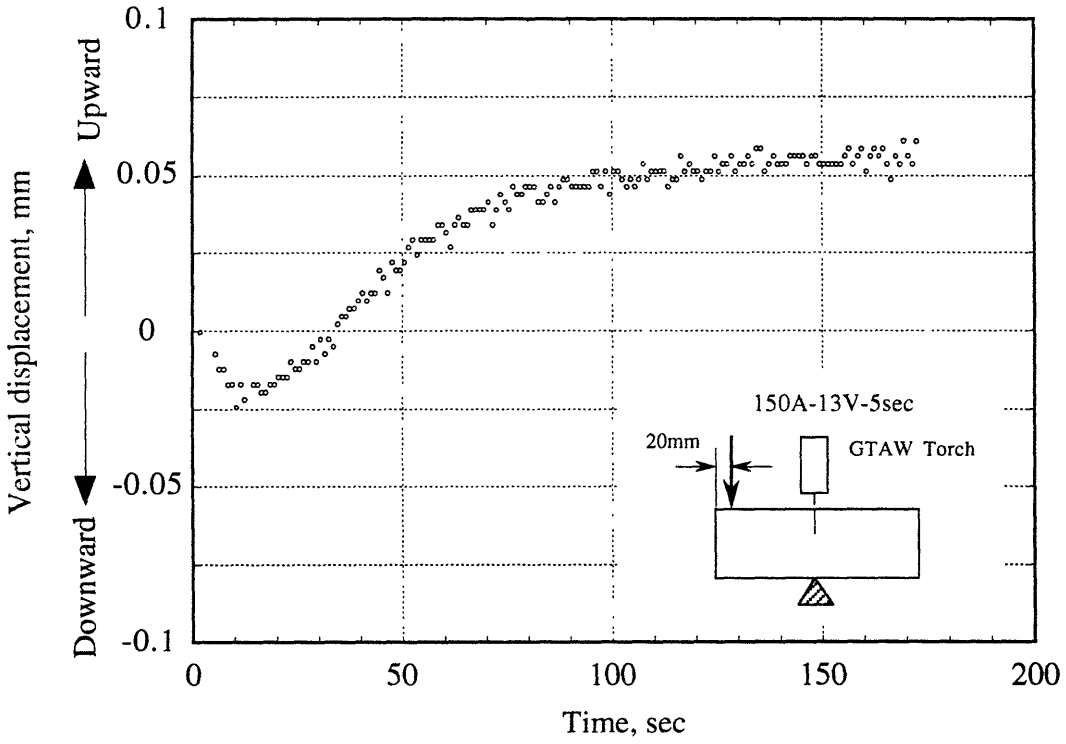

Figure 3.32 Displacement history of the plate with slit at 20 mm on the upper surface

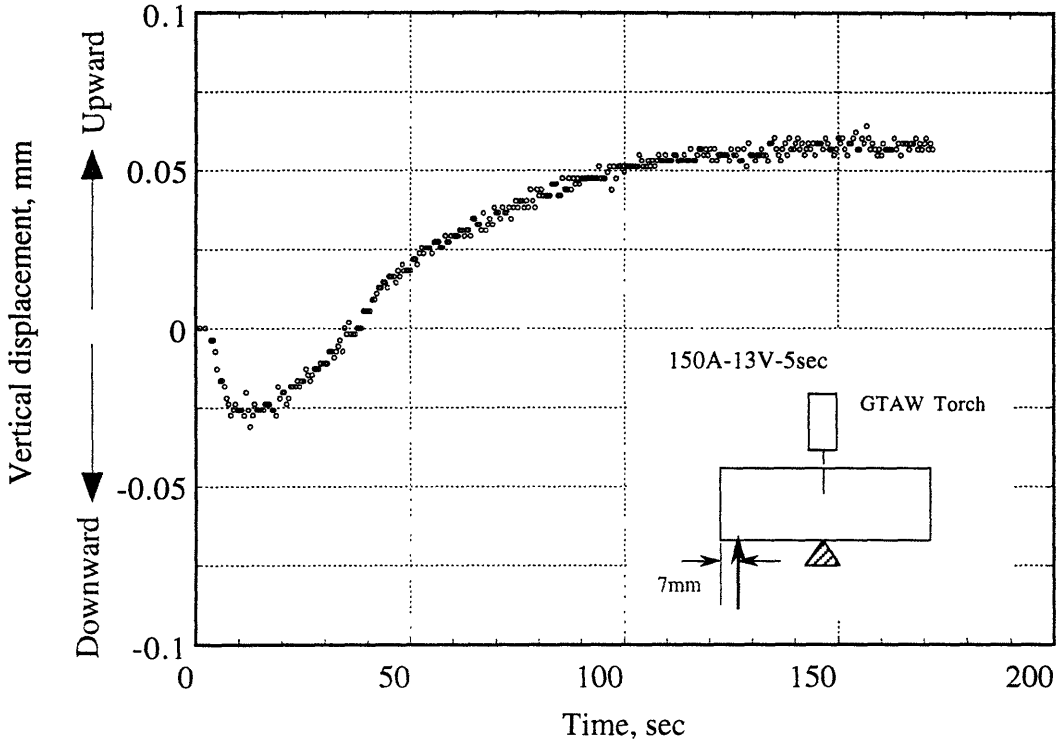

Figure 3.33 Displacement history of the plate with slit at 7 mm on the lower surface

This phenomena is more clearly observed in the welding of two separated pieces and it is covered in the next section. Proper support is required to avoid stress free rigid body motion. Figure 3.34 shows transient displacement of the plate. However, since the plates are not held in place by supports, they distort as if they are twisting on a pivot point. This state is a stress free state, because in this case it does not cause bending stress in the plate. Due to the shrinkage of the weld, plates rotate around the weld point and reach their final position.

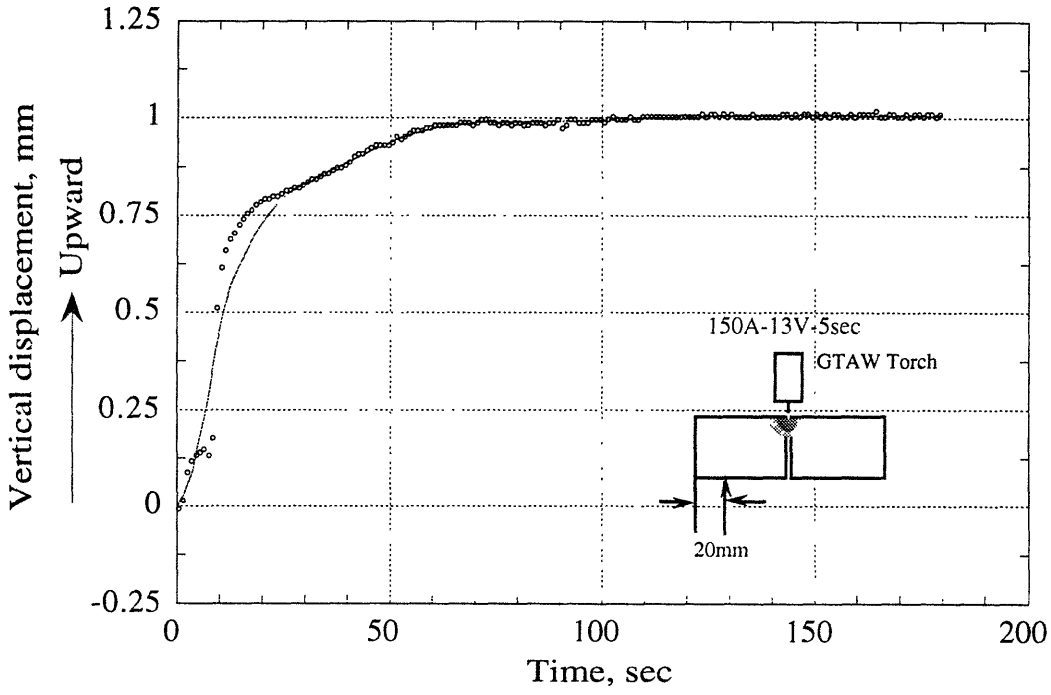

Figure 3.34 Displacement history of the plate for two separate pieces

3.6.2.2 Beam Model

In this set of experiments, the effect of restraint on distortion is investigated. Dimensions of the specimens are given in Figure 3.7. Figure 3.35 shows the different behavior of transient displacement of solid and separate beams during and after welding. While the solid beam bends into a convex shape due to compressive stresses in the region near the weld, the cut beams start to expand freely towards the center of the slit. As soon as joining occurs, the beams start to deform downward due to the temperature gradient in thickness direction. Since no compressive stresses are produced during expansion and welding, the plates reach their final position at a lower location at the end of cooling. This whole phenomena is illustrated in Figures 3.35, 3.36 and 3.37.

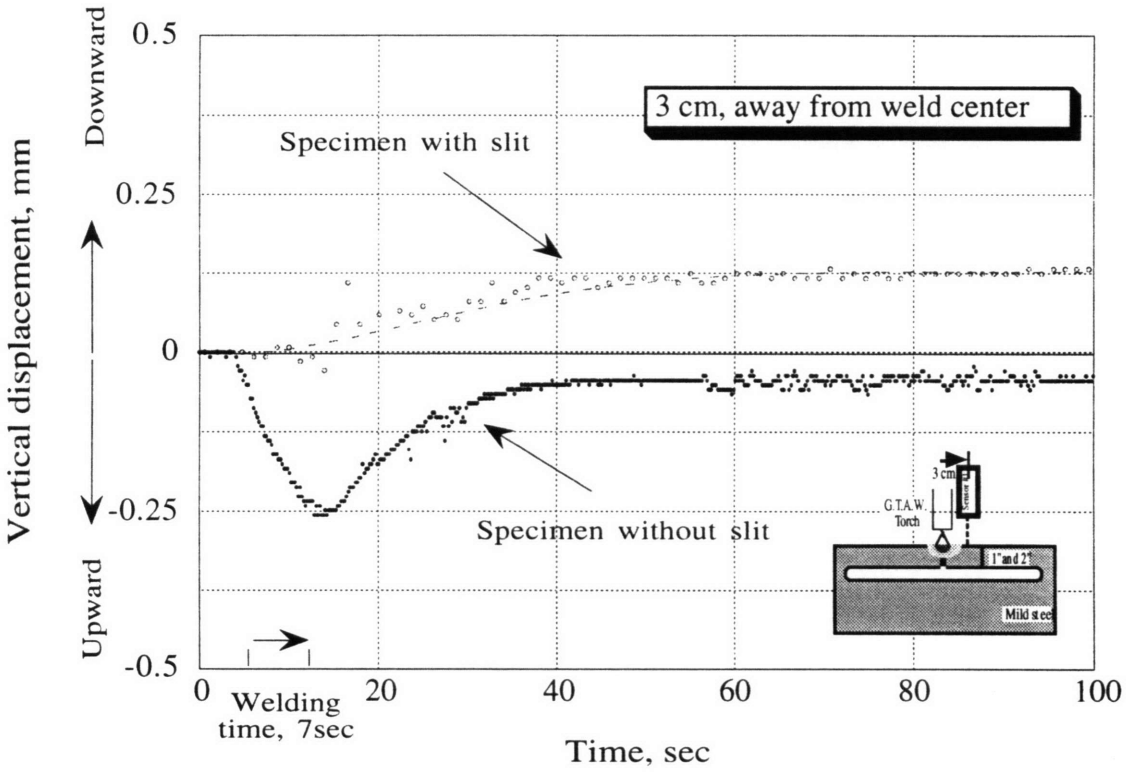

Figure 3.35 Displacement history of the beam with a different shape at 3 cm away from weld center

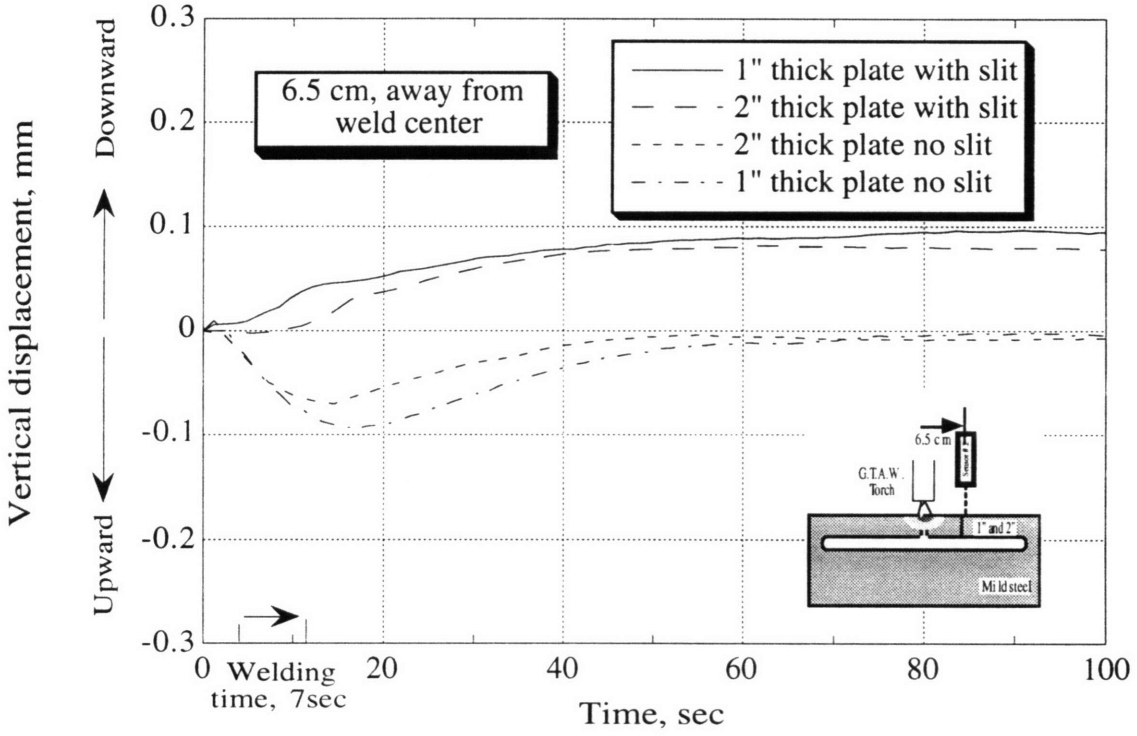

Figure 3.36 Displacement history of the beam with a different shape at 12 cm away from the weld center

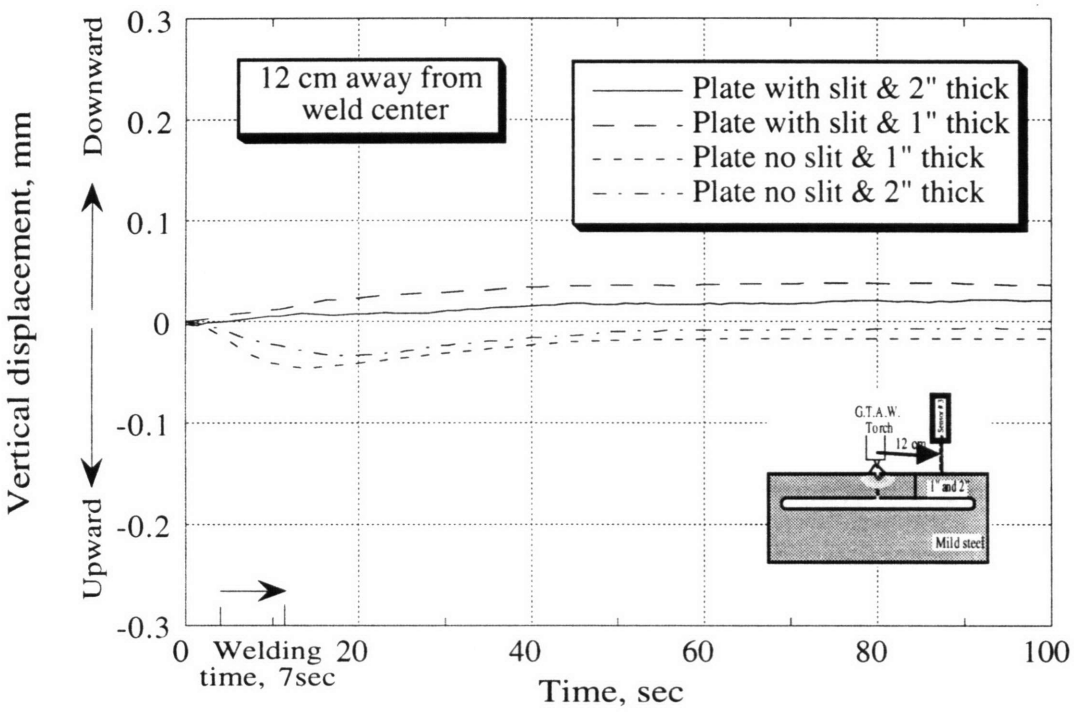

Figure 3.37 Displacement history of the beam with a different shape at 12 cm away from the weld center

3.6.2.3 The H-shaped Plate

Figure 3.38 shows transient vertical (out-of-plane) distortion detected by laser distance sensors located at 2.5 cm from the weld center line. On the Type 1 specimen, upward movement was observed during welding and then the distortion changed to the upward direction. But the amount of the final distortion was only approximately 0.06 mm. In case of the Type 2 specimen, almost no metal movement occurred during welding but the final distortion was as large as 0.45 mm which is almost 9 times that observed on a bead-on-plate welding

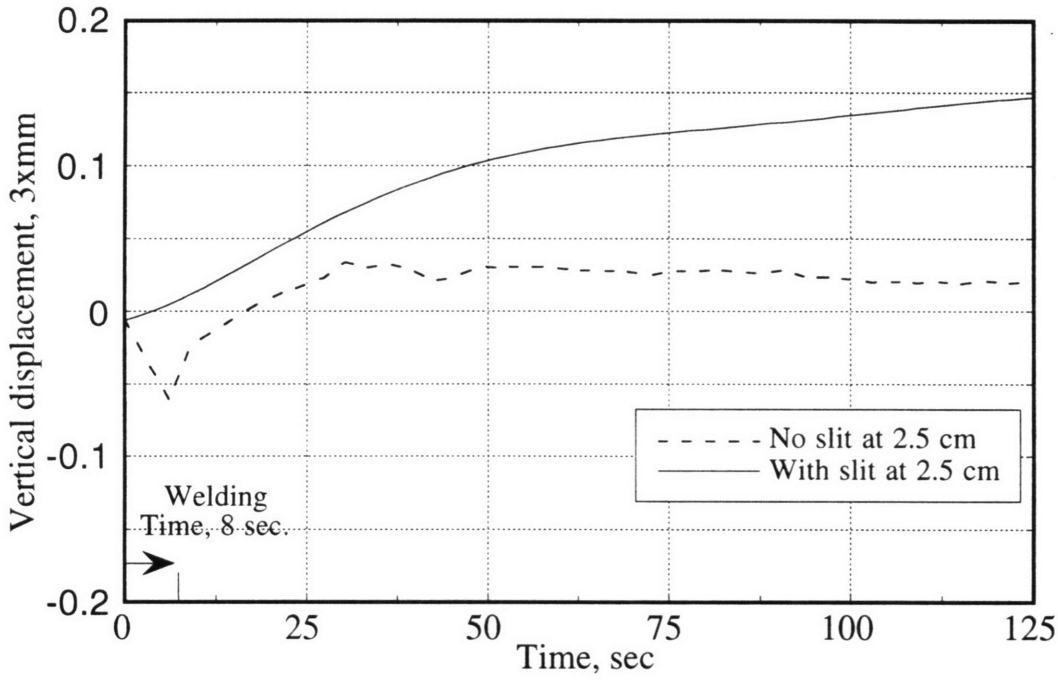

Figure 3.38 Transient out-of-plane movements during butt welding steel plates.

3.7 Discussion

3.7.1 The Observed Mechanism of the Displacement of the Tube

The mechanism of the displacement of the tube observed is shown in Figure 3.39. That is, while the welding arc is turned on, the tube moves upward with the thermal deformation of the washer. In this case, the lifting force of the tube is considered to be the friction between the tube and the washer. This upward displacement of the tube is restricted by the fixture under the washer. The tighter the tube is fixed to the package wall (the test bench in this experiment), the smaller its upward displacement becomes. After the welding arc is turned off, the washer starts returning to its initial position, and the tube also comes down with the washer. In this stage, unlike the previous stage, the tube is connected strongly to the washer by the laser welding. Therefore, the down force of the tube overcomes the strength of the fixture, and the tube goes down more than it was lifted initially by friction. Thus, the downward displacement of the tube, remains after the welding process is over.

The final downward displacement of the tube, *Df*, is considered to be determined by the following two major factors :

(a) The deformation of the washer

In our assumption, the vertical displacement of the tube is caused by the thermal deformation of the washer. Therefore, to decrease *Df*, it is important to reduce the washer's deformation.

(b) The fixing between the tube and the package wall

Df is the difference between the upward displacement of the tube during welding and its downward displacement after the arc is turned off. The amount of the tube's upward displacement is influenced by

the fixing strength to the package wall, as mentioned above. Increasing the upward displacement of the tube by releasing the tube from the fixture, is considered to be effective to reduce *Df*.

3.7.2 Decreasing the Final Displacement of the Tube

Based on the assumption mentioned above, welding trials were performed using test washers of various configurations. The tendency of the tube displacement, obtained by the experiment, coincided well with the assumption.

Concerning the influence of the washer's thickness, as described in 3.6.1.2.1, it was found that *Df* can be reduced by increasing the thickness of the washer. In other words, the thermal deformation of the washer can be reduced by increasing its rigidity. However, as shown in Figure 3.18, *Df* approaches a certain value as the thickness of the washer increases. Therefore, using a very thick washer does not have an effect on further reducing *Df*.

Next, the step washer was applied to reduce *Df*. As mentioned in 3.6.1.2.2, a small projection on the washer was found to be effective to decrease the overall deformation of the washer. The size of the projection, considering its role to absorb the thermal effects, should be small and weak in comparison to the size of the washer.

Regarding the manner in which the tube is attached in place, strong fixing was shown to have a detrimental effect on reducing the final displacement of the tube. This result also coincides with the assumption mentioned above. That is, by making the fixing stronger, the tube cannot go up sufficiently and the final downward displacement becomes larger. Based on the experimental result, it is best if the tube be longitudinally free from the fixture. Moreover, again based on the results of experiments performed thus far, a theory explaining the mechanism of

the formation of the displacement of a tube due to welding has been developed (see Figure 3.39.) The washer deforms by the welding heat while the arc is turned on, and the tube is raised by a friction force between the tube and the washer. When the tube is not attached to the washer tightly, the friction force is not being generated and the tube does not go upward. *Df* is the difference between the upward displacement during the heating stage and the downward displacement during the cooling stage, as mentioned in the Introduction. Therefore, if there is a gap between the tube and the washer, the upward displacement of the tube becomes smaller. As a result of this, *Df* becomes larger.

Experimental results mentioned in the previous chapter can be explained by using the above mechanism. Comparing Figure 3.22 with Figure 3.24, it is clearly seen that having a gap between the tube and the washer is detrimental for reducing the final displacement of the tube, *Df*.

As mentioned before, test pieces made of kovar showed the same tendency as stainless steel specimens in the previous experiments in their displacement manner during welding. However, the amount of the displacement of kovar specimens was much smaller than that of the stainless steel specimens. This is mainly because of the difference of the material properties between kovar and 304 stainless steel. That is to say, the thermal expansion rate of kovar is much lower than that of 304 stainless steel, and the heat conduction speed of kovar is much higher than in 304 stainless steel. These facts make the amount of the thermal deformation in kovar during welding much smaller than the deformation observed in stainless steel.

3.7.3 The Deformation Behavior of the Washer

As mentioned above, the thermal deformation of the washer is considered to play a major role in the displacement of the tube. To determine the motion of the washer during the welding

process, we measured its vertical displacement from the reverse side of the welding arc. However, from the experimental result described in 3.6.1.2.4, the bottom surface of the washer showed less displacement than the tube.

The displacement of the upper surface of the washer is supposed to be larger than that of the bottom surface, because of a local thermal expansion in the washer. This thermal expansion occurs in the heated area adjacent to the welding arc. The top surface in that area on the washer is raised by this expansion, in addition to its ascension by the macro deformation of the washer. The local expansion inevitably occurs during the welding process, even if the thicker washer is used. As mentioned in 3.6.2, *Df* approaches to a certain value as the thickness of the washer increases. The reason for the approach is considered to be the local thermal expansion mentioned before.

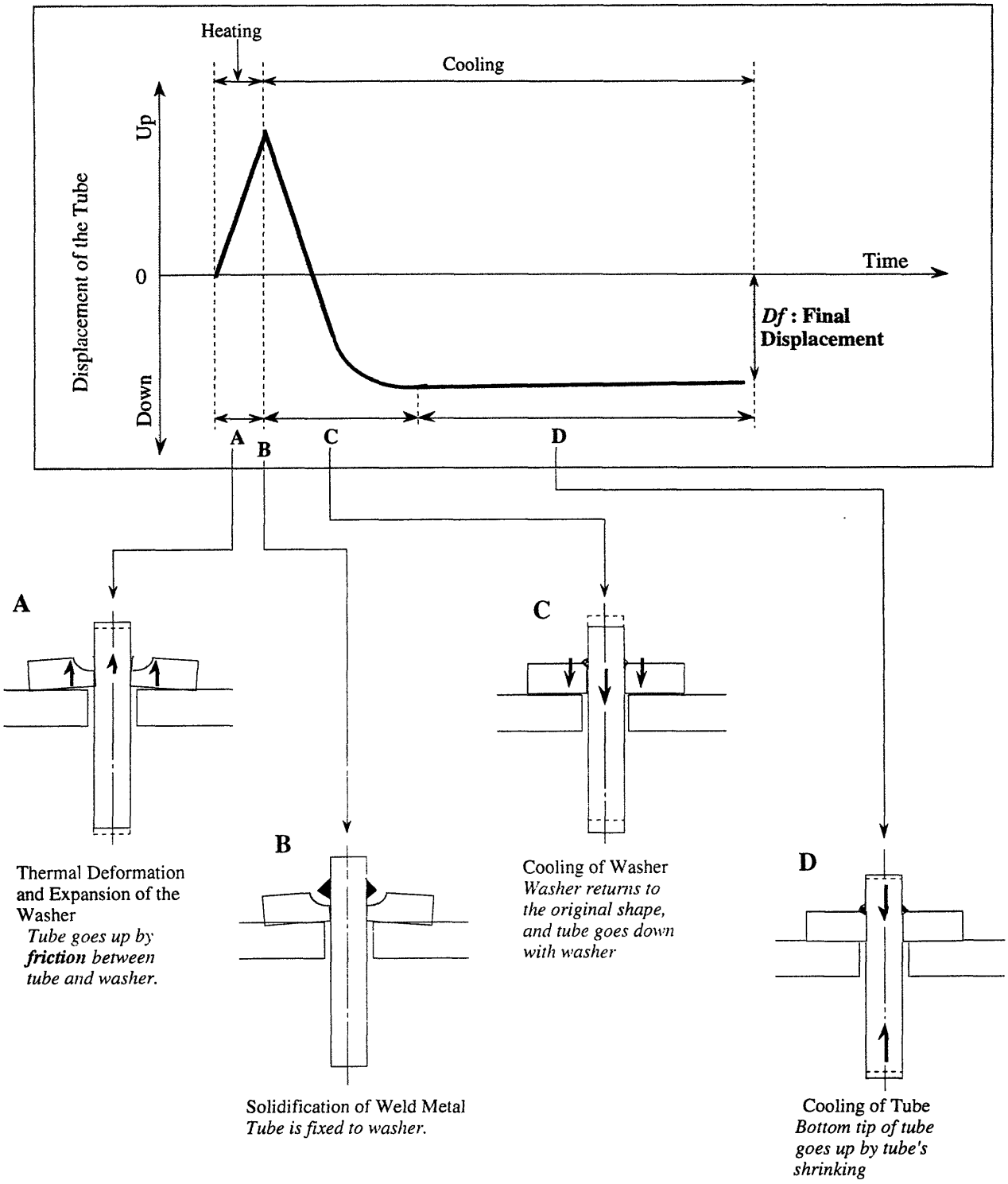

Figure 3.39 The formation of deformation due to welding for cylindrical geometry

The same steps are valid for plane geometry. In the case of the continued plate model mentioned earlier in this chapter, the welding arc increases the temperature where it is applied. This increase causes the metal to expand. However, the metal is not able to expand because of the restraining by the surrounding metal at a lower temperature. This region starts to shrink, because, plastic strains are produced under compression. As it is expected, the area under compression expands into the free direction which is the upward direction. As heat conducts over the plate, expansion takes place. This motion is shown in Figure 3.40 as part A. At the end of this period, welding is finished and cooling starts. Just after the arc is turned off, the downward motion reaches its maximum. This delay may be due to the heat conduction from the arc onto the plate surface. With cooling, the shrunken lower part of the body wants to expand as a reaction. The upward motion starts up and reaches its initial state. If the whole process was elastic, this reverse, i.e.- upward motion, would supposedly stop at this initial point. However, because of the existence of compressive plastic strains, this upward motion continues until the plate reaches a particular residual value as its final distortion. See Figure 3.39 to follow the steps of deformation through the welding and cooling period.

Hence, if one wants to reduce distortion, it has to be controlled before this compressive plastic stress and strains develop at the overheated region. In other words, the best way to control distortion is to take necessary steps during welding. Once welding is over and this plastic deformation occurs, it is very difficult to reduce distortion if not impossible.

As a final comment, on this experimental part of investigation, the formation of distortion is the same in any geometry if the constraints are the same. Here, the constraints are the restraining factors and geometrical discontinuities, such as a continuum or a pair of separate pieces to be joined.

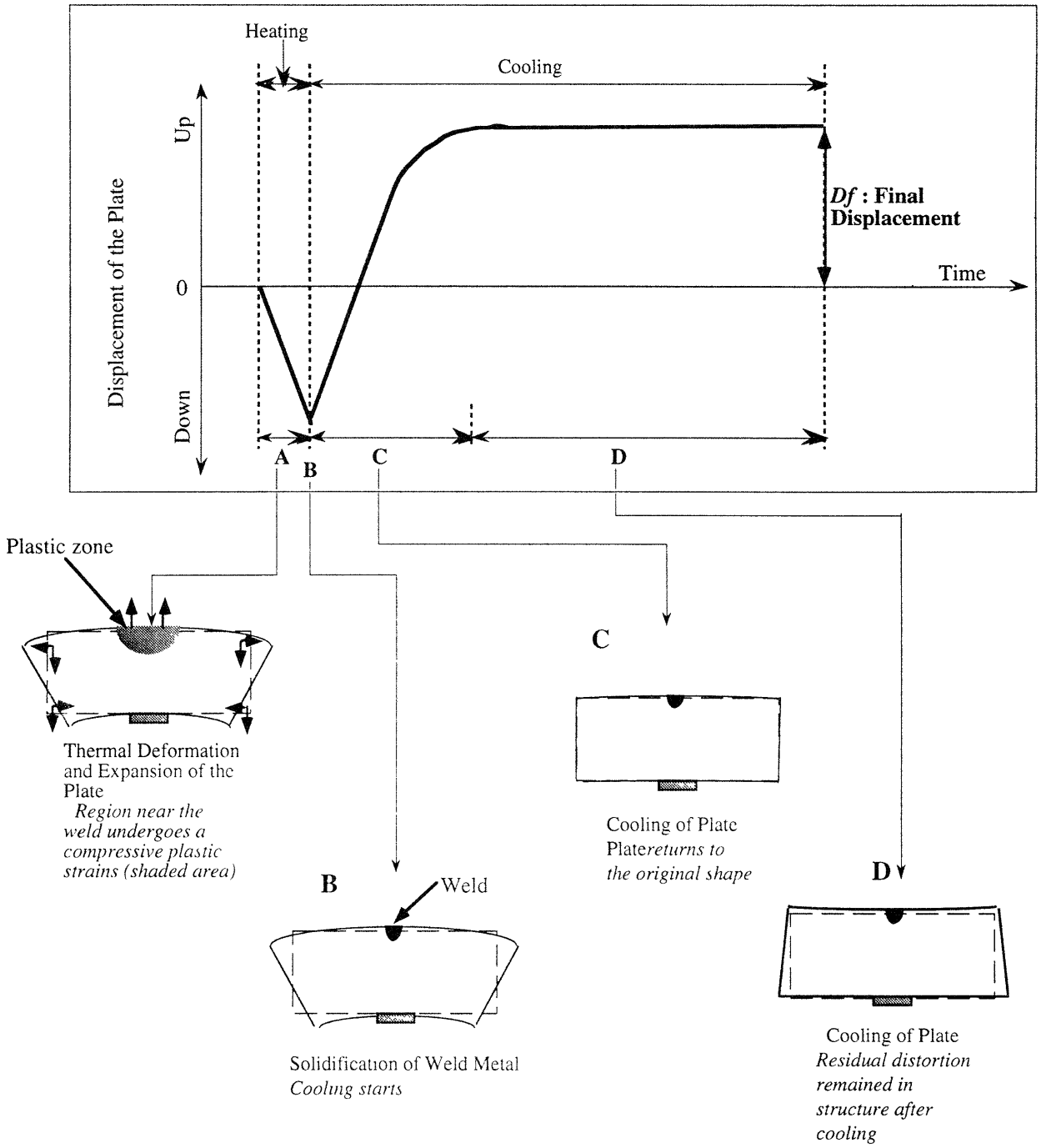

Figure 3.40 The formation of deformation due to welding for plane geometry

Chapter 4

4. Formulation of Heat Flow in Welding

4.1 Introduction

Residual stresses, distortion, metallurgical changes, mismatch, etc. are formed in the structure during the welding operation as consequences of: fast heating, cooling rates, and the uneven temperature field. Hence, an accurate prediction of temperature distribution during welding is one of the most important issues in welding problems and its importance is well understood by researchers working in related subjects.

First attempts to formulate the heat flow problem during welding were limited to analytical techniques. As a result, several simplifying assumptions were made to solve the highly nonlinear governing partial differential equation of heat flow and related boundary conditions. However, the advent of computer technology led researches to utilize computers to solve their equations using numerical methods. This numerical prediction of temperature history during welding yielded much greater accuracy than the analytical results.

In this chapter, analytical formulation and solution of heat flow will be presented first . Then towards the end, numerical formulation and computer implementation will be widely discussed. Also previous studies performed by researchers will be outlined as literature review. First, in this review, point and line heat source solutions will be reviewed. Later, the model proposed by Papazoglou[96] will be introduced. This model includes modified solutions of finite thickness and breadth with linear variations of material thermal conductivity. The model used in Automatic Dynamic Incremental Nonlinear Analysis of Temperature (ADINA-

T)[5] program to calculate the temperature history during and after welding operation, and which is developed with finite element method to solve the heat transfer problem for numerical approach, will be presented. This model takes into account the effect of temperature dependent material properties such as conductivity and specific heat. It also considers the heat loss through nonlinear convection and radiation away from the surface and in the vicinity of the weld respectively.

4.2 Analytical Formulation of Heat Flow

4.2.1 Literature Review

The fundamental equation of heat conduction in a solid can be derived from the energy conservation law as follows[62]:

Let us consider the unit volume as shown in Figure 4.2

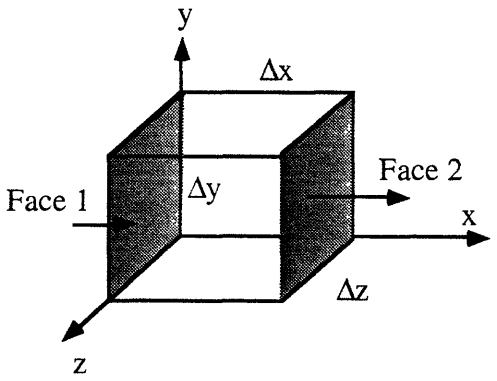

Figure 4.1 Control volume[62]

The rate of heat flow, $\frac{\partial Q}{\partial t}$ or $\dot{Q}$ across a surface A is given by:

$$\dot{Q} = -A\lambda \frac{\partial \theta}{\partial x} \tag{4.1}$$

where

t = time,

λ = thermal conductivity,

A = cross section,

θ = temperature.

The heat transfer rate across Face 1 is:

$$\dot{Q}_1 = -\left(\lambda \frac{\partial \theta}{\partial x}\right)\Big|_x \Delta y \Delta z \tag{4.2}$$

and across Face 2 is:

$$\dot{Q}_2 = -\left(\lambda \frac{\partial \theta}{\partial x}\right)\Big|_{x+\Delta x} \Delta y \Delta z \tag{4.3}$$

Net rate of heat transfer per unit volume flowing to the cube in the x-direction:

$$\frac{\dot{Q}_1 - \dot{Q}_2}{\Delta x \Delta y \Delta z} = \frac{\left(\lambda \frac{\partial \theta}{\partial x}\right)\Big|_{x+\Delta x} - \left(\lambda \frac{\partial \theta}{\partial x}\right)\Big|_x}{\Delta x} \tag{4.4}$$

By using the definition of derivative when x --> 0 at limit, one gets

$$\lim_{x \to 0} \frac{\dot{Q}_1 - \dot{Q}_2}{\Delta x \Delta y \Delta z} = \frac{\partial}{\partial x}\left(\lambda \frac{\partial \theta}{\partial x}\right) \tag{4.5}$$

When we do the same procedure for three directions, the following form of the rate of heat transfer in three dimensions is reached at limit :

$$\frac{\partial}{\partial x}\left(\lambda\frac{\partial\theta}{\partial x}\right)+\frac{\partial}{\partial y}\left(\lambda\frac{\partial\theta}{\partial y}\right)+\frac{\partial}{\partial z}\left(\lambda\frac{\partial\theta}{\partial z}\right) \tag{4.6}$$

The time rate of change of internal energy per unit volume is given by:

$$\dot{Q}_v = \rho c\frac{\partial\theta}{\partial t} \tag{4.7}$$

Lets finally define $\dot{Q}_G$ as the heat generated per unit volume and time, by heat sources or heat sinks which exist in the small unit. Hence, from the conservation of energy, the final balance becomes:

$$\rho c\frac{\partial\theta}{\partial t} = \dot{Q}_G+\frac{\partial}{\partial x}\left(\lambda\frac{\partial\theta}{\partial x}\right)+\frac{\partial}{\partial y}\left(\lambda\frac{\partial\theta}{\partial y}\right)+\frac{\partial}{\partial z}\left(\lambda\frac{\partial\theta}{\partial z}\right) \tag{4.8}$$

where

c = specific heat,

ρ = density,

$\dot{Q}_G$ = heat generated per unit time and volume,

x,y,z = stationary coordinate system.

Equation 4.8 is the three dimensional governing equation of heat conduction in a solid continuum.

4.2.1.1 Fundamental Solutions

Rosenthal [102,103] introduced the exact analytical solution to the problem of heat flow during welding in the early 1940's. He solved the conventional heat conduction differential equation, Equation 1. In his solution, he considered constant point, line, and plane heat sources moving at a constant speed with respect to a fixed Cartesian coordinate system. The coordinate system (w,y,z), which is moving with a uniform velocity, v , with respect to the stationary coordinate system (x,y,z) is shown in Figure 4.2. Here v is parallel to the x-axis. With this contrivance a stationary observer on the x-axis would notice a change in temperature of his surroundings as the source moves along, while an observer stationed on the moving coordinate (w,y,z) would notice no such change. This phenomenon is called quasi-steady or quasi-stationary state. Rosenthal obtained solutions by making the following assumptions:

- The physical properties of the medium are constant.
- The phase changes and the accompanying absorption or release of latent heat in the conducting medium are assumed as negligible.
- The joule heating in electric welding is neglected.
- The heat loss from the surface to the surrounding atmosphere is small.
- The heat source is a plane (one-dimensional infinitely long case), a line (two-dimensional infinitely large case), and a point (three-dimensional semi-infinitely case).

With these assumptions, Equation 4.8 can be rewritten as the following[1]:

$$-\frac{v}{\kappa}\frac{\partial\theta}{\partial t} = \frac{\partial^2\theta}{\partial w^2} + \frac{\partial^2\theta}{\partial y^2} + \frac{\partial^2\theta}{\partial z^2} \tag{4.9}$$

where

$w = x - vt$; moving coordinate,

v = welding speed,

---

[1] For detailed steps of formulation go to Reference [KM].

t = time,

$\kappa = \dfrac{\lambda}{\rho c}$ = thermal diffusivity.

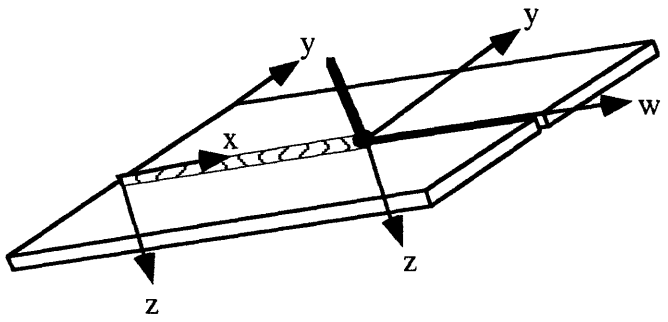

Figure 4.2 Stationary and moving coordinate system

The solutions of the Equation 2 are given for one-, two-, and three dimensional cases as (see Figure 4.3 and Figure 4.4 for schematic representations):

One-dimensional case:

$$\theta - \theta_o = \frac{q\kappa}{v\lambda 2B} e^{\left(-\frac{v}{2\kappa}(w+|w|)\right)} \tag{4.10}$$

Two-dimensional case:

$$\theta - \theta_o = \frac{q}{2\pi\lambda} e^{-\left(\frac{v}{2\kappa}\right)w} K_o\left(\frac{v}{2\kappa} r\right) \tag{4.11}$$

Three-dimensional case:

$$\theta - \theta_o = \frac{Q}{2\pi\lambda} e^{-\left(\frac{v}{2\kappa}\right)w} \frac{e^{-\left(\frac{v}{2\kappa}\right)R}}{R} \tag{4.12}$$

where

θ_0 = initial temperature,

Q = total heat input,

$q = \frac{Q}{T}$ = line heat input,

T = plate thickness,

$2B$ = plate breadth,

$r = \sqrt{w^2 + y^2}$,

$R = \sqrt{w^2 + y^2 + z^2}$,

$K_o(x)$ = modified Bessel function of second kind zero order.

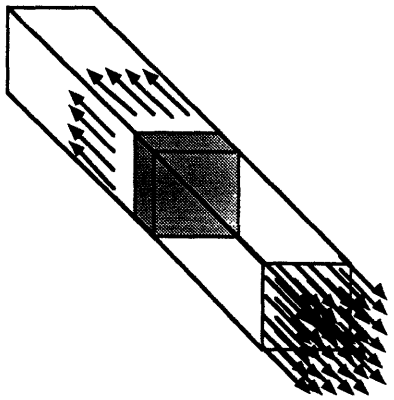

Figure 4.3 One-dimensional heat flow

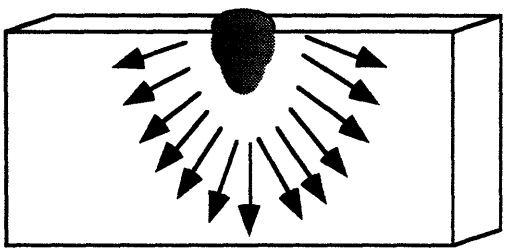

2-Dimensional strip model
no heat flow in depth direction

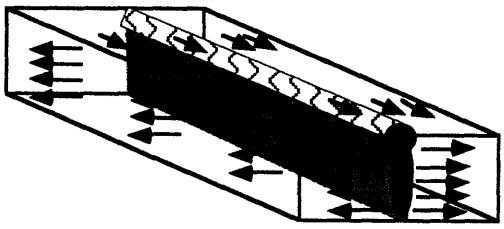

2-Dimensional thin plate theory
no heat flow in thickness direction

Figure 4.4 and Figure 4.5 Two-dimensional heat flow in strip and line heating models

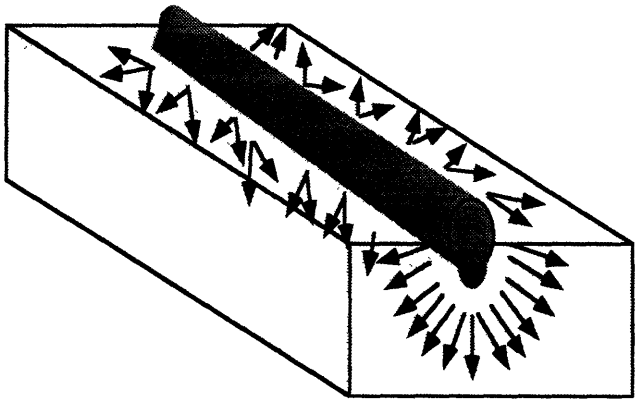

Figure 4.6 Three-dimensional heat flow

Rosenthal [104] introduced a method which takes heat losses through the surface to the surrounding environment for the thin plates in a two dimensional heat flow. In order to do this, one has to replace $\frac{v}{\kappa}$ by $\left(\frac{v}{\kappa}+\frac{h_1+h_2}{\lambda T}\right)$ in Bessel function of Equation 4.11. Where, h_1 and h_2 are the heat transfer coefficients, and assumed time and temperature are independent constants at the upper and lower surfaces of the plate, respectively.

4.2.1.2 Experimental Verification

A two dimensional model was tested experimentally by Rosenthal and Schemerber [88] in 1938. In their computations, the authors used a constant value of thermal conductivity, but a linear variation of thermal diffusivity with temperature was assumed. Under these contingencies, they reported satisfactory agreement between the measured and predicted temperature distributions for distance far from the welding arc. However, in the vicinity of the arc, the computed values of the temperature were largely different from the measured ones. This disagreement is due to the fact that assumed variation of thermal material properties is inconsistent with the assumption made in the solution procedure of the equation and also, thermal conductivity, specific heat and even density vary with temperature in practical situations.

In 1941, to solve the problem of a point source moving on a semi-infinite conducting media which is adiabatic along its boundaries, Malha and co-researchers [57] introduced a new approach which used the fact that the metallurgical structure of the base metal after welding is influenced by material composition, rate of heating, maximum temperature reached and the rate of cooling. A similar assumption, akin to the one in Rosenthal's theory was made. The equation is given by

$$\theta - \theta_0 = \frac{Q}{2\pi\lambda R} e^{-\left(\frac{v}{2\kappa}\right)(w+R)} .(1-\gamma) \tag{4.13}$$

where

$$\gamma = \beta \frac{2}{vR}\left(1+\frac{2}{vR}\right)$$

$$\beta = \frac{\left(\frac{v}{2\kappa}\right)^2}{24}\left(4p^2 + d^2\right)$$

d = weld width

b = weld penetration

here, weld cross area, $p*d$, was determined by experiment.

Comparison of experimental results with those obtained from the formula made it evident that the theory yields a very high maximum temperature and an excessive cooling rate.

Wells [141] introduced an equation which relates the width of the melting isotherm to the amount of heat input based on the moving line heat source theory of Rosenthal. Wells' equation is given by:

$$q = 8\lambda(\theta - \theta_0)\frac{e^{\left(-\frac{vs}{2\kappa}\frac{K_0\left(\frac{vs}{2\kappa}\right)}{K_1\left(\frac{vs}{2\kappa}\right)}\right)}}{K_0\left(\frac{vs}{2\kappa}\right)} \tag{4.14}$$

$$\frac{vs}{2\kappa} = \frac{vs}{2\kappa}\sqrt{1 - \left(\frac{K_0\left(\frac{vs}{2\kappa}\right)}{K_1\left(\frac{vs}{2\kappa}\right)}\right)^2} \tag{4.15}$$

When $0.1 < \frac{vs}{2\kappa} < \infty$, after simplification the theory becomes

$$q = 8\lambda(\theta - \theta_0)\left(0.2 + \frac{vs}{4\kappa}\right) \tag{4.16}$$

where s is the distance measured from the origin to the point of maximum bead width in the molten pool.

He reports a good agreement with the data from Jackson and Shrubsall [46]. Apps and Miller [**], however, during their investigation of argon arc welding, tested the validity of Well's equation and found that the equation needs less heat input to give the same weld bead obtained in the experiment. Moreover, the pool contours are narrower and more elongated than those predicted.

The effect of boundary planes on the temperature distribution due to the welding was mathematically studied by Roberts and Wells [141]. This study was based on Rosenthal's theory and Wells' correlation. Using the image source method in the numerical calculations, they reported that a plate with a half-width greater than ten times the width of fusion zone approaches the thermal condition of an infinite plate.

Adam[1] used Rosenthal's theory to derive engineering relationships which give the peak temperature and cooling rates directly as a function of geometric, thermal and welding variables. They concluded that, in the fusion zone, the cooling rate is the function of distance from the weld center line. Therefore, center line cooling rate was calculated as a function of plate thickness. Moreover, they mentioned that the transition thickness of the plate from two-dimension to three-dimension is between 0.8 and 1.2 inches. Since the effect of the phenomena of melting and solidification were not considered in their theory, the measured values of the cooling rate and peak temperatures did not match with the predicted ones. Adam's formula is given by

$$\frac{1}{\theta_p - \theta_0} = \frac{4.13\rho cTY}{H_{net}} + \frac{1}{\theta_m - \theta_0} \tag{4.17}$$

$$C_r = \frac{2\pi\lambda(\theta_c - \theta_0)^2}{H_{net}} \tag{4.18}$$

where

θ_p : peak temperature, °C,

θ_0 : initial temperature, °C,

θ_m : melting temperature, °C,

θ_c : particular temperature of interest, °C,

H_{net} : net energy heat input,

Y : the distance from the boundary of weld fusion zone,

C_r : cooling rate.

Phase changes due to the moving heat source were first studied by Jackson [46] in 1965. He introduced the solution of the one-dimensional heat flow with constant material properties.

Christensen and co-workers investigated the subject and they compared the experimental results with idealized Rosenthal's theory . They reported that they found a good agreement in the predictions of width, depth and cross-sectional area of molten pool in the three-dimensional case. Moreover, they concluded that the calculation of heat transferred from the arc to the base plate is a complicated problem to solve.

The effect of the material properties on the calculation of temperature distribution is significant. Besides, the material properties are a function of temperature. Assuming that the material properties are constant in the analytical solutions, made the results unrealistic. Especially, in the regions close to the weld, the high temperature values changed the properties of the material drastically. Moreover, this area is directly related to the size of plastic zone and the accompanying residual stresses and distortion.

Grosh, et al.,[39] have considered the temperature dependent properties by assuming that thermal conductivity, λ, and the product of density and specific heat, ρc, vary in the same manner with the temperature so that their ratio, the thermal diffusivity, κ, remains constant. He formulated the two-dimensional problem with both λ and ρc varying linearly with temperature as follows:

$$\theta = \frac{1}{\gamma}\left[\sqrt{\frac{\gamma Q}{\pi \lambda_0 T} e^{\frac{-v}{2\kappa}w} K_0\left(\frac{-v}{2\kappa} r\right) + \left(1+\gamma\theta_0\right)^2} - 1\right] \tag{4.19}$$

where

$$\lambda = \lambda_0\left(1+\gamma\theta_0\right)$$

$$\rho c = (\rho c)_0\left(1+\gamma\theta_0\right)$$

However, this assumption is limited to certain materials such as aluminum. For the other materials, λ and ρc do not vary linearly.

At M.I.T., researchers [86,87] under the supervision of Prof. K. Masubuchi have used iterative methods to take into account the temperature dependence of material properties. Papazoglou, in his thesis [96], explains this iterative method as "The fundamental heat source solution with material properties at the same temperature, say 300 °C, provides the first approximate solution at a particular point. This temperature is compared with the initial guess and if the two temperatures disagree by more than 0.5 °C, new properties are found for a temperature half-way between. These new values are used to obtain a new temperature estimation. This process is repeated until the convergence is reached. It should be pointed out that although this iteration method generally gives good predictions outside the fusion zone, there is no guarantee that it will converge to the correct solution since this approximation may violate the energy conservation law."

4.3 Heat Input Model

The amount of the heat, Q, transferred from the welding arc to the base plate is one of the most sensitive inputs required in the analysis of heat flow. Therefore, this subject went under investigation by many researchers for years. In the literature, the most common expression of the Q is

$$Q = \eta_a VI \tag{4.20}$$

where

V = arc voltage,

I = arc current ,

η_a = arc efficiency.

	Christensen	Rykalin	Tsai
Gas Metal Arc Welding (GMAW)	-	0.65-0.85	-
Mild Steel	0.66-0.70	-	0.80-0.90
Aluminum	0.70-0.85		
Submerged Arc Welding (SAW)	0.90-0.99	0.90-0.99	0.85-0.98
Shielded Metal Arc Welding (SMAW)			
Mild Steel, ac	0.66-0.85	0.65-0.85	0.55-0.90
Gas Tungsten Arc Welding (GTAW)			
Mild Steel, ac	0.22-0.48	0.20-0.50	-
Mild Steel, dc	0.36-0.46	0.45-0.75	-
Aluminum, ac	0.21-0.43	0.20-0.50	-

Table 4.1 Values of arc efficiency for various processes

The product of arc current, I, and arc voltage, V, is known as the total electric arc power. The arc efficiency, η_a, is the ratio of the power introduced into the base plate to the total electric arc power.

The value of the arc efficiency which is heavily dependent on the welding process, the depth of penetration, shielding gas etc. has been studied extensively by many researchers. They used the calorimetric method which immerses the welded metal into the water pool and measure the rise of temperature of water to estimate the values of the arc efficiency, η_a, experimentally. Rosenthal, et al. [103] showed that the arc efficiency is independent from the arc speed. Rykalin, et al.[108] proved that a 10 % drop in efficiency occurs when the welding mode is changed from continuous to pulsed. Christensen, et al. [23,24] and Rykalin, et al.[108, 110] have conducted numerous measurements using this method for various welding processes and their findings are summarized in Table 4.1. Tsai[128] formulated arc efficiency as a function of bead width in thin plates for two-dimensional heat flow. In his formulation, he divided the conducting media in solid and liquid regions. By using the appropriate boundary conditions he obtained the solution as follows:

$$Q = 2\pi\lambda_l Th(d) \tag{4.21}$$

Equation 4.36 correlates the total heat input to the width of the plate. It also says that predicted heat input is linearly dependent to the thickness of the two-dimensional plate.

4.3.1 Distribution of Arc Heat

In the accurate prediction of the heat flow due to welding, the distribution of arc heat is an important fact. Up to this point, we only dealt with either point or line heat sources. However, Rykalin [108, 110] reported that arc heat input can be modeled more accurately by

assuming a Gaussian distribution. According to Rykalin, heat flux is expressed by Gaussian normal distribution as follows:

$$q(r) = q_{max} e^{-kr^2} \tag{4.22}$$

where

q_{max} = maximum heat flux at the center of the heat spot,

k = heat flux concentration coefficient,

r = radial distance from the center of the heat spot.

The maximum heat flux is the flux value at the center of the spot and it can be calculated easily by assuming that the total heat, Q, is equal to the total heat flux under this surface, Figure 4.6. In other words mathematically:

$$Q = \int_0^\infty q(r) 2\pi r dr q \tag{4.23}$$

using the expression given in Equation 4.22 gives

$$Q = 2\pi q_{max} \int_0^\infty r e^{-kr^2} dr \tag{4.24}$$

evaluating the integral term in Equation 4. 24 yields

$$Q = \frac{\pi q_{max}}{k} \tag{4.25}$$

or a more practical expression is

$$q_{max} = \frac{Qk}{\pi} \tag{4.26}$$

Here, the concentration coefficient k determines the source concentration: the higher k is, the more concentrated the heat is, the smaller the diameter, d_h, of the heat spot is.

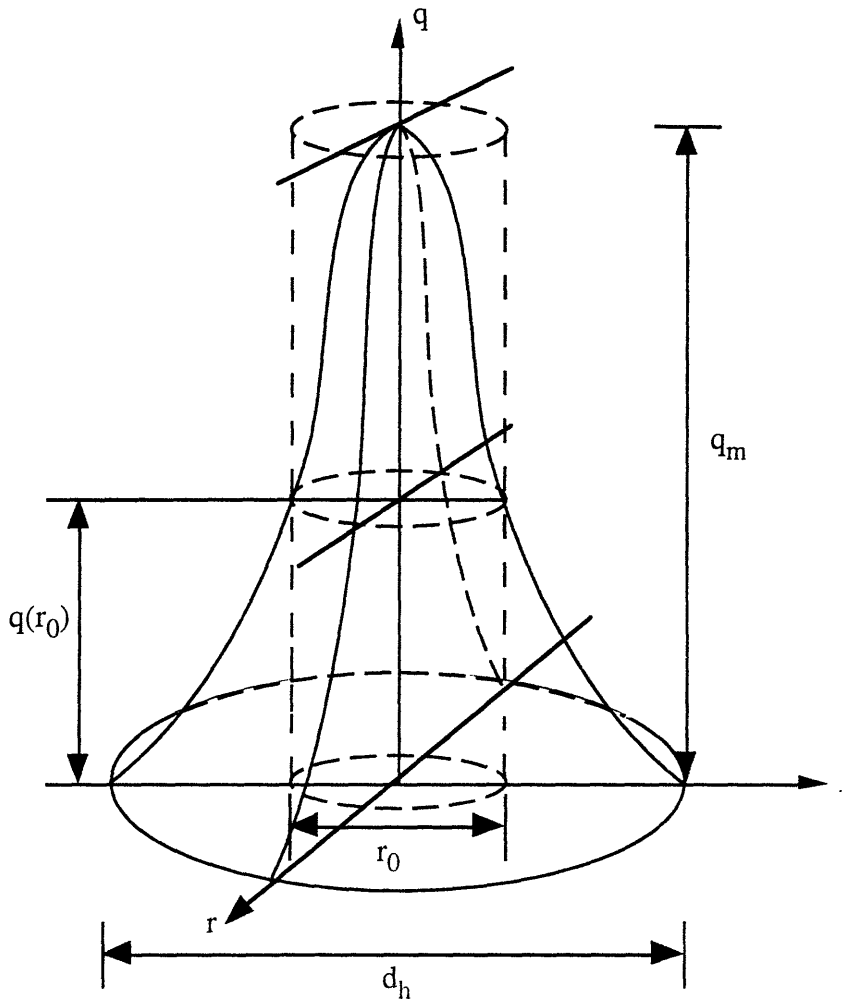

Figure 4.7 Gaussian distribution of heat flux[110]

The diameter of the heat spot d_h can be calculated as at which the heat flux $q(r_h)$ is 0.05 of the maximum heat flux q_{max}. Then

$$q(r_h) = q_{max} e^{-kr_h^2} = 0.05 q_{max} \tag{4.27}$$

where

$$r_h = \frac{d_h}{2} \tag{4.28}$$

it is clear from Equation 4.18 that

$$e^{-kr_h^2} = 0.05 \tag{4.29}$$

or

$$kr_h^2 = 3.0 \tag{4.30}$$

therefore, one gets the relation of d_h as

$$d_h = \frac{3.46}{\sqrt{k}} \tag{4.31}$$

and it is inversely proportional with the square root of the concentration coefficient *k*. The experimental values of the concentration coefficient k are summarized for various welding processes in Table 4.2.

Welding Process	**Concentration Coefficient (cm^{-2})**	**Polarity, Current**
GMAW	1.26-1.32	ac, 550-1100 A
SAW	1.00-2.50	ac, 550-1200 A
SMAW	1.26-1.32	ac, 550-1100 A
GTAW, Steel	6.0-14.00	dcsp, 40-200 A
Carbon Electrode	1.00-3.50	dcsp, 95-2500 A

Table 4.2 Experimental values of the concentration coefficient [109]

4.4 Numerical Formulation of Heat Flow

Although analytical solutions presented in the early parts of this chapter are not very accurate in the overheated area of the welded pieces, they are very useful to conduct low-cost and less time consuming parametric studies. The poor prediction of the temperature distribution in the vicinity of the weld is due to the nonlinear nature of material at high temperatures. This nonlinearity is not taken into account in analytical solutions. In this subsection, we will present a nonlinear formulation of heat transfer analysis and its application to the welding process. When we mention nonlinearity in heat transfer analysis, we mean the temperature dependent properties of material such as thermal conductivity, specific heat, density, heat transfer coefficient, etc.

On the other hand, there is a need of an accurate prediction of temperature distribution in some cases such as Heat Effected Zone calculations, weld pool characteristics, transient stress-strain predictions due to welding, etc. In order to take into account the nonlinearity in the problem, one of the best ways is to approach the solutions by using approximate methods based on variational principles.

In this study, a finite element approximation, where a continuum is replaced by a system of elements is used. ADINA-T[5], Automatic Nonlinear Incremental Nonlinear Analysis-Temperature, was chosen as finite element code. In heat conduction, an approximate solution within each element for the temperature field is assumed and heat flux equilibrium equations are introduced at a discrete number of points within the finite element system. After a basic definition of formulation, the model will be discussed in detail and the assumptions will be explained. Finally, the results obtained using the model will be presented.

4.4.1 Finite Element Formulation

Bathe and co-workers [15,17,144] formulated a nonlinear heat transfer governing equation for the finite element method. Let us rewrite the heat flow equilibrium in the interior of the body where the material obeys Fourier's law of heat conduction[2].

$$\frac{\partial}{\partial x}\left(\lambda_x \frac{\partial \theta}{\partial x}\right)+\frac{\partial}{\partial y}\left(\lambda_y \frac{\partial \theta}{\partial y}\right)+\frac{\partial}{\partial z}\left(\lambda_z \frac{\partial \theta}{\partial z}\right)=-q^B \tag{4.32}$$

where q^B *is* the heat generated per unit volume and it includes the q^{c3} in the transient heat flow formulation.

On the surface of the body the following equations must be satisfied:

$$\theta|_{S_1} = \theta_e \tag{4.33}$$

$$\lambda_n \frac{\partial \theta}{\partial n}\bigg|_{S_2} = q^s \tag{4.34}$$

where

θ_e = environmental temperature,

λ_n = body thermal conductivity,

n = the direction of normal,

q^s = the heat flow input on the surface.

---

[2] $q_x=\lambda_x\frac{\partial\theta}{\partial x}, q_y=\lambda_y\frac{\partial\theta}{\partial y}; q_z=\lambda_z\frac{\partial\theta}{\partial z}$ where q_x, q_y, and q_z are the heat flows conducted per unit area.

[3] It is defined as the rate of the heat absorption within the material and it equals to $c\dot{Q}$ where c is the material heat capacity.

The prescribed temperatures on the surface, S_1, may be taken into account in Equation 4.33. The heat flow input may be considered at the nodal points or on the surface of the body as specified in Equation 4.34. Convection boundary conditions are included in the same equation, Equation 4.34. In other words:

$$q^s = h\left(\theta_e - \theta^s\right) \tag{4.35}$$

and h was defined earlier as the convection coefficient. However, it may here be temperature-dependent.

The same method can be used to express the radiation boundary conditions as

$$q^s = \chi\left(\theta_r - \theta^S\right) \tag{4.36}$$

and

$$\chi = h_r\left(\theta_r^2 + \left(\theta^S\right)^2\right)\left(\theta_r + \theta^S\right) \tag{4.37}$$

where h_r is determined from the Stefan-Boltzmann constant, the emmissivity of the radiant and absorbing materials and the geometric view factor.

By using the variational principle, the functional governing equation of heat conduction and associated boundary conditions is

$$\begin{aligned}\Pi = \int_V \frac{1}{2}\left\{\left(\lambda_x \frac{\partial \theta_e}{\partial x}\right)^2 + \left(\lambda_y \frac{\partial \theta}{\partial y}\right)^2 + \left(\lambda_z \frac{\partial \theta}{\partial z}\right)^2\right\} dV \\ - \int_V \theta q^B dV - \int_{\Gamma_2} \theta^S q^S dS - \sum_i \theta^i Q^i\end{aligned} \tag{4.38}$$

where Q^i are the concentrated heat flow inputs. Since the only variable in the Equation 4.36 is θ, we use the stationarity of Π to obtain heat flow equilibrium at time $t+\alpha\Delta t$ with step-by-step incremental form as

$$\int_V \delta\theta'^T {}^{t+\alpha\Delta t}\lambda^{t+\alpha\Delta t}\theta' dV = {}^{t+\alpha\Delta t}Q + \int_{S_c} \delta\theta^S {}^{t+\alpha\Delta t}h\left({}^{t+\alpha\Delta t}\theta_e - {}^{t+\alpha\Delta t}\theta^S\right)dS - \int_{S_r} \delta\theta^S {}^{t+\alpha\Delta t}\chi\left({}^{t+\alpha\Delta t}\theta_r - {}^{t+\alpha\Delta t}\theta^S\right)dS \tag{4.39}$$

where

θ^S = surface temperature,

θ_e = environmental temperature,

θ_r = the temperature of radiating surface,

δ = variation symbol,

χ = radiation coefficient,

S_C = convection surface area,

S_r = radiation surface area.

$$\theta'^T = \left[\frac{\partial\theta}{\partial x} + \frac{\partial\theta}{\partial y} + \frac{\partial\theta}{\partial z}\right],$$

$$\lambda = \begin{bmatrix} \lambda_x & 0 & 0 \\ 0 & \lambda_y & 0 \\ 0 & 0 & \lambda_z \end{bmatrix}.$$

and

${}^{t+\alpha\Delta t}Q$ = the virtual work of external surface heat flow input to the system at time $t+\alpha\Delta t$.

The quantity ${}^{t+\alpha\Delta t}Q$ includes the effects of surface heat flow input, q^S, internal heat generation $\tilde{q}^B$, if any, and temperature-dependent heat capacity, c. Hence

$$ {}^{t+\alpha\Delta t}Q = \int_S \delta\theta^S {}^{t+\alpha\Delta t}q^S dS + \int_V \delta\theta\left({}^{t+\alpha\Delta t}\tilde{q}^B - {}^{t+\alpha\Delta t}c\,{}^{t+\alpha\Delta t}\dot{\theta}\right)dV \tag{4.40} $$

After linearization of Eqn. 4.39 and substituting the corresponding interpolation functions into it, one gets the heat flow equilibrium equations for a single element as follows[4]:

$$ \begin{aligned} \left({}^{t}K^{\lambda} + {}^{t}K^{c} + {}^{t}K^{r}\right)\Delta\theta^{(i)} = {}^{t+\alpha\Delta t}Q + {}^{t+\alpha\Delta t}Q^{c(i-1)} \\ + {}^{t+\alpha\Delta t}Q^{r(i-1)} - {}^{t+\alpha\Delta t}Q^{\lambda(i-1)} \end{aligned} \tag{4.41} $$

where

$$ {}^{t+\alpha\Delta t}\theta^{(i)} = {}^{t+\alpha\Delta t}\theta^{(i-1)} + \Delta\theta^{(i)} \tag{4.42} $$

α, $0 \le \alpha \le 1$, is a stability and accuracy parameter in the solution.

In most general form, the finite element heat transfer equilibrium equations can be written for any given time t as follows:

$$ C\dot{\theta} + K\theta = \overline{Q} \tag{4.43} $$

where

C = heat capacity matrix,

K = $K^{\lambda} + K^{c} + K^{r}$, heat conduction matrix,

$\overline{Q}$ = a vector of thermal nodal loads.

---

[4] for detailed steps of derivations please refer to reference [Bathe+Khoshgoftaar]

In the nonlinear analysis, $C, K, \overline{Q}$ matrices are temperature-dependent quantities. The convection and radiation boundary conditions are represented in Equation 4.41 with matrices ${}^{t}K^{c}$ and ${}^{t}K^{r}$ and the vectors ${}^{t+\alpha\Delta t}Q^{r}$ and ${}^{t+\alpha\Delta t}Q^{c}$. External heat input is included in the ${}^{t+\alpha\Delta t}Q$ as surface heat input.

4.4.2 Two-Dimensional FEM Model

In this section, all the necessary assumptions and considerations for the modeling of a bead-on-plate condition of a thin plate will be introduced. After a short explanation of the two-dimensionality of the problem is made, mesh design, boundary conditions and heat input model will be discussed in details. Finally, the results of the computational work will be presented.

In general, the heat flow distribution resulting from a moving welding arc is three-dimensional. The temperature gradients exist through thickness, transverse and longitudinal directions. However, in this particular study, the welding arc is stationary and heating is applied through the depth of the plate. The heat conduction is assumed to be zero in out-of-plane direction. Hence, heat only conducts in YZ plane into two directions. This assumption can be explained mathematically with the following equation:

$$\frac{\partial}{\partial y}\left(\lambda\frac{\partial\theta}{\partial y}\right)+\frac{\partial}{\partial z}\left(\lambda\frac{\partial\theta}{\partial z}\right)=-\rho c\frac{\partial\theta}{\partial t} \tag{4.44}$$

A similar two-dimensional approach was considered by many researchers. Papazoglou [96] used a two-dimensional approach for modeling a multi-pass weldment of relatively thicker plates. In his study, he assumed that heat conduction is negligible in the welding direction and used the quasi-stationary case. Vitooraporn [136] studied the bead-on-edge weldment. He

reduced the problem to the two-dimensional case by assuming that there is no heat flow across the thickness of plate. Three-dimensional problems were analyzed by several investigators by using the finite element method. However, the computation cost and CPU time effected the success and became a leading factor to be used in two-dimensional models. Muraki[86,87], Nishida[92], and etc. suffered from the same problem and they discontinued pursuing the detailed nonlinear transient three-dimensional analysis of heat flow.

4.4.2.1 Mesh Design

Two-dimensional heat conduction elements available in ADINA-T[4] are defined in the YZ plane. 9-node parabolic quadrilateral elements, Figure 4.8, were used to provide a higher accuracy around the weld pool and the fusion zone where the material is subjected to a very high temperature along with metallurgical changes. Moreover, the area close to the weld pool is defined with a finer mesh. The mesh used in this simulation is shown in Figure 4.9. A total of 96 two-dimensional conduction elements were defined to construct the mesh. For convective boundary conditions, 40 line convection elements were modeled at the boundaries. Also, weld pool side were modeled as radiation surface at the boundaries. 428 nodes in all were used to calculate the approximate transient temperature field. Theoretically, when the number of elements and the nodes go to infinity the approximate solution of the temperature field should approach the exact solution.

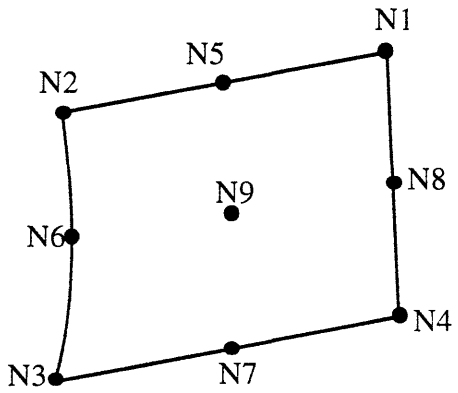

Figure 4.8 9-node two-dimensional conduction element configuration

4.4.2.2 Heat Input

The heat flux applied to the surface was modeled as a Gaussian distribution[5]. However, instead of a continuous function of heat distribution, the discrete lumped values were used as shown in Figure 4.9. The area exposed to the heat flux was measured from the experimental result. This area was used to calculate the heat flux from total heat produced by welding arc and transferred to the base plate.

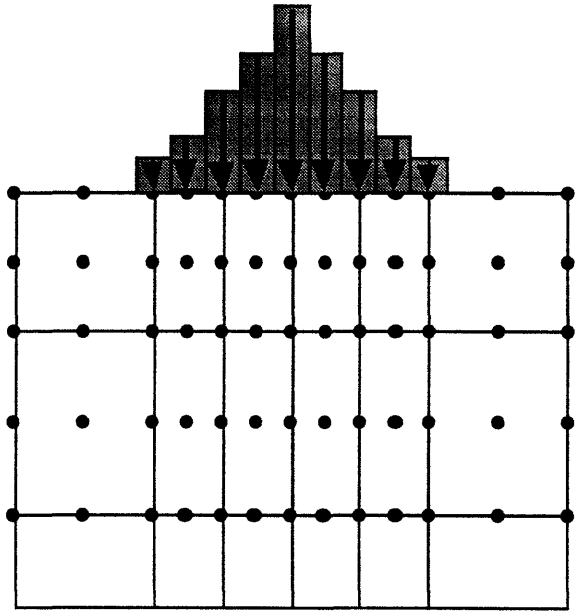

Figure 4.9 Discrete applied heat flux

On the other hand, in the heat flow analysis, a uniformly distributed heat flux gave the same results as Gaussian distribution.

---

[5] the details of this modeling were explained in section 4.3

4.4.2.3 Boundary Conditions

In this section, we will discuss the boundary conditions relevant in the modeling of the welding heat flow analysis with the finite element code ADINA-T. In the model, the nonlinear boundary conditions are considered.

4.4.2.3.1 Convection Elements

In general, in a welding application, heat from a surface is dumped into the surrounding environment in two ways. The first one is natural convection and the second one is radiation which will be discussed separately.

In ADINA-T boundary, convection elements are used to specify the convection boundary condition

$$q^S = h\left(\theta_e - \theta^S\right) \tag{4.45}$$

where h is the temperature-dependent convection coefficient, θ_e is the external environmental temperature or here, room temperature, θ^S is the unknown body surface temperature. This is also known as linear Newton convection cooling.

The estimation of the h, heat transfer coefficient is not an easy task. That is particularly true if the temperature dependent h is considered. In this study, the temperature-dependent convection coefficient, h, based on the semi-empirical correlation proposed by Lienhard[55] was used. Figure 4.10 provides the two sets of the values of h which were used.

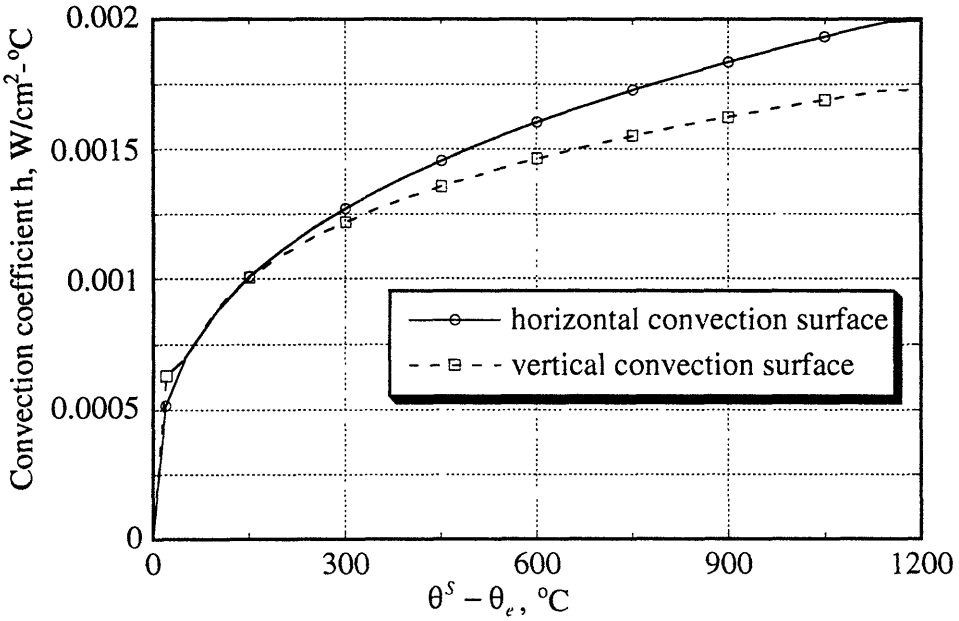

Figure 4.10 Temperature-dependent convection coefficient

4.4.2.3.2 Radiation Elements

In the vicinity of the weld metal, radiation heat losses are significant because of the large difference between the surface and environmental temperatures. These losses are modeled according to the quartic Stefan-Boltzman law. ADINA-T uses radiation elements to specify the radiation boundary condition

$$q^s = \sigma f e\left(\theta_r^4 - \left(\theta^S\right)^4\right) \tag{4.46}$$

where

σ = Stefen-Boltzman constant,

f = shape factor.

e = material emmissivity,

θ_r = temperature of radiation surface (sink)

θ^S = surface temperature.

Radiation heat loss has been taken into account by many investigators. In this study, the shape factor A was taken to be a unit and emmissivity coefficient e =0.8. The Stefen-Boltzman constant is 5.67×10^{-12} W/cm^2°K^4.

4.4.3 Temperature Dependent Material Properties

The temperature dependence of the material properties is a very critical input for the accurate calculation of temperature distribution due to welding. Tall [124] and other researchers have noticed a great variation in the temperature dependence of properties among even slightly different chemical composition of the same materials. Moreover, the literature and studies do not include the values of material properties at highly elevated temperature ranges. The reason for this is that, it becomes very difficult to measure the material properties at these temperatures.

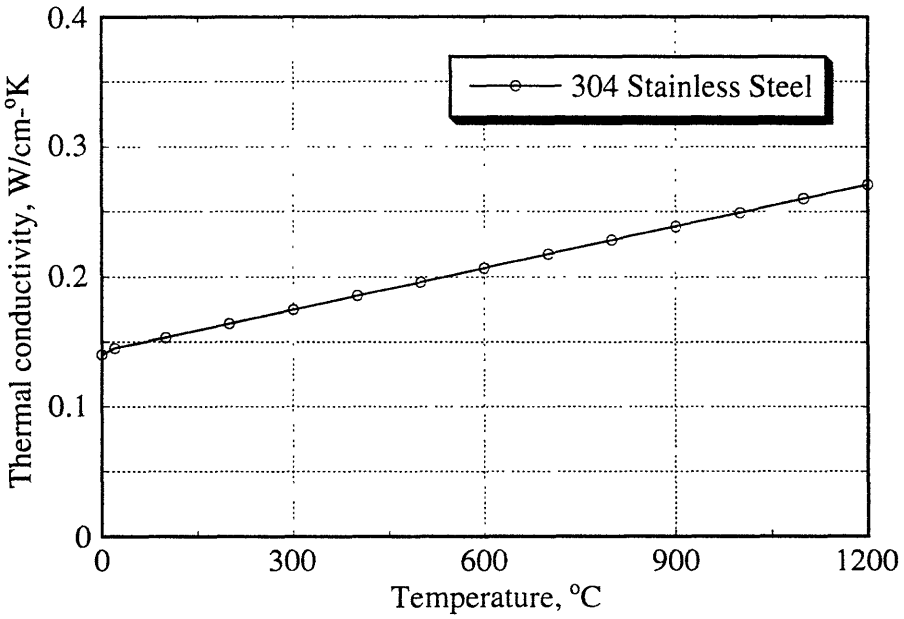

Figure 4.11 Temperature-dependent thermal conductivity

The temperature-dependent conductivity, λ, and the product of specific heat and density, ρc, are considered in the finite element analysis of heat flow with ADINA-T. The values of these quantities varying with temperature are shown in Figure 4.11 and Figure 4.12 respectively. At elevated temperatures where there was no data available, material properties were obtained through careful extrapolations.

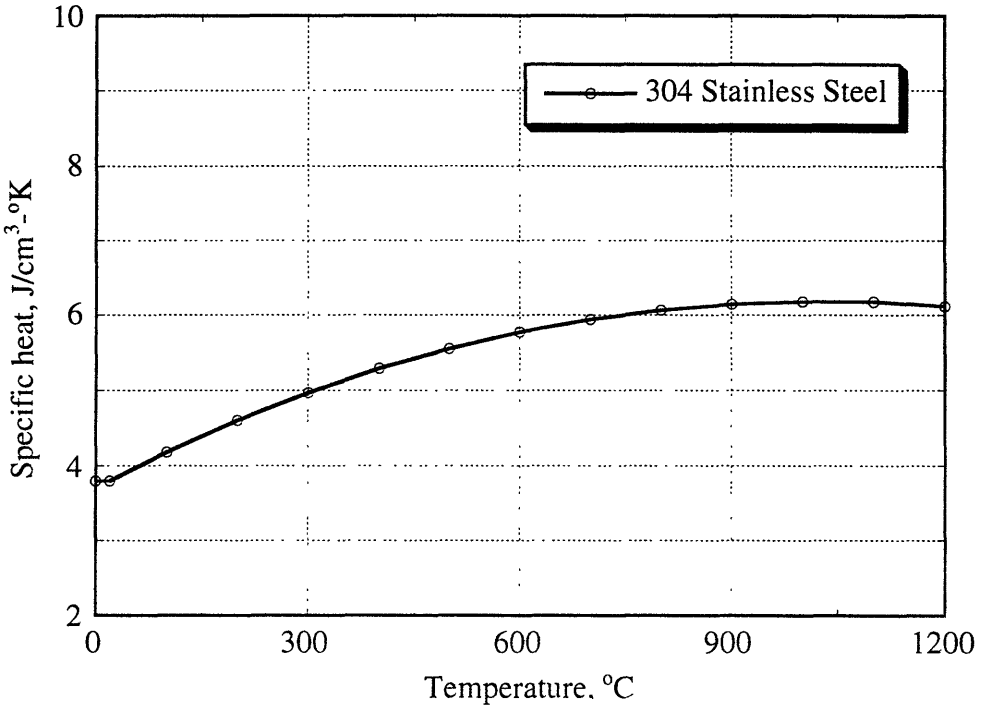

Figure 4.12 Temperature-dependent specific heat*density

4.4.3 Results of Computation

ADINA-PLOT[6] was used to reduce data obtained from ADINA-T[4]. Figures 4.13, 4.14, 4.15, 4.16, 4.17, and 4.18 show the predicted temperature contours at successive time steps. In Figure 4.13, the maximum temperature was set at the melting temperature. Therefore, the shaded area in the center of the contours refers to the weld pool. After, the welding was over, 5 sec., as can be seen in all figures, cooling starts and the heat input from the welding arc starts to conduct into the base metal. The numerical values of the color bands are printed on the right hand side of the mesh. The values of the temperatures are in °C. The compression of the numerically predicted transient temperatures and the weld pool geometry are given Chapter 6.

The welding conditions used in the numerical analysis are the same as those used in experiments. Total heat input is calculated from Equation 4.35 and arc efficiency is adjusted according to the experimental results.

After 250 sec., the temperature on the plate becomes almost uniform. This can be seen in Figure 4.18.

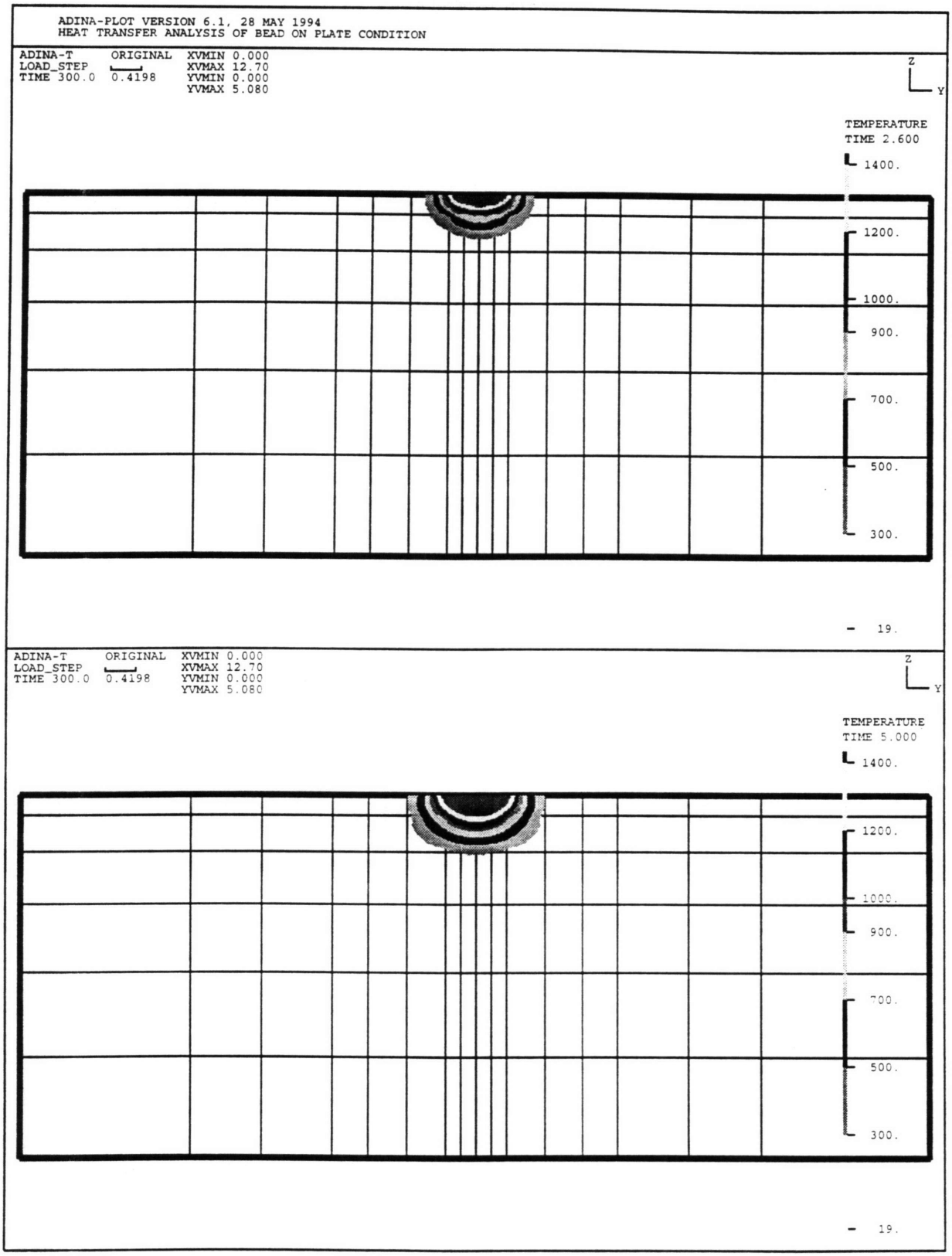

Figure 4.13 Predicted weld pool geometry and related temperature field during welding

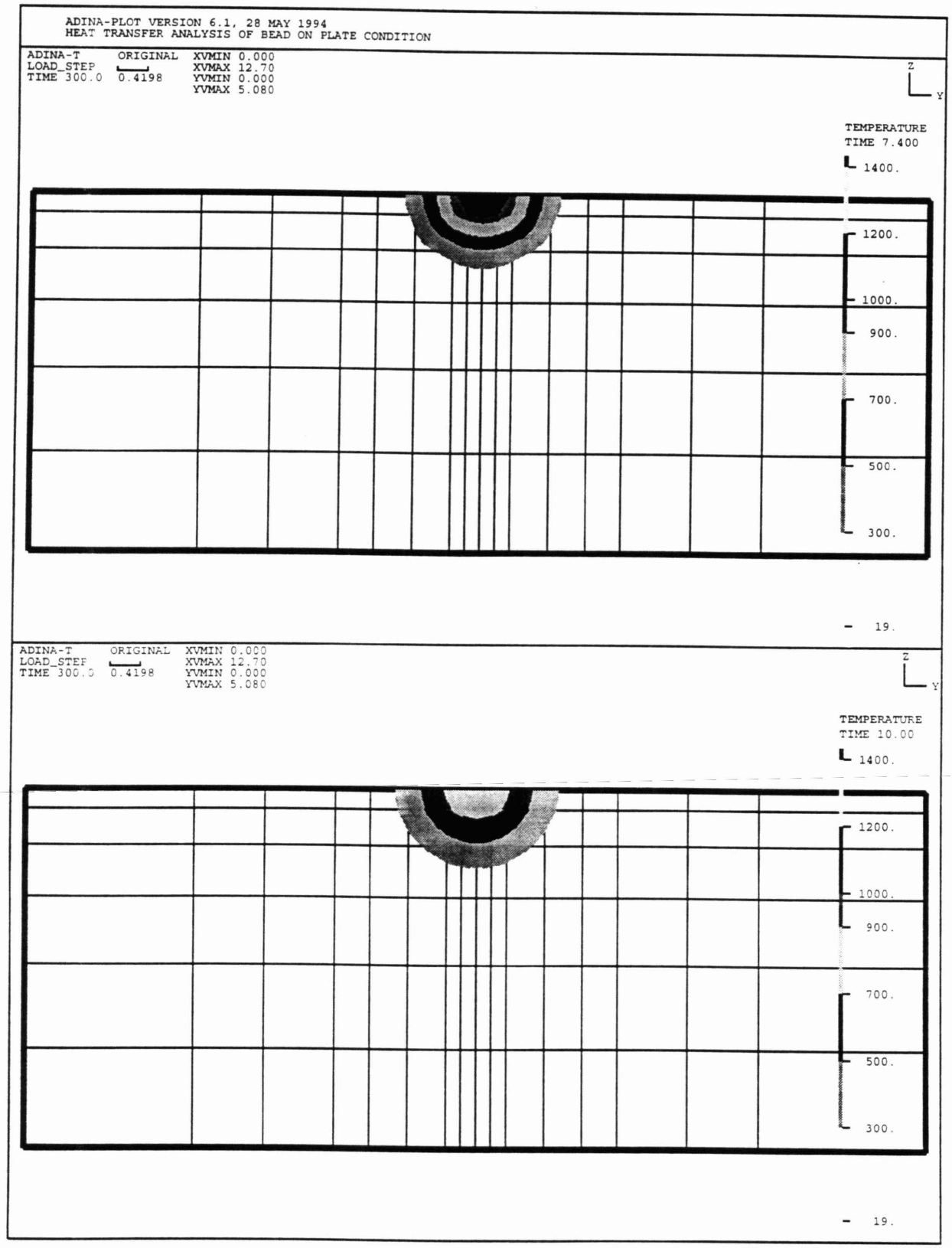

Figure 4.14 Predicted temperature contours after welding at 7.4th and 10th sec.

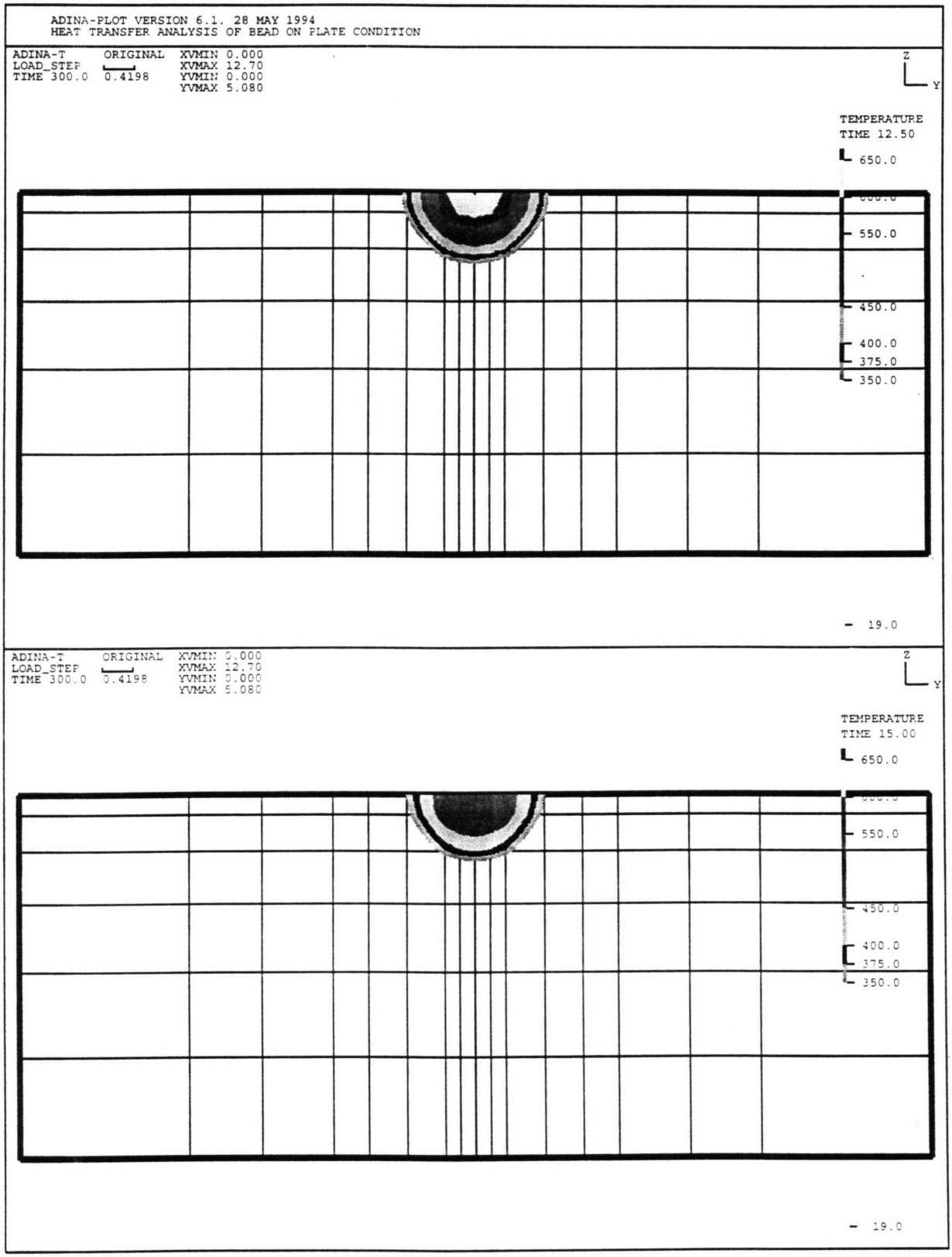

Figure 4.15 Predicted temperature contours after welding at 12th and 15th sec.

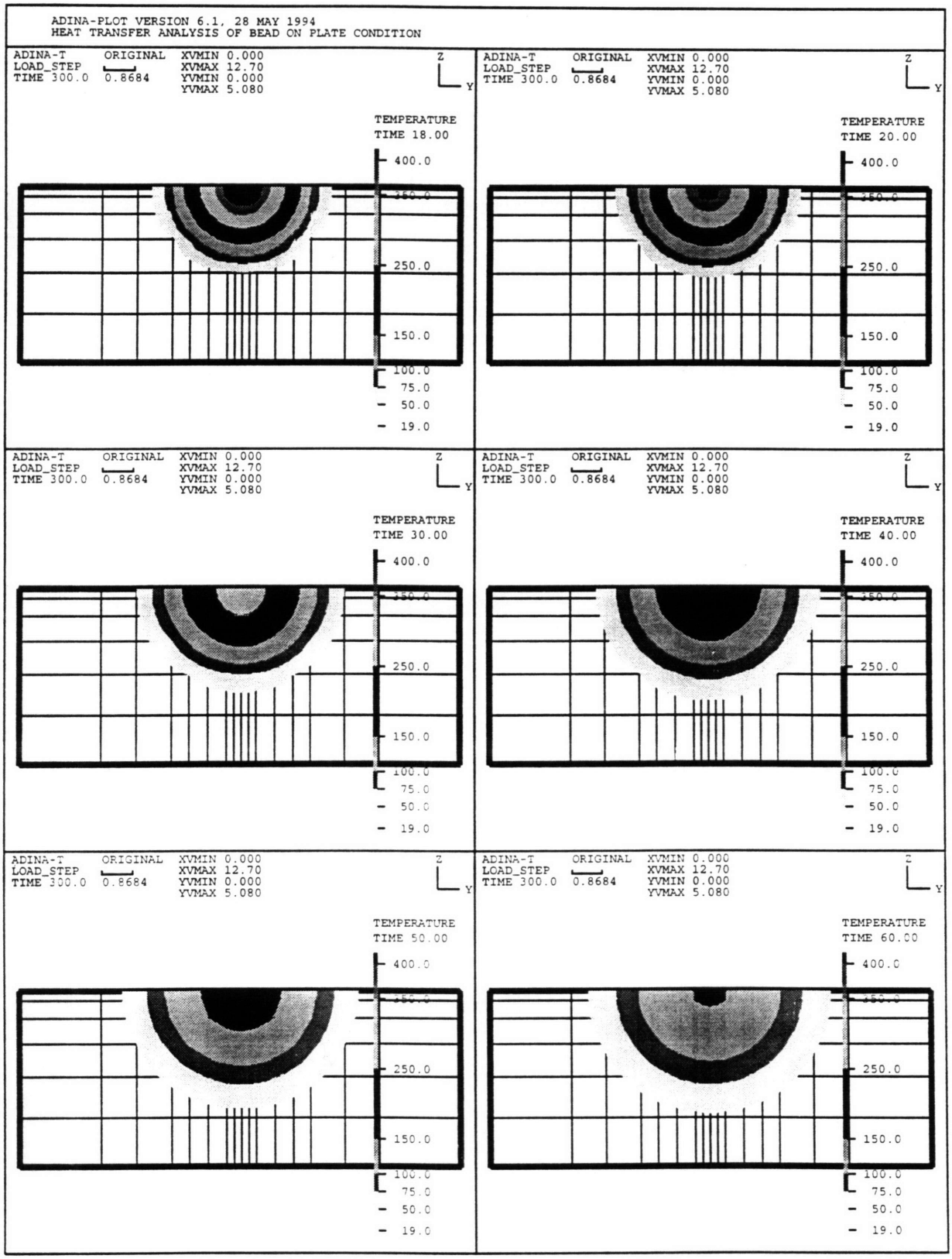

Figure 4.16 Predicted temperature contours after welding at 18th, 20th, 30th, 40th, 50th, and 60th sec.

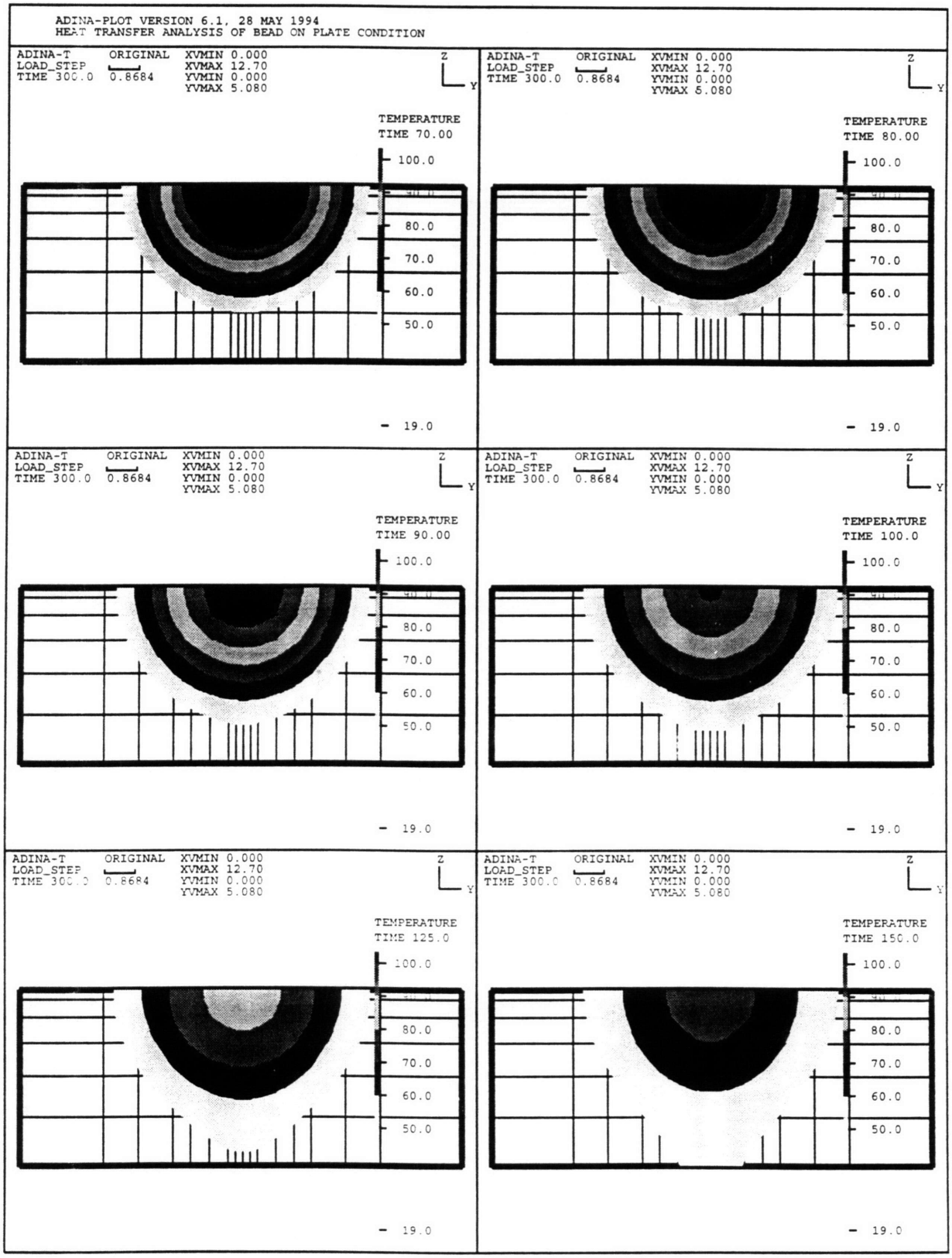

Figure 4.17 Predicted temperature contours after welding at 70th, 80th, 90th, 100th, 125th, and 150th sec.

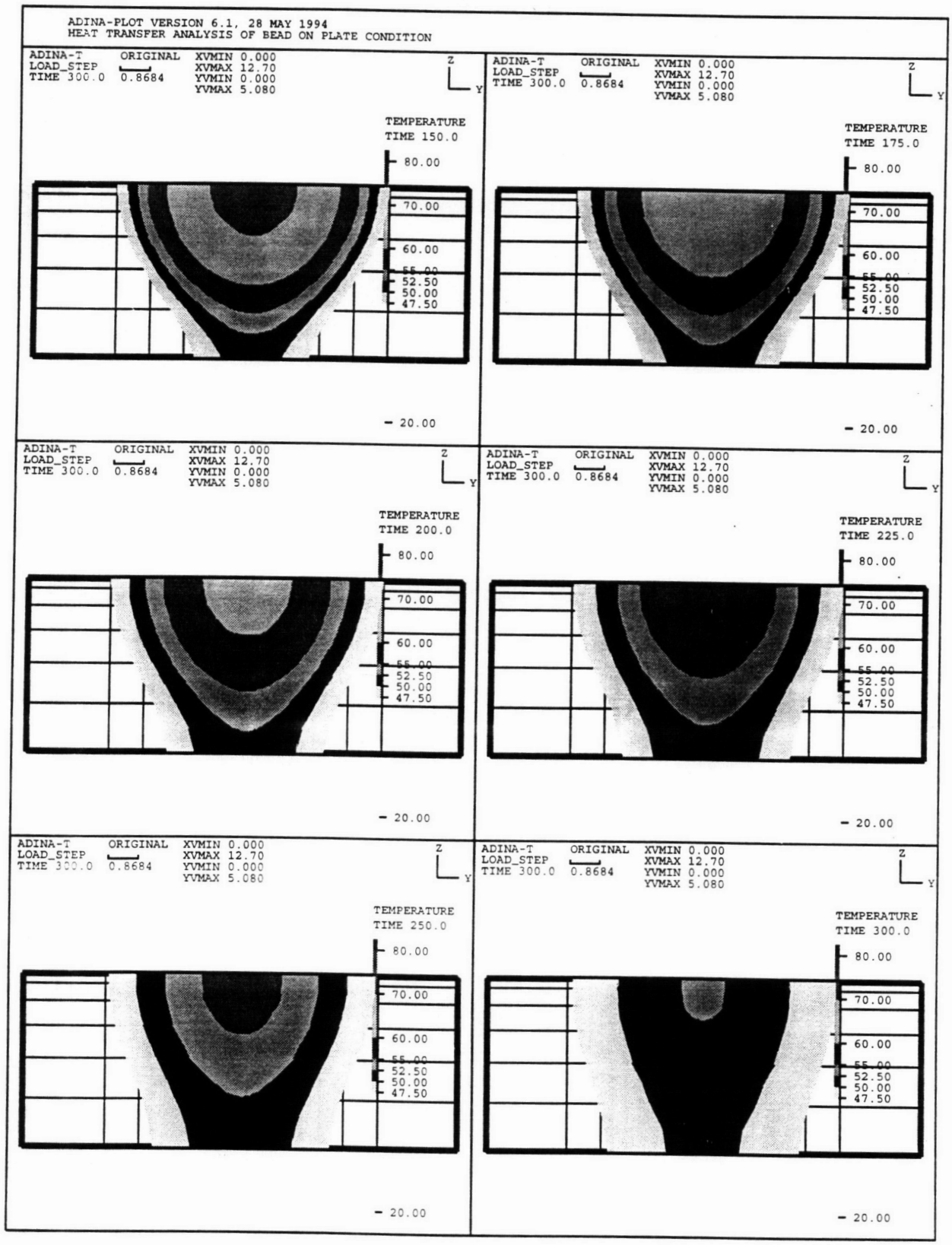

Figure 4.18 Predicted temperature contours after welding at 150th, 175th, 200th, 225th, 250th, and 300th sec.

Figure 4.19 shows the transient temperature histories of the nodes at 0.6, 0.8, 1.2, and 1.6 inches away from the weld center as explained in Figure 3.12. Special attention was paid to locate nodes at the points where thermocouples were placed. In Chapter 6, the results shown in Figure 4.19 were compared with experimental thermocouple readings.

Figure 4.20 shows the predicted transient temperature of the nodes at 1.0, 1.25, 1.50 and 2.0 inches from the weld surface into the direction of the thickness. This figure demonstrates temperature profile under the weld.

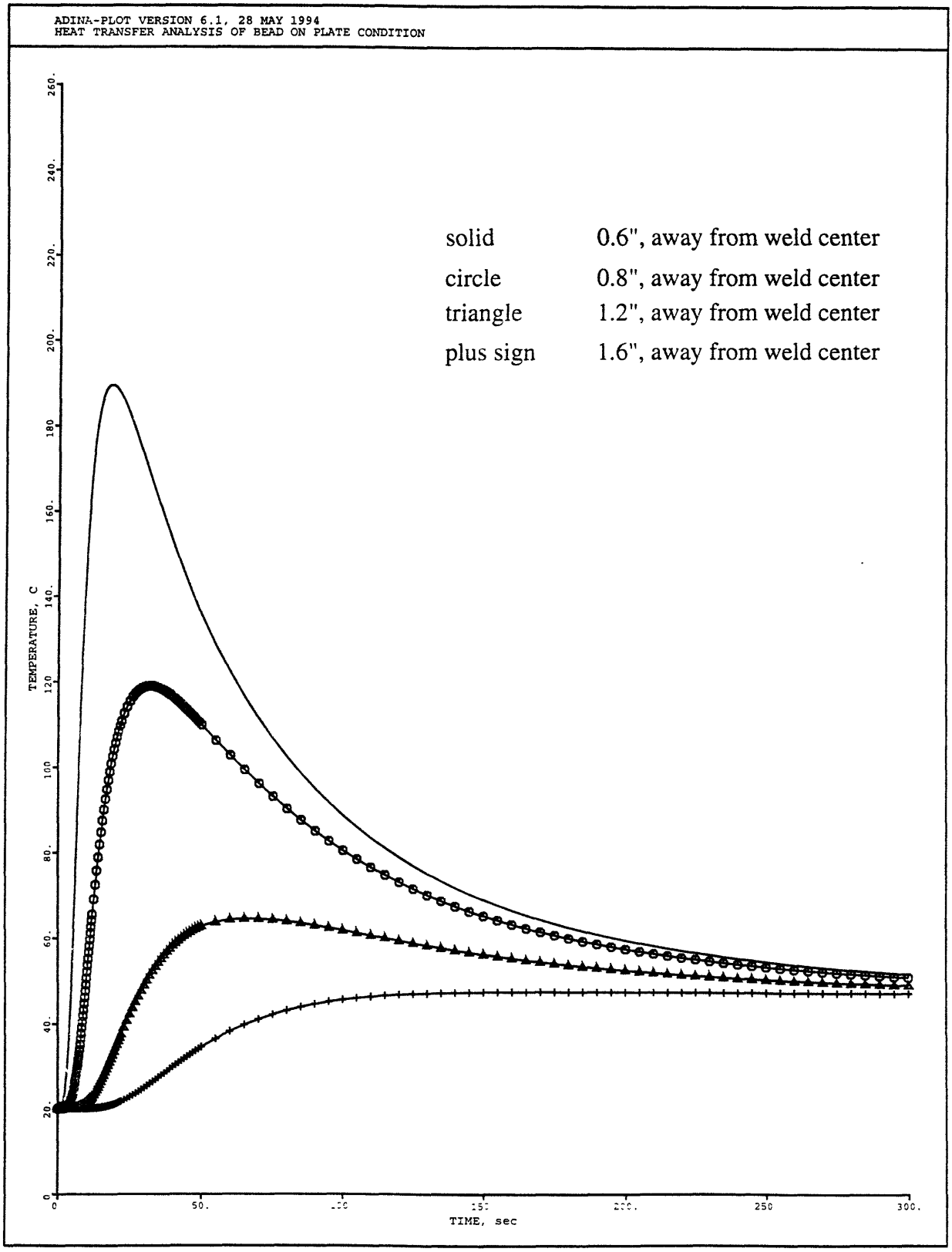

Figure 4.19 Predicted transient temperature at points 0.6", 0.8", 1.2", and 1.6" from weld center

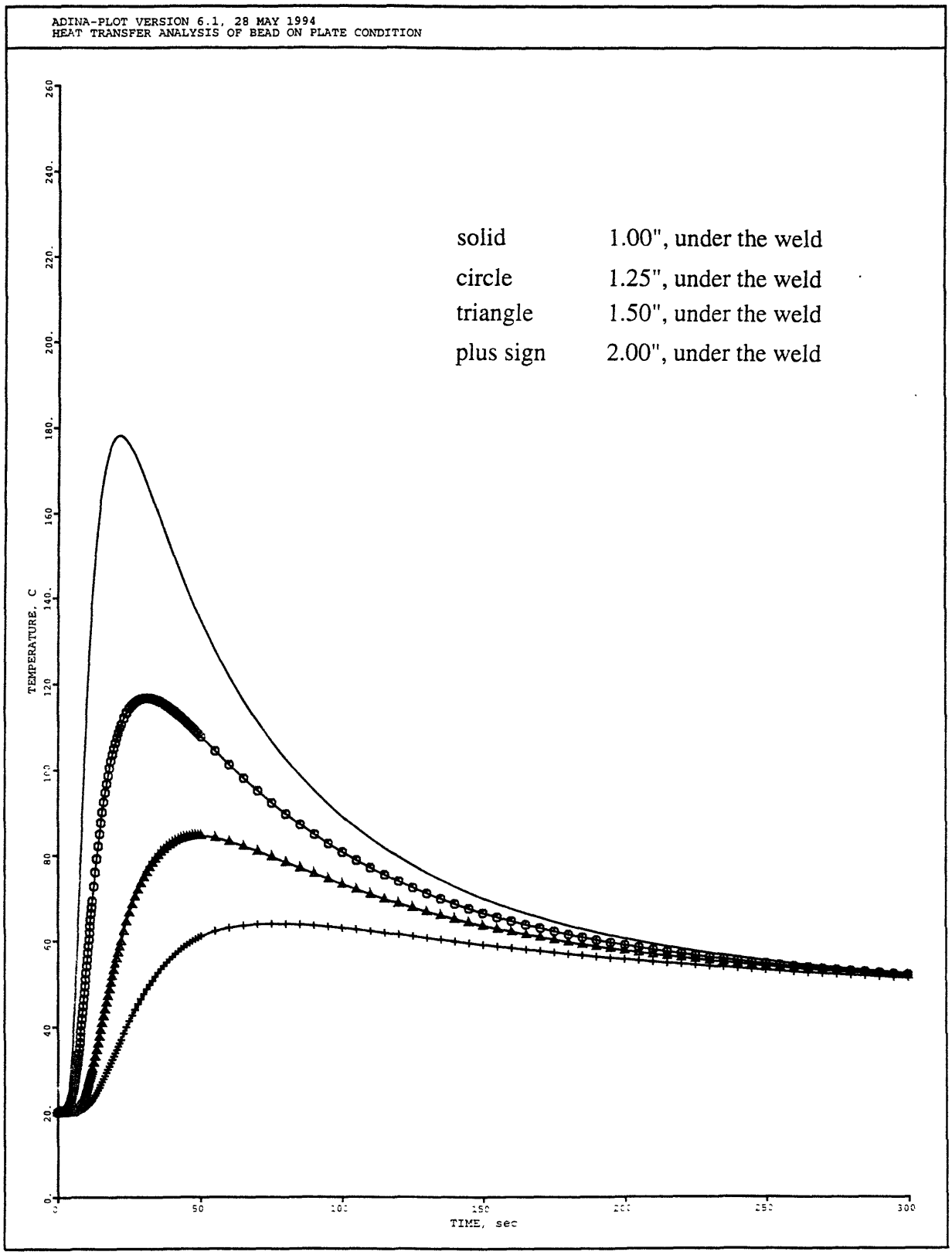

Figure 4.20 Predicted transient temperature at points 1.0", 1.25", 1.50", and 2.0" under the weld

The successive temperature profiles on the top of the plate surface are shown in Figures 4.22, 4.23, 4.24, and 4.25. The maximum of the temperature curve was set at 1400 °C which is the melting range for stainless steel (304 SUS).

Similarly, the same plots were prepared in the thickness direction (see Figure 4.20.) Figures 4.24, 4.25, 4.26, and 4.27 show the temperature profiles in the thickness direction just under the weld bead.

It can be seen from figures 4.23 and 4.28 that after 250 sec., the temperature is uniform all over the plate. As soon as welding is over, the systems cool down very rapidly. Moreover, the weld freezes in less than one second (Figures 4.20 and 4.27.)

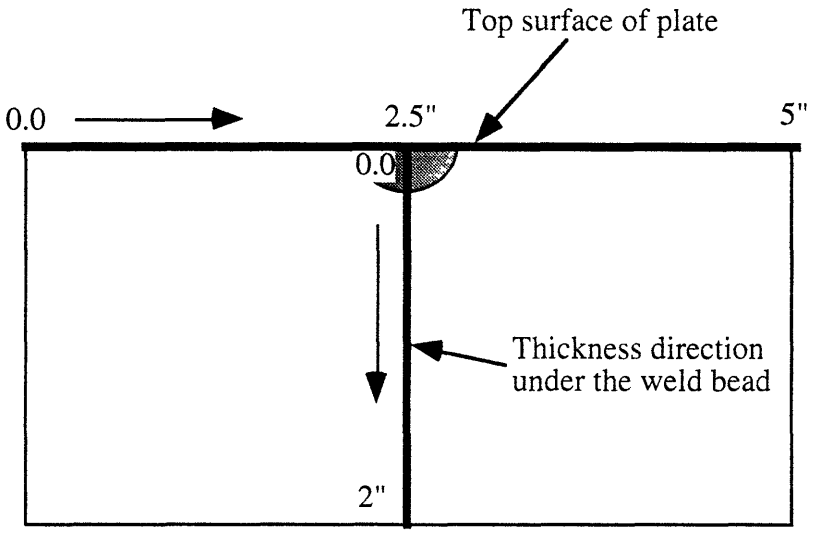

Figure 4.21 Schematic representation of lines defined in the figures for successive temperature profiles

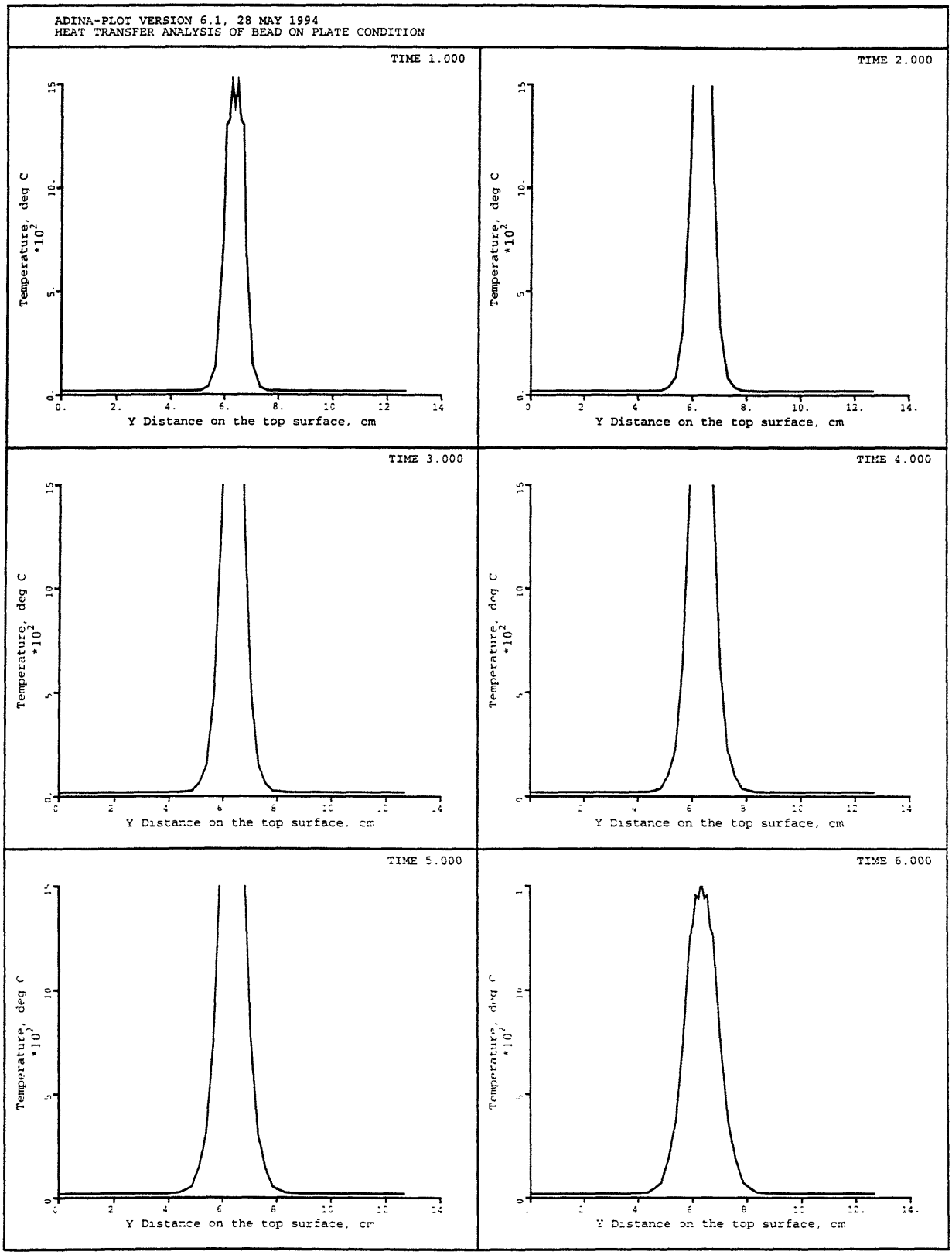

Figure 4.22 Successive temperature profiles on the top surface of plate at 1st, 2nd, 3rd, 4th, 5th, and 6th sec.

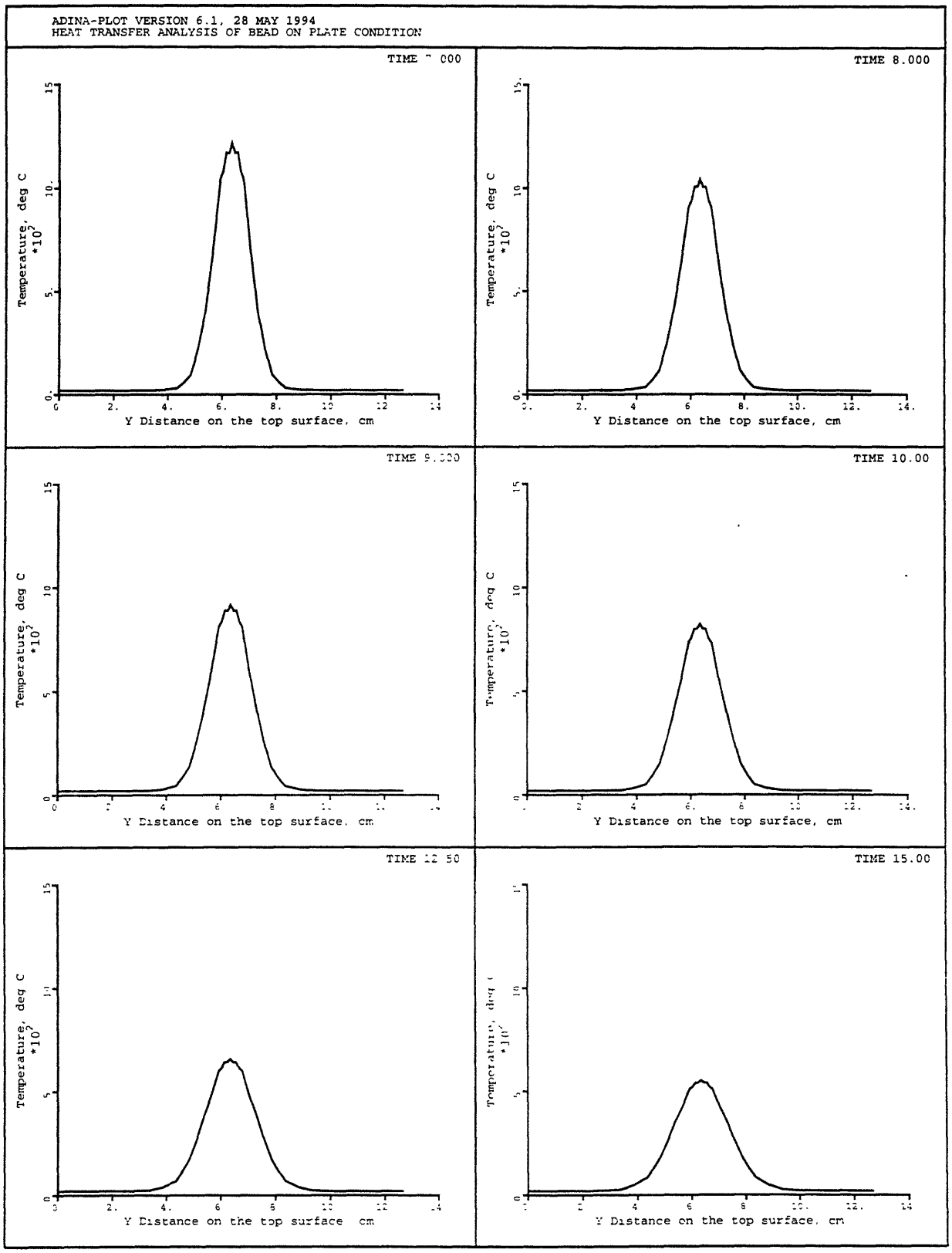

Figure 4.23 Successive temperature profiles on the top surface of plate at 7th, 8th, 9th. 10th, 12.5th. and 15th sec.

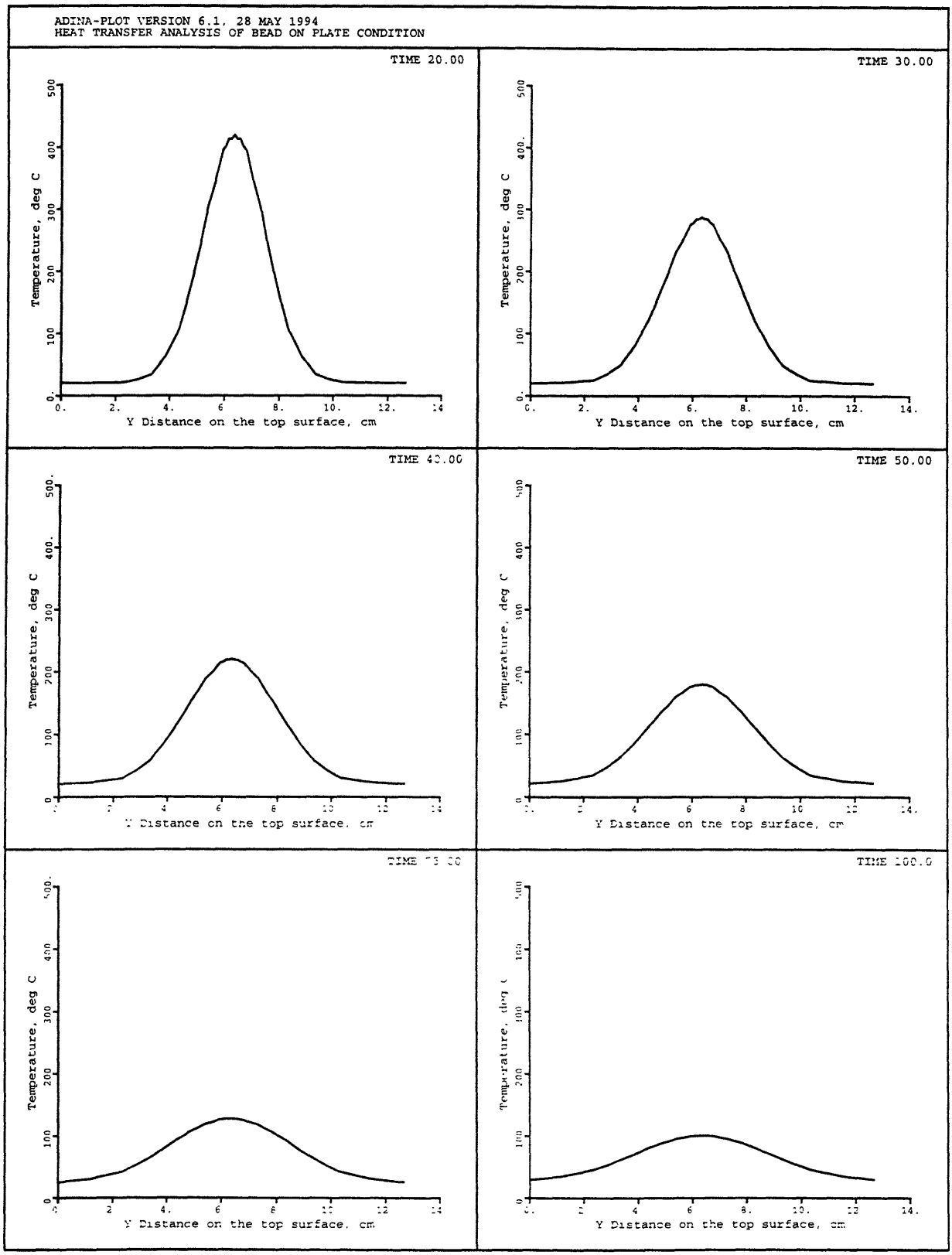

Figure 4.24 Successive temperature profiles on the top surface of plate at 20th, 30th, 40th, 50th. 75th. and 100th sec.

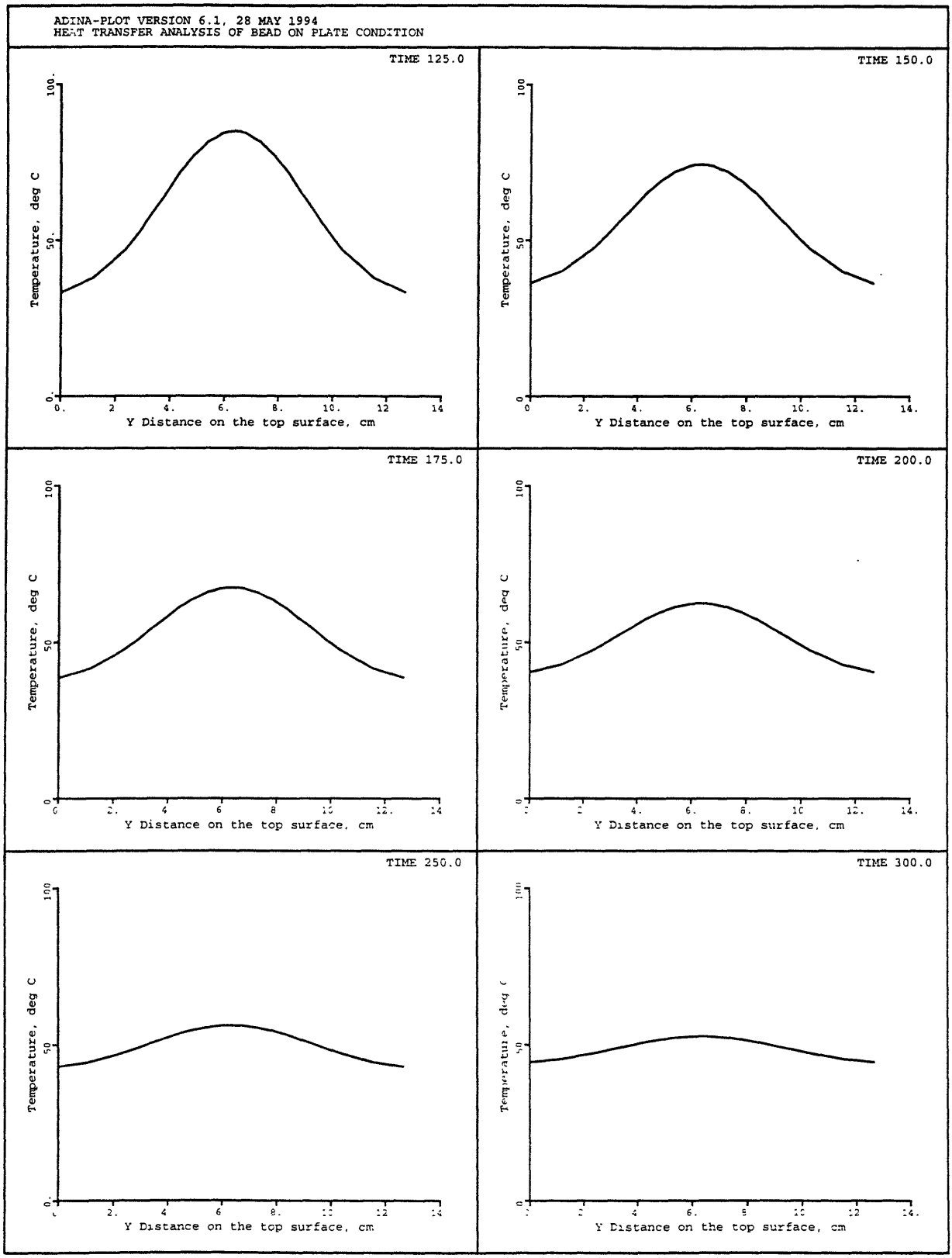

Figure 4.25 Successive temperature profiles on the top surface of plate at 125th, 150th, 175th, 200th, 250th, and 300th sec.

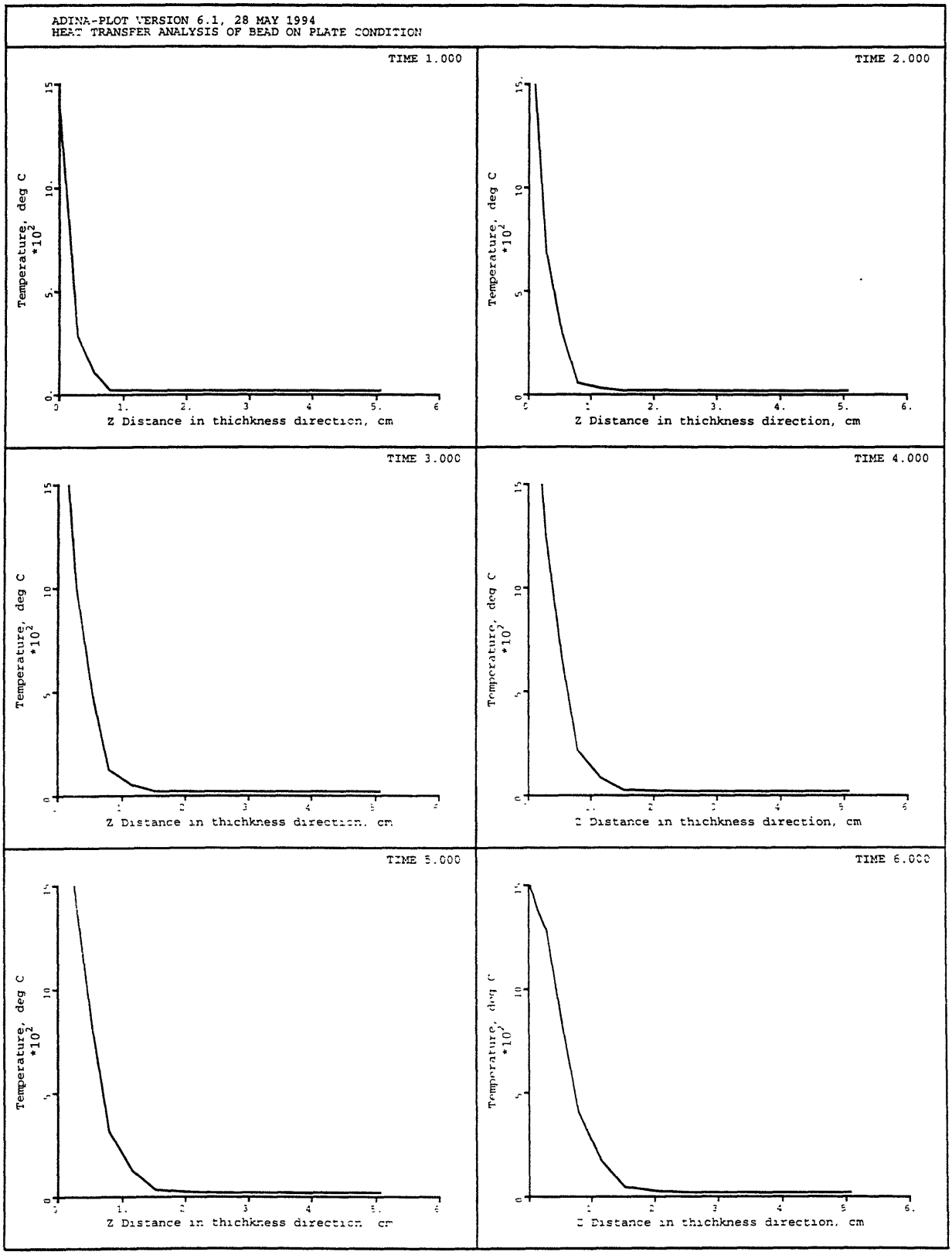

Figure 4.26 Successive temperature profiles in the thickness direction of plate at 1st, 2nd, 3rd, 4th, 5th, and 6th sec.

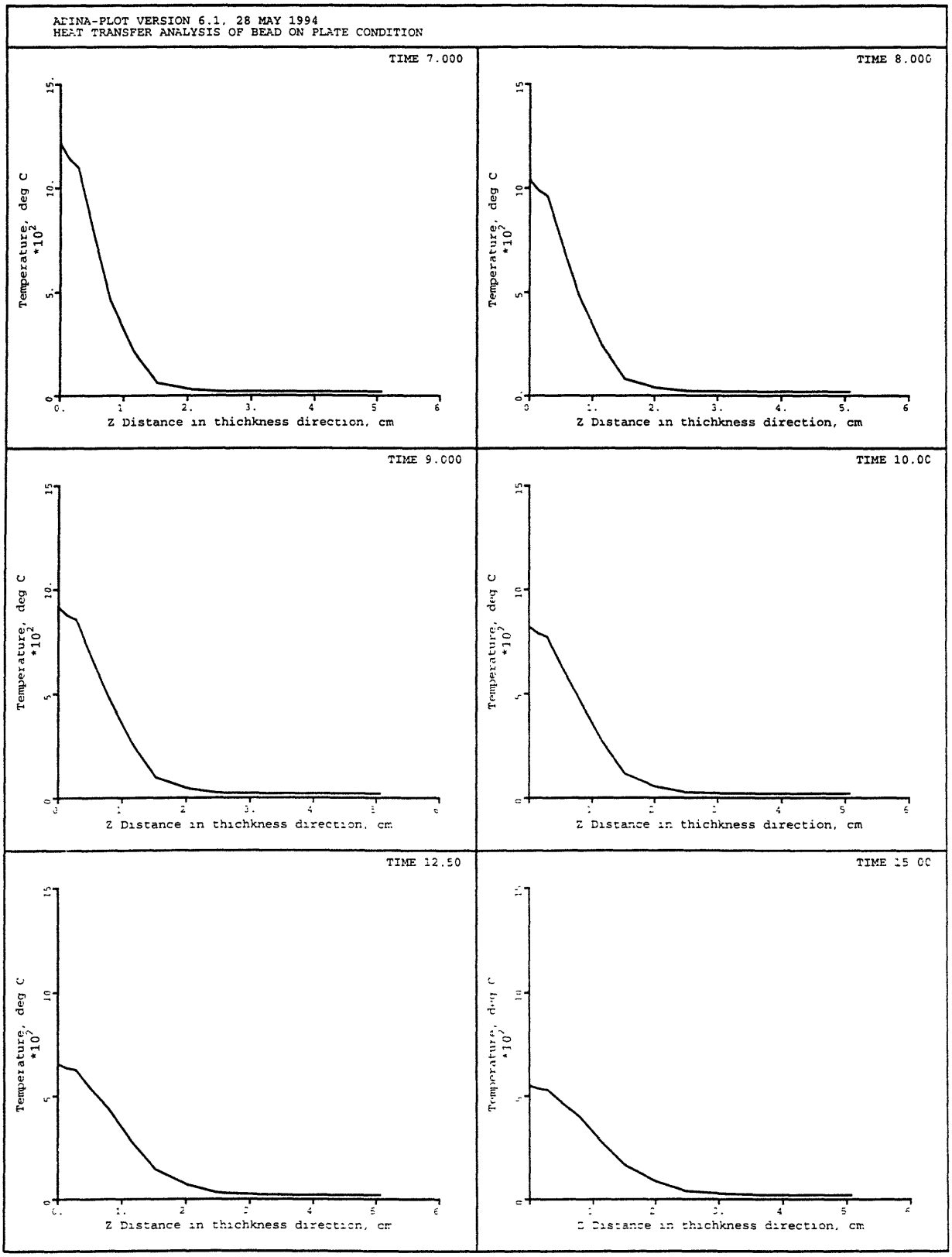

Figure 4.27 Successive temperature profiles in the thickness direction of plate at 7th. 8th. 9th. 10th. 12.5th, and 15th sec.

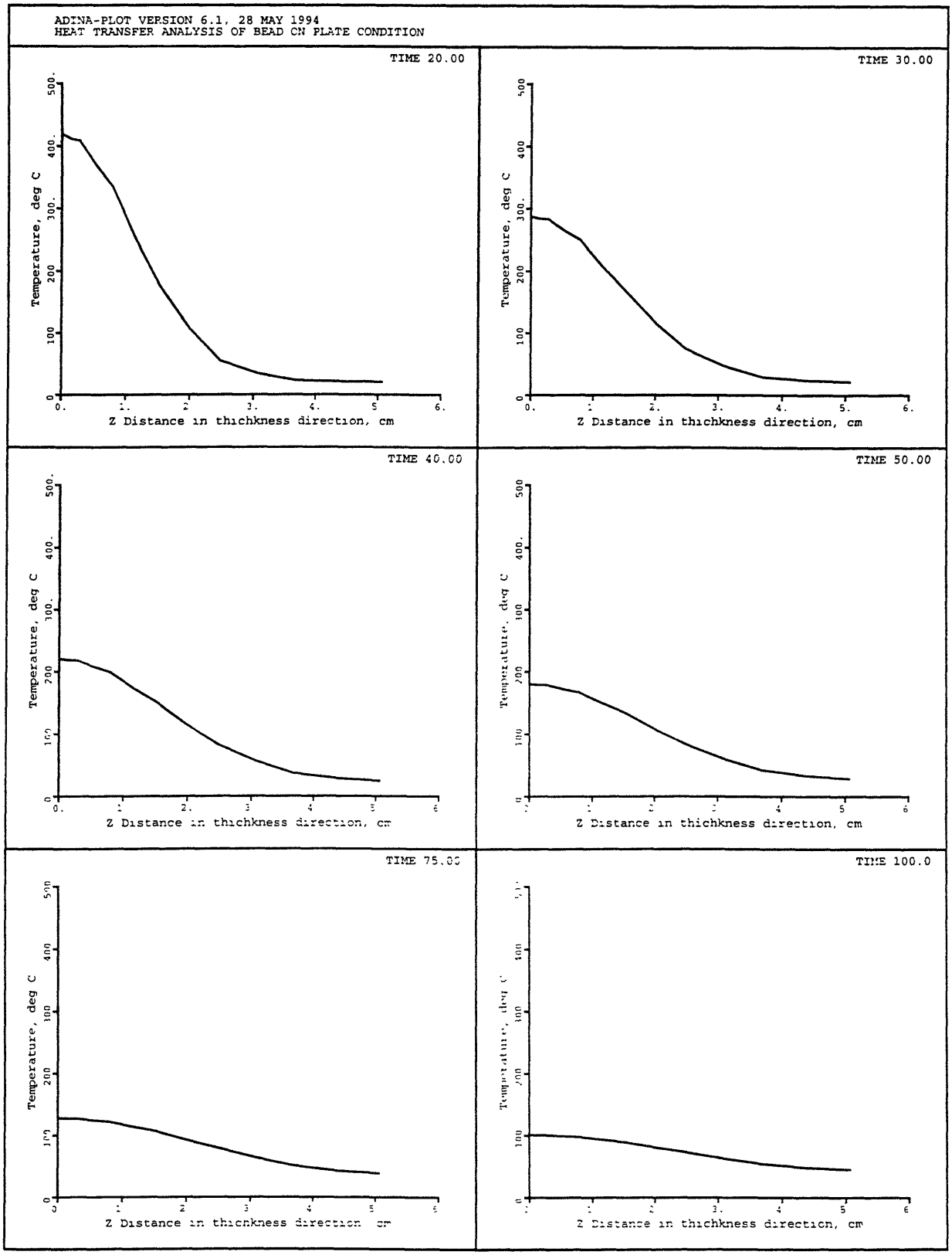

Figure 4.28 Successive temperature profiles in the thickness direction of plate at 20th. 30th. 40th. 50th. 75th. and 100th sec.

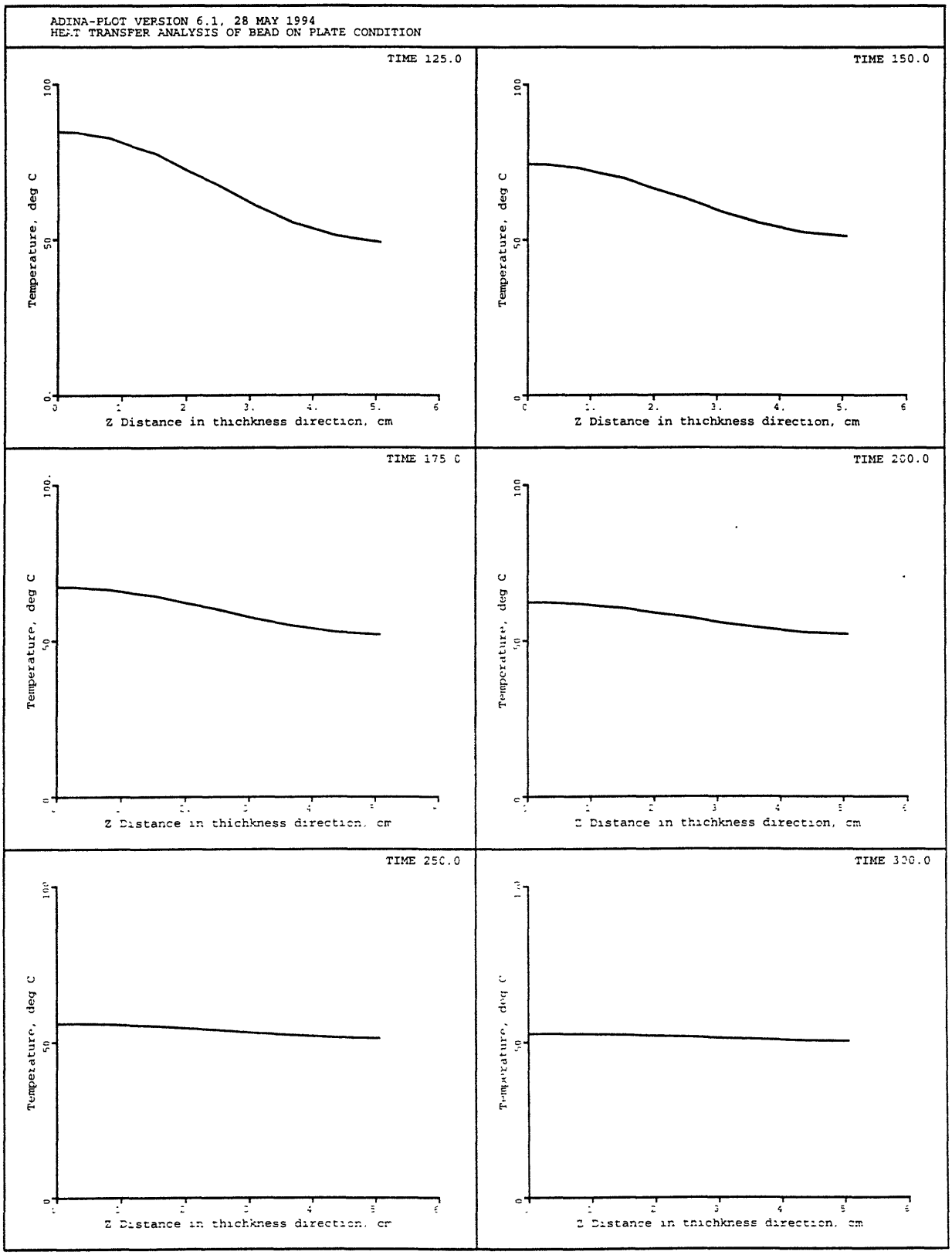

Figure 4.29 Successive temperature profiles in the thickness direction of plate at 125th, 150th, 175th, 200th, 250th and 300th sec.

The last figure in this chapter, Figure 4.30 shows the heat flux entering the base metal from the welding arc. The time steps are in welding time. The distribution of the flux input is clearly shown. It looks like the original welding process. After the welding time, heat just conducts into the base metal

.

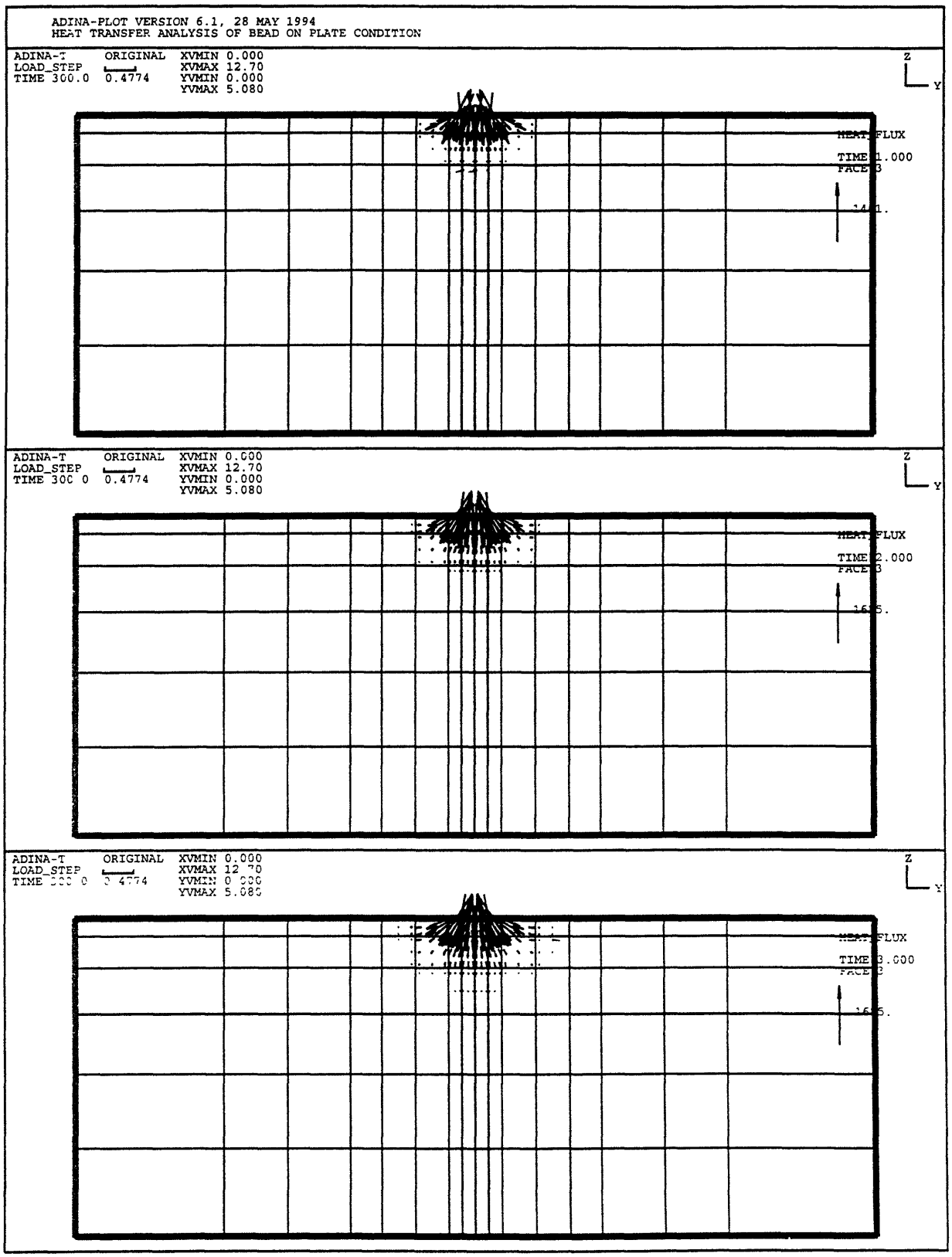

Figure 4.30 Heat flux input during welding

Chapter 5

5. Prediction of Stresses and Distortion in Plane Geometry

After successful prediction of the transient temperature field, the transient stresses and the distortion due to welding can be calculated independently from the heat flow analysis. This temperature distribution is applied to the mechanical model at discrete steps as the driving input. The calculation of the transient stress field and deformations is much more complicated than the heat transfer analysis of welding. This difficulty rises from the thermal-elastic-plastic state produced around the weld metal during welding.

In general there are two methods widely used to solve the problem described above. In this thesis the first method, so-called one-dimensional analysis, will be addressed but not used. The second one is the numerical method, a more sophisticated one based on the finite element method.

At first, a short review of literature survey of the subject will be outlined. Secondly, a one-dimensional analysis and its applications will be addressed. Third, the finite element formulation of the problem will be discussed. In the formulation, Bathe's notation[15,117] will be adopted, and his steps will be followed. Fourth, the two-dimensional finite element model for plane-strain and plane-stress cases will be introduced. Fifth, the corresponding boundary conditions and the temperature-dependent nonlinear material properties will be given. As a final step, the results of the computational analysis will be presented.

Although the transient and residual stresses will be computed in this study, particular emphasis will be given to the transient distortion and metal movement during the welding and cooling stage.

5.1 Literature Survey

A number of research programs have been carried out on residual stresses and distortion in weldments. The initial studies in this subject were started as early as 1930's. Boulton and Lance-Martin[19] discussed the transient stresses during welding along the edge of a plate in their paper published 1936. They assumed that the weld bead created a plastic zone in the vicinity of the weld and an elastic zone elsewhere. In order to estimate the plastic zone size, they used the results of experiments carefully. In following years of, 1937, 1944 and 1950, Spraragen and colleagues[119, 120, 121] conducted a series of research projects on distortion. In the 1950's, scientists in Japan performed extensive studies on residual stress and distortion. Another contribution into this field came from Russian researchers in the late 50's. In 1958, Okerblom[95] introduced a new look into the phenomena of welding distortion and residual stresses. He proposed a classification for existing approximate methods for the analysis of welding deformation. Although all of his approaches were applicable, he chose the simulation technique to solve the problem. However, simulation methods depend heavily on computers and their technology. Therefore, with the present computer technology, his efforts did not improve the situation noticeably.

The first significant attempt to use computers in the analysis of residual and transient stresses was taken by Tall[124]. While he was using the available closed form solutions of the two-dimensional heat flow analysis in welding, he introduced a step-by-step method for the calculation of thermal and residual stresses resulting in a plate welded either to the center line or edge by a moving heat source at a constant speed. Tall [124] assumed temperature-dependent

physical properties of material in his mechanical analysis. However, in order to reduce computer time he used tables to read the values instead of computing them. Consequently, he predicted the longitudinal stress, σ_x, to be a function of lateral distance y. Later, since this method assumes that the transverse stress, σ_y, and τ_{xy} are zero, it became known as the one-dimensional analysis in the literature. Based on Tall's analysis, Masubuchi[63,62] et al. developed a computer code to calculate the transient stresses and residual stress in bead-on-plate condition. Later, this program was improved by the researchers at M.I.T. under the supervision of Prof. Masubuchi.

Due to the complexity of the problem characterized by large temperature changes in small areas near the welding arc with its resulting non-elastic deformation, temperature dependency of the material properties and/or phase transformations and complex boundary conditions, resulting geometry and multipass welding, there were limited further attempts to develop this kind of analytical approach. As a result of this, the researchers were forced to attack this complex problem using numerical methods. Among the numerical methods, the finite element method is the most suitable one to apply to welding problems with a highly nonlinear inelastic nature. A wide range of nonlinear problems have been solved by using the finite element method. Moreover, at universities and private companies, many different kinds of commercial software tools have been developed. Some of these nonlinear thermo-elastic-plastic formulations were described in the papers by Bathe and co-workers[117]. The first researchers who applied the finite element method to welding problems were Hibbitt and Marcal [42]. They produced a model which treated the weld process as a thermo-mechanical problem. The proposed finite element formulation was based on uncoupled thermal and mechanical parts and it took temperature dependent properties into account. After this pioneering research, many researches including Nickel and Hibbitt [89], Hsu [43], Lobitz and co-workers, Rybicky and co-workers [106], etc. developed finite element procedures based on the first method introduced by Hibbitt and Marcal [42] to calculate residual stresses and distortion. However, these analyses

were limited to planer and axismetric problems of welding with a bead-on-plate condition. Masubuchi and his research team at the Massachusetts Institute of Technology became very active in the field towards the late 70's and developed finite element programs for plane-stress and plane-strain states. Muraki [86,87] developed a two-dimensional finite element code to calculate the thermal stress and distortion during butt welding and bead-on-plate.

Japanese investigators have also contributed to the field. Ueda and co-workers [132,133,134], Satoh et al. [111] and later Fujita and Nomoto [34] developed programs for transient stresses and distortion. Ueda and co-workers [131,132,133,134] published numerous papers in the calculation of residual stresses and developed finite element programs for computation.

In the last decade, researchers started using commercial finite element programs. However, these commercial finite element programs are general purpose programs, and welding applications require a specific model which simulates the physical behavior of the welded structure. In other words, there is no way to get the program to calculate residual stresses, transient stresses and deformation unless one makes a thermo-mechanical model that takes into account the behavior of the physical system and represents it mathematically. One of the first studies was carried out at M.I.T. by Papazoglou [96]. He developed a two-dimensional weld model which incorporated the phase deformation strains for butt welding of thick plates with multipass GMAW [96]. In 1989, Vitooraporn [136] developed his model for edge-bead-on-plate condition. He assumed a two-dimensional plane stress field to compute the transient stresses, distortion and residual stresses for high strength steels such as HY-80, HY-100, etc. Shim et al. [115] used ABAQUES to model a thermo-mechanical uncoupled system for predicting the distribution of residual stresses through the thickness of a thick plate with multipass welding process. They reported that this plane strain assumption gave reasonably good results and correlation with the experiment. Johnson et al.[47] studied residual stresses and distortion in circular welds of thin plates. A plane strain, two-dimensional, model was

used in the computation. The results were that if only the prediction of residual stresses were desired a simpler axisymmetric analysis might suffice. However, in the case of deformations, a full model of systems had to be considered and a fully transient analysis had to be performed. Chidiac and Mirza [22] developed a three dimensional nonlinear model to compute the thermal stresses, transient deflections and stresses. They reported a good agreement of the results with available results from literature and experiments.

5.2 One-Dimensional Analysis

The one-dimensional program, based on the method of successive elastic solutions introduced by Mendelson [84], was first developed for welding problems by Tall [125], and was later improved by Masubuchi. Although this method was not used in the present study, very thorough definitions of the formulation will be outlined because it is a very practical and inexpensive method to compute the stresses and distortion during the welding of thin plates. However, more detailed analyses using this method can be found in references [20, 96, 136].

As can be easily understood from the name, only the component of the stress, σ_x, in the parallel to the welding direction is considered. The other components, σ_y and τ_{xy} are assumed to be zero. Hence, under the absence of external forces the stresses equilibrium equation reduces to the following equation:

$$\frac{\partial \sigma_x}{\partial x} = 0. \tag{5.1}$$

The meaning of this equation is that $\sigma_x = \sigma_x(y)$ does not vary in the direction of x and y is the transverse distance from the weld line (Figure 5.1). Consequently, since the temperature does vary in the direction of x, equilibrium conditions are not satisfied. In order to eliminate this

incompatibility, it must be assumed that at time t, the strip is a part of an infinitely long plate subjected to a known temperature distribution $\theta(y)$ which is non-varying along its entire length.

For given Δt, the stress strain relation can be written

$$\varepsilon_x = \frac{\sigma_x}{E} + \alpha\Delta\theta + \varepsilon_x^p \tag{5.2}$$

where

ε_x^p = plastic strain,

$\alpha\Delta\theta$ = thermal strain,

$\frac{\sigma_x}{E}$ = elastic strain,

$\Delta\theta = \theta - \theta_0$.

If a single longitudinal position is considered, the entire welding process may be divided into a number of time steps, Δt. During each time step, the transverse temperature distribution was assumed to be constant. At each new time step, the temperature changed and a new stress distribution was obtained. Each time step in the fixed system corresponded to a given transverse strip in the moving system. The width of each strip was produced of the length of the time step and travel speed.

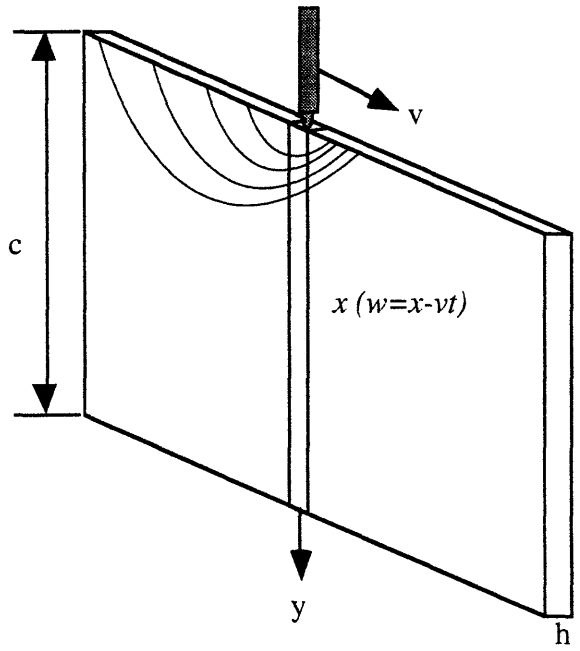

Figure 5.1 Stripped element for one-dimensional analysis

The stress, Equation 5.2, at each time step is calculated using the method of successive elastic solution. The stress-strain relation is used and the strain obtained is also made to satisfy the compatibility equation for one-dimensional analysis.

$$\frac{\partial^2 \varepsilon_x}{\partial y^2} = 0 \tag{5.3}$$

hence

$$\varepsilon_x = c_1 + c_2 y \tag{5.4}$$

which essentially states that plane sections remain plane and this is the usual assumption of simple beam theory. The boundary conditions are used to determine the c_1 and c_2. Under the presence of external forces, the equilibrium equations, force and moment, are

$$\int_{-c}^{c} \sigma_x dy = 0 \tag{5.5}$$

$$\int_{-c}^{c} \sigma_x y dy = 0 \tag{5.6}$$

where c is the plate width.

Rewriting Equation 5.2 in the form of

$$\sigma_\lambda = E\left(\varepsilon_x - \alpha\Delta\theta - \varepsilon_x^p\right) \tag{5.7}$$

and substituting this equation with Equation 5.4 into Equation 5.5 and Equation 5.6 enables one to have five equations with five unknowns, ε_λ, and four constants. However, one of the unknowns, ε_x, is not independent of the other four. Hence, there is one more equation needed to solve the problem. The strain-stress relation must be used as fifth equation.

5.3 Finite Element Formulation

The multipurpose finite element program ADINA (Automatic Dynamic Incremental Nonlinear Analysis)[2,3] will be used to predict the thermal stresses, thermal strains, plastic stresses in the vicinity of the weld, displacement and residual stresses. The solution procedure and formulation of thermo-elastic-plastic problems including creep were introduced by Snyder and Bathe [117]. In this section, this model will be discussed and Bathe's formulation will be adopted[15].

5.3.1 Thermo-Elastic-Plastic Model

The model presented includes the combined effects of thermoelasticity and thermoplasticity. All material properties are assumed to vary with temperature. Von Misses yield function is considered in the thermoplasticity part. Moreover, this model can utilize the creep as well. However, the particular problem in this study did not consider the creep because the total welding time is around 5 seconds. This duration is small enough to neglect the effect of the creep.

5.3.1.1 Formulation and FEM Discretization

The formulation of the model with small strains assumption can be written as

$$^{\tau}e_{ij}=^{\tau}e_{ij}^{E}+^{\tau}e_{ij}^{P}+^{\tau}e_{ij}^{TH} \tag{5.8}$$

where

$^{\tau}e_{ij}$ = component of total strain tensor,

$^{\tau}e_{ij}^{E}$ = component of elastic strain tensor,

$^{\tau}e_{ij}^{P}$ = component of plastic strain tensor,

$^{\tau}e_{ij}^{TH}$ = component of thermal strain tensor,

and τ is the time of interest.

The constitutive law in stress strain relation for an isotropic continuum can be written for thermoelastic model temperature dependent modulus as follows:

$$^{\tau}\sigma_{ij}=^{\tau}C_{ijrs}^{E}\,^{\tau}e_{ij}^{E} \tag{5.9}$$

or using the relation given in Equation 5.8, the component of the Couchy stress tensor is

$$^{\tau}\sigma_{ij}={}^{\tau}C^{E}_{ijrs}\left({}^{\tau}e_{rs}-{}^{\tau}e^{P}_{rs}-{}^{\tau}e^{TH}_{rs}\right). \tag{5.9}$$

where

$^{\tau}C^{E}_{ijrs}$ = component of elastic constitutive tensor,

$$= {}^{\tau}\lambda\delta_{ij}\delta_{rs}+{}^{\tau}\mu\left(\delta_{ir}\delta_{js}+\delta_{is}\delta_{jr}\right),$$

$$^{\tau}\lambda = \frac{{}^{\tau}E\,{}^{\tau}\nu}{\left(1+{}^{\tau}\nu\right)\left(1-2\,{}^{\tau}\nu\right)},$$

$$^{\tau}\mu = \frac{{}^{\tau}E}{2\left(1+{}^{\tau}\nu\right)},$$

$^{\tau}E$ = Young's modulus,

δ_{ij} = Kronecker delta,

The thermal stresses are $^{\tau}e^{TH}_{rs}$ and it is given as

$$e^{TH}_{rs}={}^{\tau}\alpha_{m}\left({}^{\tau}\theta-\theta_{R}\right)\delta_{rs} \tag{5.10}$$

where

$^{\tau}\theta$ = material temperature at time τ,

θ_{R} = reference temperature,

$^{\tau}\alpha_{m}$ = mean coefficient of thermal expansion.

The plasticity equations, which consider the plastic behavior of material, such as the yield condition, the flow rule and the hardening rule are presented[1]. Plastic flow starts when the stress field reaches a certain state. The researchers defined this state with several yield criteria. Among those, this study utilizes the von Misses yield criteria. The flow rule model relates to

---

[1]A hardening rule describes the change in the yield surface with the continuing plastic deformation.

the plastic strain increment with stress conditions which include current stresses and stress increments after yielding occurs. There are two way of hardening rule. The first one is isotropic which assumes that the size of the yield surface increases uniformly while its center remains fixed in a nine-dimensional stress space. The second is kinematic hardening rule that assumes that both the size of the yield surface and the hardening of the material can depend on temperature. In ADINA, either isotropic or kinematic hardening can be assumed.

The general form of yielding condition is defined as follows:

$$^{\tau}F = {}^{\tau}F\left({}^{\tau}\sigma_{ij}, {}^{\tau}\alpha_{ij}, {}^{\tau}\sigma_{y}\right) \tag{5.11}$$

where

$^{\tau}\alpha_{ij}$ = coefficient of thermal expansion,

$^{\tau}\sigma_{y}$ = yield stress.

Moreover, these two quantities are the functions of plastic deformation and temperature. Plastic deformation starts when $^{\tau}F = 0$, and for the elastic deformations, $^{\tau}F$ is less then zero, $^{\tau}F < 0$.

As a consequence of Drucker's postulate for stable inelastic materials, $^{\tau}F$ defines a convex yield surface in a ten-dimensional stress-temperature space. Moreover, when stress and plastic strain rate axes are coincident the plastic strain rate vector is normal to the yield surface. Hence, the plastic strain rate is defined by

$$^{\tau}\dot{e}_{ij}^{P} = {}^{\tau}\Lambda \frac{\partial {}^{\tau}F}{\partial {}^{\tau}\sigma_{ij}} \tag{5.12}$$

where ${}^{\tau}\Lambda$ is a positive scalar variable and the dot indicates the differential increment in time. Here, in order to define the values of ${}^{\tau}\Lambda$, we have to choose one of the hardening rules we mentioned earlier. The values of ${}^{\tau}\Lambda$ for both hardening rules were derived by Snyder and Bathe[117]. However, in the expression of ${}^{\tau}\Lambda$, there are two terms, $\partial^{\tau}\sigma_y/\partial^{\tau}e^P$ and $\partial^{\tau}\sigma_y/\partial^{\tau}\theta$, remaining as unknowns. In order to evaluate these terms, a relationship between ${}^{\tau}\sigma_y$, ${}^{\tau}\theta$, and ${}^{\tau}e^P$, had to be derived from the experimental data obtained from a series of tensile tests at different temperatures using virgin material specimens.

At time $t+\Delta t$, the finite element discretization of constitutive equations are given in vector form as follows [117]:

$$ {}^{t+\Delta t}\sigma = {}^{t+\Delta t}C^E\left({}^{t+\Delta t}e - {}^{t+\Delta t}e^P - {}^{t+\Delta t}e^{TH}\right) \tag{5.13}$$

and the equilibrium equation is

$$ {}^{t+\Delta t}K^E\,{}^{t+\Delta t}U = {}^{t+\Delta t}R - \int_{v} B_L^T\,{}^{t+\Delta t}C^E\left({}^{t+\Delta t}e^P + {}^{t+\Delta t}e^{TH}\right) \tag{5.14}$$

where the first term, K^E, is the elastic stiffness matrix and it is given by

$$ {}^{t+\Delta t}K^E = \int_{v} B_L^T\,{}^{t+\Delta t}C^E B_L\,dv \tag{5.15}$$

$$ {}^{t+\Delta t}e^P = {}^{t}e^P + e^P \tag{5.16}$$

R = nodal external force vector,

U = nodal point displacement vector,

C^E = stress-strain matrix,

B_L = total strain-displacement transformation matrix,

e^P = plastic strains given by

$$e^P = \Delta t^{t+\Delta t} \Lambda D^{t+\Delta t} \sigma \tag{5.17}$$

D = deviatoric stress operator matrix.

In the solution steps of these incremental equations, a very important issue is the accuracy of the numerical integrations at time $t + \Delta t$ and increment i. In these cases, the integrations are performed using the a-method where a=0 and 1 corresponds to the Euler forward (explicit) and backward (implicit) methods, respectively. The implicit schema may produce a better stability state. However, it is more expensive since it uses iterations for equilibrium state. Furthermore, by using the sub increments at each time step, the accuracy of integration may be enhanced.

5.4 Two-Dimensional Weld Model Using FEM

An important subject in modeling of welding problems is dealing with the stress state in the near regions of weld. In this analysis of thermal stresses and strains during bead-on-plate welding, the following assumptions were made:

- The molten zone is state of zero stress. In other words, stresses are zero in the regions where temperatures exceed the melting temperature.
- Solidified material recovers its initial material properties. In other words, the material, under welding temperature, behaves like the original material at corresponding temperature.
- No creep occurred due to the very short duration of welding process, 5 seconds.

The two-dimensional finite element weld model for bead-on-plate condition will be introduced under these assumptions. The temperature data obtained from ADINA-T analysis and stored in a file will be used as external forcing function in ADINA program. In order to perform a thermo-elastic-plastic analysis without creep, the creep law number was set to zero. The

deformed mesh, transient stresses, accumulated effective plastic strains, plastic stress, transient thermal stress, and transient displacements are calculated. Graphic illustrations of this will be shown in corresponding figures.

After presenting the mesh design consideration, boundary conditions will be handled. The temperature-dependent material properties will be discussed and their variations with temperature will be graphically illustrated. The plane-stress and plane-strain cases will be considered separately. At the end of the section, the results of the computer simulation will be presented.

5.4.1 Mesh Design

The same finite element mesh, whose number and type of elements, etc., and number of nodal points are the same as in heat transfer analysis, ADINA-T[4] is used in ADINA[2,3] analysis. Two-dimensional nine-node solid elements are used in the ADINA analysis. All the nodes except for those constraints, have two degrees of freedom, namely y and z translations. As shown in Figure 5.2, a total of 428 nodes and 96 elements were utilized.

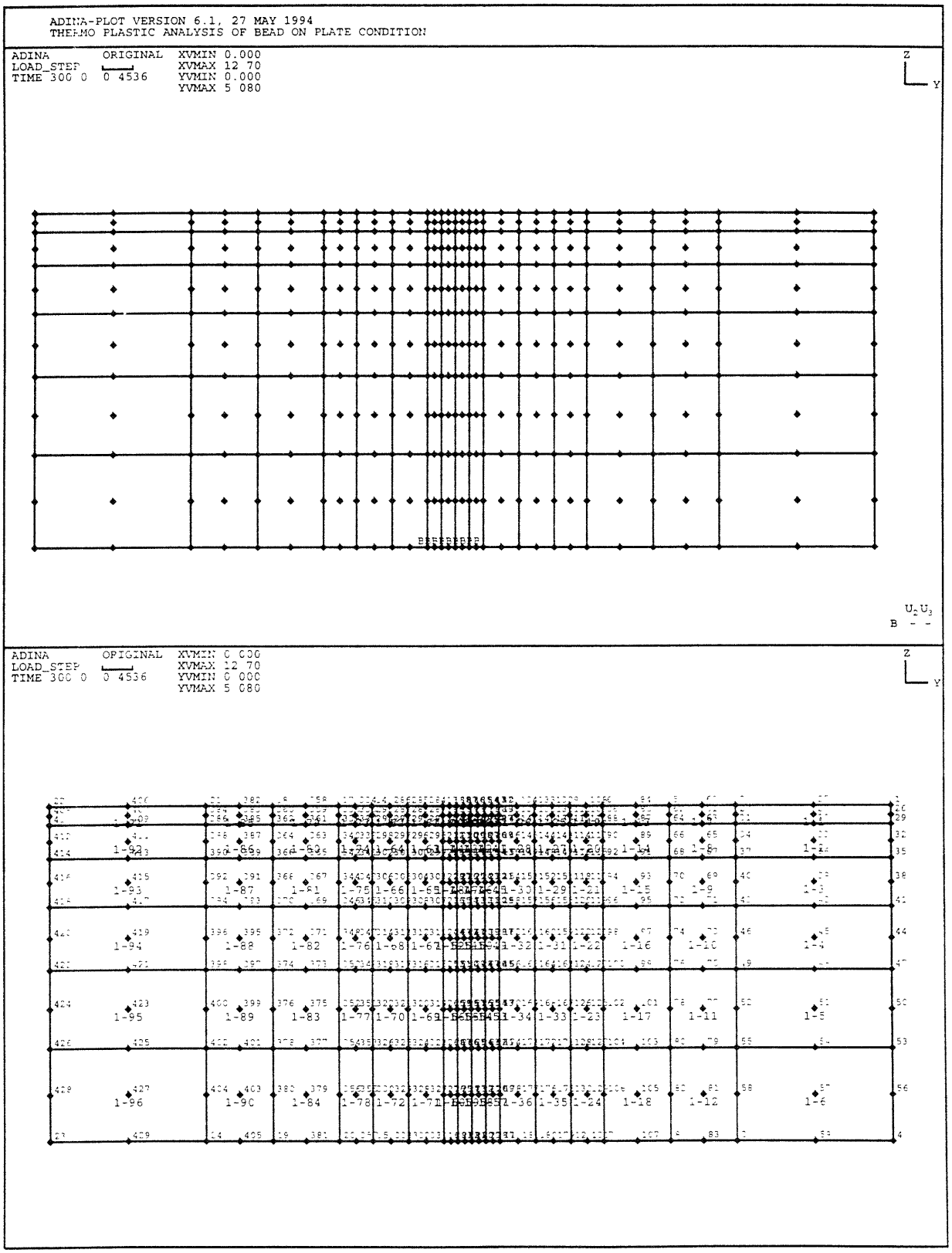

Figure 5.2 Finite element mesh and imposed boundary conditions

5.4.2 Boundary Conditions

The boundary conditions are chosen in such a way that they simulate the behavior of the physical system. Moreover, they are restrained as they are used in the experiment to eliminate possible rigid body motion, otherwise one cannot obtain a positive definite stiffness matrix. The Figure 5.2 shows the constraints imposed: nodes 11, 16, 277, 278, 279, 280, 281, and 282 are fixed in y and z directions.

5.4.3 Temperature Dependent Material Properties

The temperature-dependent material properties are accepted in ADINA program to perform non-linear thermo-elastic-plastic model. As an input, temperature dependent variations of Young's modules, E, virgin yield stress, σ_y, Poisson's ratio, ν, strain hardening modules, E_T, and the thermal expansion coefficient, α, are specified in input file.

As it was mentioned earlier, at elevated temperatures where the metal is like liquid, the molten material does not have any strength. Hence, the values of the mechanical properties at this temperature are equal to zero. However, the zero properties cannot be defined as input in the program. Therefore, to avoid the instability conditions, very small values of Young's module, virgin yield stress and strain hardening modules should be used above the liquidus temperature.

Papazoglou[], pointed out that the accumulation of plastic strains in the regions which become molten during the welding cycle needs to be considered. When the temperature reaches liquidus, these plastic strains are physically relieved, starting to accumulate again when the metal solidifies. The presence of non-zero material properties above the liquidus, however,

would cause the plastic strains not only to continue accumulating but also to reach artificially high values caused by the very low values of material properties.

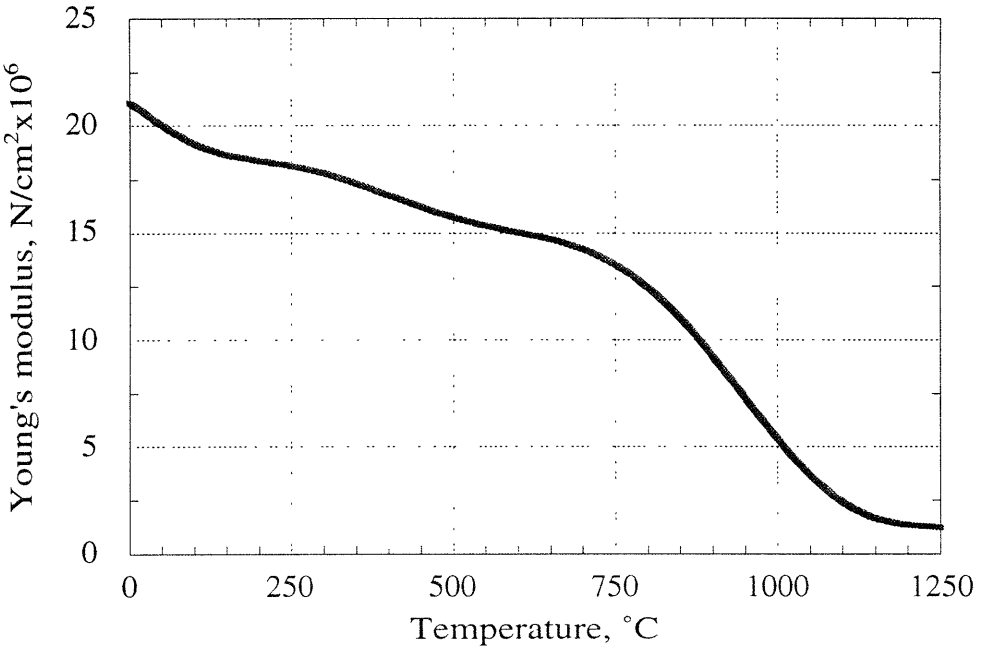

Figure 5.3 Temperature-dependent Young's modulus (304 SUS)[7]

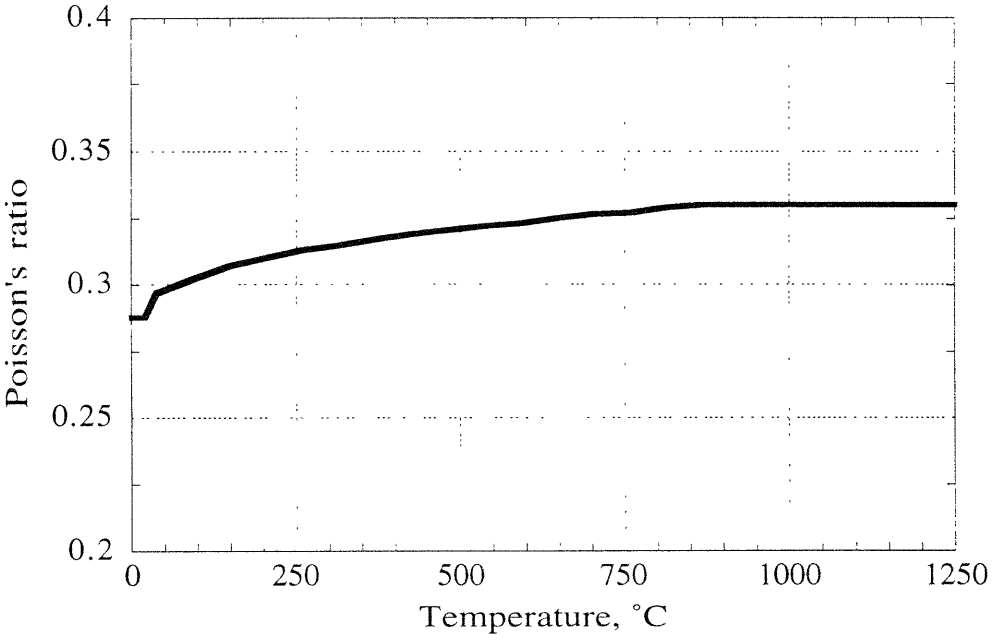

Figure 5.4 Temperature-dependent Poisson's ratio (304 SUS)

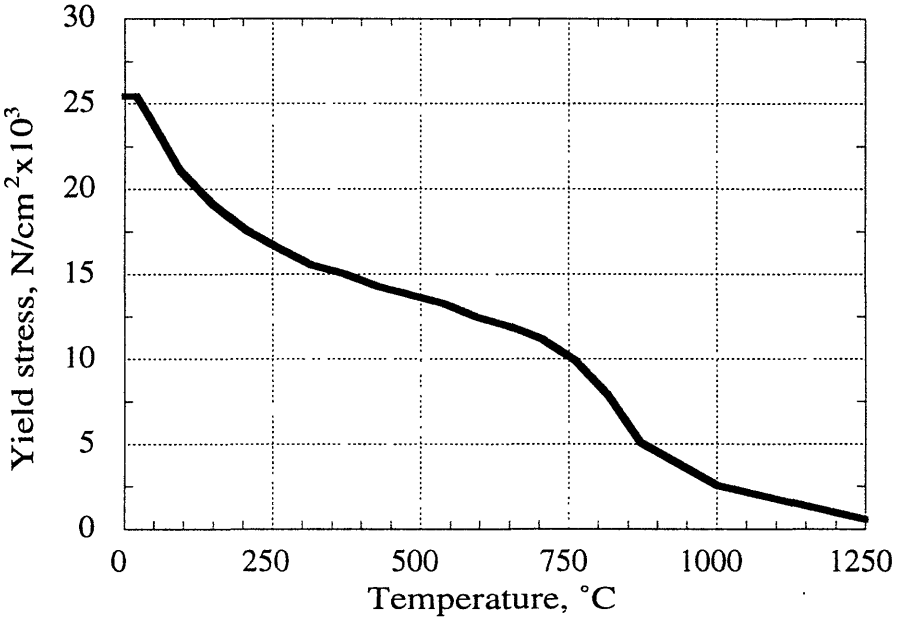

Figure 5.5 Temperature-dependent yield stress (304 SUS)[7]

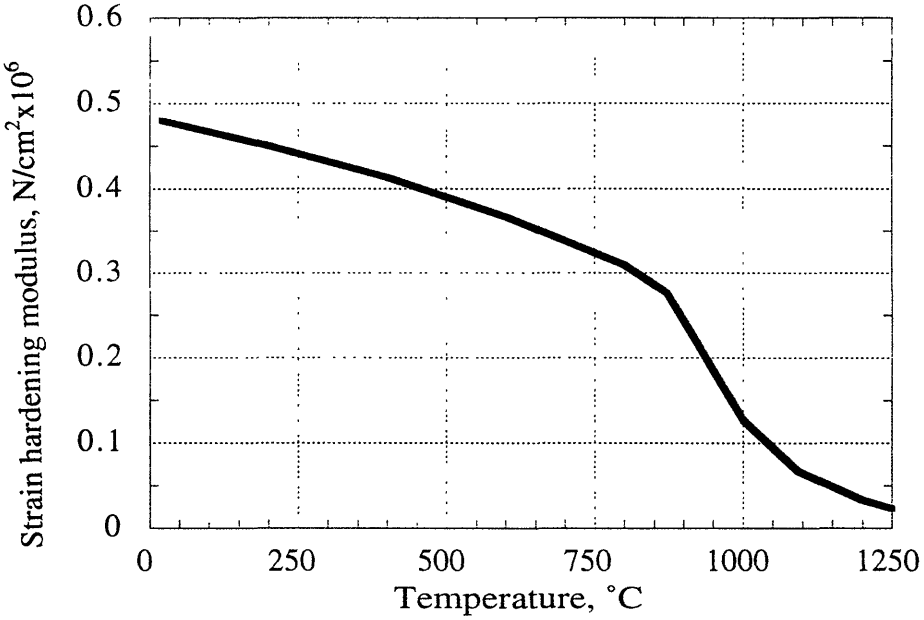

Figure 5.6 Temperature-dependent strain hardening modulus (203 SUS)[7]

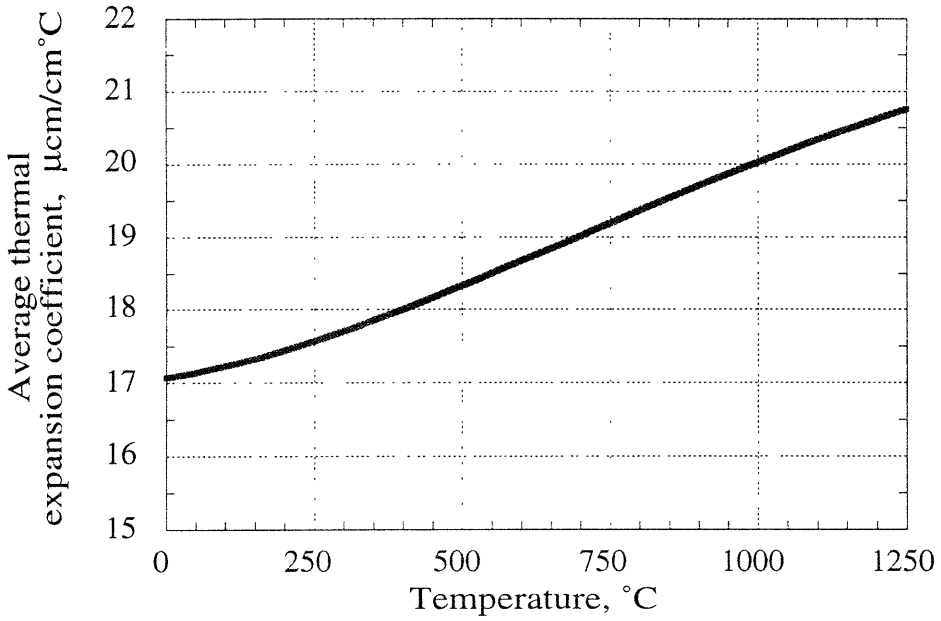

Figure 5.7 Temperature-dependent average thermal expansion coefficient (304 SUS)[7]

5.4.4 Solution Strategy

In the modeling of the two-dimensional welding problems, plane-stress and plane-strain states are widely used. In this study, both states are considered for a welding model. However, our experimental geometry and the problem is in the state of plane stress. Therefore, the most important stress component is σ_y. Since the analysis involves plastic deformation at elevated temperatures, the analysis requires a very long CPU time. One of the simplest welding models considered in this study required 2.5 hours CRAY time. If the same geometry was modeled as three dimensional stress-strain field, it would be just too expensive.

5.4.4.1 Plane Stress Case

The plane stress state assumes that stress component is not present in thickness direction. In other words, the plane stress σ_z, σ_y, and τ_{yz} are functions in the plane defined by z and y. Hence, the other components of the stress tensor, namely σ_x, τ_{yx}, and τ_{zx}, are identically equal to zero. Plane stress assumption is mostly used in bead-on-edge welding conditions and stationary welding processes, such as spot and pulse welding. In this case, the in-plane transient stresses, $\sigma_z(t)$ and $\sigma_y(t)$, distortion, $u_z(t)$, and $u_y(t)$, residual stresses, and accumulated plastic stresses can be computed. Moreover, as is very obvious, the distortion ahead of the arc can easily be predicted.

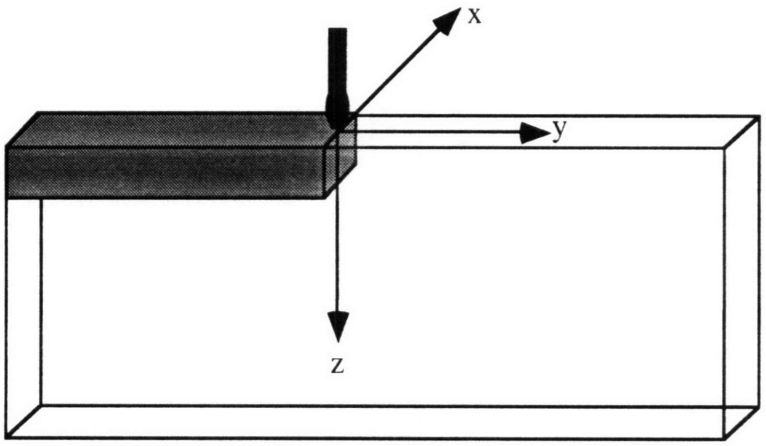

Figure 5.8 Plane stress geometry

5.4.4.2 Plane Strain Case

This assumption implies that all sections normal to the weld line remain plane during the entire welding process. In other words, the out of plane displacement is zero, σ_z, σ_y, σ_x, and τ_{yz} are functions of y and z and $\varepsilon_x = \tau_{yx} = \tau_{zx} = 0$. Although this assumption is adequate in regions somewhat removed from the weld puddle, it may not be valid in the neighborhood of the weld pool. This approach, therefore, prevents the calculation of distortion ahead of the welding arc, and may inhibit accurate computations of deformations in the immediate vicinity of the weld puddle. Plane strain assumption enables one to determine complete transient strains, transient stress and residual stress distributions, transverse distortion, and plastic stresses.

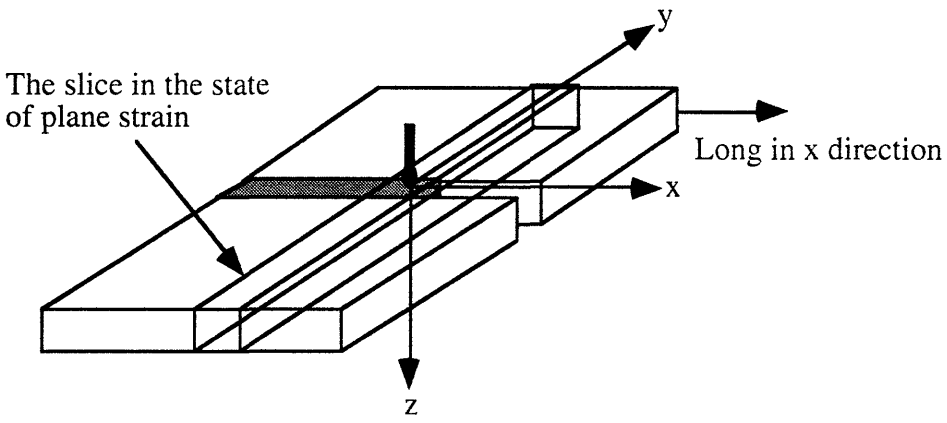

Figure 5.9 Plane strain state of welding problem

The typical applications of plane strain case are bead-on-plate of long plates, butt welded plates, etc.

5.5 The Results of Computations

The computations were carried out at CRAY X-MP supercomputer installed at M.I.T. Super Computing Facility. Pre and post processing, ADINA-IN and ADINA-PLOT, were performed with DEC 5000 workstation in the Welding Systems Laboratory. The results, the computed transient stresses, deformation, thermal strains, and plastic strains are presented in the following figures.

ADINA-PLOT was used to perform the graphical presentations of data. The output of ADINA was processed by using ADINA-PLOT and the following plots were obtained.

ADINA-PLOT is able to plot the transient stresses, strains, and distortions. In addition, accumulated effective plastic strains were plotted successively.

As it was mentioned earlier, compressive plastic strains are developed in the vicinity of the weld due to the restraining of surrounding metals. The plastic strains cause plastic deformations after welding. Figures 5.10, 5.11 and 5.12 show the successive development of plastic strains along the top surface of plate. As soon as welding starts, the metal under the welding arc starts to expand but the surrounding metals at lower temperatures do not allow this expansion. Consequently, under a reduced yield stress at high temperatures, the area around the weld starts to yield plastically under compression. This phenomena is well established in the Figures 5.10 and 5.11. Immediately after welding is completed, that is after 5 seconds, the development of these compressive plastic strains come to a stop but they remain in the structure. In Figure 5.12, the upper left corner corresponds to the state of plastic strains at sixth second, one second after welding, and the lower right corner is the end of cooling time. The difference between these pictures is very small. Similarly, these compressive plastic strains reached the maximum value as soon as welding was completed.

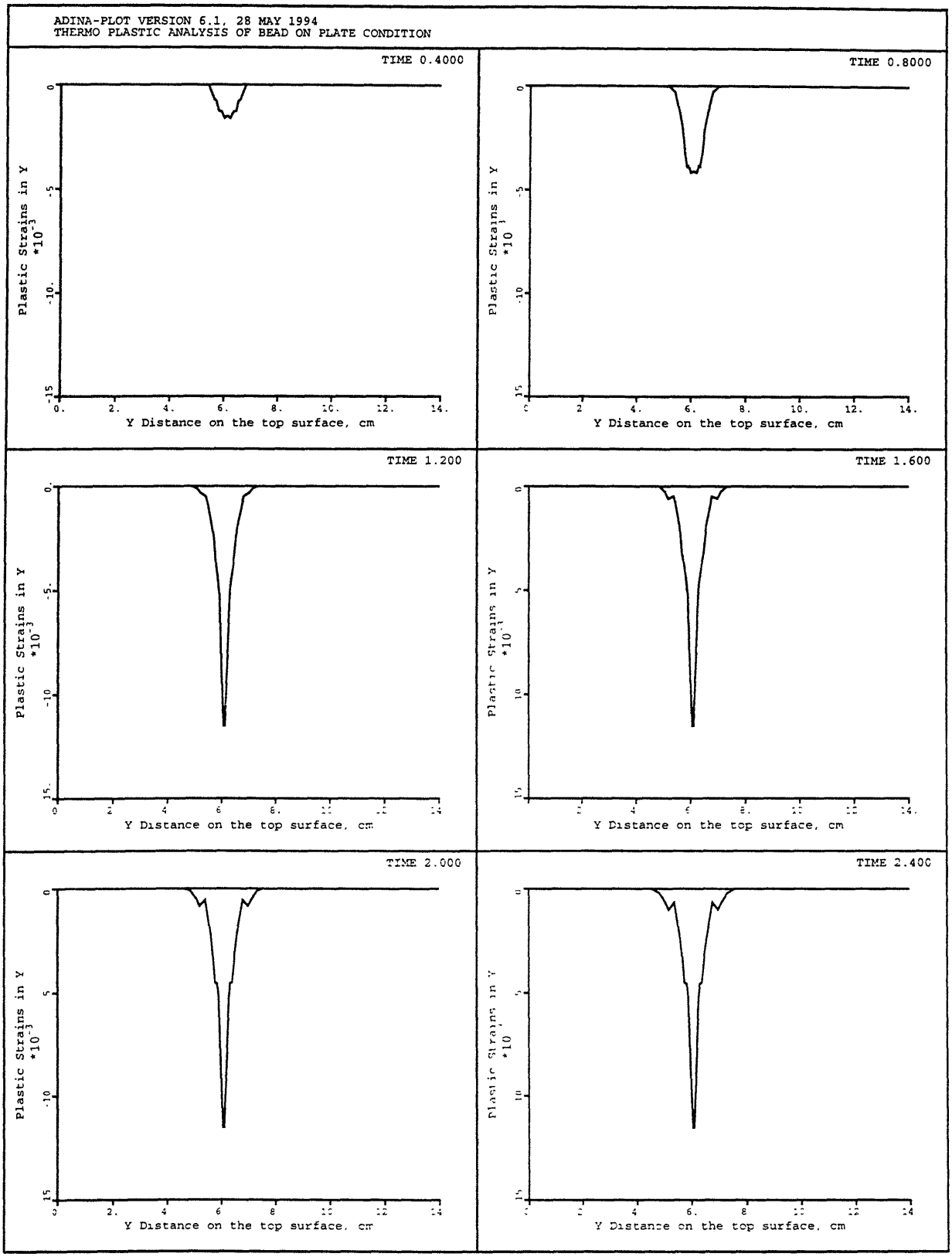

Figure 5.10 Successive development of compressive plastic strains in the neighborhood of the weld during welding

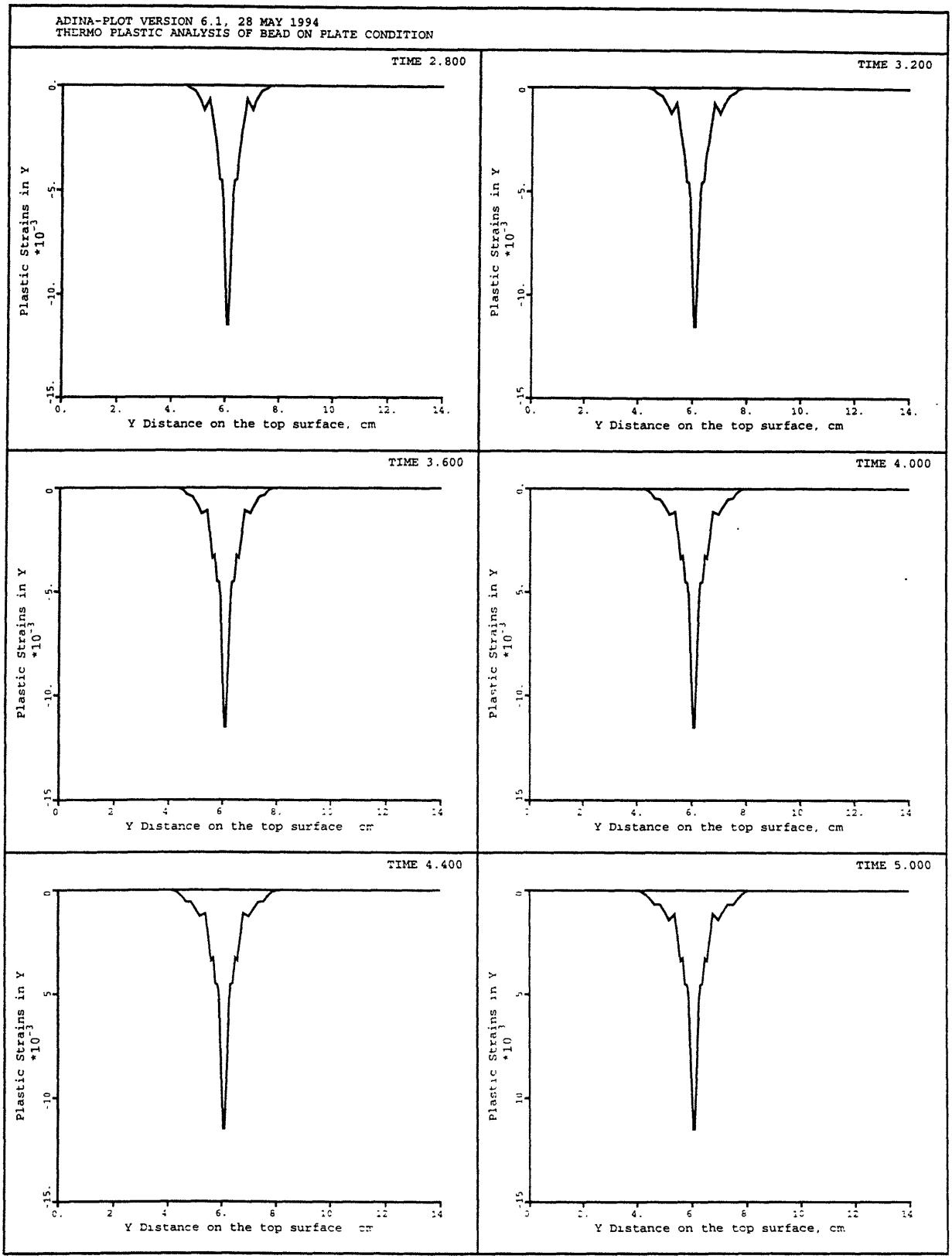

Figure 5.11 Successive development of compressive plastic strains in the neighborhood of the weld immediately after welding

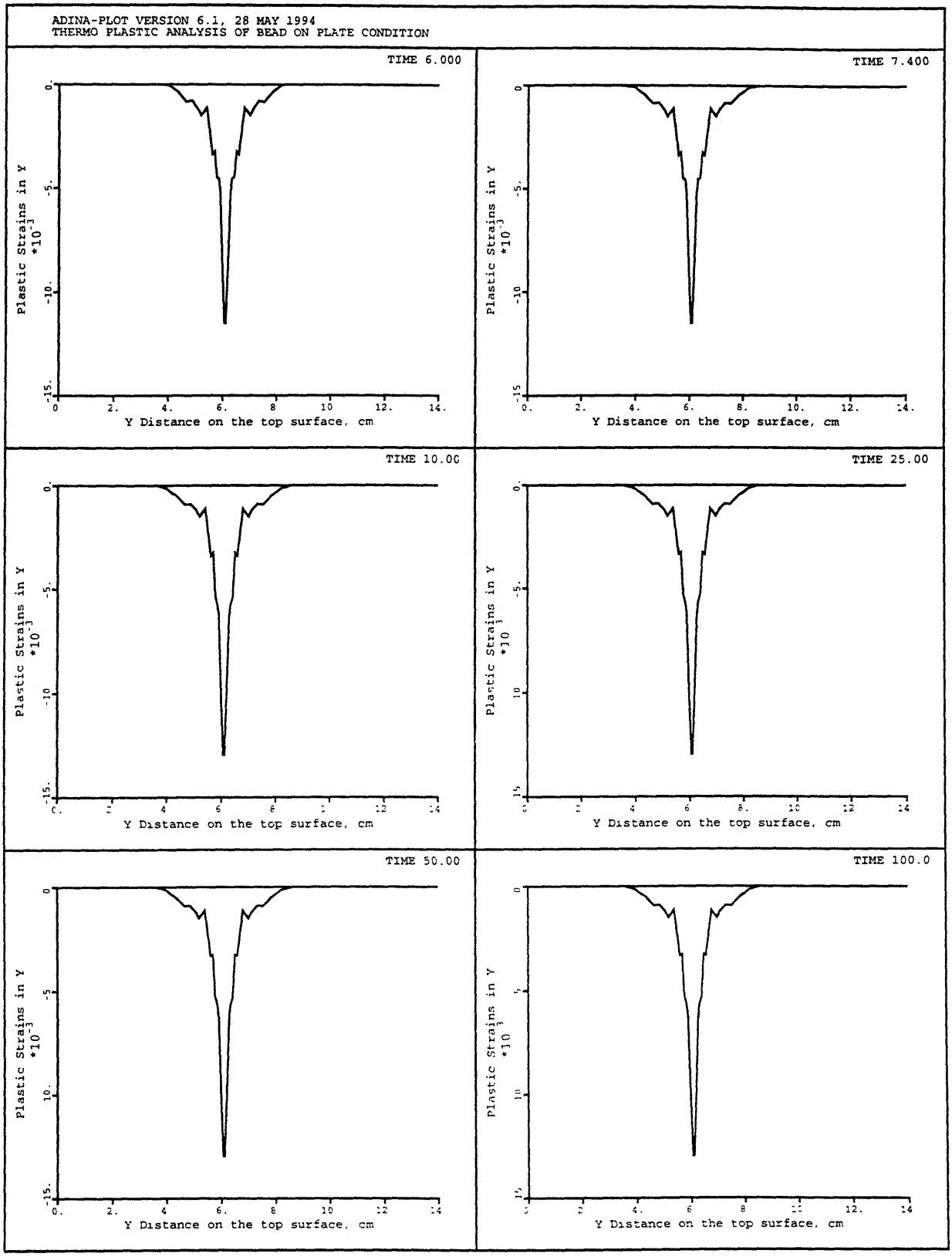

Figure 5.12 Successive development of compressive plastic strains in the neighborhood of the weld at the end of cooling

The same steps are followed in the thickness direction. Figure 5.13, 5.14, and 5.15 show the development of plastic strains in the thickness direction. Here again, just after welding, the plastic strains approach their maximum values rapidly and remain in the structure afterwards.

A more complete history of the accumulated plastic strain is shown in Figures 5.16, 5.17, 5.18, 5.19, 5.20, and 5.21. Plots of accumulated plastic strain versus time at various locations on the surface of the plate are shown in Figure 5.16. In the weld metal zone, plastic strain builds rapidly as the material yields in compression. At the melting region those plastic strains are completely relieved, to rapidly reach again a level in close proximity to that of the existing level prior to melting upon solidification. As cooling continues and yielding in tension progresses, the plastic strain steadily increases but at a smaller rate. In the heat affected zone, plastic strain is accumulated during heat-up in much the same way as in the weld metal zone but not quite as rapidly.

The successive accumulation of plastic strains are presented step by step in Figures 5.17, 5.18, 5.19, 5.20 and 5.21. The rapid accumulation of plastic strains , e^p, was observed during and just after welding and the development of these strains slowed down during cooling. After a certain time, that is eight seconds, the accumulation stopped and these values remained in the structure.

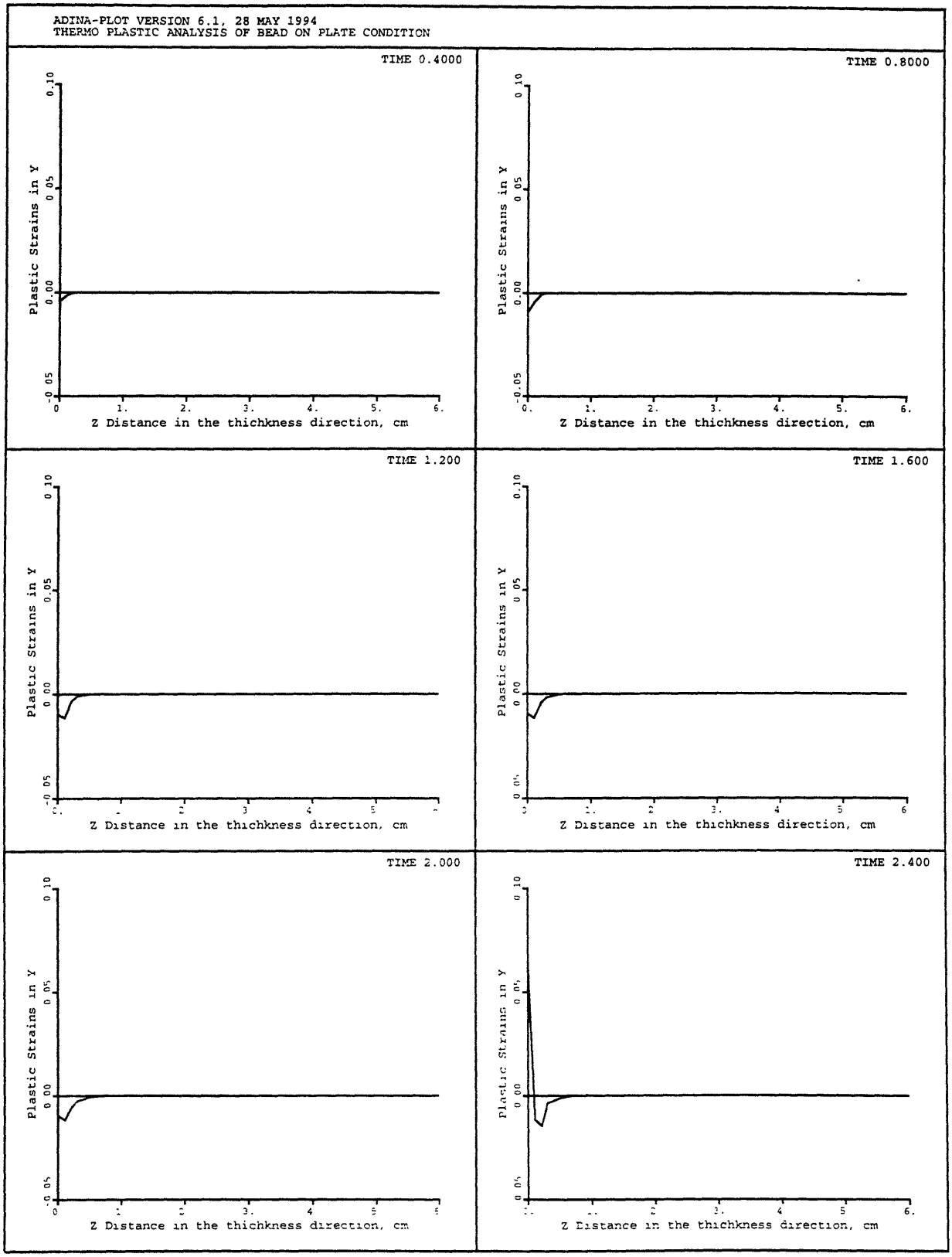

Figure 5.13 Successive development of compressive plastic strains in thickness direction during welding

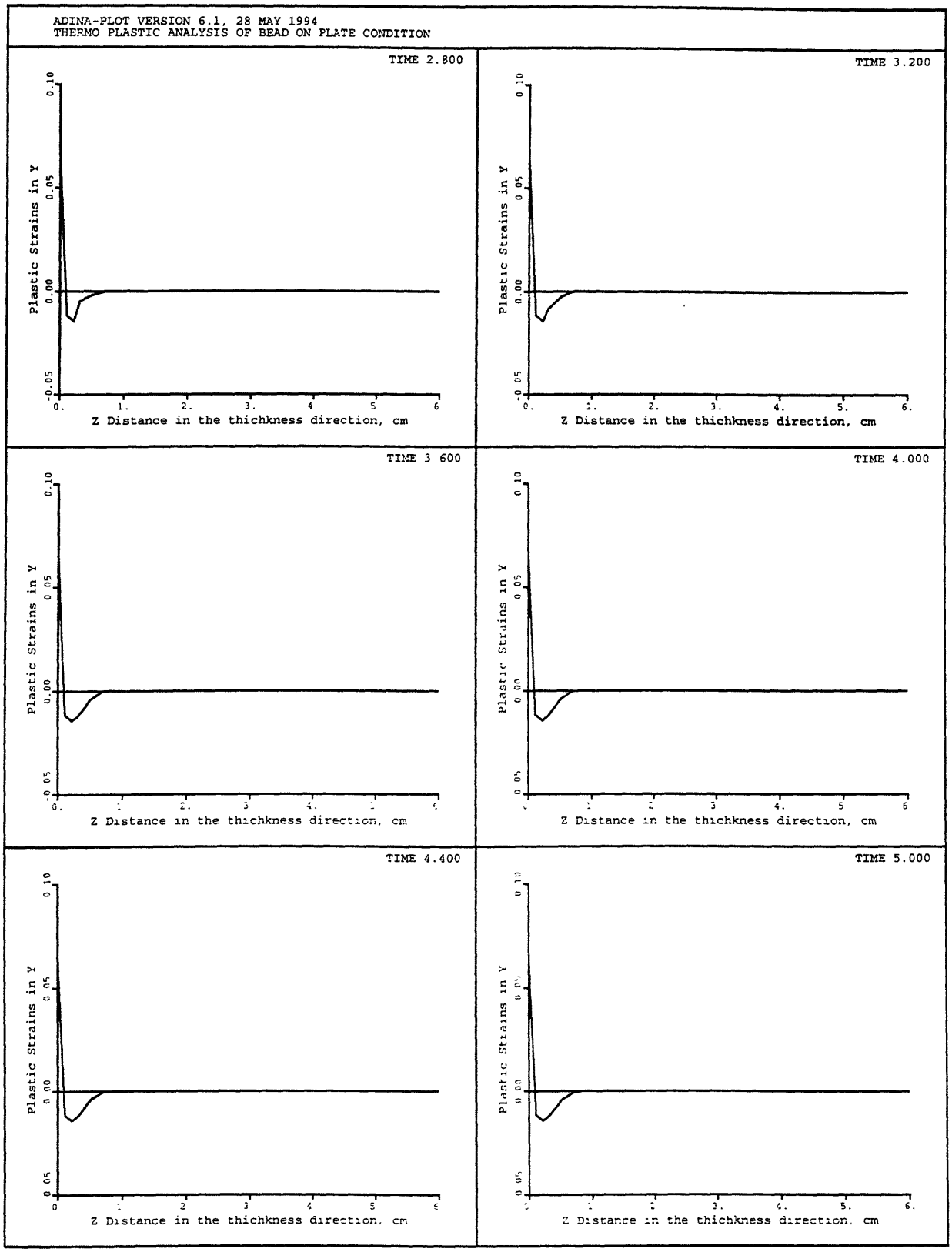

Figure 5.14 Successive development of compressive plastic strains in thickness direction after welding

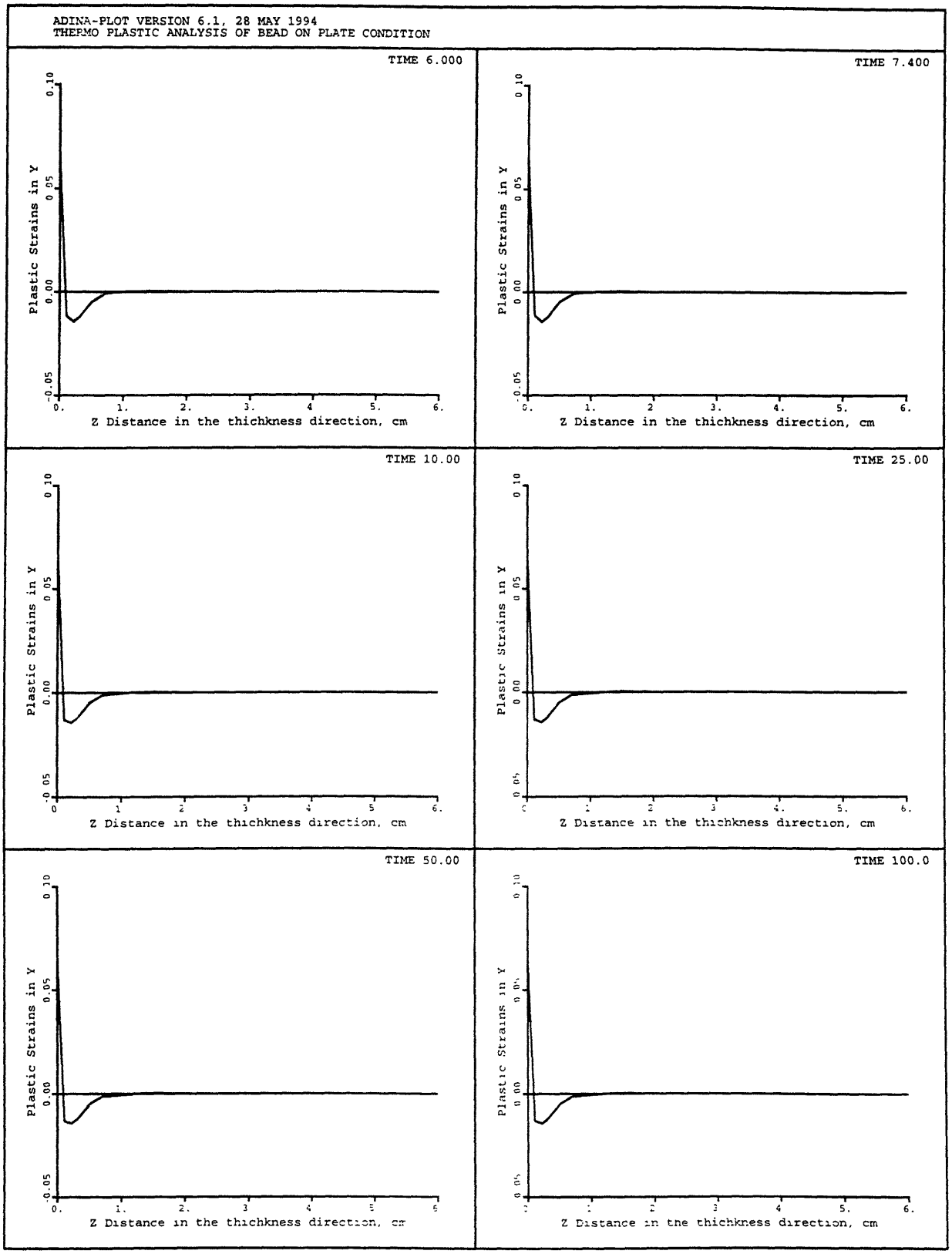

Figure 5.15 Successive development of compressive plastic strains in thickness direction during cooling

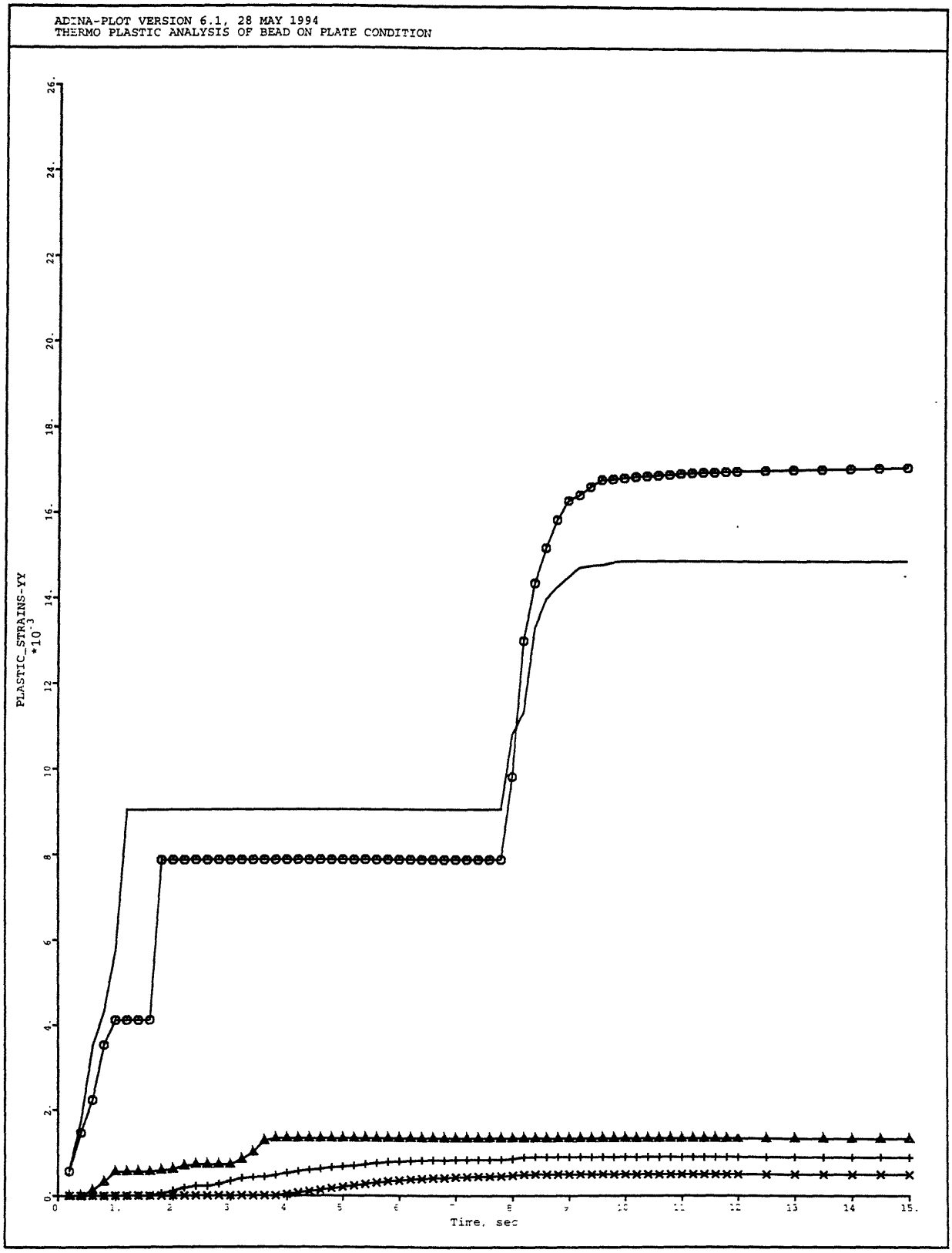

Figure 5.16 Accumulated effective plastic strain history at various distances from the weld center line

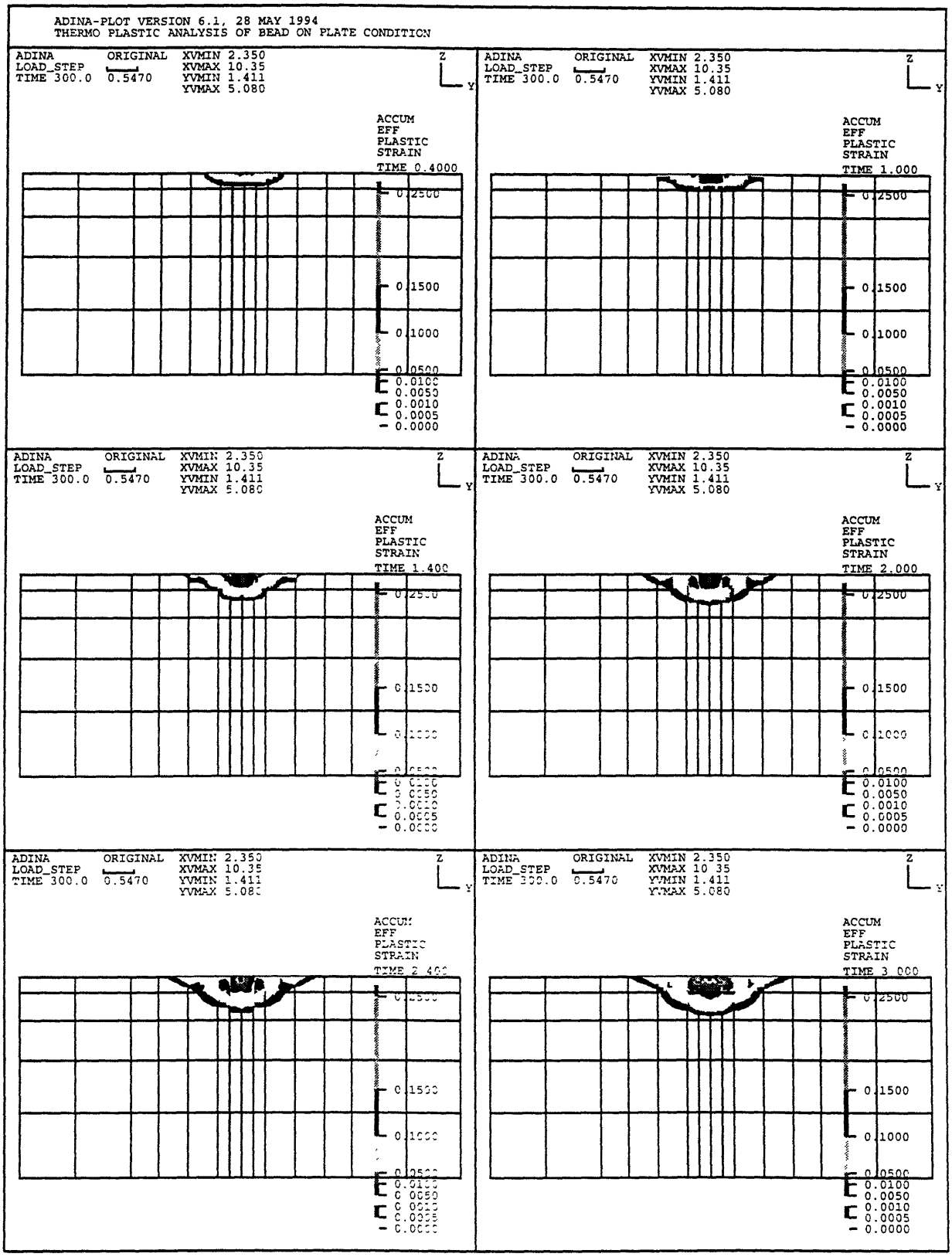

Figure 5.17 Successive accumulated effective plastic strains during welding

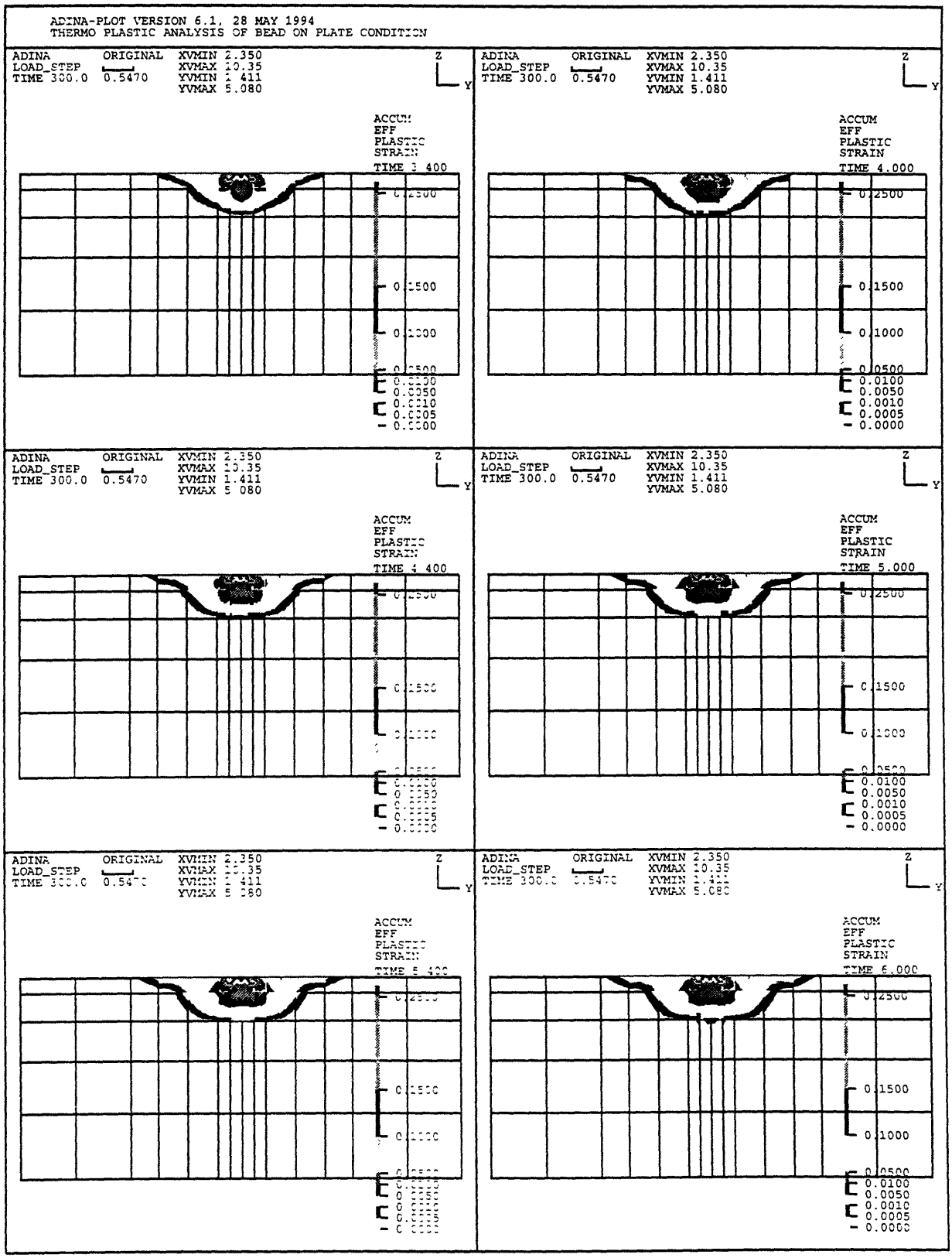

Figure 5.18 Successive accumulated effective plastic strains during welding

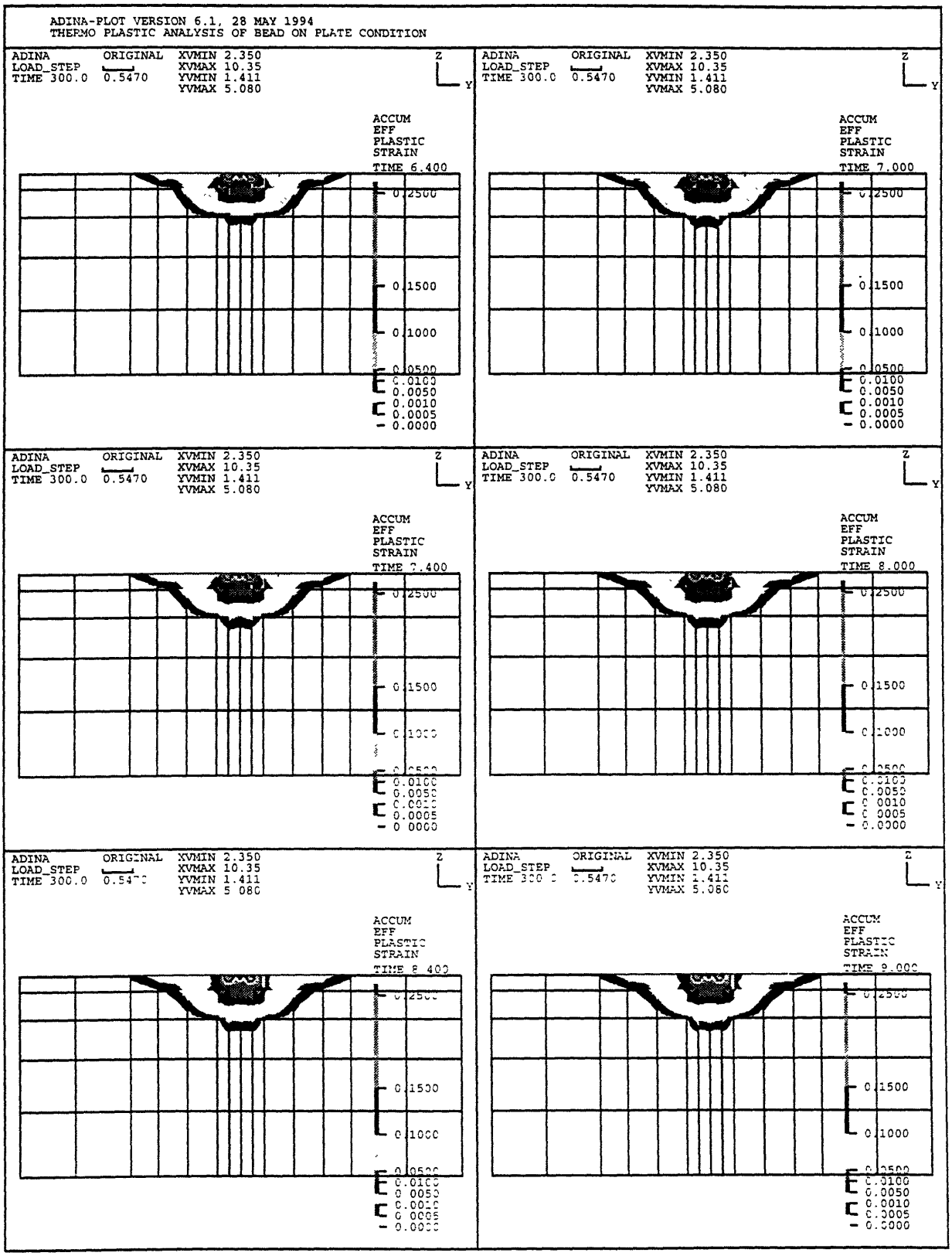

Figure 5.19 Successive accumulated effective plastic strains immediately after welding

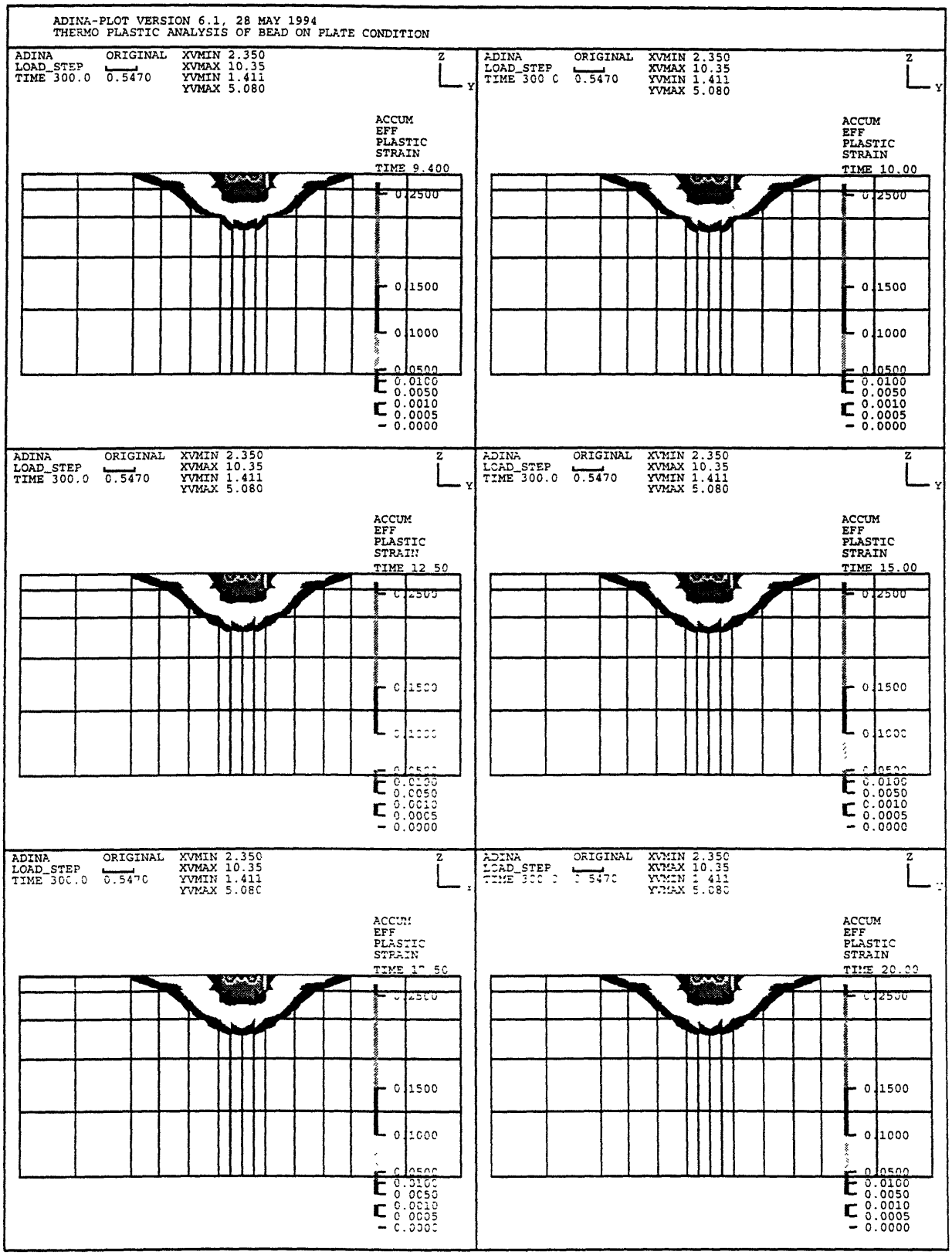

Figure 5.20 Successive accumulated effective plastic strains during cooling

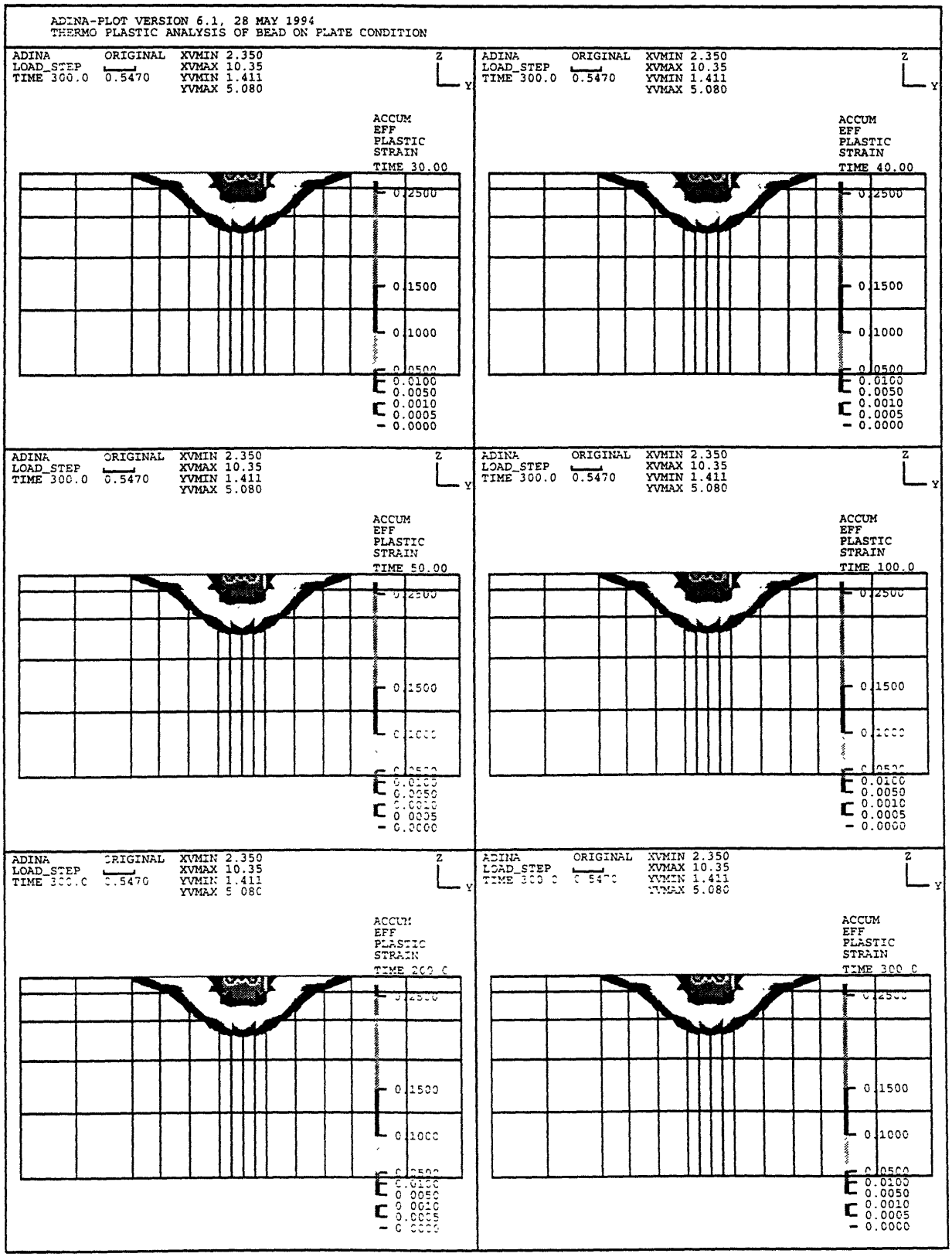

Figure 5.21 Successive accumulated effective plastic strains at the end of cooling

The transient displacement was computed at various distances on the surface of the plate. The deformation phenomena showed the same tendency as was observed in the experiments. Figure 5.22 shows the displacement history of points 0.6", 0.8", 1.2", and 1.6" away from the weld center line. During welding, the heated top surface of the plate expands and the points on the surface start bending and it reaches maximum immediately after welding is completed. With cooling, deformation reverses the direction and starts coming back to its initial position. This state can be seen in Figure 5.23 at time 10 second. At around the 50th second, the plate is at its initial state. After this, the plate passes its initial state and deforms plastically, due to the existence of compressive plastic strains developed during welding, as shown in Figures 5.23 and 5.26. This whole scenario was explained in Figure 3.43 and experimentally verified in Figure 3.33.

Figures 5.23, 5.24 and 5.25 show the deformation of the plate at selected times. Figure 5.23 corresponds to the actual welding period and the period immediately after completion. Figure 5.24 shows the deformation incidents during the cooling period. In Figure 5.25, the formation of the residual distortion is illustrated.

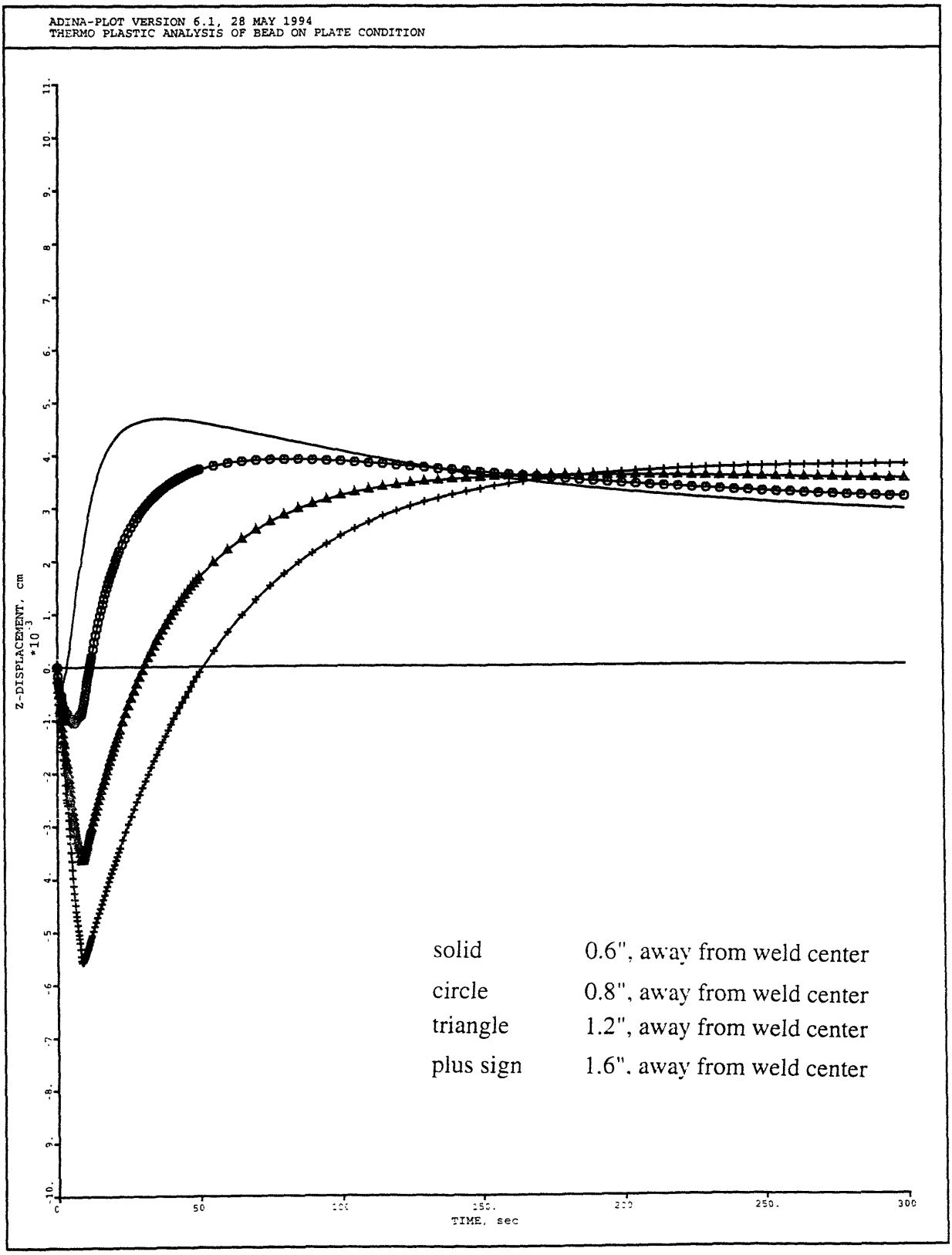

Figure 5.22 Transient displacement of the selected points on the surface of the plate

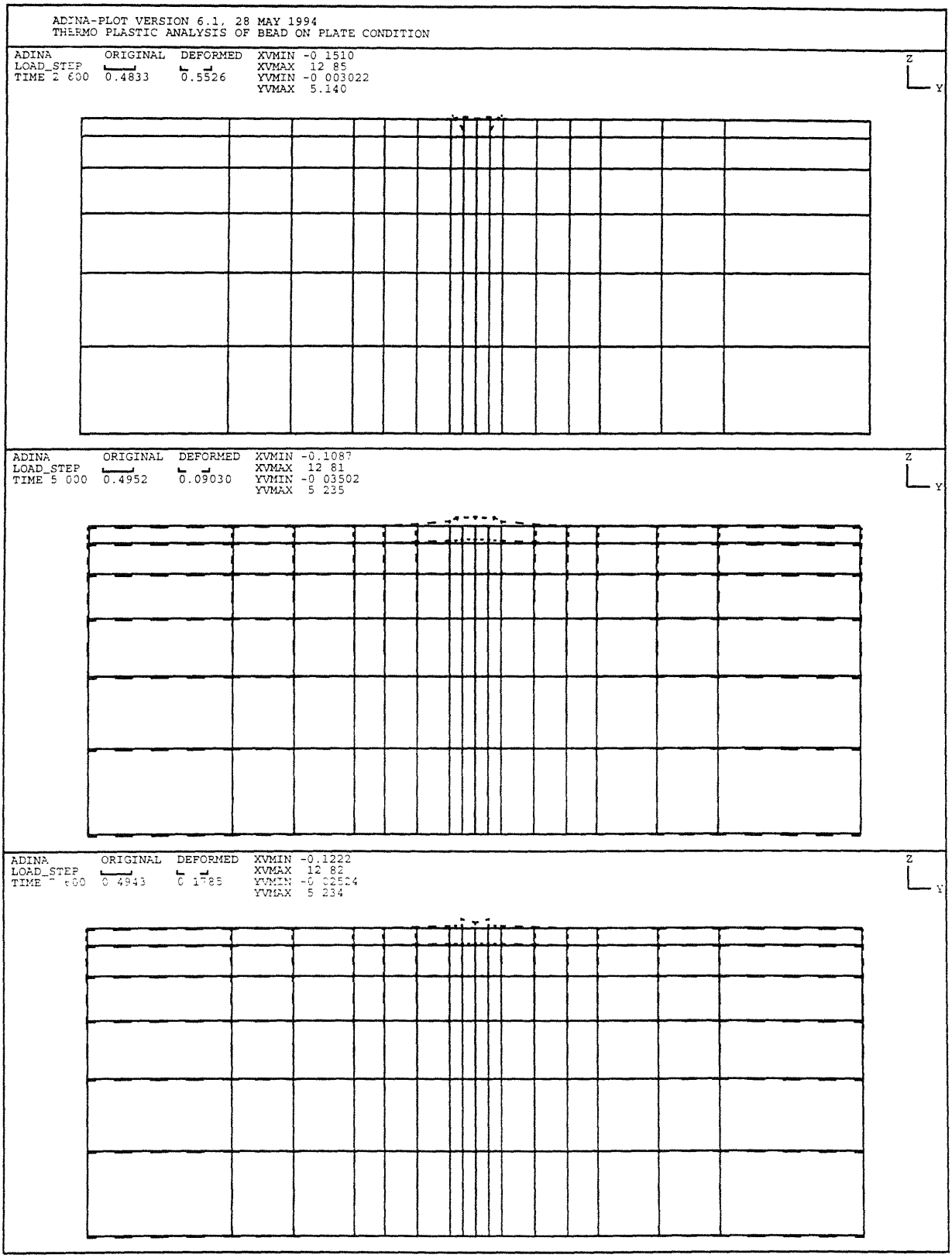

Figure 5.23 Successive deformation of plate during welding

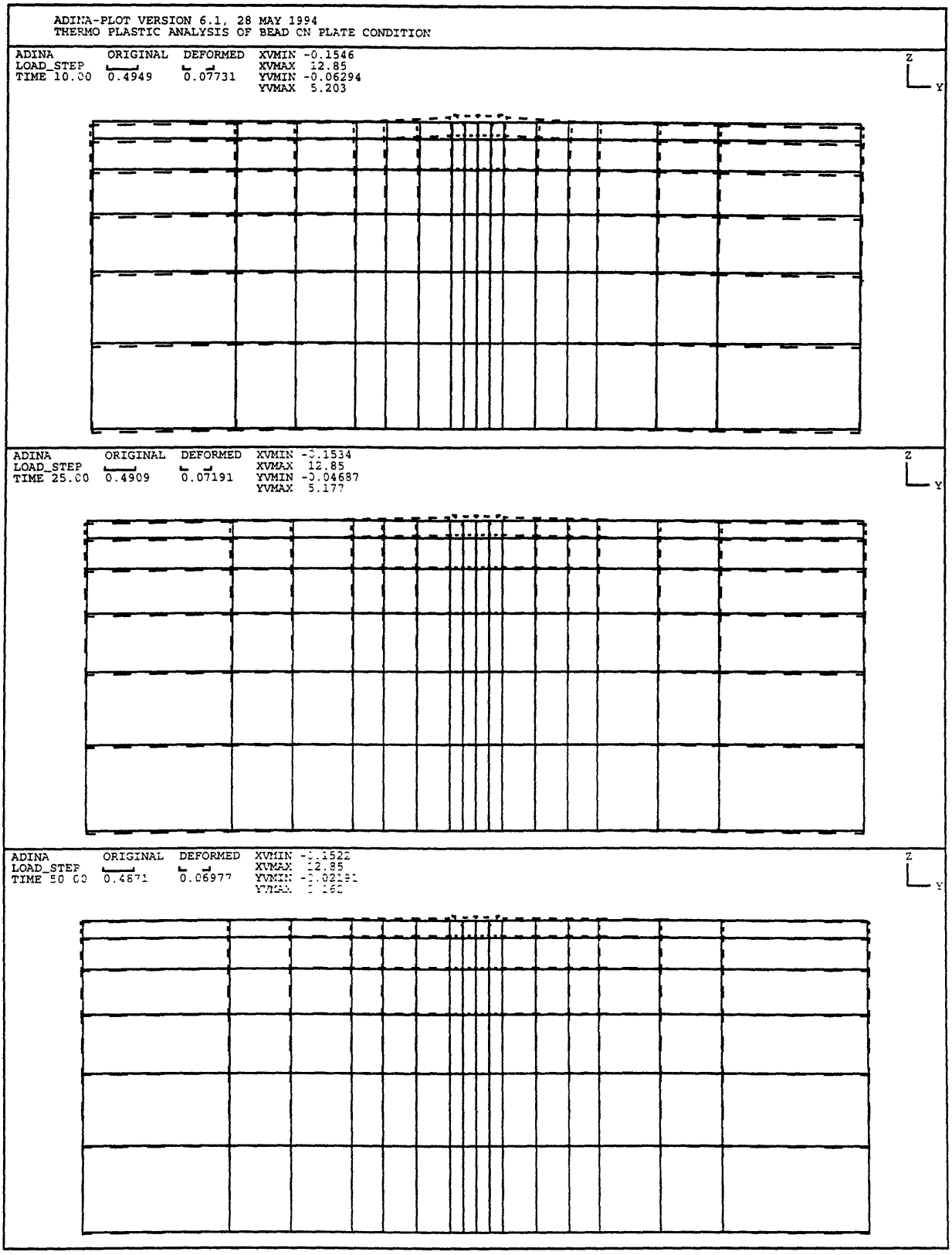

Figure 5.24 Successive deformation of plate during cooling

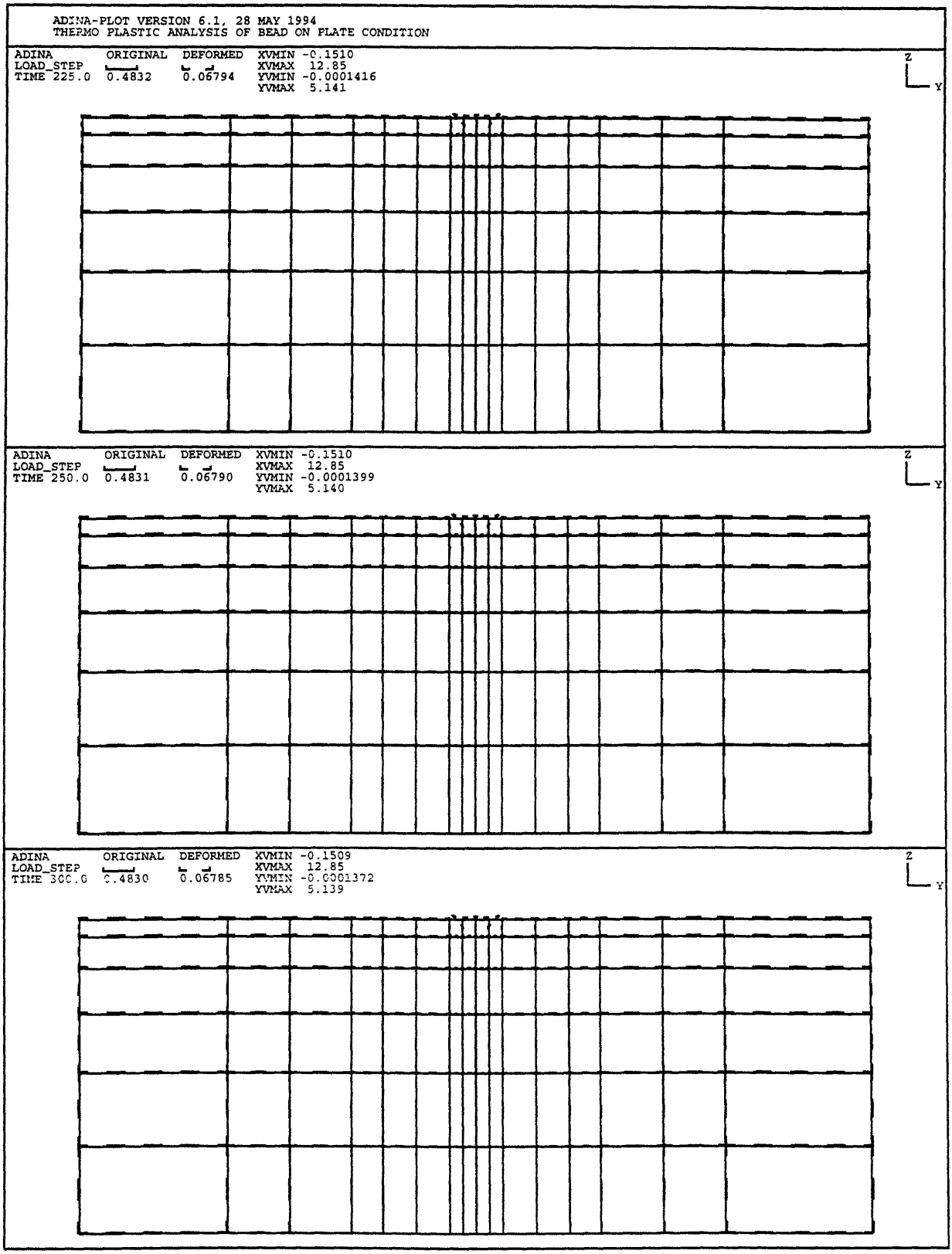

Figure 5.25 Successive deformation of plate at the end of cooling

The correlation is relatively good if the various assumptions involved in modeling the complex welding problem are taken into account. A delay in the transition from the tensile to the compressive and again from compressive to tensile strains is observed in the analysis. The same delay as far as the occurrence of the maximum strain is also exhibited. It is believed that the reason for this is the complex loading history due to welding.

Summarizing, it can be said that the finite element model developed based on ADINA is able to predict most of the scenarios presented in the complex behavior of metals during welding. The ability of ADINA for highly nonlinear phenomena is excellent. However, it is an expensive method to perform because welding problems consist of a coupled equation of thermo-mechanics. Due to the limitation of CPU expenses, in this study only 2-dimensional problems were considered and modeled. An attempt was made to model a 3-dimensional welding problem for the washer-pipe connection. However, it failed due to the time required to perform the analysis. Since the loading was neither symmetric nor axisymmetric, the problem could be modeled as a two-dimensional welding problem.

The total CPU time used through this thesis work was more than 50 hrs. on CRAY X-MP and this does not include the pre and post processing steps.

Chapter 6

6. Comparison of Experimental and Predicted Results

In this chapter, the predicted transient temperatures and distortions are compared with experimental results explained in Chapter 3.

6.1 Heat Transfer Analysis

In welding, the whole process is a very complicated problem. It first starts with the melting of weld pool. During melting, material is subjected to a set of phase transformations and state changes. Although the solidified material has entirely different properties, such as hardness, ductility, and non homogeneity, it is mostly assumed that the original material regains its initial properties after cooling. Weld pool geometry and physics are individual fields in which many researchers are involved. Therefore, the present study does not aim to elaborate on this field. However, the size of the molten pool and the heat affected zone, HAZ, are important factors to estimate the temperature distribution over the welded structure. Consequently, experimental results were used to estimate the transient temperature distribution in the heat flow analysis. The predicted temperature field, however, is used in the strain-stress analysis to predict the distortion and stresses.

Figure 6.1 shows the predicted weld pool and HAZ facing the experimental specimen. The red color represents the area which has reached the melting temperature and above. The other color contours correspond to the transition temperatures of 304 stainless steel. As seen easily, the results are in very good agreement.

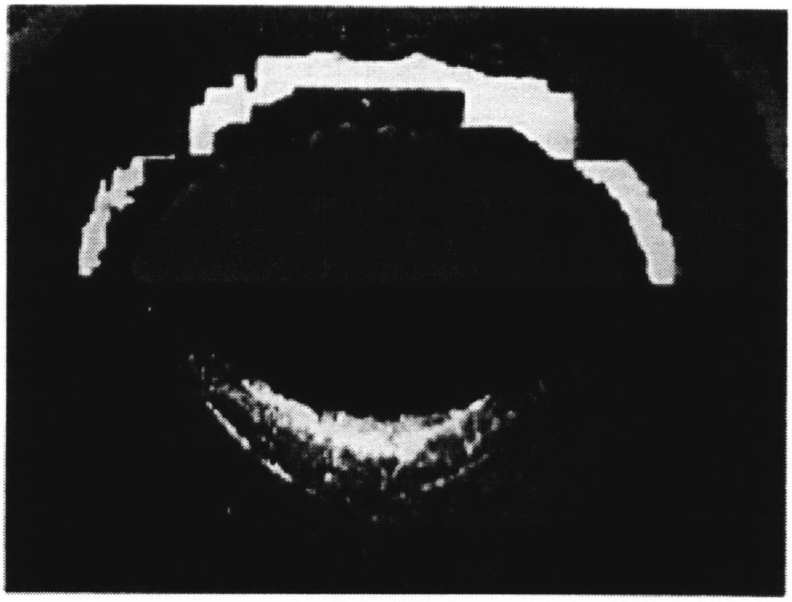

Figure 6.1 The experimental and predicted weld pool geometry and HAZ

The transient temperatures were measured with thermocouples as explained in Chapter 3. The predicted model transient temperatures were plotted against the experimentally measured data at 0.6, 0.8, 1.2, and 1.6 inches away from the weld center, in Figures 6.2, 6.3 and 6.4 respectively. Over all, the results yield a good correlation with experimental data. The peak temperatures are estimated quite accurately with FEM analysis. However, at the cooling stage, which is the long term behavior of the system, the results do not show as close an agreement as before. This disagreement may result from the assumption made when the FEM model was developed. Since the FEM model is a 2-D heat flow model, the heat losses from the plate surface, in the out-of-plane direction, were neglected. The only heat losses allowed were from the edges of plate as linear Newton convection and from the vicinity of the weld pool as radiation, utilizing the quartic Stefan-Boltzmann law. During the conduction of heat from the source as it reaches the boundary, there is a moment when heat is kept in the domain. Since no heat leaves the body, at this moment, the increasing temperature causes a separation between the lines (see following figures.)

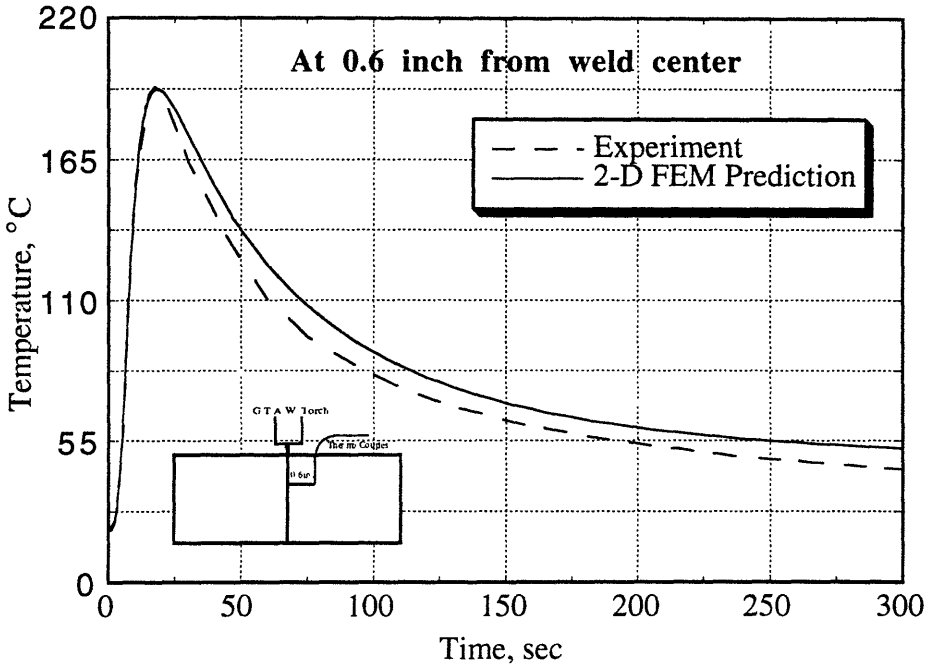

Figure 6.2 Comparison of predicted transient temperature history vs. experimental result

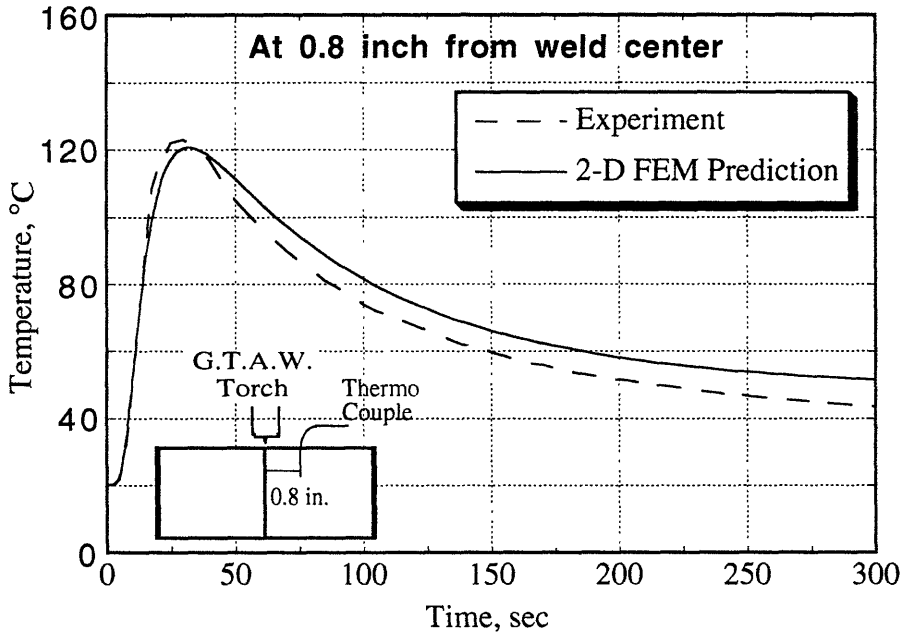

Figure 6.3 Comparison of predicted transient temperature history vs. experimental result

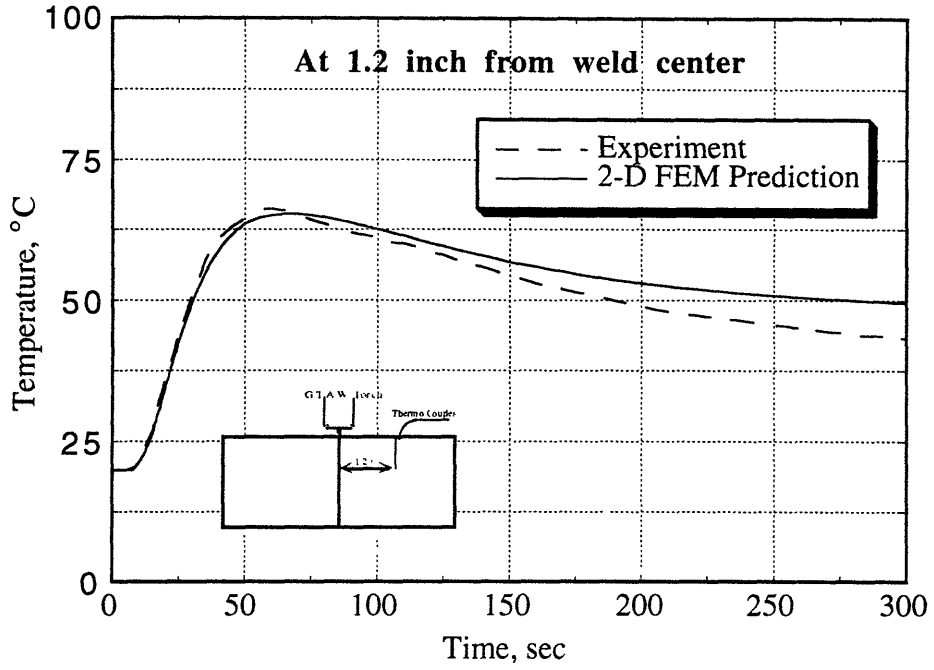

Figure 6.4 Comparison of predicted transient temperature history vs. experimental result

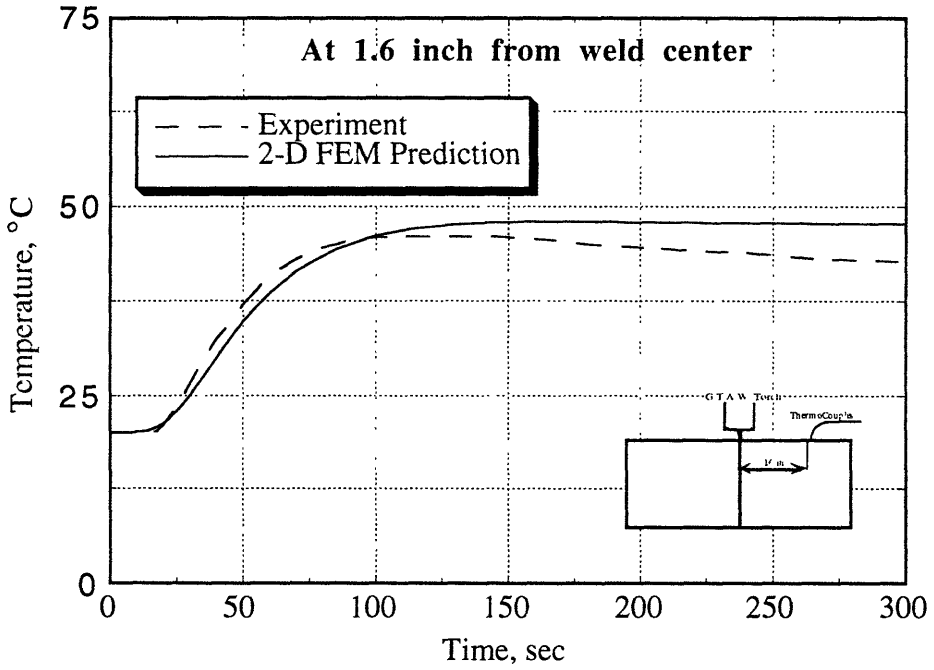

Figure 6.5 Comparison of predicted transient temperature history vs. experimental result

After a certain time, this difference remains constant and the two lines run together. This behavior is not valid at distances far away from the weld line. Moreover, the heat transfer coefficient, h, is a correlation estimation. Therefore, the cooling rate depends on this value as well. However, in reality, the heat loss starts in three directions as soon as the external heat source is applied. Consequently, while the FEM model shows a very good agreement during the rise of temperature, it overestimates the temperature values during cooling stage in the vicinity of the weld and underestimates it at distances far away from the weld due to a fast cooling rate.

6.2 Displacement Analysis

In the experiment, only transient displacements were measured. Due to the size of the specimens, the transient stresses and strains were not obtained. In this section, the transient displacements of the plate in vertical direction is compared with the values of transient displacement predicted by FEM. In order to see the effect of the modeling assumptions, the resulting plane stress and plane strain cases are compared with experimental data in the same picture. It is observed that the values of the deformation in the plastic zone, that is in the vicinity of weld, are higher in the plane strain case than in the plane stress case. That is because the equilibrium equations are different in plasticity for the two cases. Plane stress prediction gives a closer estimation to the experimental data. Plane strain case tends to overestimate the displacement.

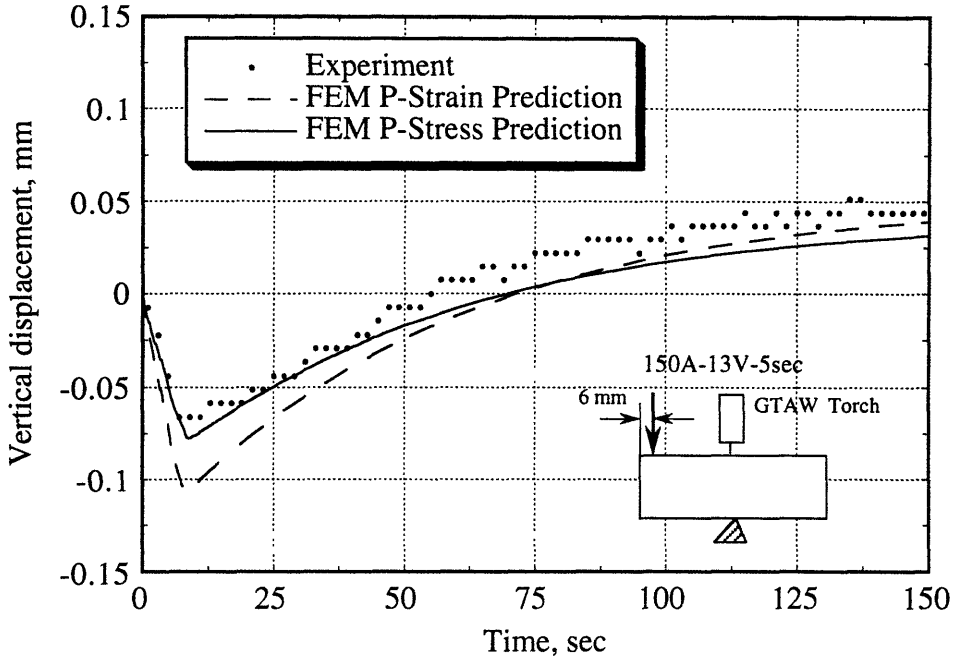

Figure 6.6 Comparison of predicted transient displacement vs. experimental result

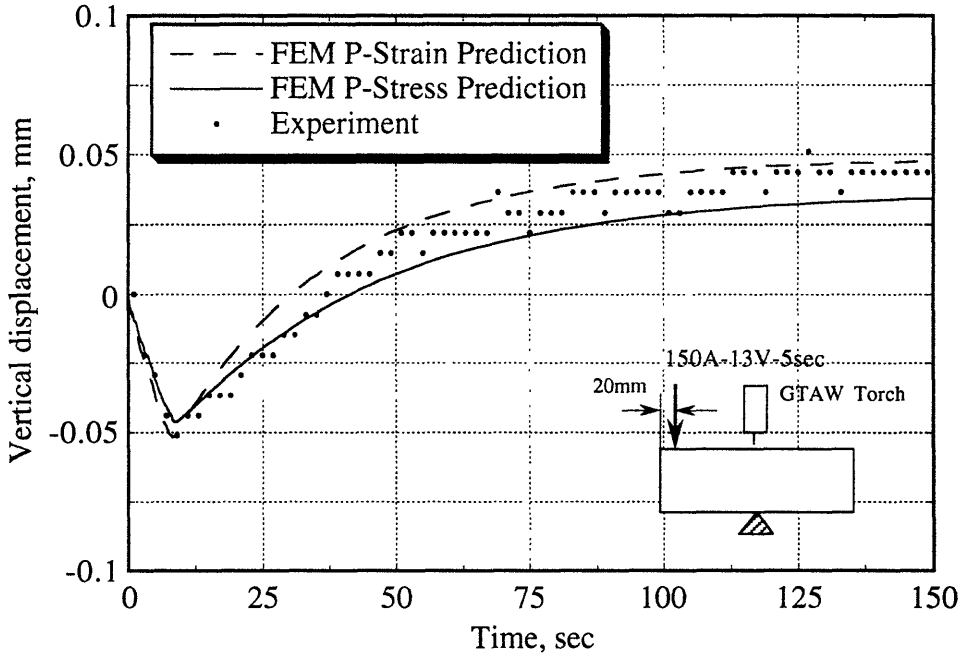

Figure 6.7 Comparison of predicted transient displacement vs. experimental result

Chapter 7

7. Conclusion and Recommendations

This study showed the importance of the metal movement during welding and presented it quantitatively. The effect of rigid-body motion and its occurrence during solidification of the weld metal was measured. It was found that the distortion caused by the rigid-body motion of the unrestrained free joints is 10 to 20 times larger than the distortion caused by the thermal elastic-plastic strains. Hence, it is extremely important to provide proper restraining. High restraint can result in cracking in welding steels, especially thick plates made of high-strength steels. Moreover, it has been regarded that welds made under restraint tend to have higher residual stresses.

A real-time non-contact measurement technique, which is capable of measuring out-of-plane transient metal movement during welding without any limitations of geometrical shape of specimens, has been developed and it was applied to the most common geometries used in joining processes. This technique uses KEYENCE laser displacement sensors which are very suitable to measure the metal movement during and after heating even in severe welding environments.

To determine the principal displacement behavior of the tube and the washer during the laser welding of the SL-2000 laser package, a set of experiments was carried out using larger scale specimens and G.T.A.W. processes. Through the experiments, the displacement history of the tube was determined. Based on the experimental results, the following several practical industrial recommendations were given to the AT&T Bell Laboratories to reduce the final deformation of the fiber optic connectors by up to 70%:

(1) To reduce the final displacement of the tube, using a thicker washer is recommended. But too much thickness (more than a half of the outer diameter) has less effect in decreasing the displacement of the tube.

(2) The step washer is also effective to reduce the displacement of the tube. The size of the projection on the washer should be small enough to absorb the thermal stress by deforming itself.

(3) The tube should be longitudinally free from the fixture in its longitudinal direction. By keeping the tube unfixed, it is possible for the tube to go up with the washer during welding and finally return almost to its initial position.

(4) With the loosely fitted tube and washer combination, the tube does not follow the upward expansion of the washer while the welding arc is turned on. Hence, the value of Df with the loosely fitted washer and tube combination was much larger than the value of Df with the tightly fitted combination obtained by the previous experiments. Therefore, a tightly fitted tube should be preferred during joining.

(5) Kovar had the same tendency of displacement as stainless steel, though kovar had a much smaller final displacement than stainless steel due to different material properties. Hence, kovar is a better material to have less distortion.

The other experiments showed that real-time measurements must be performed in order to control distortion during welding. Compared to phenomena involved in the formation of weld metals (solidification), the phenomena involved in transient metal movement are slower. Formation of non-elastic strains, or in other words, the metal movement as an elastic-plastic

body, is slower than those involved in solidification. However, the metal movement as a rigid body that takes place in an unrestrained (free) joint is fast. Since the amount of the rigid body movement is far greater than that caused by non-elastic strains, it is essential to reduce the rigid body motion to a minimum in order to develop technologies for minimizing weld distortion. Unlike the solidification, actions necessary for distortion control can be corrected in real-time if necessary.

Proper restraining is required in order the avoid rigid-body motion during solidification of weld metal in the joining of unrestrained free parts. In reality, let us assume that the pieces lie on the ground while welding is performed. As soon as the forces generated by the solidification of weld metal overcome the friction between the plates and ground, rigid-body motion starts. This motion which is 10 to 20 times larger than the ones produced by incompatible strains can be eliminated by restraining the plates from the edges. However, the forces generated may easily exceed the expected values and this may cause the cracking in the weld metal. Moreover, this cracking is a very serious problem in high strength steels.

The restrained plate and beam models showed the same deformation tendency in the bead-on-plate and butt welding conditions. Moreover, the deformation patterns are the same for all geometries the with same welding conditions. In other words, when the pieces were butt welded no plastic strains were produced because both sides were free to expand until the weld metal solidified. As soon as solidification occurred deformation continued in the same direction until ambient conditions were reached. In the case of bead-on-plate condition, the expanded side reversed the direction of deformation after the weld solidified and reached final deformation either before or after its initial position. This was due to the compressive plastic strains produced while welding was being performed. Additionally, it is observed that the final position is the function of several parameters such as the thickness of the specimen, and the length and location of restraining.

Stainless steel plate specimens measuring 5"X2"X0.25" were welded with a stationary GTAW process. Temperatures and the transient deformations were measured during and after welding. The collected data were compared with numerical predictions as explained in the following lines.

ADINA-T, a multipurpose nonlinear finite element program, was used to develop a model for the aforementioned experiment. The temperature variation of the material properties, nonlinear convection and radiation heat losses were taken into account. A very good agreement with the experiments of the results was reached upon comparison

Finally, a stress-strain analysis of the welding problem was performed using a thermo-elastic-plastic model predefined in ADINA. This model included the effect of temperature dependent mechanical properties of material such as yield stress, Young's modulus, Poisson's ratio, tangent modulus and thermal expansion coefficient. The comparison of the predicted data with the experiment results showed good agreement.

Based on the outcome and observations made in this study the following topics for future studies are recommended:

- Experimental work was performed with a limited number of specimens. As was mentioned earlier, the effect of the geometrical constraints such as the thickness of plate and the length is significant. Therefore, it is recommended that a more detailed experimental study be carried out to understand the restraining conditions.

- Since the specimens are a great deal smaller than real structures, the scale effect should be studied using larger specimens.

- The metal movement during joining should be studied in more detail in order to develop a more sophisticated model to perform the numerical prediction of joining when weld metal solidifies.

- One of the most important factors regarding the accuracy of numerical prediction is the temperature dependence of the physical and material properties of the material under consideration. Hence, since there is a serious lack of data on these properties at elevated temperatures, it is recommended that a better estimation of this data be obtained through experiments.

- Two dimensional models were adequate for the beam and plate models for plane stress cases. However, if one wants to predict the out-of-plane distortion on the butt welded short plates, there is a need to perform a three dimensional analysis.

Chapter 8

8. References

[1] Adams, C. M., Jr., *Cooling Rate and Peak Temperature in Fusion Welding.* Welding Journal, 37, pp. 97-104, 1958.

[2] ADINA R&D, Inc., *ADINA Verification Manual-Nonlinear Problems*, Report ARD 87-10, Watertown, Massachusetts, December 1987

[3] ADINA R&D, Inc., *ADINA Theory and Modeling Guide*, Report ARD 87-8, Watertown, Massachusetts, December 1987

[4] ADINA R&D, Inc., *ADINA-IN: User's Manual, Report*, ARD 87-4, Watertown, Massachusetts, December 1987.

[5] ADINA R&D, Inc., *ADINA-IN for ADINA-T User's Manual,*, Report ARD 92-5, Watertown, Massachusetts, December 1992.

[6] ADINA R&D, Inc., *ADINA-PLOT: User's Manual,* Report ARD 87-7, Watertown, Massachusetts, December 1987.

[7] Agapakis, J., E., *Welding of High Strength and Stainless Steels: A Study on Weld Metal Strength and Stress Relieving,* SM. Thesis, M.I.T., May 1982.

[8] Agapakis, J., E., and Masubuchi, K., *Analytical Modeling of Thermal Stress Relieving in Stainless and High Strength Steel Weldments,* Welding Journal, AWS, pp. 187-196, June 1984.

[9] American Welding Society, *Welding Handbook,* Volume 2, Eighth Edition 1991.

[10] Anderson, J. E. and Stesino, E. F., *Heat Transfer from Flames Impinging on Flat and Cylindrical Surfaces.* Journal of Heat Transfer (ASME), pp. 49-54, 1963.

[11] Andrews, J. B., Arita, M., and Masubuchi, K., *Analysis of Thermal Stresses and Metal Movement During Welding*, NASA Contractor Report NASA CR-61351, prepared for the G. C. Marshall Space Flight Center, December 1970.

[12] Apps, R. and Milner, D., *Heat Flow in Argon Arc Welding*. British Welding Journal, 2 (10), pp. 475-485, 1955.

[13] Barnes, P. K., *Reduction of Residual Stresses and Distortion in Girth-Welded Pipes.* Master's Thesis, M.I.T., June, 1987.

[14] Bathe, K. J., *ADINA-T - A Finite Element Program for Automatic Dynamic Incremental Nonlinear Analysis of Temperature*. Technical Report 82448-5, Department of Mechanical Engineering, M.I.T., May, 1977.

[15] Bathe, K. J., *Finite Element Procedures in Engineering Analysis*. Prentice-Hall, Inc., Englewood Cliffs, NJ, 1982.

[16] Bathe, K. J., and Cimento, A. P., *Some Practical Solutions for the Solution of Nonlinear Finite Element Equation*. Journal of Computational Methods in Mechanics and Engineering. 22, pp. 59-85, 1980.

[17] Bathe, K.J. and Khoshgoftaar, M. R., *Finite Element Formulation and Solution of Nonlinear Heat Transfer*. Journal of Nuclear Engineering and Design, 51, pp. 389-401, 1979.

[18] Becker, E. B. and Parr, C. H., *Application of Finite Element Method to Heat Conduction in Solids*. Technical Report S - 117, Rohm and Haas Redstone Research Laboratories, 1967.

[19] Boulton, N. S., and Lance Martin, H. E., *Residual Stresses in Arc Welded Plates*, Proceedings of the Institution of Mechanical Engineers, Volume 133, pp. 295-339, 1936.

[20] Chang, I. H., *Analysis and Control of Root Gap During Butt Welding*, Ph. D. Thesis, M.I.T., January 1988.

[21] Chang, I. H., Miyachi, H., and Masubuchi, K., *Instrumentation, Measurement, and Analysis for Controlling Residual Stresses and Metal Movement - Especially Reducing Joint Mismatch and Force Acting on Tack Welds During Butt Welding.* The Fifth Symposium on Energy Engineering Sciences, Instrumentation, Diagnostic, and Material Behavior, pp. 161-167, Argonne National Laboratory, June, 1987.

[22] Chidiac, S. E., and Mirza, F. A., *Thermal Stress Analysis due to Welding Processes by the Finite Element Method.* Computers and Structures, 46(3), pp. 407-412, 1993.

[23] Christensen, N., Davies, V. and Gjermundsen, K., *Distribution of Heat Around Finite Moving Sources.* Technical Report CA-91-508-EVC-378, U.S. Army, September 1959.

[24] Christensen, N., Davies, V. and Gjermundsen, K., *The Distribution of Temperature in Arc Welding.* British Welding Journal, 12(1), pp. 54-75, 1965.

[25] Christie, H., K.J., *3-D FEM Analysis of Electron Beam Butt Welding of a Flat Plate,* SM. Thesis, M.I.T. June, 1990.

[26] *Aerospace Structural Metals Handbook*, Mechanical Properties Data Center, A Department of Defense Materials Information Center, Watertown, Massachusetts, 1977.

[27] DeBiccari, A., *A Control of Distortion and Residual Stresses in Girth-Welded Pipes.* Ph.D. Thesis, M.I.T. June, 1986.

[28] Degarmo, et. al., *The Effect of Weld Length Upon Residual Stresses of Unrestrained Butt Welds.* Welding Journal, 25 (8), pp. 485-486, 1946.

[29] Duffy, D. K., *Distortion Removal in Structural Weldments*, M. S. Thesis, M.I.T., May 1970.

[30] Eagar, T. and Tsai, N. S., *Temperature Fields Produced by Traveling Distributed Heat Sources.* Welding Journal, 62 (12), pp. 346-355, 1983.

[31] Friedman, E., *Numerical Simulation of the Gas Tungsten Arc Welding Process*, Proceedings of Numerical Modeling of Manufacturing Processes, ASME Winter Annual Meeting, Atlanta, GA, pp. 35-47, 1977.

[32] Friedman, E., *Thermomechanical Analysis of the Welding Process Using the Finite Element Method*, Journal of Pressure Vessel Technology, ASME, pp. 206-213, August 1975.

[33] Friedman, E., and Glickstein, S. S., *An Investigation of the Thermal Response of Stationary Gas Tungsten Arc Welds*, Welding Journal, Volume 55, No. 12, Research Supplement pp. 408s - 420s, 1976.

[34] Fujita, Y., Nomoto, T., and Hasegawa, H., *Thermal Stress Analysis Based on Initial Strain Method*, International Institute of Welding, Document X-926-79, April 1979.

[35] Fujita, Y., Terai, K., Matsui, S., Matsumura, H., Nomoto, T., and Otsuka, M., *Studies on Prevention of End Cracking in One-Side Automatic Welding*, Journal of the Society of Naval Architects of Japan, Vol. 136, pp. 450-465, 1974.

[36] *Welder's Handbook for Welding HY80, HY100, and HY130.* General Dynamics Corporation, 1975.

[37] Goktug, G., *On the Effect of Environmental Pressure on Gas Tungsten Arc Welding Process*, Ocean Engineer and S.M. Thesis, M.I.T., May 1994.

[38] Greene, T. W., and Holzbaur, A. A., *Controlled Low-Temperature Stress Relieving.* Welding Journal, 25 (3), pp. 1715-1855, March, 1946. Research Supplement.

[39] Grosh, R. J., and Trabant, E. A., *Arc Welding Temperatures.* Welding Journal, 35, pp. 396-400, 1956.

[40] Gurtis, M. E., *Variational Principles for Linear Initial Value Problems.* Quarterly Applied Mechanics, 22(3), 1964.

[41] Hardt, D. E., Masubuchi, K., Paynter, H. M., and Unkel, W. C., *Improvement of Welding by In-Process Sensing and Control (Development of Smart Welding Machines*

for Girth Welding of Pipes, Final Report under Contract No. DE-AC02-79ER10474, A000 from M.I.T. to Department of Energy, April 1983.

[42] Hibbitt, H. D., and Marcal, P. V., *A Numerical, Thermomechanical Model for the Welding and Subsequent Loading of a Fabricated Structure*, Computers and Structures, Vol. 3, pp. 1145-1174, 1973.

[43] Hsu, M. B., *Analysis of Welds by the Finite Element Method.* Proceedings of Numerical Modeling of Manufacturing Processes, pp. 97-115, ASME, 1977.

[44] Hwang, J. S., *Residual Stresses in Weldment in High Strength Steels.* Master's Thesis, M.I.T., February, 1976.

[45] *Control of Weld Distortion*, Institute of Welding, London, U.K., 1957.

[46] Jackson, C. E. , and Shrubsall, A. E., *Energy Distribution in Energy Welding.* Welding Journal, 29, pp. 231-141, 1950. Research Supplement.

[47] Jonsson, M., Karlsson, L. and Lindgren, L. E., *Simulations of Tack Welding Procedures in Butt Joint Welding of Plates.* Welding Journal, pp. 296-301, 1985.

[48] Johnson, B., K., Emery, A., F., and Marburger, S., J., *An Analytical and Experimental Study of the Effects of Welding Parameters on Fusion Welds,* Welding Journal, AWS, pp. 51-s-59-s, February 1993.

[49] Janca, L. L., *Removal of Out-of-Plane Distortion in Mild Steel Plates Using Flame Heating*, M. S. Thesis, M.I.T., May 1987.

[50] *Laser Displacement Sensors, LB-1000 Series*, Instruction Manual, Keyence Corporation, Osaka, Japan, 1992.

[51] Kihara, H., Watanabe, M., Masubuchi, K., and Satoh, K., *Researches on Welding Stress and Shrinkage Distortion in Japan*, Volume 4 of the 60th Anniversary Series of the Society of Naval Architects of Japan, 1959.

[52] Kolodziejczak, G. C., *GMAW Control to Minimize Interference from Tack Welds*, Ph. D. Thesis, M.I.T., May 1987.

[53] Kumose, T., Yoshida, T., Abe, T., and Onoue, H., *Prediction of Angular Distortion Caused by One-Pass Fillet Welding*, The Welding Journal, Vol. 33, pp. 945-956, 1954.

[54] Legatt, R. H., *Finite Element Analysis of the Bending of Plates During Welding*, Proceedings of the Colloquium on Applications of Numerical Techniques in Welding held during the 1978 Annual Assembly of the International Institute of Welding, Dublin, Ireland

[55] Leinhard, J., H., *A Heat Transfer Textbook,* Prentice-Hall, Inc., Englewood Cliffs, New Jersey, 1987.

[56] Lobitz, D. W., McClure, J. D., and Nickell, R. E., *Residual Stresses and Distortion in Multipass Welding*. Proceedings of Numerical Modeling of Manufacturing process, pp. 81-96, ASME, 1977.

[57] Malha, E., Rowland, M., Shook, C., and Doan, G., *Heat Flow in Arc Welding.* Welding Journal, 20(10), pp. 559-568, 1941. Research Supplement.

[58] Malisius, R., *Electroschweissen*, Vol. 7, pp. 1-7, 1936.

[59] Malisius, R., *Practical Steps Against Shrinkage Effects in Welded Constructions-Economic Aspects*, Schweissen und Schneiden, Vol. 7, pp. 119-133, April 1955.

[60] Masubuchi, K., *Advances in Analysis and Control of Residual Stresses and Distortion.* 1987 Annual Convention of the American Welding Society, American Welding Society, April, 1987.

[61] Masubuchi, K. *Analysis of Welded Structures*, a video course developed by the Center for Advanced Engineering Study, M.I.T., Cambridge, MA, 1990.

[62] Masubuchi, K. *Analysis of Welded Structures - Residual Stresses, Distortion, and Their Consequences*, Pergamon Press, 1980.

[63] Masubuchi, K., *Applications of Numerical Analysis in Welding*, Welding in the World, Volume 17, No. 11/12, pp. 268-291, 1973.

[64] Masubuchi, K., *Control of Distortion and Shrinkage in Welding*, Welding Research Council Bulletin No. 149, Welding Research Council, New York, April 1970.

[65] Masubuchi, K., *Materials for Ocean Engineering*. M.I.T. Press, 1970

[66] Masubuchi, K., *Models of Stresses and Deformation Due to Welding-A Review, Journal of Metals,* Volume 33, No. 12, pp. 19-23, December 1981.

[67] Masubuchi, K., *Nondestructive Measurement of Residual Stresses in Metals and Metal Structures*, RSIC-410, Redstone Scientific Information Center, Redstone Arsenal, Alabama, April 1965.

[68] Masubuchi, K., *The Need for Analytical/Experimental Orchestrated Approaches to Solve Residual Stress Problems in Real Structures*, Nondestructive Methods for Material Property Determination, edited by Ruud, C. O., and Green, R. E., Plenum Press, New York and London, pp. 123-134, 1983.

[69] Masubuchi, K., *Numerical Analysis of Stresses, Strains and Other Effects Produced by Welding*. Technical Report Document X-1087-85-, A.W.S., 1985

[70] Masubuchi, K., *Recent M.I.T. Research on Residual Stresses and Distortion in Welded Structures*, Journal of Ship Production, Volume 9, No. 3, pp. 137-145, August 1993.

[71] Masubuchi, K., *Residual Stresses and Distortion in Welded Aluminum Structures and Their Effects on Service Performance*, Welding Research Council Bulletin No. 174, Welding Research Council, New York, July 1972.

[72] Masubuchi, K., *Studies at M.I.T. Related to Applications of Laser Technologies to Metal Fabrication*, Proceedings of International Conference on Laser Advanced Materials Processing LAMP'92, Nagaoka, Japan, Vol. 2, pp. 939-946, June 7-12 1992.

[73] Masubuchi K., et al., *Research on High -Strength Steels with an Improvement Against Weld Cracking - Evaluation of Weld Cracking Sensitivities* . The First OMAE Specialty Symposium on Offshore and Arctic Frontiers, pp. 429-437, ASME, 1986.

[74] Masubuchi, K., and Agapakis, J. E., *Analysis and Control of Residual Stresses, Distortion and Their Consequences.* Trends in Welding Research in the United States, pp. 153-172. American Society of Metals, November, 16-18, 1981.

[75] Masubuchi, K., and Chang, I. H., *Hybrid Experimental-Analytical Approach for Controlling Distortion and Residual Stresses in Weldments.* International Conference in Computational Engineering Science, pp. viii 1-4, Springer Verlag, 1988.

[76] Masubuchi, K., Cook, W. J. C., Deacon, D. L., Fan, J. S., Haidemenopoulos, G., Johnson, R. C., and McCarthy, R. W., *Phase I Report on Laser Forming of Steel Plates for Ship Construction*, from M.I.T. to Todd Pacific Shipyards Corporation, February 1985.

[77] Masubuchi, K., DeBiccari, A., and Cook, W. J. C., *Non-Contact Measurement of Out-Of-Plane Distortion as a Means for Controlling Distortion in Welded Structures,* Advances in Welding Science and Technology, ASM International, pp. 529-532, 1987.

[78] Masubuchi, K., and Luebke, W. H., *Phase II (Final) Report on Laser Forming of Steel Plates for Ship Construction*, from M.I.T. to Todd Pacific Shipyards Corporation, March 1987.

[79] Masubuchi, K., Luebke, W. H., and Itoh, H., *Novel Techniques and Their Applications for Measuring Out-of-Plane Distortion of Welded Structures, Journal of Ship Production*, Vol. 4, No. 2, pp. 73-80, May 1988.

[80] Masubuchi, K., and Martin D. C., *Investigation of Residual Stresses by Use of Hydrogen Cracking.* Welding Journal, 40 (12), pp. 401-418, 1966. Research Supplement.

[81] Masubuchi, K., Ogura, Y., Ishihara, Y., and Hoshino, J., *Studies on the Mechanisms of the Origin, and Methods of Reducing the Deformation of Shell Plating in Welded Ships*, International Shipbuilding Progress, Vol. 3, No. 19, pp. 123-133, 1956.

[82] Masubuchi, K., Simmons, F. B., Monroe, R. E., *Analysis of Thermal Stresses and Metal Movement During Welding*, RSIC-820, Redstone Scientific Information Center, Redstone Arsenal, Alabama, July 1968.

[83] Matsui, S., *Investigation of Shrinkage, Restraint Stresses and Cracking in Arc Welding,* Ph.D. Thesis, Osaka University, 1964.

[84] Mendelson, A., *Plasticity: Theory and Application.* The MacMillan Company, New York, 2nd Ed., 1968.

[85] Miyachi, H., *Control of Thermal Stresses Acting on Tack Welds During Butt Welding*, Ph. D. Thesis, M.I.T., February 1989.

[86] Muraki, T., Bryan, J. J., and Masubuchi, K., *Analysis of Thermal Stresses and Metal Movement During Welding, Part I: Analytical Study, and Part II: Comparison of Experimental Data and Analytical Results*, Journal of Engineering Materials and Technology, ASME, pp. 81-84, and 95-91, January 1975.

[87] Muraki, T., and Masubuchi, K., *Manual on Finite-Element Program for Two-Dimensional Analysis of Thermal Stresses and Metal Movement During Welding*, Department of Ocean Engineering, M.I.T., April 1975.

[88] Naka, T., *Shrinkage and Cracking in Welds*, Komine Publishing Co., Tokyo, Japan, 1950

[89] Nickell, R. E., and Hibbitt, H. D., *Thermal and Mechanical Analysis of Welded Structure*. Journal of Nuclear Engineering and Design, 32, pp. 110-120, 1975.

[90] Nikolaev, G. A., *Stresses and Strains in Welding*, Trudy MVTU, No. 6., Moscow, 1949

[91] Nippes, E. F., and Savage, W. F., *Residual Stresses in Welded Titanium Plates*. Welding Journal, 37 (10), pp. 433-439, 1958. Research Supplement.

[92] Nishida, M., *Analytical Prediction of Distortion in Welded Structures*, M. S. Thesis, M.I.T., March 1976.

[93] Nowacki, W., *Thermoelasticity*. Pergamon Press Ltd., New York, 1962.

[94] Oden, J. T., and Kross, D. A., *Analysis of General Coupled Thermo-Elasticity Problems by the Finite Element Method.* The Second Conference on Matrix Methods in Structural Mechanics, ASME, October, 1968.

[95] Okerblom, N. O., *The Calculation of Deformations of Welded Metal Structures*, Her Majesty's Stationary Office, London, U. K., 1958.

[96] Papazoglou, V. J., *Analytical Techniques for Determining Temperatures, Thermal Strains, and Residual Stresses During Welding*. Ph.D. Thesis, M.I.T., May, 1981.

[97] Papazoglou, V. J., Manual #2, *Computer Programs for the One-Dimensional Analysis of Thermal Stresses and Metal Movement During Welding*, Department of Ocean Engineering, M.I.T., January 1977.

[98] Papazoglou, V. J., and Masubuchi, K., *Numerical Analysis of Thermal Stresses During Welding Including Phase Transformation Effects*, Journal of Pressure Vessel Technology, ASME, Vol. 104, pp. 198-203, August 1982.

[99] Papazoglou, V. J., Masubuchi, K., Goncalves, E., and Imakita, A., *Residual Stresses Due to Welding: Computer-Aided Analysis of Their Formation and Consequences*, Transactions of the Society of Naval Architects and Marine Engineers, Vol., 90, pp. 365-390, 1982.

[100] Park, S. W., *In-Process Control of Distortion During Aluminum Welding*, M.S. Thesis, M.I.T., August 1988.

[101] Pavlovski, V. I., and Masubuchi, K., *Research in the U.S.S.R. on Residual Stresses and Distortion in Welded Structures*, Welding Research Council Bulletin No. 388, Welding Research Council, New York, January 1994.

[102] Rosenthal, D., *Mathematical Theory of Heat Distribution During Welding and Cutting.* Welding Journal, 20 (5), pp. 220-234, 1941. Research Supplement.

[103] Rosenthal, D., *The Theory of Moving Sources of Heat and its Application to Metal Treatment.* Transactions ASME, pp. 849-866, November, 1946.

[104] Rosenthal, D., and Schmerber, R., *Thermal Study of Arc Welding.* Welding Journal, 17 (4), pp. 208, 1948. Research Supplement.

[105] Rybicki, E. F., Ghadiali, N. D., and Schmueser, D. W., *An Analytical Technique for Evaluating Residual Deformations in Butt Weld Plates*, Special Publication of PVP-P8-025, ASME Winter Annual Meeting held November 27 through December 2, 1977.

[106] Rybicki, E. F., and Schmueser, D. W., Stonesifer, R. W., Groom, J. J., and Mishler, H. W., *A Finite-Element Model for Residual Stresses and Deflections in Girth-Butt Welded Pipes, Journal of Pressure Vessel Technology*, ASME, Volume 100, pp. 256-262, August 1978.

[107] Rybicki, E. F., and Stonesifer, R. B., *Computation of Residual Stresses due to Multipass Welds in Piping Systems*, Journal of Pressure Vessel Technology, ASME, Volume 101, pp. 149-154, May 1979.

[108] Rykalin, N. N., *Calculation of Heat Processes in Welding.* Lecture presented before the A.W.S., April, 1961.

[109] Rykalin, N. N., *Energy Sources Used for Welding.* Welding in the World, 12, pp. 227-247, 1974.

[110] Rykalin, N. N., and Nikolaev, A., *Welding Arc Heat Flow.* Welding in the World, pp. 112-132, September, 1971.

[111] Satoh, K., et al., *Thermal Elastic-Plastic Analysis of Stress and Strain in Weld Metal During Multipass Welding*, International Institute of Welding, Document X-760-73, May 1973.

[112] Satoh, K., Terasaki, T., and Nohara, K., *Changes of Root Gap During Welding in Case of Butt Weld Joint*. Journal of Japanese Welding Society, 50, pp. 76-82, 1981.

[113] Scully, K., *Laser Line Heating*, Journal of Ship Production, Vol. 3, No. 4, pp. 237-246, November 1987.

[114] Serotta, M. D., *Reduction of Distortion in Weldment*. Master's Thesis, M.I.T., March, 1975.

[115] Shim, Y., Feng, Z., Lee, S., Kim, D., Jaeger, J., Papritan, J., C., and Tsai, C., L., *Determination of Residual Stresses in Thick-Section Weldments,* Welding Journal, AWS, pp. 305s-312s, September, 1992.

[116] Shin, D. B., *Finite Element Analysis of Out-of-Plane Distortion of Panel Structures*, M. S. Thesis, M.I.T., May 1972.

[117] Snyder, M. D., and Bathe, K. J., *A Solution Procedure for Thermo-Elastic-Plastic and Creep Problems*. Journal of Nuclear Engineering and Design, 64, pp. 49-80, 1981.

[118] Soete, W., *Measurement and Relaxation of Residual Stresses*. Welding Journal, 28 (8), pp. 354-364, 1949. Research Supplement.

[119] Spraragen, W., and Claussen, G. E., *Shrinkage Distortion in Welding, a review of the literature to January 1, 1937*, The Welding Journal, Vol. 16, No. 7, Research Supplement, pp. 29-40, 1937.

[120] Spraragen, W., and Cordvi, M. A., *Shrinkage Distortion in Welding*, The Welding Journal, Vol. 23, No. 11, Research Supplement, pp. 545s-559s, 1944.

[121] Spraragen, W., and Ettinger, W. G., *Shrinkage Distortion in Welding*, The Welding Journal, Vol. 29, Nos. 6 and 7, Research Supplement, pp. 292s-294s, and 323s-335s, 1950.

[122] Strang, G., and Fix, G. J., *An Analysis of the Finite Element Method*, Prentice-Hall, Inc., Englewood Cliffs, NJ, 1973.

[123] Sussman, T., and Bathe, K. J., *A Finite Element Formulation for Nonlinear Incompressible Elastic and Inelastic Analysis.* Computers and Structures, 26 (1/2), pp. 357-409, 1987.

[124] Tall, L, *Residual Stresses in Welded Plates - A Theoretical Study*, Welding Journal, Volume 43, No. 1, Research Supplement, pp. 10s - 23s, 1964.

[125] Tall, L., *The Strength of Welded Built-up Columns*, Ph. D. Dissertation, Lehigh University, 1961.

[126] Talykov, G. B., *Approximate Theory of Deformation and Stresses in Welding*, Izd-vo Leningrad, Iniv-ta, 1957

[127] Terai, K., et al., *Study on Prevention of Welding Deformations in Thin-Plate Structures*, Kawasaki Technical Review, No. 61, pp. 61-66, August 1978.

[128] Tsai, C. L., *Parametric Study on Cooling Phenomena in Underwater Welding.* Ph.D. Thesis, M.I.T., September, 1977.

[129] Ueda, Y., *Simulation of Welding Deformation for Accurate Ship Assembling (1st Report)*, Journal of the Society of Naval Architects of Japan, Vol. 171, pp. 395-404, 1992.

[130] Ueda, Y., *Simulation of Welding Deformation for Accurate Ship Assembling (2nd Report)*, Quarterly Journal of the Japan Welding Society, Vol. 172, pp. 559-566, 1992.

[131] Ueda, Y., Fukuda, K., and Nakacho, K., *Basic Procedures in Analysis and Measurement of Welding Residual Stresses by the Finite Element Method*, Proceedings of the International Conference on Residual Stresses in Welded Construction and Their Effects, The Welding Institute, London, pp. 27-37, 1977.

[132] Ueda, Y. and Fukuda, K., *Analysis of Welding Stress Relieving by Annealing Based on Finite Element Method.* Technical Report IIW Doc X-773-75, A.W.S. 1975.

[133] Ueda, Y., and Yamakawa, T., *Analysis of Thermal Elastic-Plastic Stress and Strain Analysis During Welding by Finite Element Method.* Transactions of Journal of Welding Society, 2, pp. 90-100, September, 1971.

[134] Ueda, Y., and Yamakawa, T., *Thermal Stress Analysis of Metals with Temperature Dependent Mechanical Properties.* Proceedings of International Conference on Mechanical Behavior of Materials, pp. 10-20, Journal of Welding Society, 1971.

[135] Vinokurov, V. A., *Welding Distortions and Stresses*, Machinostroemiye, Moscow, 1968

[136] Vitooraporn, C., *Experimental and Analytical Study on Reduction of Residual Stresses and Distortion During Welding in High Strength Steel.* Ph.D. Thesis, M.I.T., 1986.

[137] Watanabe, M., and Satoh, K., *Effect of Welding Conditions on the Shrinkage and Distortion in Welded Structures*, The Welding Journal, Vol. 40, No. 8, Research Supplement, pp. 377s-384s, 1937.

[138] Watanabe, M., and Satoh, K., *Welding Mechanics and Its Applications*, Asakura Publishing Co., Tokyo, Japan, 1965

[139] Watanabe, M., Satoh, K., Morii, H., and Ichikawa, I., *Distortion in Web Plate of Welded Built-up Girders Due to Welding of Stiffeners and Methods for Reducing It*, Journal of the Japan Welding Society, Vol. 26, pp. 591-596, 1957.

[140] *Weld Distortion Handbook*, Battelle Memorial Institute, Columbus, Ohio, 1969 (not published.)

[141] Wells, A., *Heat Flow in Welding.* Welding Journal, 31 (6), pp. 263-267, 1952. Research Supplement.

[142] *Control of Distortion in Welding Fabrication*, The Welding Institute, London, U.K., 1968.

[143] Wilkening, W. W., and Snow, J. L., *Analysis of Welding-Induced Residual Stresses with the ADINA System.* Computers and Structures, 47 (4/5), pp. 767-786, 1993.

[144] Wilson, E. L., Bathe, K. J., and Peterson, F. E., *Finite Element Analysis of Linear and Non-Linear Heat Transfer.* Journal of Nuclear Engineering and Design, 29, pp. 110-124, 1974.

[145] Wilson, E. L., and Nickell, E. L., *Application of the Finite Element Method to Heat Conduction Analysis.* Journal of Nuclear Engineering and Design, 4(30< pp. 276-286, October, 1966.

[146] Zienkiewicz, O. C., and Cheugn, Y. K., *The Finite Element Method in Structural and Continuum Mechanics*, McGraw-Hill Publishing Co., New York, 1967.

[147] Zienkiewicz, O. C., and Parekh, C. J., *Transient Field Problems: Two Dimensional and Three Dimensional Analysis of Isoparametric Finite Elements.* International Journal for Numerical Methods in Engineering, 2(1), pp. 61-71, 1970.